EXPERIMENTAL INVESTIGATION INTO ELECTROCHEMICAL DISCHARGE MILLING PROCESS

THESIS SUBMITTED BY

SUDIP SANTRA

DOCTOR OF PHILOSOPHY (ENGINEERING)

DEPARTMENT OF PRODUCTION ENGINEERING

FACULTY COUNCIL OF ENGINEERING & TECHNOLOGY

JADAVPUR UNIVERSITY

KOLKATA, INDIA

2026

JADAVPUR UNIVERSITY

KOLKATA-700 032

Index No. 276/20/E
Registration No. 1012016001

TITLE OF THE Ph.D. (ENGG.) THESIS:

EXPERIMENTAL INVESTIGATION INTO ELECTROCHEMICAL DISCHARGE MILLING PROCESS

NAME, DESIGNATION & INSTITUTION OF THE SUPERVISORS:

DR. BIPLAB RANJAN SARKAR
Professor,
Department of Production Engineering,
Jadavpur University,
Kolkata–700032, India.

DR. BISWANATH DOLOI
Professor,
Department of Production Engineering,
Jadavpur University,
Kolkata–700032, India.

List of Publications

INTERNATIONAL JOURNALS:

(i) **Sudip Santra**, Biplab Ranjan Sarkar, Biswanath Doloi, Bijoy Bhattacharyya, Investigation through novel tool-electrode feeding approach on electrochemical discharge machining of glass, **Proceedings of the Institution of Mechanical Engineers Part B: Journal of Engineering Manufacture,** 2023, Vol. 237, No. 8, pp. 1207–1219. (**SCI Indexed**)

(ii) **Sudip Santra**, Biplab Ranjan Sarkar, Biswanath Doloi, Bijoy Bhattacharyya, Experimentation into Electrochemical Discharge Milling for Generation of Cavity on Glass, **Journal of Advanced Manufacturing Systems**, 2024, Vol. 24, No. 2, pp. 283-308. (**ESCI & Scopus Indexed**)

(iii) **Sudip Santra**, Biplab Ranjan Sarkar, Biswanath Doloi, Bijoy Bhattacharyya, Machining of Silica Glass with ECD Milling Using Vertically Upward Tool Feeding Technique, 2024, **Sādhanā**, Vol. 49, Article no. 128. (**SCI Indexed**)

(iv) **Sudip Santra**, Biplab Ranjan Sarkar, Biswanath Doloi, Bijoy Bhattacharyya, Fabrication of Micro Channels on Polycarbonate using Electrochemical Discharge Milling, **Journal of Materials Engineering and Performance**, 2025, Vol. 34, pp. 26050-26057. (**SCI Indexed**)

(v) **Sudip Santra**, Biplab Ranjan Sarkar, Biswanath Doloi, Investigation on electrochemical discharge milling by side feeding technique, **Materials Today: Proceedings,** 2022, Vol. 62, No. 13. (**Scopus Indexed**)

NATIONAL JOURNALS:

(i) **Sudip Santra**, Biplab Ranjan Sarkar, Biswanath Doloi, Bijoy Bhattacharyya, "On Electrochemical Discharge Milling of Glass with Horizontal Tool and Vertically Upward Feeding Technique," **CMTI-Manufacturing Technology Today (MTT)**, 2023, 22(5): 18-23. (**UGC Approved**)

BOOK CHAPTERS:

(i) **Sudip Santra**, Biplab Ranjan Sarkar, Biswanath Doloi, Bijoy Bhattacharyya, Experimental Investigation into Electrochemical Discharge Milling of Glass by Bottom Feeding the Tool Electrode. **Advances in Modern Machining Processes**,

Lecture Notes in Mechanical Engineering, Springer, pp. 65-75, 2022, DOI: 10.1007/978-981-19-7150-1_6

(ii) **Sudip Santra**, Biplab Ranjan Sarkar, Biswanath Doloi, Bijoy Bhattacharyya, Advancement of Electrochemical Discharge Machining Process—A Review, **Advances in Forming, Machining and Automation**, **Lecture Notes in Mechanical Engineering**, Springer, pp.173-187, 2022, DOI:10.1007/978-981-19-3866-5_15

(iii) **Sudip Santra**, Biplab Ranjan Sarkar, Biswanath Doloi, Bijoy Bhattacharyya, Analysis of Fabricated Channels on Glass by Electrochemical Discharge Milling (ECDmilling), **Materials Science and Engineering**, accepted for publication, considered from COPEN 13, 2024

INTERNATIONAL CONFERENCES:

(i) **Sudip Santra**, Biplab Ranjan Sarkar, Biswanath Doloi, Bijoy Bhattacharyya, Advancement of Electrochemical Discharge Machining Process—A Review, **8th International and 29th All India Manufacturing Technology, Design and Research (AIMTDR 2021)**, 09th – 11th December 2021, organised by Mechanical Engineering Department, PSG College of Technology, Coimbatore.

(ii) **Sudip Santra**, Biplab Ranjan Sarkar, Biswanath Doloi, Bijoy Bhattacharyya, Experimental Investigation into Electrochemical Discharge Milling of Glass by Bottom Feeding the Tool Electrode, **8th International and 29th All India Manufacturing Technology, Design and Research (AIMTDR 2021)**, 09th – 11th December 2021, organised by Mechanical Engineering Department, PSG College of Technology, Coimbatore.

(iii) **Sudip Santra**, Biplab Ranjan Sarkar, Biswanath Doloi, Investigation on electrochemical discharge milling by side feeding technique, **International Conference on Advances in Materials, Mechanics, Mechatronics and Manufacturing (IC4M 2022),** organised by An Association for Educational Empowerment and Social Welfare, 9th-10th April, 2022.

(iv) **Sudip Santra**, Biplab Ranjan Sarkar, Biswanath Doloi, Bijoy Bhattacharyya, On Electrochemical Discharge Milling of Glass with Horizontal Tool and Vertically Upward Feeding Technique, **International Conference on Precision, Micro, Meso and Nano Engineering (COPEN 12)**, 08th–10th December 2022, organised by Mechanical Engineering Department, IIT Kanpur.

(v) **Sudip Santra,** Biplab Ranjan Sarkar, Biswanath Doloi, Bijoy Bhattacharyya, On the ECD milling of Polycarbonate using Vertically Upward Tool Feeding Technique, **9th International and 30th All India Manufacturing Technology, Design and Research (AIMTDR 2023)**, 08th–10th December 2023, organised by Mechanical Engineering Department, IIT BHU, Varanasi.

(vi) **Sudip Santra**, Biplab Ranjan Sarkar, Biswanath Doloi, Experimental Investigation into Electrochemical Discharge Turning of Cylindrical Glass, **9th International and 30th All India Manufacturing Technology, Design and Research (AIMTDR 2023),** 08th–10th December 2023, organised by Mechanical Engineering Department, IIT BHU, Varanasi.

(vii) **Sudip Santra**, Biplab Ranjan Sarkar, Biswanath Doloi, Bijoy Bhattacharyya, Analysis of Fabricated Channels on Glass by Electrochemical Discharge Milling (ECDmilling), **13th International Conference on Precision, Micro, Meso and Nano Engineering (COPEN 13)**, 13th–15th December 2024, organised by Mechanical Engineering Department, NIT Calicut.

(viii) **Sudip Santra,** Biplab Ranjan Sarkar, Biswanath Doloi, Bijoy Bhattacharyya, Quantitative Study of Energy Utilisation and Machining Accuracy in ECD milling of Glass, **10th International and 31st All India Manufacturing Technology, Design and Research (AIMTDR 2025)**, 11th–13th December, 2025, organised by Mechanical Engineering Department, IIT Indore, Madhya Pradesh.

LIST OF AWARDS

(i) **Best Paper Award** for Investigation on electrochemical discharge milling by side feeding technique, **International Conference on Advances in Materials, Mechanics, Mechatronics and Manufacturing (IC4M 2022),** An Association for Educational Empowerment and Social Welfare, 9th -10th April, 2022.

PATENTS: NIL

Sudip Santra
13/07/2026

13/07/2026
Professor
Production Engineering Department
Jadavpur University
Kolkata - 700 032

13/07/2026
Professor
Production Engineering Department
Jadavpur University
Kolkata - 700 032

PROFORMA – I

"Statement of Originality"

I, Sudip Santra, registered on 21st December, 2020, do hereby declare that this thesis entitled "EXPERIMENTAL INVESTIGATION INTO ELECTROCHEMICAL DISCHARGE MILLING PROCESS" contains a literature survey and original research work done by the undersigned candidate as part of doctoral studies.

All the information in this thesis has been obtained and presented in accordance with existing academic rules and ethical conduct. I declare that, as required by the relevant rules and code of conduct, I have fully cited and referenced all materials and results that are not original to this work.

I also declare that I have checked this thesis as per the "Policy on Anti Plagiarism, Jadavpur University, 2019", and the level of similarity as checked by iThenticate software is **4%**.

Sudip Santra

Signature of the Candidate

(SUDIP SANTRA)

Date: 13/07/2026

Certified by Supervisors:

(Signature with date & seal)

13/07/2026

1. Dr. Biplab Ranjan Sarkar

Professor
Production Engineering Department
Jadavpur University
Kolkata - 700 032

13/07/2026

2. Dr. Biswanath Doloi

Professor
Production Engineering Department
Jadavpur University
Kolkata - 700 032

JADAVPUR UNIVERSITY
FACULTY OF ENGINEERING AND TECHNOLOGY
DEPARTMENT OF PRODUCTION ENGINEERING

CERTIFICATE FROM THE SUPERVISORS

This is to certify that the thesis entitled "EXPERIMENTAL INVESTIGATION INTO ELECTROCHEMICAL DISCHARGE MILLING PROCESS" submitted by Mr. Sudip Santra, who got his name registered on 21st December 2020 for the award of Ph.D. (Engg.) degree of Jadavpur University, is absolutely based upon his work under the supervision of Prof. Biplab Ranjan Sarkar and Prof. Biswanath Doloi and that neither his thesis nor any part of the thesis has been submitted for any degree/diploma or any other academic award anywhere before.

13/07/2026	13/07/2026
Professor Production Engineering Department Jadavpur University Kolkata - 700 032	Professor Production Engineering Department Jadavpur University Kolkata - 700 032
Prof. Biplab Ranjan Sarkar	Prof. Biswanath Doloi
(Signature of the supervisor and date with official seal)	(Signature of the supervisor and date with official seal)

ACKNOWLEDGEMENT

I would like to express my sincere gratitude to my esteemed guides, Prof. Biplab Ranjan Sarkar and Prof. Biswanath Doloi, Professor, Department of Production Engineering, Jadavpur University, for the inspiration, encouragement, and assistance they provided throughout the research work. It is due to their continuous guidance, encouragement, and valuable advice at every step, from the embryonic to the developmental stage. I am deeply indebted to them and would like to express my sincere gratitude.

Additionally, I would like to express my heartfelt thanks to my respected teachers, Prof. Bijoy Bhattacharyya and Prof. Shankar Chakraborty, for their valuable advice and suggestions. I am grateful to the Head of the Production Engineering Department at Jadavpur University for providing the departmental facilities, a healthy work environment, and moral support.

The author expresses his wholehearted thanks and gratitude to AICTE for offering the fellowship throughout the entire tenure of the PhD research work. Thanks are also extended to the FET office and the Research section for their cordial assistance and administrative support. I acknowledge and extend special thanks to Mr. Biswajit Pathak, librarian, and the staff of the Production Engineering Department, Jadavpur University, for their support, suggestions, immense help, and cooperation during this thesis work.

I am highly thankful to Dr. Santosh Kumar, Dr. Kaushik Mishra, Dr. Mohit Pandey, Dr. Naresh Besekar, Dr. Himadri Sekhar Panda, Mr. Dwarika Pratap Singh, Mr. Kailash Roy, and all other research scholars of the Production Engineering Department, Jadavpur University, for their support and encouragement during my research work. I gratefully acknowledge the support of all other people who helped me, directly or indirectly, at various stages of this work.

I want to express my deepest gratitude to my parents, Rabindranath Santra and Mana Santra, for their unconditional love and unwavering support throughout my life's journey. I also thank my beloved maternal grandparents and maternal uncle for their love and blessings. I am grateful to my dear sister, Dipika Karmakar, my brother-in-law, Rathin Karmakar, my dear aunt, and my elder brother, Samanway Santra, for their affection and encouragement. I thank my childhood teachers, Mr. Bijoy Roy and Mr. Chapal Kanti Roy; whose mentorship has profoundly influenced my life. I thank my beautiful nieces, Aaradhya Karmakar and Shreya Santra; their laughter brings light to our family.

I am indebted to my loving wife, Rita Santra, and my daughter, Ritanya Santra, who fill my life and encourage me to continue my research work smoothly. Each of you has played a significant role in shaping me, and I am deeply grateful for your love, support, and presence in my life.

Sudip Santra

…………………………………

(Sudip Santra)

Preface

Electrochemical Discharge Milling (ECD milling) arises from the inherent limitations of Electrical Discharge Machining and Electrochemical Machining when dealing with hard, brittle, and non-conductive materials. ECD milling offers a viable solution by leveraging electrochemical processes to achieve precise, efficient, and high-quality machining of such materials, making it indispensable in various industrial applications. In ECD milling, an electrolyte solution is used as a conductive medium, facilitating the flow of electrical current between the tool electrode and the workpiece. When a voltage is applied across the electrodes immersed in the electrolyte, electrochemical reactions occur, leading to the generation of hydrogen gas and electrolyte vapour due to Joule heating. These generated gas bubbles adhere around the tool electrode and form a gas film. The formed gas film breaks down with a spark discharge between the tool electrode and the electrolyte at a threshold or critical voltage. As a result, ECD milling enables the machining of non-conductive materials while achieving intricate shapes and features that would be difficult or impossible to produce using conventional methods. Moreover, ECD milling offers several advantages when machining non-conductive materials. Unlike traditional machining methods that generate significant heat during machining, ECD milling operates at lower temperatures due to the predominance of electrochemical reactions. This minimizes the risk of thermal damage, such as cracks or distortion, particularly in heat-sensitive materials like glass and ceramics. ECD milling can create very smooth surfaces on tough and fragile materials if the right settings and machining methods are used. The ability of ECD milling to effectively machine non-conductive materials with high precision, minimal thermal damage, and excellent surface finish makes it a valuable technique in various industries, including aerospace, electronics, and biomedical engineering.

Significant research has been conducted since the discovery of the electrochemical discharge machining (ECDM) process. This technique has been widely utilized for drilling holes in electrically non-conductive materials. Some researchers have extended its application to create channels and various patterns on materials such as glass, ceramics, and polymers. However, electrochemical discharge milling (ECD milling) has not been extensively studied. Additionally, researchers have implemented various techniques and accessories to enhance the performance of ECDM.

One of the major challenges in ECDM is the inadequate supply of fresh electrolyte and the presence of gas bubbles in the machining zone. These gas bubbles, which rise from the tool-electrode tip due to the buoyancy of the electrolyte, hinder effective machining at deeper zones. Techniques such as tool vibration, tool rotation, different tool shapes, and the introduction of magnetic fields have yielded some improvements by reducing the thickness of the gas film and controlling electrolyte flow at the machining zone. However, no research has been conducted on tool electrode feeding techniques that could regulate the movement of gas bubbles and ensure a consistent supply of fresh electrolyte at the machining zone. This study focuses on the milling operation using electrochemical discharge, employing various tool feeding techniques to ensure proper circulation of fresh electrolyte and formation of gas bubbles at the machining zone. Using Electrochemical Discharge Milling (ECD milling), various patterns have been fabricated on glass and polymers, demonstrating the potential of this technique to enhance machining performance. So, keeping the drawbacks of the ECDM process in mind, the following objectives are set to be fulfilled during my Ph.D. (Engg.) research work:

(i) To develop an Electrochemical Discharge Milling setup.

(ii) To investigate the possibility of fabricating high aspect ratio features, such as channels, using Electrochemical Discharge Milling on glass.

(iii) To investigate the effects of different process parameters during Electrochemical Discharge Milling with vertically upward tool feeding technique.

(iv) To fabricate various patterns, such as zigzag channels, rectangular-shaped cavity, using Electrochemical Discharge Milling on glass.

(v) To investigate the effects of various process parameters on Electrochemical Discharge Milling of different types of polymers.

The thesis has been structured and describes all the investigations and research work in a well-organized manner into eight chapters in detail as follows:

Chapter 1 delves into the principles and advancements of Electrochemical Discharge Milling (ECD milling), beginning with an in-depth exploration of its fundamental processes. It details the electrolysis process involved in ECD milling, including how the electrolyte facilitates material removal through electrochemical reactions. The formation and impact of gas films, which can affect machining efficiency, are examined, alongside the generation of spark discharge a crucial element in material removal. The chapter further explains the mechanisms by which material is removed during the milling process. It addresses the necessity of ECD milling, highlighting its advantages over conventional machining methods, particularly in complex and precision applications. The chapter reviews past research efforts focused on reducing gas film thickness, controlling spark discharge, and improving material removal rates (MRR) and surface quality. By identifying existing gaps in the current research and technological landscape, the chapter sets the stage for the objectives of the present study, which aims to address these gaps and contribute to the evolution of ECD milling technology.

Chapter 2 outlines the development of an Electrochemical Discharge Milling (ECD milling) setup, detailing its critical components and their functions. It begins with an introduction to the setup, then describes key elements including the X-Y-Z translation stage for precise tool and workpiece movement, the Automated Programmed Tool (APT) software for process control, and the tool and workpiece holding devices for stability. The chapter also covers the tool and auxiliary electrodes, the main machining chamber, and the power supply unit, which is essential for generating spark discharges. Additionally, it addresses the equipment used for measurements and data collection to monitor the milling process. Finally, it integrates these components into a complete ECDM setup, highlighting their collective role in ensuring efficient and accurate milling operations.

Chapter 3 investigates the effectiveness of various tool feeding techniques in Electrochemical Discharge Milling (ECD milling). The chapter includes numerical analyses of gas film shape generation for various tool feeding techniques, including the existing, bottom, and upward tool feeding methods. It then simulates temperature distributions for the gas films created by these techniques. Results and discussions examine the impact of various tool feeding methods on electrochemical spark discharge, including the effects of electrolyte concentration and tool feed rate on channel width. The chapter compares the width and depth of channels produced by different feeding techniques, examining their relative performance and effects on the tool electrode. Finally, it summarizes the study's outcomes, highlighting the most suitable tool feeding techniques based on the experimental data and simulations.

Chapter 4 explores the application of the Upward Tool Feeding Technique in Electrochemical Discharge Milling (ECD milling) on silica glass. The results and discussion section examines how different process parameters affect material removal rate (MRR), surface quality, channel width, and channel taper. Additionally, it assesses the generation of various patterns on silica glass using this technique. The chapter concludes with a summary of the study's outcomes, highlighting the effectiveness of the Upward Tool Feeding Technique in achieving precise milling and pattern creation on silica glass.

Chapter 5 presents the optimization of Electrochemical Discharge milling (ECD milling) using Response Surface Methodology and a Box-Behnken experimental design. Electrolyte concentration, voltage, and tool feed rate were systematically varied to model their effects on channel width, surface roughness, taper angle, and material removal rate. ANOVA confirmed all quadratic models as statistically significant, with electrolyte concentration emerging as the dominant factor for width and MRR, while voltage and feed rate strongly influenced roughness and taper. Multi-objective optimization identified 20 wt% electrolyte concentration, 35 V, and 44 µm/s feed rate as the best compromise setting. Experimental validation showed errors below 5%, and SEM images confirmed smoother, crack-free channel edges, verifying the accuracy and reliability of the optimized RSM models.

Chapter 6 examines the process of creating rectangular cavities in glass using Electrochemical Discharge Milling (EDM, also known as ECD milling). It begins with an overview of the experimental goals and setup, which includes testing three different strategies for inter-channel distances, i.e. matching the width of a single channel, matching the tool diameter, and setting the distance smaller than the tool diameter. The results section discusses the impact of these strategies on the width of individual channels and their effectiveness in forming rectangular cavities. The analysis evaluates the success of the strategy in cavity formation, leading to the identification of the most effective approach for this purpose. The chapter concludes with a summary of the key findings and the recommended strategy for the precise fabrication of rectangular cavities in glass.

Chapter 7 investigates ways to enhance the performance of Electrochemical Discharge Milling (ECD milling) when applied to polymers using the Upward Tool Feeding Technique. The experimental plan involves analysing the effects of milling process parameters on different polymers, specifically PMMA and polycarbonate, using NaOH and KOH electrolytes. The chapter examines how these parameters influence the milling process, including their effects on material removal and the Spark Affected Zone (SAZ) for each polymer-electrolyte combination. The chapter concludes by summarizing the findings and providing recommendations for ECD Milling performance on polymers using the Vertically Upward Tool Feeding Technique.

Finally, **Chapter 8** presents the general conclusions drawn from the research on Electrochemical Discharge Milling (ECD milling) and its various applications. It summarizes the key findings from the studies covered in previous chapters, highlighting the effectiveness of different tool feeding techniques, parametric combination for various polymers and glass machining, and advancements in surface quality enhancement for stainless steel. The chapter then outlines potential directions for future research, suggesting areas where further investigation could build on the current findings to advance the technology and address existing challenges.

The outcomes of this study on electrochemical discharge milling (ECD milling) present substantial benefits to various industries, particularly those engaged in precision and high-tech manufacturing. The enhanced precision and efficiency achieved through the integration of advanced X-Y-Z translational stages and APT software enable exceptional accuracy and minimal tolerance deviations, which are crucial for sectors such as aerospace, automotive, and electronics. Additionally, the upward tool feeding technique's ability to reduce tool-electrode wear translates into longer tool life and lower operational costs. The study also offers improved machining performance by identifying effective tool path strategies and feeding techniques, which can improve surface quality and dimensional accuracy for complex components, essential in medical device manufacturing and precision engineering. Furthermore, the research highlights material-specific machining strategies, providing insights into how different materials, such as glass, polycarbonate, and PMMA, respond to ECD milling. This enables industries to tailor their processes for optimal performance across various materials, enhancing versatility and adaptability. Overall, the findings of the study demonstrate how advanced technological integration and parameter adjustments can drive manufacturing advancements, enhance product quality, and reduce operational costs, ultimately leading to increased competitiveness and efficiency in industrial operations.

VITA

The author, Sri Sudip Santra, son of Sri Rabindranath Santra and Smt. Mana Santra, was born on January 16, 1994, in the district of Hooghly, West Bengal, India. He studied in Bhurkunda High School (H.S.) and passed the Secondary Examination from WBBSE in 2009. Then he studied in Arambagh High School (H.S.) and passed the Higher Secondary Examination from WBCHSE in 2011. The author graduated in Mechanical Engineering in 2015 from Kalyani Government Engineering College under Maulana Abul Kalam Azad University of Technology (Formerly WBUT), Kalyani, Nadia, West Bengal. The Author worked as a machine shop supervisor at Carnation Industries Limited, Uluberia, Howrah, West Bengal, from 2016 to 2017. After that, the author completed his Master of Technology with a specialisation in Production Engineering in 2019 from the Mechanical Engineering Department at Kalyani Government Engineering College, under Maulana Abul Kalam Azad University of Technology (Formerly WBUT), Kalyani, Nadia, West Bengal. The author stood second in the University and won a silver medal during his master degree course.

In 2019, the author joined as a junior research fellow and, after two years, was promoted to senior research fellow under the AICTE Doctoral Fellowship (formerly known as the National Doctoral Fellowship) in the Production Engineering Department of Jadavpur University, Kolkata. Author was registered as a PhD student in Jadavpur University on 21st December, 2020, in the Department of Production Engineering. The author continued his research work in the area of Electrochemical Discharge Milling during the entire tenure of his research. Currently, the author is working as a CSIR Research Associate in the Department of Production Engineering, Jadavpur University, Kolkata.

The author has published seven research papers in national and international refereed journals, as well as presented more than eight research papers at reputed international conferences related to advanced machining processes. Author received the “BEST PAPER AWARD” in the International Conference on Advances in Materials, Mechanics, Mechatronics and Manufacturing, 2022 (IC4M-2022) for his research work.

DEDICATED TO MY PARENTS, MATERNAL GRANDPARENTS, LATE GRANDPARENTS AND WELL-WISHERS

Table of Contents

List of Figures

Figure No.	Title of the Figure	Page No.

List of Tables

List of Abbreviations

Abbreviation	Meaning
MEMS	Micro-Electro-Mechanical Systems
EDM	Electrical Discharge Machining
ECM	Electrochemical Machining
DC	Direct Current
ECDM	Electrochemical Discharge Machining
ECD milling	Electrochemical Discharge Milling
NEMS	Nano-Electro-Mechanical Systems
MRR	Material Removal Rate
MHD	Magnetohydrodynamic
KOH	Potassium Hydroxide
NaOH	Sodium Hydroxide
SACE	Spark Assisted Chemical Engraving
SACM	Spark Assisted Chemical Machining
ECAM	Electrochemical Arc Machining
UAECDM	Ultrasonic Assisted Electrochemical Discharge Machining
SDS	Sodium Dodecyl Sulfate
CTAB	Cetyltrimethylammonium Bromide
HAZ	Heat Affected Zone
CMC	Critical Micelle Concentration
WOC	Width Overcut
ECF	Electrochemical Finishing
TGV	Through Glass Vias
EWR	Electrode Wear Ratio
TWR	Tool Wear Rate
TEWR	Tool Electrode Wear Ratio
TTR	Tool Travel Rate
SEM	Scanning Electron Microscopy
EDS	Energy Dispersive Spectroscopy
EDAX	Energy Dispersive X-Ray Analysis
EDX	Energy Dispersive X-ray Spectroscopy

G-ECDM	Grinding-aided Electrochemical Discharge Machining
ECDD	Electro-Chemical Discharge Drilling
WEDM	Wire Electrical Discharge Machining
PECMM	Pulsed Electrochemical Micromachining
ECSM	Electrochemical Spark Machining
TSECDD	Tube Electrode High-Speed Electrochemical Discharge Drilling
FEM	Finite Element Method
WC	Tungsten Carbide
TFR	Tool Feed Rate
TEFR	Tool Electrode Feed Rate
PECDM	Pulse Electrochemical Discharge Machining
FESEM	Field Emission Scanning Electron Microscopy
FRP	Fibre Reinforced Polymer
CLECDM	Closed-loop ECDM
PDMS	Polydimethylsiloxane
APT	Automated Programmed Tool
OFAT	One Factor at a Time
SAZ	Spark Affected Zone
EC DISCHARGE	Electrochemical Discharge
PMMA	Polymethyl Methacrylate

Chapter 1

INTRODUCTION

Since ancient times, humanity has been deeply invested in refining the art of material processing, a fundamental aspect underpinning technological progress. This enduring pursuit has been evident from prehistoric times to the present, with the mastery of machining playing a pivotal role in shaping civilizations and driving innovation across various fields. As technological advancements surged in the last century, the demand for specialized materials grew exponentially. Silicon, composites, ceramics, Polymers, and other advanced materials have become essential components across a wide range of industries, from electronics to aerospace. This proliferation of materials necessitated the development of new machining techniques tailored to their unique properties. A significant milestone in machining history was the advent of micromachining. This breakthrough enabled the fabrication of intricate microstructures with unprecedented precision, laying the foundation for the miniaturization of devices and systems. In tandem with the rise of micromachining, attention also turned to electrically non-conductive materials, such as glass, composites, polymers, etc. These materials, once considered challenging to machine, gained newfound importance in various applications. Glass, in particular, emerged as a versatile material in the realm of Micro-Electro-Mechanical Systems (MEMS). MEMS, a revolutionary technology that integrates microsensors and actuators on a single chip, ushered in a new era of miniaturized devices and systems. The unique properties of glass, including its chemical resistance, biocompatibility, and transparency, make it invaluable in a myriad of applications. From optical devices to medical implants, glass finds utility in diverse fields where precision, reliability, and functionality are paramount. In the dynamic landscape of MEMS, glass holds immense promise for future innovations. Micro accelerometers, micropumps, microreactors, and medical devices such as flow sensors and drug delivery systems are just a few examples of the amazing capabilities glass enables in MEMS technology. Overall, the evolution of material processing and machining techniques has been instrumental in driving technological progress, paving the way for breakthroughs in fields ranging from electronics and healthcare to aerospace and beyond. As advancements continue to unfold, the role of materials like glass in shaping the future of technology is poised to become even more significant.

Electrochemical Discharge, an innovative machining technique, was initially developed in Japan during the late 1950s and initially found its early applications in diamond die workshops. The seminal work of Kurafuji and Suda **[1]** in 1968 marked a significant milestone in the evolution of the process. The pioneering paper introduced the concept, which was coined 'electrical discharge drilling', showcasing its ability to create micro-holes in glass. Additionally, the study explored the intricate effects of the electrolyte's chemical composition and the choice of tool-electrode materials, laying the groundwork for further exploration. Nonetheless, the innovation of this technology sparked discussions about its similarity to established techniques, such as Electrical Discharge Machining (EDM) and Electrochemical Machining (ECM). This ambiguity persisted for five years until it was clarified by Cook et al. **[2]** in 1973, who proposed the term "Discharge machining of non-conductors". This term highlighted its unique applicability across a broad spectrum of nonconductive materials and prompted deeper investigations into its mechanisms and capabilities. Throughout the years, researchers continued to refine and expand upon this technique. Tsuchiya et al. **[3]** introduced a novel variant in 1985, employing a wire as a tool electrode, which was termed 'wire electrochemical discharge machining'. This innovation opened up new possibilities, allowing the cutting of not only glass but also various ceramics. Further advancements came with the work of Jain et al. **[4]** in 1991, where 'electrochemical spark machining' was introduced, drawing parallels with electrochemical arc machining and broadening its scope of application. The 1990s witnessed the first applications of Electrochemical Discharge in the expanding field of Micro-Electro-Mechanical Systems (MEMS), alongside rigorous fundamental studies. Notably, Ghosh et al. **[5]** in 1999 established a crucial link between the machining process and the electrochemical discharge phenomenon, shedding light on the underlying mechanisms. As the new millennium dawned, researchers intensified their efforts to unravel the intricacies of material removal mechanisms. In 2001, Yang et al. **[6]** defined the process as a high-temperature etching phenomenon, deepening the understanding of its chemical aspects. Subsequent investigations by Fascio et al. **[7]** in the early 2000s further elucidated the electrochemical contributions, culminating in the publication of the first comprehensive review paper by Wuthrich et al. [8] in 2005. Since 2006, there has been a remarkable resurgence of interest in Electrochemical Discharge technology, with a proliferation of studies that refine process fundamentals, systematically characterize various machining strategies, and propose novel process improvements.

1.1 Fundamentals of Electrochemical Discharge Milling

Electrochemical Discharge is a sophisticated machining method that harnesses a combination of electrochemical reactions and electrical discharge to shape electrically non-conductive materials. The process entails immersing the workpiece in a carefully chosen electrolytic solution, commonly sodium or potassium hydroxide, while applying a steady DC voltage between the machining tool or tool-electrode and a larger counter-electrode, as shown in **Fig. 1. 1**.

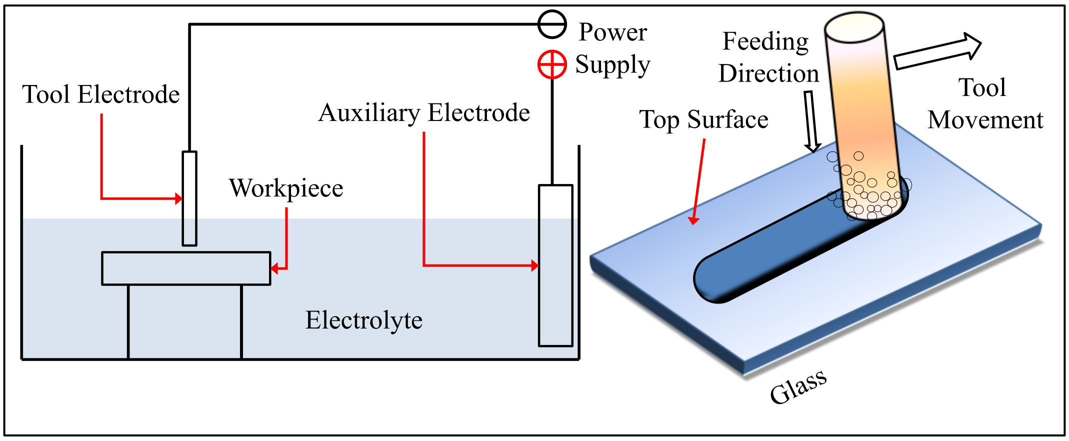

Fig. 1. 1 Schematic diagram of electrochemical discharge machining

The tool electrode, positioned a few millimeters into the electrolytic solution, has a notably smaller surface area than the counter electrode. This size discrepancy, typically by a factor of around 100, ensures effective machining conditions. Initially, at lower terminal voltages, the process resembles traditional electrolysis. Depending on the polarization and the specific electrolyte used, hydrogen bubbles form at the tool electrode, while oxygen bubbles form at the counter electrode. As the terminal voltage rises, the current density at the tool electrode increases, leading to greater bubble generation. These bubbles accumulate around the electrodes, forming a layer. When the voltage exceeds the critical voltage (typically 20-30 V), the bubbles coalesce into a cohesive gas film that envelops the tool electrode. Within this gas film, electrochemical discharges occur intermittently between the tool and the surrounding electrolyte, manifesting as observable light emissions. This phenomenon signifies the intricate interplay between electrical and chemical processes within the machining environment. The temperature of the electrolyte solution around the tool electrode increases due to electrochemical action. This elevated temperature facilitates the machining process, particularly when the tool electrode is positioned in proximity (typically less than 25 μm) to the glass workpiece. Despite its apparent simplicity, Electrochemical Discharge Machining is not devoid of challenges. The stability of the gas film surrounding the tool electrode can be precarious, leading to potential microexplosions that may compromise the integrity of the machined structure. Moreover, during drilling, localized temperature spikes can occur, resulting in heat-affected zones or even cracking the glass. In essence, Electrochemical Discharge machining represents a delicate balance of electrochemical and physical factors, offering precise control over the machining process while demanding careful attention to operational parameters to ensure optimal outcomes.

1.1.1 Electrolysis Process during ECD milling

Understanding electrochemical discharges requires a deep dive into the intricate processes occurring at gas-evolving electrodes. These electrodes produce gases according to Faraday's law, which relates the amount of substance produced in an electrolytic reaction to the quantity of electricity passing through the cell. However, the formation and growth of gas bubbles on the electrode surface introduce a complicating factor, as they can impede the area available for electrochemical reactions.

In alkaline solutions, hydrogen production is a multi-step process. Initially, water molecules chemically adsorb onto the free electrode as shown in equation (1.1).

$$2H_2O + 2e^- \rightarrow H_2 \uparrow + 2(OH)^- \qquad \dots (1.1)$$

In an acidic solution, the reaction occurs as shown in equation (1.2)

$$2H^+ + 2e^- \rightarrow H_2 \uparrow \qquad \dots (1.2)$$

Similarly, the oxygen evolution reaction, like the hydrogen evolution reaction, involves several intermediate steps. In acidic solutions, the overall reaction is influenced by electrode corrosion, as the overpotential required for oxygen evolution can lead to electrode material corrosion and passivation. The reaction in an acidic solution is as shown in equation (1.3)

$$2H_2O \rightarrow O_2 \uparrow + 4H^+ + 4e^- \qquad \dots (1.3)$$

The reaction in an alkaline solution is as shown in equation (1.4)

$$4OH^- \rightarrow O_2 \uparrow + 2H_2O + 4e^- \qquad \dots (1.4)$$

Conversely, in alkaline electrolytes, electrodes are typically more resistant to corrosion. However, the formation of metal oxides during the reaction adds another layer of complexity. In summary, understanding electrochemical discharges is hindered by the intricate nature of the reactions at gas-evolving electrodes. Despite efforts to model these reactions, a multitude of factors are involved, and parameter adjustments based on experimental data are needed.

1.1.2 Mechanism of Gas Film Formation

The gas film in electrochemical machining serves a dual role: it is both a prerequisite for the machining process and a significant factor affecting the quality of the machining outcome. Thus, gaining a deep understanding of the mechanisms underlying the formation and behavior of this gas film is crucial for optimizing machining processes. When water undergoes electrolytic decomposition, gas bubbles are generated at the electrodes. This bubble formation comprises two distinct steps. Initially, at the microscopic level, gas is formed through electrochemical reactions as shown in equation (1.5).

$$2H^{+} + 2e^{-} \rightleftharpoons H_2 \uparrow \qquad \dots (1.5)$$

Subsequently, at the macroscopic level, these gases accumulate near the electrode surface, leading to bubble formation. This process primarily occurs at defects or irregularities on the electrode surface and relies on the surrounding electrolyte being supersaturated with dissolved gas.

Once formed, the behavior of these bubbles is influenced by various forces acting upon them. Buoyancy and capillary forces, as shown in equations (1.6) & (1.7), play crucial roles, determining whether bubbles detach from the electrode surface.

$$F_B = \frac{4}{3}\pi R_b^3 \rho g \qquad \dots (1.6)$$

$$F_B = 2\pi D\gamma \sin\vartheta \qquad \dots (1.7)$$

where ρ is the density of the electrolyte, γ is the surface tension of the electrolyte, R_b is the bubble radius, D is the order of magnitude of the aperture of an active nucleation site, and ϑ is the contact angle.

The mean bubble departure radius, a key parameter, is influenced by electrode properties (such as surface roughness and wettability) and electrolyte characteristics (such as density and surface tension). The applied current density may also influence the activation of nucleation sites, thereby affecting bubble formation rates. Research indicates that the mean bubble departure radius exhibits a complex relationship with current density. At low current densities, the radius decreases, whereas at higher values it tends to stabilize as the number of growing bubbles increases. Additionally, the coalescence of bubbles becomes more prevalent at higher current densities, as demonstrated by Vogt **[9],** and shows an increase in the number of merging bubbles. Furthermore, the quality of the electrode material can significantly affect bubble behavior. Studies have shown differences in bubble behavior between unused electrodes and used electrodes, suggesting that electrode quality affects bubble dynamics. The region surrounding a gas-evolving electrode forms a structured bubble layer that can be divided into three distinct regions, as shown in **Fig. 1. 2**.

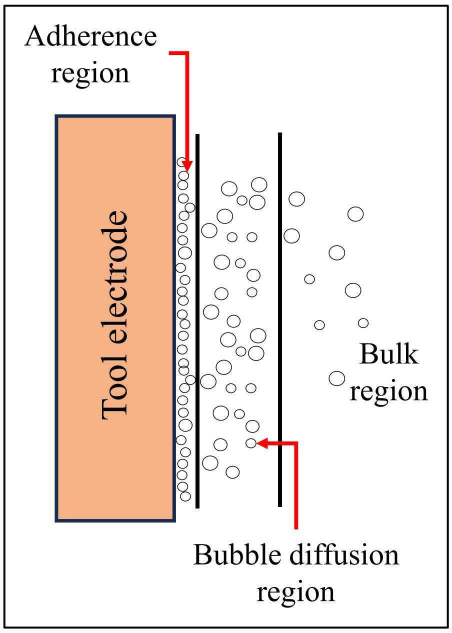

Fig. 1. 2 Schematic diagram of different bubble layers in the ECD milling process

The regions surrounding a gas-evolving electrode are as follows:

(i) The adherence region,
(ii) The bubble diffusion region, and
(iii) The bulk region.

Each of these regions plays a specific role in bubble dynamics and machining processes. For instance, the adherence region is where bubbles initially form and grow, often coalescing upon contact. The bubble diffusion region is characterized by high bubble concentration, while the bulk region contains dispersed bubbles and marks the end of significant bubble growth due to reduced gas supersaturation. In summary, a comprehensive understanding of gas-film dynamics in electrochemical discharge machining is essential for optimizing processes and achieving desired outcomes. This understanding encompasses bubble formation, growth, detachment, and coalescence, as well as the influence of electrode properties and current density on these processes.

1.1.3 Generation of Spark Discharge

The formation of a gas film around an electrode significantly alters the distribution of electrical potential within the electrochemical cell. In the presence of a gas film, the current flow through the system diminishes considerably, resulting in a minimal voltage drop within the electrolyte due to its low conductivity. Consequently, most of the electrical potential drop occurs across the gas film itself, resulting in localized, elevated electric fields near the electrode surface. This alteration in the distribution of electrical potential, combined with the elevated temperature of the electrode, facilitates the occurrence of electrochemical discharges as shown in **Fig. 1.3**. For an active cathode, these discharges are often facilitated by thermal-assisted field emission, wherein the elevated temperature of the electrode assists in the emission of charged particles necessary for electrochemical reactions.

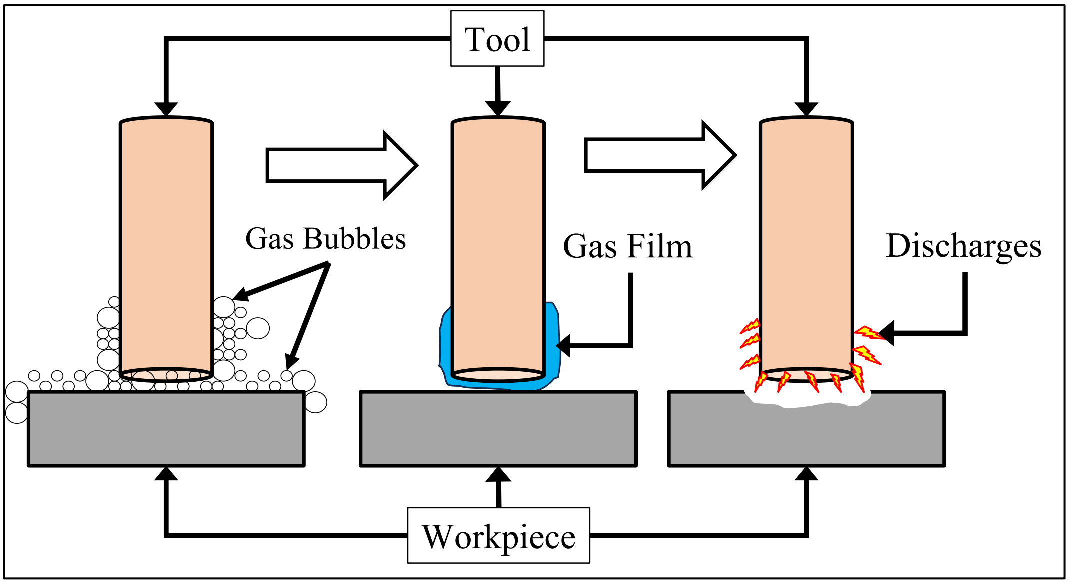

Fig. 1. 3 Schematic of gas film formation and spark discharge

Conversely, for an active anode, electrochemical discharges are typically attributed to mechanisms such as the Hickling and Ingram mechanisms, in which gas bubbles serve as nucleation sites for discharge. Furthermore, because the voltage drop across the electrolyte is minimal, most of the heat generated during the electrochemical process is concentrated within the gas film. This heat concentration further raises the electrode temperature, creating an environment conducive to enhanced electrochemical activity. As the applied voltage surpasses a critical threshold, typically 20 to 30 volts, the individual gas bubbles coalesce, forming a continuous gas film that envelops the tool-electrode interface. Within this cohesive gas film, electrochemical discharges occur intermittently between the tool and the surrounding electrolyte. These discharges are often accompanied by observable light emissions, as shown in **Fig. 1. 3**, which serve as visual indicators of spark discharges within the gas film. The formation of a gas film around the electrode profoundly influences the electrochemical processes within the cell, shaping the distribution of electrical potential, facilitating electrochemical discharges, and ultimately enhancing the efficiency and effectiveness of the machining process.

1.1.4 Mechanism of Material Removal

Since Kurafuji and Suda demonstrated the feasibility of electrochemical discharge machining for glass microdrilling in 1968, it has been established that this method extends beyond glass substrates to various other non-conductive materials. Despite this understanding, ongoing investigations examine the mechanisms underlying material removal. Multiple processes contribute to material removal, including.

(i) Melting and vaporization due to electrochemical discharges,
(ii) High-temperature etching,
(iii) Thermal stresses, and
(iv) Mechanical shock.

To date, systematic exploration has primarily focused on thermal effects and etching, especially in glass machining utilizing an active cathode. It is widely acknowledged that localized heating of the workpiece induced by electrochemical discharges drives the machining process. Depending on the material being worked on, material removal occurs through melting, which may lead to vaporization, or via high-temperature etching. The simultaneous operation of both mechanisms is also feasible. Numerous experimental studies corroborate the significance of the thermal mechanism in machining. For example, studies have shown that during micro drilling, the temperature of the tool electrode can reach up to 500°C. Demonstrative experiments, such as those conducted by Allesu et al. **[10]** and Kulkarni et al. **[11]**, showcase the ability of heat generated by electrochemical discharges to impact glass and metallic workpieces, respectively. Observations of thermal cracks in machined materials at elevated machining voltages made by Gautam and Jain **[12]**. Maillard et al. **[13]** further support the role of thermal effects. Conversely, there is compelling evidence suggesting a chemical contribution to machining, particularly in the context of smooth surface finishes achieved in glass machining at low voltages. Chemical analysis of the electrolyte post-machining by Jain et al. **[14]** reveals products indicative of etching reactions. Recent experimental findings have shed light on the temperature conditions within the machining zone, revealing temperatures around 500–600°C, or even as low as 200°C, depending on the machining strategy. Despite these relatively low temperatures, glass still exhibits high viscosity, prompting the consideration of etching as a necessary mechanism for material removal. The high-temperature chemical etching of glass during Electrochemical Discharge Milling is confirmed by the thermal–chemical reaction between silica (SiO_2) and sodium hydroxide (NaOH). At spark-induced temperatures above 800 °C, silica reacts rapidly with NaOH to form soluble sodium silicate, as shown in equation (1.8).

$$SiO_2 + 2NaOH \rightarrow Na_2SiO_3 + H_2O \quad \text{... (1.8)}$$

This temperature-activated dissolution proves that chemical etching, enhanced by localized thermal energy from discharges, plays a dominant role in the material removal mechanism in ECD milling of glass. These chemical reactions occur predominantly during Electrochemical Discharge Milling, not during simple NaOH etching, because the dissolution of silica in alkaline solutions requires a very high activation energy. At room temperature, NaOH attacks the Si–O–Si network of glass extremely slowly, resulting in negligible material removal. However, in ECDM, the spark discharges generated at the tool–electrolyte interface produce localized temperatures ranging from several hundred to over a thousand degrees Celsius. Such extreme thermal conditions rapidly break the strong Si–O–Si bonds and soften the glass surface, enabling hydroxyl ions from NaOH to react instantly with silica to form soluble sodium silicate species. This synergistic effect of thermal softening and chemical attack accelerates the otherwise sluggish reaction, demonstrating that significant etching of glass occurs only under the high-temperature conditions produced by electrochemical discharges, not in simple ambient-temperature NaOH solutions. In summary, electrochemical discharge machining involves a complex interplay between thermal and chemical effects. While thermal mechanisms are integral to initiating material removal, chemical etching processes also play a significant role, particularly in achieving precise finishes on glass substrates. Continued research is essential to understand the relative contributions of these mechanisms better and to optimize machining processes accordingly.

1.2 Need for Electrochemical Discharge Milling

The need for electrochemical discharge milling arises from the inherent limitations of conventional machining techniques when dealing with hard, brittle, and non-conductive materials. ECDM offers a viable solution by leveraging electrochemical processes to achieve precise, efficient, and high-quality machining of such materials, making it indispensable in various industrial applications. Traditional machining methods, such as milling, drilling, and turning, rely on mechanical cutting or abrasion, which necessitates the workpiece to conduct electricity effectively. However, non-conductive materials such as ceramics and glass have low electrical conductivity, rendering traditional machining techniques ineffective. ECDM circumvents this limitation by employing electrochemical processes rather than relying solely on mechanical force. In ECDM, an electrolyte solution serves as a conductive medium, facilitating the flow of electric current between the tool electrode and the workpiece. When a voltage is applied across the electrodes immersed in the electrolyte, electrochemical reactions occur, leading to the dissolution of material from the workpiece. This electrochemical dissolution enables precise material removal without requiring the workpiece to conduct electricity. As a result, ECDM enables the machining of non-conductive materials with high precision, achieving intricate shapes and features that would be difficult or impossible to produce using conventional methods. Moreover, ECDM offers several advantages when machining non-conductive materials. Unlike traditional machining methods, which generate significant heat during cutting, ECDM operates at lower temperatures because electrochemical reactions predominate. This minimizes the risk of thermal damage, such as cracks or distortion, particularly in heat-sensitive materials like glass and ceramics. The non-contact nature of electrochemical machining in ECDM eliminates the risk of tool wear and deflection, ensuring consistent dimensional accuracy even in intricate geometries. This is particularly important for applications that require tight tolerances. The electrochemical dissolution process produces surfaces with minimal roughness and subsurface damage, making them suitable for applications requiring high-quality surface finishes, such as optics and microelectronics. Since material removal in ECDM primarily occurs through electrochemical reactions rather than mechanical abrasion, tool wear is significantly reduced. This results in longer tool life and lower maintenance costs, making ECDM a cost-effective machining. The ability of ECDM to effectively machine non-conductive materials while offering high precision, minimal thermal damage, and excellent surface finish makes it a valuable technique in aerospace, electronics, and biomedical engineering.

1.3 Applications of Electrochemical Discharge Milling

Electrochemical Discharge Milling (ECD milling) finds applications across various industries due to its ability to machine hard, brittle, and non-conductive materials with high precision and efficiency. It enables the fabrication of microelectromechanical systems (MEMS), integrated circuits, and other electronic components with high precision and minimal subsurface damage. In the optics and photonics industry, ECD milling is used to manufacture precision optical components such as lenses, mirrors, and diffraction gratings. It enables the creation of complex surface profiles with sub-micron accuracy, meeting the stringent requirements of optical systems in fields like astronomy, telecommunications, and laser technology. ECD milling plays a crucial role in biomedical engineering for fabricating miniaturized medical devices, implants, and surgical instruments. It enables the machining of biocompatible materials such as titanium alloys, stainless steel, and bio ceramics with high precision, making it suitable for applications in orthopedics, dentistry, and implantology. ECD milling is utilized in the fabrication of microelectromechanical systems (MEMS) and nanoelectromechanical systems (NEMS) for various applications such as sensors, actuators, and microfluidic devices. It enables the creation of intricate microstructures and features on substrates like silicon, quartz, and polymers, contributing to advancements in sensing, biomedical diagnostics, and lab-on-a-chip technologies. ECD milling is employed for precision machining of hard and brittle materials, including ceramics, glass, and composites. It enables the production of complex components with tight tolerances and fine surface finishes, making it suitable for applications in the aerospace, automotive, and tooling industries. ECD milling is used in microfabrication to create microchannels, micro-holes, and micro-patterns on substrates for applications such as microfluidics, microreactors, and microelectrodes. It offers high precision and repeatability in producing microstructures with sub-micron resolution, contributing to advancements in lab-on-a-chip devices, biochemical analysis, and microscale manufacturing. ECD milling is used in the glass industry to machine precision glass components, such as microfluidic devices and glass lenses. It allows for the creation of intricate shapes and features on glass substrates with high precision and minimal edge chipping, making it suitable for applications in telecommunications, biotechnology, and precision optics. The versatility, precision, and efficiency of ECD milling make it a valuable machining technique across a wide range of industries, contributing to technological and manufacturing advancements.

1.4 Review of Past Research

In the past, research work had been carried out in various fields of electrochemical discharge processes. Some focused on machining performance, while others concentrated on the fundamentals of the electrochemical discharge process. The number of research papers on ECDM published in international journals is increasing day by day, as shown in **Fig. 1. 4**.

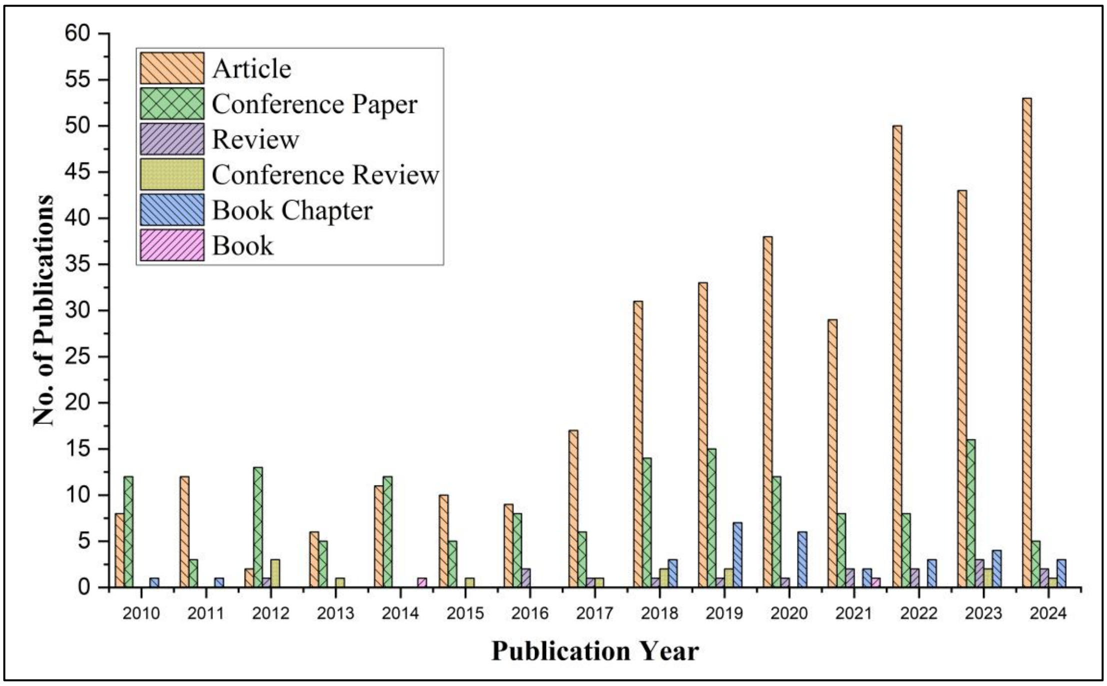

Fig. 1. 4 Graphical representation of research publications on ECDM

Still, research into the fundamentals of the process is ongoing to better understand it. Researchers studied the fundamentals of Electrochemical Discharge Machining and its machining performance. Overall, previous research can be categorized as follows by its nature.

(i) Reduction of gas film thickness
(ii) Controlling the Spark Discharge Phenomenon
(iii) Improvement of Material Removal Rate (MRR) and Machined Quality
(iv) Fabrication of Various Geometrical Shapes by ECD milling

1.4.1 Reduction of Gas Film Thickness

Reducing the gas film thickness in Electrochemical Discharge Machining (ECDM) is critical for optimizing machining performance. Thinner gas films facilitate higher material removal rates, improved surface finishes, and greater machining accuracy by enabling better electrolyte access to the workpiece surface and finer control over process parameters. Additionally, minimizing gas film thickness helps prevent gas bubble formation, optimize heat dissipation, and reduce electrolyte consumption, thereby promoting cost-effectiveness and environmental sustainability. Overall, reducing the gas film thickness in ECDM is pivotal to achieving efficient and precise machining of conductive materials.

Han et al. **[15]** introduced a partially side-insulated electrode to maintain a consistent contact surface area with the electrolyte during the ECDM process, ensuring uniform gas film formation and stable spark discharges. Visual inspections revealed that this electrode configuration facilitated the formation of single bubbles, improving the geometric uniformity of the gas film compared to conventional electrodes. Experimental results demonstrated enhanced discharge current uniformity with the side-insulated electrode, thereby significantly reducing fluctuations. The study also theoretically determined the minimum bubble radius required for spark generation and evaluated film thickness limits, which were experimentally verified using microchannels fabricated with a cylindrical electrode. The geometric accuracy of the channels improved, and surface roughness decreased when the side-insulated electrode was used, demonstrating its potential to enhance ECDM performance.

Cheng et al. **[16]** investigated magnetic-field-assisted Electrochemical Discharge Machining (ECDM) to improve micro-hole drilling performance by enhancing electrolyte circulation via magnetohydrodynamic (MHD) convection. The applied magnetic field generated a Lorentz force on charged ions, promoting electrolyte flow in the narrow tool–workpiece gap. This improved bubble removal and maintained a stable gas film, ensuring consistent electrochemical discharges. As a result, machining accuracy and efficiency were significantly enhanced. Micro-holes with depths up to 450 μm were successfully drilled in less than 20 s, while stable machining conditions were maintained even at greater depths. The entrance hole diameter decreased from 470 μm to 358 μm, and machining time was reduced from 41.4 s to 17.6 s, corresponding to a 23.8% improvement in geometric accuracy and a 57.4% increase in machining efficiency.

Cheng et al. **[17]** investigated gas-film dynamics in Electrochemical Discharge Machining (ECDM) by analyzing current signals and machined contours to assess gas-film quality. They introduced the concept of a transition voltage, defined as the applied voltage above the critical level at which a stable, dense gas film forms, thereby enabling steady discharges and improved machining accuracy. During deep-hole drilling, trapped bubbles increased gas film thickness near the hole entrance, reducing discharge stability and machining quality. Higher electrolyte concentration enhanced electrolysis, lowered the transition voltage, and produced a thinner, more stable gas film due to increased hydroxyl (OH^-) ions, thereby improving chemical etching and surface finish. Additionally, current signals effectively monitored gas film behavior, while a flat-sidewall tool minimized gas film deterioration, enhancing machining accuracy and efficiency.

Huang et al. **[18]** proposed a novel Electrochemical Discharge Machining (ECDM) technique for micro-hole drilling in stainless steel using a high-speed rotating micro-electrode and pure water as the electrolyte. Despite the challenges associated with machining stainless steel due to its high hardness and toughness, the proposed method successfully produced micro-holes with improved performance. Experimental results showed that increasing the electrode rotation speed significantly reduced tool wear while enhancing discharge stability. Machining voltage and electrode diameter also had a considerable influence on the process. An empirical mathematical model developed from the experimental data revealed that machining voltage had the greatest effect on tool wear, followed by electrode rotational speed and diameter. Overall, high-speed electrode rotation improved machining accuracy, efficiency, and tool life.

Gao et al. **[19]** investigated spark-assisted chemical engraving (SACE) for micro-machining glass using a 200 µm tungsten carbide drill instead of a conventional cylindrical electrode. The rotating micro-drill enhanced electrolyte circulation through its micro-grooves, improving machining performance and reducing micro-cracking. The effects of machining time, drill rotation direction, rotation speed, and contact force were systematically evaluated, showing significant influence on drilling performance. Under optimal conditions, a micro-hole with an entrance diameter of 245 µm and an aspect ratio of 8.8 was achieved. The study also highlighted reduced tool wear and improved electrolyte supply with the micro-drill electrode. Using the proposed configuration, a 2 mm deep hole was successfully drilled in Pyrex glass, with entrance and exit diameters of 245 µm and 210 µm, respectively.

Razfar et al. **[20]** investigated the effect of longitudinal oscillation of the cathode electrode during electrochemical discharge micro-drilling of glass by modifying electrolyte flushing in both discharge and hydrodynamic regimes. Experiments were performed at different vibration frequencies and amplitudes, using two tool geometries: a cylindrical rod and a micro-drill. For the cylindrical rod, square-wave oscillation significantly increased the material removal rate (MRR), whereas sinusoidal oscillation produced only a modest improvement. In contrast, vibration had little influence on the rotating micro-drill because its flutes naturally enhanced electrolyte circulation. Square-wave excitation increased MRR by up to 40% and enabled deeper holes in shorter machining time, while sinusoidal excitation improved MRR by approximately 20%, demonstrating the importance of oscillation waveform in ECDM performance.

Jiang et al. **[21]** comprehensively investigated gas film dynamics in Electrochemical Discharge Machining (ECDM) through analytical modeling and experimental validation. High-speed imaging confirmed that gas film formation governs discharge initiation and machining performance. Experimental gas film thickness closely matched analytical predictions, underscoring the importance of controlling film thickness to improve productivity, accuracy, and repeatability. The study showed that electrolyte surface tension and density strongly influence bubble growth and gas film evolution. Thinner gas films lowered the critical voltage and current, reducing overcut and improving machining quality. The addition of surfactants was suggested to achieve thinner films. Furthermore, increasing current density near the tool electrode through appropriate tool size and immersion depth enhanced spark initiation without requiring additional electrolysis power.

Krotz et al. **[22]** investigated Spark-Assisted Electrochemical Machining (SAEM), an advanced process derived from Electrochemical Arc Machining (ECAM), for machining electrically conductive materials. SAEM utilizes electrochemical discharges to drill micro-holes and can be integrated with Electrochemical Machining (ECM) for electrochemical finishing. The study refined the material removal mechanism by incorporating the contact arc, enabling efficient micro-hole drilling. Optimizing the inter-electrode gap ensured the contact arc occurred at an optimal frequency, reducing machining time by nearly 50%. Micro-holes were successfully produced using different electrolytes, and their surface characteristics and heat-affected zones were systematically evaluated. The results demonstrated SAEM's potential as an efficient and versatile technique for precision micro-machining of conductive materials.

Elhami et al. **[23]** investigated ultrasonic-assisted Electrochemical Discharge Machining (UAECDM) by applying ultrasonic vibration directly to the tool tip to improve machining precision and efficiency. A vibration system was designed using modal analysis and analytical modeling. Experimental and analytical results showed that ultrasonic vibration significantly reduced gas film thickness, leading to higher material removal rates (MRR) and improved machining accuracy. The tapering zone and entrance overcut decreased by up to 50% and 40%, respectively, while increasing the voltage to 37 V produced more uniform wall surfaces. UAECDM also achieved substantially greater machining depths, with increases of 82% at 15 μm vibration amplitude and 60% at 10 μm compared with conventional ECDM, demonstrating the effectiveness of localized ultrasonic assistance.

Elhami et al. **[24]** employed modal analysis to design an ultrasonic-assisted Electrochemical Discharge Machining (ECDM) system, focusing on machining speed, gas film thickness, and discharge characteristics. Gas film thickness, discharge location, and discharge patterns were experimentally analyzed, while current signals were used to monitor machining phenomena. The application of ultrasonic vibration reduced gas film thickness by approximately 65%, with a vibration amplitude of 10 μm producing the most stable current signal and significantly improving the material removal rate (MRR). Furthermore, ultrasonic vibration increased machining speed under both discharge and hydrodynamic regimes. The findings demonstrated that vibration effectively stabilized the machining process by improving discharge characteristics and electrolyte behavior, thereby enhancing machining efficiency.

Sabahi et al. **[25]** investigated the influence of gas film thickness on microchannel quality in Electrochemical Discharge Machining (ECDM). Theoretical analysis showed that tool wettability and electrolyte surface tension strongly affect gas film formation. Experiments using the surfactants Sodium dodecyl sulfate (SDS) and Cetyltrimethylammonium bromide (CTAB) modified electrolyte properties and improved machining performance. Surfactant addition increased the material removal rate (MRR), reduced overcut and heat-affected zones (HAZ), and enhanced surface quality. At 35 V with 0.036 wt% CTAB in KOH, surface quality improved by 73%, while channel edge hardness increased by 144%, indicating reduced thermal damage. CTAB outperformed SDS because of its lower critical micelle concentration and superior chemical etching capability.

Elhami et al. **[26]** introduced technical enhancements to electrochemical discharge machining (ECDM) to improve machining efficiency. The study of the ECDM process at the single-discharge level focused on understanding its complexities and the effects of technical augmentations. In the research, ultrasonic vibration was incorporated as a technical enhancement, resulting in a method termed ultrasonic vibration-assisted electrochemical discharge machining (UAECDM). Special configurations and equipment were employed to apply ultrasonic vibration and generate single discharges. Material removal and tool wear were assessed as key indicators of machining efficiency. Analysis of the current signal revealed that ultrasonic vibration increased the number of discharges under constant conditions. Furthermore, ultrasonic vibration led to a significant increase in material removal, up to 35%, while reducing tool wear by 3% to 14%. These findings highlight the potential of UAECDM as an efficient machining method.

Xu et al. **[27]** investigated the magnetohydrodynamic (MHD) effect in electrochemical discharge machining (ECDM) to address the challenges posed by the unstable gas film around the tool electrode, which often leads to inaccuracies and reduced material removal rates, especially in the hydrodynamic regime. The analysis and experimental observations revealed that the MHD effect induced by a magnetic field improved electrolyte circulation and machining efficiency, thereby decreasing the thickness of the gas film. Through high-speed camera recordings, a reduction in the machined hole radius from 528 μm to 430 μm was observed, along with a decrease in machining time from 50 to 16 s. Additionally, a hybrid approach combining the counter-resistant feeding method with a magnetic field was introduced, which significantly enhanced the accuracy, throughput, and roundness of the machined holes, offering promising advances in the ECDM process.

Singh et al. **[28]** investigated textured tools for Electrochemical Discharge Machining (ECDM) of microchannels in borosilicate glass. The textured surface created micro-gaps that promoted the formation of thin, stable gas films, producing high-frequency, low-intensity discharges and improving machining performance. Compared with smooth tools, textured tools increased the material removal rate (MRR) by 19.27% and channel depth by 64.81%, while reducing width overcut (WOC) and surface roughness by 122.26% and 26.96%, respectively. The tools were also capable of producing both smooth and textured surfaces, making them suitable for microfluidic applications. Multi-criteria optimization identified optimal conditions of 59 V, 3 ms pulse on/off time, 12 mm/min feed rate, and 21 wt.% electrolyte concentration, resulting in improved machining accuracy and surface quality.

Kolhekar et al. **[29]** investigated the influence of gas-film thickness and stability on Electrochemical Discharge Machining (ECDM) using a full factorial experimental design. The effects of electrolyte concentration, electrolyte level, inter-electrode distance, and machining time were systematically examined. A novel approach correlated mean discharge energy with gas-film thickness, while the standard deviation of discharge current was used to evaluate gas-film stability. ANOVA confirmed that both parameters significantly affected overcut and taper during micro-hole machining. Optimal conditions consisting of low electrolyte concentration, low electrolyte level, high electrode spacing, and short machining time produced thinner, more stable gas films, minimizing machining errors. Experimental validation verified the predictive capability of the discharge current-based gas-film model, providing an effective method for process monitoring and control.

Lin et al. **[30]** enhanced Electrochemical Discharge Machining (ECDM) of quartz glass by combining ethanol with a 3 T magnetic field. Ethanol improved tool wettability by reducing the contact angle between gas bubbles and the electrode, resulting in thinner gas films and more stable discharges. Simultaneously, the magnetic field generated magnetohydrodynamic (MHD) effects that improved electrolyte flow and stabilized bubble behavior. These combined effects produced more uniform discharge zones, improved hole roundness, reduced taper by approximately 30%, and significantly decreased undercut. The technique enabled smoother machining profiles and higher dimensional accuracy, making it particularly suitable for fabricating precise micro-holes and grooves in quartz for MEMS applications while minimizing residual stress and fracture compared with conventional machining methods.

Arab et al. **[31]** investigated the influence of tool electrode roughness on through-hole quality during Electrochemical Discharge Machining (ECDM) of glass substrates. Single-tip electrodes with different surface roughness levels were fabricated using wire electrical discharge machining, while electrochemical finishing (ECF) was employed to improve surface quality and tool reusability. Rougher electrodes generated unstable and aggressive discharges, resulting in greater radial overcut and larger heat-affected zones. In contrast, smoother ECF-finished electrodes produced thinner hydrogen gas films, lower mean discharge currents, and improved hole geometry. The fabricated through-holes were successfully filled by bottom-up copper electrodeposition to produce through-glass vias (TGVs), demonstrating the applicability of the process for radio-frequency MEMS and advanced electronic packaging.

Singh et al. **[32]** investigated ultrasonic-assisted Electrochemical Discharge Machining (UA-ECDM) using high-frequency (35 kHz), low-amplitude ultrasonic vibrations. High-speed imaging, discharge signal analysis, simulations, and surface characterization demonstrated that ultrasonic assistance redirected machining energy from the tool edges toward the center, improving energy channelization. Material removal occurred through cavitation, pressure-assisted debris evacuation, melting, vaporization, and chemical etching. Compared with conventional ECDM, UA-ECDM consumed 2.23 times less energy while improving the energy channelization index fivefold. It also reduced the heat-affected zone and eliminated the alkali-deficient layer on machined surfaces. Enhanced sludge removal and electrolyte replenishment significantly improved the material removal rate and depth-to-diameter ratio, demonstrating the effectiveness of ultrasonic assistance.

Rashedul et al. **[33]** experimentally evaluated the influence of electrode material on Electrochemical Discharge Machining (ECDM) performance using titanium alloy (TC4), stainless steel (SS304), brass, and three copper–tungsten (CuW) alloys. Material removal rate (MRR), electrode wear ratio (EWR), overcut, and surface quality were analyzed. Electrical conductivity primarily affected MRR, whereas thermal conductivity governed electrode wear. Among the tested materials, the W70Cu30 electrode exhibited the best performance, achieving an MRR of 70 µg/s, the lowest EWR of 8.1%, and a minimum overcut of 0.05 mm. Its superior thermal conductivity enhanced heat dissipation, reduced electrode erosion and oxygen deposition, and produced smoother surfaces with fewer defects, thereby improving discharge stability, machining accuracy, and tool life.

1.4.2 Controlling the Spark Discharge Phenomenon

Controlling the spark discharge in Electrochemical Discharge Machining (ECDM) is essential for achieving precise machining outcomes. Effective control over the spark discharge ensures uniform material removal and prevents surface damage to the workpiece. This control involves regulating parameters such as pulse frequency, pulse duration, voltage, and electrolyte flow rate. Adjusting these parameters allows fine-tuning of the discharge process to match desired machining requirements, such as material removal rate, surface finish, and dimensional accuracy. Additionally, monitoring and feedback systems can be employed to maintain consistent spark discharge conditions throughout the machining operation, ensuring optimal performance and quality of the machined components. By mastering the control of spark discharge, ECDM processes can deliver high-precision machining results across a wide range of conductive materials.

Liu et al. **[34]** investigated the discharge mechanism in Electrochemical Discharge Machining (ECDM) of particulate-reinforced metal matrix composites by modeling the electric field around hydrogen bubbles and predicting the critical breakdown voltage. The maximum electric field intensity was found at 90° to the vertical electrode axis, and the predicted breakdown voltage (26.2–34.2 V) closely matched experimental values (26–30 V). Increasing current, duty cycle, pulse duration, and electrolyte concentration promoted arc formation. Waveform analysis showed that ECDM spark discharges gradually transition into EDM-like arcs, although ECDM produced smaller craters. XRD analysis detected the Al_4C_3 phase in EDM but not in ECDM, indicating lower machining temperatures or electrochemical dissolution. The study provided valuable insights into discharge behavior, crater formation, and material removal mechanisms in ECDM.

Wei et al. **[35]** developed a finite element model for the discharge regime of Electrochemical Discharge Machining (ECDM), focusing on machining depths below 300 μm where most material removal occurs. Unlike previous models, the proposed approach specifically addressed the discharge regime, improving prediction accuracy at shallow depths and lower voltages. The model simulated single-spark material removal and predicted the evolution of drilling depth with good agreement with experimental results. Approximately 29.1% of the spark energy was transferred to the workpiece, and the maximum machinable depth in this regime was estimated at 303 μm. Although the model excluded tool wear, thermal expansion, phase transformation, and hydrodynamic effects, it provided a reliable foundation for understanding and optimizing precision micro-drilling using ECDM.

Krotz et al. **[36]** investigated single discharges in electrochemical arc machining by analyzing the heat-affected zone (HAZ) and by developing a heat-transfer model. Simulation results showed that the HAZ diameter was mainly governed by the arc spot diameter rather than discharge duration or heat flux. Variations in the melting zone were attributed to differences in plasma channel diameter caused by changes in electrolyte composition and temperature. Continuous pulsing increased the electrolyte temperature, leading to evaporation and changes in gas composition, which influenced plasma formation and arc spot size. These findings clarified the factors governing melting zone dimensions and provided useful guidance for improving micro-drilling processes in electrically conductive materials by better controlling discharge characteristics.

Jiang et al. **[37]** developed an experimental stochastic model to estimate spark energy in Electrochemical Discharge Machining (ECDM). Tapered tool electrodes fabricated by electrochemical machining (ECM) improved the consistency of spark generation, while spark energy was modeled with a two-component log-normal distribution. A finite element model correlated spark energy with material removal by treating the process as a heat-transfer problem, in which electrical energy was converted into thermal energy, causing melting and chemical etching. Model predictions agreed well with experimental observations. The study demonstrated that tapered electrodes suppressed minor discharges and improved spark consistency, providing a reliable framework for predicting material removal and advancing process modeling in ECDM.

Hajian et al. **[38]** investigated the influence of machining parameters on tool bending force during Electrochemical Discharge Machining (ECDM). The effects of tool diameter, electrolyte concentration, magnetic field, and tool feed rate were systematically evaluated to determine the maximum feed rate that maintains stable tool bending forces. Experimental results showed that higher applied voltage and electrolyte concentration significantly reduced bending force and increased the optimum feed rate. The magnetic field had a more pronounced effect at lower electrolyte concentrations by further decreasing tool deflection. The study emphasized the importance of monitoring horizontal tool force for selecting optimal machining conditions and demonstrated that appropriate parameter selection can minimize tool bending, improve machining stability, and enhance overall process efficiency.

Saranya et al. **[39]** conducted systematic experimental investigations to analyze the electrical and 2-D machining characteristics of the electrochemical discharge machining (ECDM) process. The study examined the effects of various process parameters, including electrolyte type, electrolytic concentration, tool travel rate (TTR), and applied voltage, on critical voltage (Vc) and critical current (Ic). Two electrolytes, KOH and NaOH, at concentrations ranging from 10% to 50% were used. A cylindrical tungsten carbide tool with a diameter of 0.4 mm and varying TTRs (from 0.3 to 4 mm/min) was employed to fabricate microchannels. Results indicated that precise channels with smooth surfaces and regular outlines could be achieved at an applied voltage of Vc + 4 V and TTRs between 1 and 2 mm/min, as observed through optical images of the machined channels.

Sabahi et al. **[40]** investigated microchannel machining in soda-lime glass under different electrolyte concentrations and magnetic field conditions. Nanoindentation tests were used to evaluate the hardness of the channel edges and assess the heat-affected zone (HAZ). Applying a magnetic field increased edge hardness by up to 87% and 24% at 15% and 30% electrolyte concentrations, respectively. Magnetohydrodynamic (MHD) convection enhanced hydrogen bubble movement and electrolyte conductivity, resulting in more stable electrical discharges and a smaller HAZ. Higher electrolyte concentration and applied voltage generated greater thermal energy, increasing the HAZ. Nanoindentation results also showed that KOH-machined samples exhibited lower hardness than NaOH-machined samples because larger potassium ions reduced material strength and enlarged the heat-affected zone.

Singh et al. **[41]** proposed a pressurized feeding system to improve precision and deep-hole drilling in Electrochemical Discharge Machining (ECDM) of borosilicate glass. The fixture-based mechanism maintained a near-zero working gap by applying constant pressure, promoting the formation of thin, stable gas films and high-frequency, low-intensity discharges. Compared with conventional feeding methods, the pressurized system increased machining depth by 207.4%, achieving micro-holes up to 1537 μm deep with reduced hole overcut and taper. Optimal machining conditions included 55 V, 3 ms pulse-on time, 1 ms pulse-off time, 20 wt.% electrolyte concentration, and 3 N/mm^2 applied pressure. The simple design eliminated the need for complex feedback control, providing improved process stability and making the technique highly suitable for precision microfluidic device fabrication.

Gupta et al. **[42]** investigated the influence of electrolyte level on the performance of Electrochemical Discharge Machining (ECDM) during micro-hole drilling in glass. Electrolyte height above the workpiece was varied from 0.1 to 4 mm, and its effects on material removal rate (MRR), depth of cut, heat-affected zone (HAZ), and overcut (OC) were evaluated using spark waveform analysis and microscopic observations. An electrolyte level of approximately 1 mm provided the best balance between machining efficiency and quality by producing higher MRR, greater drilling depth, and lower HAZ and overcut. Electrolyte levels below 1 mm caused unstable discharges and poor hole geometry, whereas a 4 mm level reduced HAZ and overcut but significantly decreased MRR and machining depth. The findings provide practical guidelines for optimizing electrolyte level in ECDM microfabrication.

Sabahi et al. **[43]** investigated the impact of electrolyte composition on electrochemical discharge machining (ECDM). A blend of NaOH and KOH in equal proportions was found to yield higher electrical conductivity and improved surface quality than using them separately. This blend enabled the creation of deeper microchannels with sharper sidewalls. Mixed electrolytes at various concentrations also enhanced surface quality due to increased viscosity. The study revealed that salt electrolytes produced low-energy, unstable sparks, thereby affecting material removal rates and surface quality. Additionally, SEM and EDX analyses showed more severe tool wear with NaOH and NaNO3 than with KOH and mixed electrolytes. Erosion was exacerbated at higher voltage. These findings emphasize the importance of electrolyte composition in optimizing ECDM processes to improve performance and surface finish.

Liu et al. **[44]** investigated the working mechanism and tool behavior in Grinding-aided Electrochemical Discharge Machining (G-ECDM) for machining metal matrix composites. The study examined tool electrode clogging, grit volume fraction, and average grit height under different machining conditions. Experimental results showed that although grinding caused material clogging on the tool surface, spark discharges effectively removed the deposited material, maintaining stable machining conditions. The remaining clogged material protected the bonding layer between the diamond grits, thereby extending tool life. Compared with conventional ECDM, G-ECDM exhibited significantly greater tool durability. While rapid diamond grit loss occurred during the initial run-in stage, the tool surface gradually stabilized, resulting in more predictable wear. These findings demonstrate that balancing clogging removal and protective buildup improves machining stability and tool longevity, making G-ECDM suitable for machining hard and composite materials.

Madhavi et al. **[45]** investigated the μ-Electrochemical Discharge Machining (μ-ECDM) of channels in 4 mm-thick quartz glass using a 370 μm-diameter stainless steel tool. Various levels of voltage (V), electrolyte concentration (wt.%), and duty factor (%DF) were explored for optimization using the Signal-to-Noise (S/N) ratio and Grey Relational Analysis (GRA). S/N ratio optimization identified parameters to maximize Material Removal Rate (MRR), minimize Tool Wear Rate (TWR), and minimize channel width. GRA optimization identified parameters (40 V, 20 wt%, 50 %DF) resulting in 81 μg/m of MRR, 2.99 μg/m of TWR, and a channel width of 557.6 μm. The study also delved into machining textures on the quartz surface, including 45° hatch, square hatch, and 45° criss-cross hatch, using the optimized parameters.

Kolhekar et al. **[46]** investigated the influence of gas-film characteristics on machining performance in Electrochemical Discharge Machining (ECDM) of glass, using finite-element-based multiphase simulations and experimental validation. The study examined how electrolyte level affects gas film formation, stability, and machining overcut. Simulation results showed that increasing the electrolyte level produced thicker, less stable gas films, which enhanced convective heat transfer around the tool and altered discharge behavior, resulting in greater overcut. In contrast, lower electrolyte levels produced thinner, more stable gas films, resulting in reduced overcut and improved machining precision. Experimental observations closely matched the simulation results, confirming the relationship between electrolyte level, gas film thickness, and machining accuracy. The study highlights the importance of optimizing electrolyte levels to control gas-film behavior and improve precision in ECDM micro-machining.

Zhang et al. **[47]** investigated the impact of solution conductivity on tool electrode wear in the Electro-Chemical Discharge Drilling (ECDD) process. Using deionized water and $NaNO_3$ solutions with varied conductivities, the study aimed to understand the relationship between solution conductivity and the reduction in tool electrode wear while maintaining high-quality drill holes through ECDD. Results indicated that using a NaNO3 working fluid with a conductivity of approximately 4.0 mS/cm yielded optimal outcomes, with high-quality holes and minimal tool electrode wear. The tool electrode relative wear ratio decreased by 65.4% as the working fluid conductivity changed from 0.005 to 4.0 mS/cm. These findings underscore the importance of selecting a suitable solution conductivity to improve efficiency and precision in the ECDD process.

Mishra et al. **[48]** explored the impact of parameters on microchannel fabrication in soda-lime glass. Using NaOH and KOH electrolytes at varying concentrations and tool-electrode/workpiece gaps, the study employed a DC power supply and high-carbon steel needles. Finite element analysis correlated predicted and experimental values for microchannel depth and width. NaOH outperformed KOH, showing higher depth and width. Increasing the tool electrode-workpiece gap and feed rate reduced microchannel depth, while wider channels were achieved at specific gaps. Additionally, tool wear decreased with higher gaps and feed rates, and KOH resulted in lower wear than NaOH. The research provides valuable insights into optimizing microchannel fabrication processes.

Rathore et al. **[49]** investigated incorporating sonication into the tool electrode in the Electrochemical Discharge Machining (ECDM) process to enhance discharge energy. Experimental findings highlighted sonication's role in regulating gas-bubble departure and controlling gas-film thickness. Higher electrolyte concentration reduced gas film thickness, resulting in intensified electric discharges. Sonication improved electrolyte replenishment and sludge removal. The study introduced a mathematical model of the effects of process parameters on gas bubble departure. Furthermore, when comparing Ultrasonic-Assisted ECDM (UAECDM) with traditional ECDM, sonication during UAECDM resulted in an

11.13% increase in material removal rate (MRR), a 27.17% increase in diameter overcut percentage (DOP), and a 23.10% reduction in hole overcut (HOC) compared to standard ECDM. This research offers insights into the potential benefits of sonication in ECDM and compares UAECDM with conventional ECDM.

Jawalkar et al. **[50]** proposed a hybrid Electrochemical Discharge Machining (ECDM) process combining electrolyte stirring and tool rotation to improve machining performance. Using a custom-built setup and Taguchi's L_{18} orthogonal array, the study evaluated the effects of these enhancements on material removal rate (MRR) and surface quality. The hybrid process achieved a maximum MRR of 1.282 mg/min and an improved surface roughness (R_a) of 0.4 µm. FESEM analysis revealed smoother channel surfaces, reduced recast layers, and well-defined tool feed marks due to enhanced electrolyte flushing and rotational tool motion. A regression model was also developed to predict MRR under different conditions. The results demonstrated improved machining efficiency, surface integrity, and economic feasibility, highlighting the potential of this hybrid approach for precision micro-machining.

Elhami et al. **[51]** developed a comprehensive multiphysics simulation model to predict discharge behavior and material removal in Electrochemical Discharge Machining (ECDM). Unlike conventional thermal models, the proposed approach incorporated electric current, electromagnetic fields, plasma fluid behavior under local thermodynamic equilibrium (LTE), and heat transfer using COMSOL. Single-discharge experiments validated the model, with the critical discharge voltage determined as 37 V. The simulation predicted a maximum plasma temperature of 3650 °C and accurately represented phase-change-induced material removal. Predicted material removal and hole diameter deviated from experimental values by 31.5% and 14.33%, respectively. The model provides a more realistic understanding of discharge phenomena and offers a valuable physics-based tool for analyzing and optimizing ECDM processes.

Singh et al. **[52]** evaluated the environmental impact of Electrochemical Discharge Machining (ECDM) by analyzing fumes generated using HCl, NaOH, and NaCl electrolytes. Fume mass concentration increased with electrolyte concentration due to intensified electrochemical reactions, with HCl producing the highest emissions and NaOH the lowest among the alkaline electrolytes. Nanometer-sized particles (<100 nm) exhibited different morphologies and agglomeration characteristics depending on the electrolyte.

Elemental analysis identified toxic metals, including Al, Mg, Fe, Ni, Cr, and Ti, while FTIR spectroscopy detected hazardous gases, including CH_4, NO_2, SO_2, CO_2, amines, disulfides, and halogenated hydrocarbons. The study concluded that low-concentration NaOH generates the least toxic emissions, making it the safest electrolyte for environmentally sustainable ECDM.

Ho et al. **[53]** proposed two auxiliary techniques to improve Electrochemical Discharge Machining (ECDM) of sapphire: micro-nano bubble (MNB) enriched electrolytes and hollow electrodes. MNBs increased spark intensity and electrolyte activity, reducing machining time by 31% and increasing average current by 26.7%. Hollow electrodes enhanced electrolyte replenishment and debris removal, reducing gas film formation time by 34.5% and gas film thickness by 54%, resulting in more stable discharges. Combining MNB electrolytes with a cone-shaped hollow electrode increased machining depth by 3.8 times compared with conventional ECDM, achieving a maximum depth of 440.08 μm. The study demonstrated that controlling gas-film behavior and current characteristics significantly improves discharge stability, material removal, and machining performance in hard, non-conductive materials.

Rajput et al. **[54]** developed an improved numerical model to predict the material removal rate (MRR) in Electrochemical Discharge Machining (ECDM) using randomly oriented multi-spark discharges. Unlike conventional single-spark models, the approach accounted for crater overlap, spark growth, and a Gaussian heat distribution to simulate realistic machining conditions. The effects of applied voltage, electrolyte concentration, and energy transfer were analyzed. Increasing electrolyte concentration from 10 wt.% to 30 wt.%, voltage from 35 V to 55 V, and energy transfer from 15% to 35% significantly increased MRR. The predicted temperature distribution followed a Gaussian profile with maximum heating at the spark center. Simulation results closely matched experimental data, demonstrating the model's reliability for analyzing spark interactions and optimizing ECDM performance.

Rajput et al. **[55]** developed a finite element thermal model to compare the performance of NaOH, KOH, and NaCl electrolytes in Electrochemical Discharge Machining (ECDM). The model predicted temperature distribution and material removal rate (MRR) by considering electrolyte concentration, applied voltage, spark radius, and duty ratio. Simulation results closely agreed with experiments, showing that NaOH produced the highest MRR due to its superior chemical-etching capability and a peak temperature of 2970.1 K. MRR increased with voltage, duty ratio, and electrolyte concentration, but decreased with larger spark radius. Experimental evaluation further showed that KOH provided better geometric accuracy, reducing overcut by 32.1% and improving hole circularity by 40.8% compared with $NaNO_3$. Overall, NaOH and KOH were identified as the most effective electrolytes for ECDM.

1.4.3 Improvement of Material Removal Rate (MRR) and Machined Quality

Improving the Material Removal Rate (MRR) and machined quality in Electrochemical Discharge Machining (ECDM) is crucial for enhancing productivity and achieving high-quality surface finishes. Several strategies can be employed to achieve these goals. Firstly, optimizing process parameters such as voltage, pulse frequency, pulse duration, and electrolyte flow rate can significantly enhance MRR while maintaining machined quality. Additionally, using advanced tool electrode materials and designs can improve material removal efficiency and reduce tool wear, leading to higher MRR and better surface finishes. Furthermore, implementing intelligent process monitoring and control systems enables real-time adjustments to machining parameters, ensuring consistent, optimal performance throughout the process. Moreover, integrating advanced surface treatment techniques, such as surface roughness prediction models and post-processing methods like electrochemical polishing, can further enhance machined quality by refining surface texture and minimizing defects. Overall, a combination of parameter optimization, tool enhancement, process monitoring, and surface treatment strategies is essential for achieving simultaneous improvements in MRR and machined quality in ECDM.

Han et al. **[56]** experimented with the ECDM process using electrolytes mixed with powder to improve the surface integrity of the machined product. An investigation was conducted on 1 mm-thick borosilicate glass using a 0.2 mm-diameter tungsten carbide tool electrode to machine the glass in a NaOH solution. It was observed that the surface roughness (Ra) decreased with increasing tool feed rate up to a certain point; beyond that, Ra increased due to irregular material removal from the workpiece. It was also observed that surface roughness improved when 1 wt% conductive powder was added to the electrolyte; however, higher powder concentrations led to a deterioration in the surface quality of the machined product.

Han et al. **[57]** enhanced Electrochemical Discharge Machining (ECDM) micro-hole drilling by introducing ultrasonic electrolyte vibration, a side-insulated electrode, and a pulse-power generator to improve electrolyte flow, gas film stability, and spark generation. The side-insulated electrode concentrated discharges at the tool tip, while pulsed voltage minimized thermal damage and improved surface quality. Ultrasonic vibration promoted electrolyte circulation, efficient chip removal, and modified the bubble layer to produce more stable and active spark discharges. Experimental results showed significant improvements in hole geometry, with the hole diameter decreasing from 426 μm to 328 μm and the machining depth increasing from 320 μm to 550 μm using a 200 μm electrode. The combined approach also reduced overcut and taper, demonstrating superior machining accuracy and efficiency compared with conventional ECDM.

Yang et al. **[58]** investigated the influence of the surface roughness of the tool electrode in the ECDM process. A 200 μm-diameter tool electrode was fabricated by WEDM under varying process parameters to obtain different surface roughnesses. The study revealed that the wettability of the tool electrode varied with its surface roughness, and poor wettability led to thicker gas film formation due to increased surface tension of gas bubbles adhered to the tool electrode. Furthermore, three different tool electrode materials tungsten, stainless steel, and tungsten carbide were used, among which tungsten carbide exhibited the highest machining speed compared to the other two materials.

Yang et al. **[59]** investigated Electrochemical Discharge Machining (ECDM) using a spherical-end tool electrode to improve micro-hole drilling in hard and brittle materials. The spherical electrode, with a 150 μm tip and 100 μm cylindrical body, reduced the contact area with the workpiece, promoting better electrolyte flow, gas film formation, and uniform bubble growth. These improvements increased discharge frequency and machining efficiency. Compared with a conventional cylindrical electrode, the spherical tool reduced machining time by 83% and hole diameter by 65%. It also minimized cracking and exit damage, producing through-holes with improved roundness and dimensional accuracy. The study demonstrates that spherical tool geometry significantly enhances machining performance and feature quality in ECDM micro-hole drilling.

Jui et al. **[60]** investigated micro-Electrochemical Discharge Machining (micro-ECDM) for high-aspect-ratio micro-hole drilling in glass using in-house fabricated tungsten carbide microtools produced by Pulsed Electrochemical Micromachining (PECMM). Employing a low-concentration NaOH electrolyte (1 M) achieved an aspect ratio of 11 while reducing overcut, tool wear, and hole taper by 22%, 39%, and 18%, respectively. Tool rotation improved hole circularity without affecting the critical voltage or current. The lower electrolyte concentration also enhanced surface finish, producing roughness values between 250 and 350 nm. The study demonstrates that combining high-aspect-ratio microtools with low-concentration electrolytes effectively improves machining accuracy, surface quality, and tool life during deep micro-hole fabrication.

Jain et al. **[61]** investigated Electrochemical Spark Machining (ECSM) for micromachining quartz, optimizing the machining voltage and table feed rate to fabricate high-aspect-ratio microchannels. The study showed that higher voltage increased the material removal rate (MRR) and channel width but produced non-uniform channel depth, whereas lower voltage reduced depth fluctuations. Increasing table feed decreased channel width and the heat-affected zone but increased depth variation due to the absence of feedback control. Optimal machining conditions were identified within a voltage range of 30–60 V and a feed rate of 3–10 mm/min. The authors emphasized the importance of implementing servo or feedback-controlled tool feeding to maintain a constant working gap and achieve uniform microchannel depth in non-conductive materials.

Kamaraj et al. **[62]** investigated the influence of electrolyte concentration on overcut during Electrochemical Discharge Machining (ECDM) of high-aspect-ratio microholes in glass. An analytical thermal model was developed to predict overcut by considering electrolyte concentration and machining time. The study found that tool diameter had negligible influence on microscale overcut, whereas electrolyte concentration significantly affected dimensional accuracy. Using a 1 M electrolyte, microholes with an aspect ratio of 12 were successfully fabricated in 1.2 mm-thick borosilicate glass using tungsten carbide tools. The proposed model predicted overcut with less than 15% error, providing an effective approach for controlling dimensional accuracy in high-aspect-ratio ECDM applications.

Zhang et al. **[63]** developed Tube Electrode High-Speed Electrochemical Discharge Drilling (TSECDD), a hybrid process combining Electrochemical Machining (ECM) and Electrical Discharge Machining (EDM) using a low-conductivity salt solution for machining superalloys. Material removal occurred primarily through EDM in the frontal gap and ECM in the lateral gap, with ECM removing the recast layer produced by EDM. Experimental results demonstrated improved machining speed, material removal rate, surface finish, hole diameter, and taper compared with conventional EDM. The study confirmed that low-conductivity electrolytes enhance both machining efficiency and accuracy, establishing TSECDD as an effective technique for precision micro-hole fabrication in difficult-to-machine conductive materials.

Gupta et al. **[64]** investigated the effect of pulse duration on aspect ratio and machining quality during Electrochemical Discharge Machining (ECDM) of glass. Experimental results identified an optimal pulse condition of 1 ms pulse-on time and 3 ms pulse-off time, which produced quasi-continuous discharges and efficient thermal energy for material removal. Similar trends were observed for both NaOH and NaCl electrolytes, although NaOH exhibited stronger chemical etching and benefited from longer pulse durations. High-speed imaging showed that spark discharges ceased when the gas film collapsed, while tool wear remained negligible within the investigated pulse range. The study provides useful guidelines for selecting pulse parameters to achieve high-aspect-ratio microholes with improved machining quality.

Behroozfar et al. **[65]** investigated plasma channel characteristics and material removal in Electrochemical Discharge Machining (ECDM) of glass using controlled single-spark discharges. A pulsed voltage with an offset below the critical voltage enabled the generation of isolated sparks, allowing detailed analysis of individual discharge craters. The average plasma channel diameter was measured at approximately 260 μm, and a finite-element thermophysical model incorporating this value accurately predicted crater dimensions and material removal. Experiments also demonstrated that tapered-tip electrodes effectively localized spark generation. The proposed approach provides valuable insights into plasma behavior and offers an improved modeling framework for predicting material removal during ECDM.

Behroozfar et al. **[66]** investigated the wear characteristics of brass, steel, and tungsten carbide (WC) tool electrodes during Electrochemical Discharge Machining (ECDM). Tool wear initiated at approximately 46 V for brass, 48 V for steel, and 53 V for WC, reflecting differences in melting temperature. Brass exhibited the highest wear because of its lower melting point, whereas WC showed the greatest wear resistance. Surface analysis estimated a tool temperature of nearly 2800 °C at 50 V, indicating severe thermal loading that can cause plastic deformation and accelerated wear. The study recommended improving tool cooling by reducing machining time and using pulsed-voltage operation to enhance tool life and machining stability.

Zhu et al. **[67]** introduced a novel uniform annular-area, layer-by-layer feeding strategy for the fabrication of high-aspect-ratio, small-radius rotational components on a conventional Wire Electrical Discharge Machining (WEDM) machine with an auxiliary spindle. This strategy encompassed both roughing and finishing stages, with theoretical determinations of Material Removal Rate (MRR) and radial infeed rate in the roughing phase, and investigation into theoretical surface roughness (Rz) in the finishing phase. Subsequent optimization experiments were conducted to analyze the influence of parameters on MRR and surface roughness. Employing this feed strategy with optimized parameters, the researchers successfully machined a group of pin electrodes, achieving a minimum diameter of 40 µm with an impressive aspect ratio of 60. Furthermore, micro electrodes for an injection nozzle were produced using this innovative process, culminating in the fabrication of a qualified injection nozzle for powder metallurgy applications.

Goud et al. **[68]** aimed to determine the optimal combination of control parameters for machining micro-channels on quartz glass. Taguchi's standard orthogonal array (L9), combined with Grey Relational Analysis (GRA), was employed to identify optimal parametric conditions to reduce the Width Overcut (WOC) and increase the Material Removal Rate (MRR). Experimental results validated the effectiveness of this method in assessing the performance of the electrochemical discharge machining process. The Signal-to-Noise (S/N) ratio analysis served as an initial process monitoring parameter, yielding different optimal conditions for MRR and WOC. Specifically, the GRA converted multi-objective optimization into single-objective optimization problems, enabling the determination of optimal control parameters for both MRR and WOC. The study identified the feed rate as the most dominant factor influencing micro-channel machining of quartz glass, surpassing the influence of applied voltage and electrolyte concentration.

Rattan et al. **[69]** explored the application of magnetohydrodynamic (MHD) convection to enhance the performance of electrochemical spark machining (ECSM), particularly in the traveling wire (TW)-ECSM method. Restricted electrolyte circulation around the machining zone was observed to reduce the material removal rate (MRR). By introducing a magnetic field during electrolysis, Lorentz forces were induced, thereby driving MHD convection and improving electrolyte flow. Experimental findings demonstrated that MHD convection significantly increased MRR compared to machining without a magnetic field, with improvements ranging from 9.09% to 200% across various processing conditions. Moreover, applying a magnetic field reduced the discharge current during machining. The

Lorentz force induced by the magnetic field facilitated ion motion and improved electrolyte circulation between the wire tool and workpiece, leading to higher MRR.

Han et al. **[70]** introduced a novel approach to create high-aspect-ratio microgrooves in hard, brittle materials using electrochemical discharge machining (ECDM) with a microtextured machining tool. The tool side surface was treated using micro-electrical discharge machining to produce fine micro-protrusive patterns, enhancing the electric field and improving step-milling depth in the ECDM process. The field enhancement factor was evaluated through finite element method (FEM) analysis. Experimental results demonstrated the successful fabrication of microgrooves with a 1:4 aspect ratio, high geometric accuracy, and crack-free surfaces using one-step ECDM. Notably, the use of the textured surface tool significantly reduced the taper angle of the machined grooves to less than 3°, compared with ~13° with a conventional electrode. Additionally, the proposed tool enabled higher-quality microgroove fabrication with greater edge linearity and improved surface quality. Future research aims to enhance further machining performance for rapid prototyping of microfluidic devices across various hard and brittle materials.

Hajian et al. **[71]** conducted a study evaluating the bending force applied to the tool in electrochemical discharge machining (ECDM), considering factors such as tool diameter, electrolyte concentration, presence of a magnetic field, and tool feed rate. Experimental results indicated a decrease in bending force with increased electrolyte concentration and applied voltage. Additionally, the presence of a magnetic field notably reduced the bending force, particularly in lower electrolyte concentrations (15 wt%). Optimal feed rates were significantly influenced by applied voltage and electrolyte concentration, with higher values at elevated voltage and electrolyte concentration. Notably, the magnetic field's effects on raising the optimum feed rate were more pronounced at lower electrolyte concentrations (15 wt%) than at higher concentrations (25 wt%).

Goud et al. **[72]** presented a three-dimensional finite element model to simulate material removal in electrochemical discharge machining (ECDM) drilling and to elucidate the mechanism, correlating the findings with experimental data. The model outputs were compared with existing experimental results, demonstrating good agreement. Despite minor differences attributable to assumptions about parameters such as spark radius and energy partition, the model accurately captured the shape of material removal due to a single spark. Furthermore, comparisons between 3D and 2D FEM simulations revealed similar trends, albeit with slight variations attributable to differences in machining conditions, such as the type of voltage supply used. The study also noted a significant increase in material removal rate (MRR) with increasing electrolyte concentration, with a more pronounced effect observed in soda lime glass compared to alumina.

Mehrabi et al. **[73]** addressed a significant challenge in drilling operations using the electrochemical discharge phenomenon: limited electrolyte access in deep holes. The performance of electrochemical discharge processes in mesoscale drilling operations was enhanced by employing hollow electrodes and a high-pressure electrolyte injection system to deliver electrolyte to the machining area of deep holes. Experimental investigations were conducted at various pressure levels and electrode diameters. Results indicated that electrolyte injection through the hollow cathode significantly increased material removal rate (MRR) and drilling speed, with these effects further amplified by larger electrode diameters and injection pressures. Hole depth improvement relative to effective pressure ranged from 50% to 70% across different electrode diameters. Additionally, higher injection pressures resulted in larger hole diameters and conical-shaped holes. These findings demonstrate the efficacy of using hollow electrodes with high-pressure electrolyte injection systems to enhance electrochemical discharge drilling at the mesoscale.

Xu et al. **[74]** introduced a hybrid electrochemical discharge drilling method employing a metal tube as the cathode tool and the workpiece as the anode. A liquid with low conductivity flows at high speed between the metal tube and the workpiece, where electrical discharge primarily occurs at the frontal gap, with electrochemical processes at both the frontal and side gaps. The recast layer generated by electrical discharge at the side gap can be removed electrochemically. Observations of the machining phenomenon at the gap were made using a designed transparent clamping fixture, while voltage and current waveforms during machining were recorded. Analysis of machining products and the removal effects of the recast layer was conducted, along with analysis of the hole cross-section and the machining surface. Tool wear and machining efficiency were compared with those of other processes, demonstrating that a 4-mm-deep, 0.5-mm-diameter hole can be produced with low tool wear and almost no recast layer using this method.

Saranya et al. **[75]** conducted a detailed experimental investigation of a constant-velocity feed drilling technique within electrochemical discharge machining (ECDM) to create micro-holes in quartz substrates. Cylindrical micro-tools of various diameters and tool feed rates (TFRs) were examined along with a 30 wt% NaOH solution as the electrolyte, a machining voltage of 30 V, and an initial working gap of 5 μm. The findings revealed that the minimum micro-hole diameter and overcut were achieved at a TFR of 0.8 μm/s for all cylindrical tool diameters. Further analysis focused on the influence of tool shape, using a spherical tool electrode, which resulted in improved quality metrics compared to cylindrical tools. Specifically, micro-holes created with the spherical tool showed reductions of 12% in entrance diameter, 29% in entrance overcut, 28% in central diameter, and 67% in central overcut compared to those made with cylindrical tools under the same parameters.

Kang et al. **[76]** investigated electrochemical discharge machining (ECDM) for fabricating film cooling holes in components with thermal barrier coatings. It was found that ECDM can effectively machine both conductive and non-conductive materials by utilizing a gas film formed around the electrode. While electrochemical discharge was predominant during coating machining, both electrochemical and electrical discharges occurred during substrate machining. Analysis revealed that electrical discharge primarily removed material from the substrate, while electrochemical discharge contributed to secondary material removal on the machined surface. Surface roughness measurements showed R_a = 10.2 μm for the coating and R_a = 5.6 μm for the substrate, with a 15 μm recast layer observed on the machined surface of the substrate.

Hajian et al. **[77]** proposed a thermal model based on the finite element method (FEM) to predict machining depth in ECD milling. The FEM model's input parameters were determined based on various machining conditions, including machining voltages and electrolyte concentrations. Experimental validation was conducted under identical ECD milling conditions. Within the FEM model, different criteria for material removal temperature (Teq) were employed to calculate machining depths. Comparative analysis revealed a strong agreement between FEM predictions and experimental results when Teq fell within the range of 600 to 850 °C. Notably, the softening Littleton point at 720 °C emerged as a promising criterion for material removal temperature in ECD milling processes.

Dhanvijay et al. **[78]** conducted an experimental investigation of the Electrochemical Discharge Machining (ECDM) process on fiberglass-reinforced plastic (FRP) using a mixed electrolyte of NaOH and KOH in equal proportions. The study aimed to optimize key process parameters voltage, duty factor, electrolyte concentration, and tool rotation speed to enhance the material removal rate (MRR). Both static and dynamic (with electrolyte flow) machining conditions were examined, and optimization was carried out using Taguchi and Grey Relational Analysis techniques. Results indicated that the continuous flow of electrolyte marginally improved MRR due to the consistent supply of fresh electrolyte, which facilitated stable gas film formation and discharge activity. Taguchi analysis revealed voltage as the most influential parameter, where higher voltage increased current, promoting rapid hydrogen bubble generation and higher discharge rates. ANOVA confirmed that voltage, duty factor, and electrolyte concentration significantly affected MRR during machining with electrolyte flow. Optimal machining conditions with electrolyte flow were identified as 90 V voltage, 75% duty factor, 30% electrolyte concentration, and 360 rpm tool rotation. For operations without flow, the same voltage and duty factor were optimal, but tool rotation was reduced to 310 rpm. This study emphasizes the positive impact of electrolyte flow on MRR and provides a data-driven basis for optimizing ECDM parameters in FRP machining.

Antil et al. **[79]** employed Response Surface Methodology (RSM) using a Box-Behnken design to optimize the machining parameters of the Electrochemical Discharge Machining (ECDM) process for hybrid polymer matrix composites (PMCs). The study focused on three key input parameters: electrolyte concentration, applied voltage, and inter-electrode gap, and their influence on output characteristics, specifically material removal rate (MRR) and overcut. Voltage emerged as the most significant factor affecting MRR, with the optimal range identified between 60–70 V, while the inter-electrode gap was the primary factor influencing overcut. Surface plots were generated to understand the individual and interaction effects of parameters on output responses. A novel approach using the adjusted delamination factor (Fda) was introduced to assess surface integrity, providing a reliable metric for quantifying irregular damage patterns in composite drilling. The study also included scanning electron microscopy (SEM) analysis to evaluate hole morphology. ANOVA results confirmed the statistical validity of the developed quadratic models for both MRR and overcut, reinforcing the significance of voltage and inter-electrode gap. The proposed models offer an effective predictive tool for optimizing machining conditions. Overall, this work highlights the potential of ECDM for precision machining of non-conductive hybrid PMCs and provides practical guidelines to improve performance and surface quality.

Singh et al. **[80]** conducted a study to drill micro-holes in silicon wafers, focusing on applied voltage and tool feed rate as input parameters, with overcut and hole taper as output quality characteristics. Results revealed that increasing voltage amplified overcut and hole taper, whereas elevated tool feed rates mitigated them. Scanning electron microscopy characterization showcased small debris, overcut, and a heat-affected zone on the machined surface. Optimal conditions, identified at an applied voltage of 60 V and a tool feed rate of 250 μm/min, resulted in minimized overcut and hole taper. Additionally, the study noted axial, lateral, and flank erosion on the micro tool used for silicon wafer machining, providing comprehensive insights into parameter optimization and the associated tool-erosion characteristics in micro-hole drilling.

Arya et al. **[81]** addressed a critical limitation of conventional Electrochemical Discharge Machining (ECDM), the restricted drilling depth due to inadequate replenishment of vaporized electrolyte in deep micro-holes, by developing a Pressurized Flow-ECDM (PF-ECDM) system. In this method, fresh electrolyte is precisely injected into the machining zone through a tubular electrode using controlled electrolyte flow rates (EFR). An analytical model was developed to predict electrolyte vaporization rates at various thermal energy levels, enabling estimation of the required EFR to maintain stable discharge conditions. Experimental validation confirmed that optimized EFR significantly enhances machining performance. The study revealed that adequate EFR ensures effective electrolyte replenishment, stabilizes spark activity, and enables deeper, cleaner hole formation. The PF-ECDM process achieved a maximum hole depth of 2478 μm in borosilicate glass, an improvement of 61.22% over conventional ECDM. Furthermore, multi-criteria optimization using the desirability function approach was employed to determine the optimal process parameters (voltage, pulse-on time, concentration, and EFR) to achieve the best outcomes. Results demonstrated that machining depth increased and entrance diameter reduced significantly when EFR was matched to the thermal energy input. The proposed PF-ECDM system offers precise control without major tool modification and expands ECDM's applicability in microfabrication fields such as microfluidics, MEMS, and lab-on-a-chip devices.

Madhavi et al. **[82]** conducted a study on micro-hole machining in 500 μm-thick borosilicate glass using a 370 μm-diameter Stainless Steel (SS) tool via Micro-Electro Chemical Discharge Machining (μ-ECDM). Analyzing Voltage (V), Duty Factor (% DF), and Sodium Hydroxide (NaOH) Electrolyte Concentration (wt% C) as machining parameters, and Material Removal Rate (MRR), Tool Wear Rate (TWR), and Radial Over Cut (ROC) as output responses, experiments were conducted using a Taguchi L16 Orthogonal Array (OA). Signal-to-Noise (S/N) ratio technique optimized individual responses, resulting in parameters of 65 V, 35 wt% C, 65% DF for maximum MRR (890 μg/min), and 50 V, 20 wt% C, 50% DF for minimum TWR (25 μg/m) and ROC (10.16 μm). Subsequently, the Grey Relational Analysis (GRA) technique refined the parameters to 50 V, 20 wt% C, and 60% DF, resulting in MRR of 365 μg/m, TWR of 25 μg/m, and ROC of 33.8 μm.

Sundaram et al. **[83]** investigated the influence of pulse current parameters and tool immersion depth on gas film formation and machining quality in Pulse Electrochemical Discharge Machining (PECDM) of glass-fiber epoxy-reinforced composites. By carefully controlling pulse frequency and duty cycle to ensure no more than one spark per cycle, the study aimed to optimize discharge characteristics and minimize thermal damage. Compared with conventional ECDM using DC, PECDM significantly reduced the hole diameter and the heat-affected zone (HAZ), thereby enhancing overall machining precision. The study found that lowering the duty cycle in PECDM increases gas film formation time while decreasing its thickness, thereby reducing sparking energy and frequency. This results in more controlled material removal, producing smaller hole diameters and minimizing thermal damage. Additionally, shallower tool immersion depth contributed to thinner gas films and smaller HAZ. However, an optimal balance between duty cycle and electrolyte level was necessary. In contrast, higher electrolyte levels helped reduce hole diameter at low duty cycles; the extent of HAZ was also increased. Overall, the findings highlight the effectiveness of PECDM in achieving higher machining accuracy and reduced thermal impact by fine-tuning pulse parameters and electrolyte conditions, particularly for delicate composite materials.

Chen et al. **[84]** introduced an innovative composite machining aid featuring a self-developed auxiliary nozzle. The design ensures the rotating tool electrode remains submerged in electrolyte at a low level during Electrochemical Discharge Machining (ECDM). The study focused on investigating the surface quality of the entrance and exit, as well as the roundness of the hole. Using 0.1 mm-thick quartz glass drilled in a 5 M KOH electrolyte at 50 V, the results showed a 48.23% reduction in the heat-affected zone area compared to an unassisted process. Additionally, the HAZ area at the exit decreased by 53.21%, leading to improved surface quality and roundness at the start and end of the hole.

Singh et al. **[85]** developed a finite element analysis (FEA) model to simulate heat generation in the spark region of the Electrochemical Discharge Machining (ECDM) process, aiming to predict the Material Removal Rate (MRR) in quartz and soda lime glass. The model accounts for both melting and evaporation mechanisms driven by the intense thermal energy from spark discharges, as well as convective heat transfer. A 3D spark model was adopted to improve accuracy over traditional 2D simulations. Simulation results closely matched experimental data, with a maximum deviation of 1.95 mg/min, attributed to simplifying assumptions in the model. The study also confirmed that MRR increases with higher electrolyte concentration, due to enhanced discharge activity and thermal input. Notably, the 3D model demonstrated superior predictive accuracy compared to previous 2D models, indicating its effectiveness in capturing complex thermal behavior in the ECDM process. While the model effectively estimates thermally driven material removal, the authors suggest that future work should incorporate chemical interactions near the electrodes through mathematical modeling. This would enable a more comprehensive simulation of the ECDM process, thereby further improving predictive accuracy and expanding the model's applicability to industrial research and development.

Antil **[86]** investigated the Electrochemical Discharge Machining (ECDM) process for machining silicon carbide (SiC)- reinforced epoxy composite materials, known for their high strength but poor machinability due to increased tool wear in conventional drilling. To overcome this limitation, the study employed a non-contact machining approach using ECDM and developed a hybrid prediction-optimization model integrating Response Surface Methodology (RSM) and Artificial Neural Networks (ANN). Key process parameters, voltage, electrolyte concentration, inter-electrode gap, and duty factor, were varied to study their influence on material removal rate (MRR) and taper angle. RSM-based experimentation followed a Central Composite Design, and the results were used to train a feed-forward backpropagation neural network in MATLAB. ANOVA analysis confirmed that voltage and electrolyte concentration significantly enhance MRR, while minimizing the inter-electrode gap reduces taper. Using the desirability function, the optimal parameters identified were voltage 65 V, electrolyte concentration 90 g/L, inter-electrode gap 70 µm, and duty factor 0.535. The ANN model with 10 hidden layers achieved excellent accuracy, with deviations of only 0.40% and 0.32% in MRR and taper predictions, respectively, compared to RSM results. This study confirms the viability of ECDM for machining SiC composites and demonstrates the effectiveness of AI-based models in optimizing and validating non-traditional machining processes.

Mishra et al. **[87]** presented a combined numerical and experimental investigation of microchannel fabrication in glass using Electrochemical Discharge Machining (ECDM)-based micro milling. A stainless steel needle tool was used with alkaline electrolytes

(NaOH and KOH), and the effects of machining voltage, pulse frequency, and tool feed rate on material removal rate (MRR) and surface roughness (SR) were analyzed. The study revealed that both MRR and SR increased with higher voltage and feed rate, while increasing pulse frequency reduced both outcomes. A 3D finite element model (FEM) was developed to simulate thermal effects and showed good correlation with experimental MRR. However, deviations were observed in cross-sectional profiles due to simplifications such as the the Gaussian heat flux assumption. Optical inspection indicated that KOH outperformed NaOH by producing cleaner microchannels with fewer thermal cracks and lower overcut. Multi-objective optimization was performed using utility theory coupled with Taguchi's method, revealing optimal machining conditions of 60 V, 50 kHz pulse frequency, and feed rates of 50 µm/s (KOH) and 100 µm/s (NaOH). The study also demonstrated the versatility of ECDM in fabricating complex microstructures, such as sinusoidal channels and engraved patterns, suggesting its broader applicability to other brittle materials, such as quartz and ceramics.

Charak et al. **[88]** employed Electrochemical Discharge Machining (ECDM) to fabricate microchannels in borosilicate glass and used Response Surface Methodology (RSM) to model and optimize the process. The study analyzed the influence of key parameters applied voltage, electrolyte concentration, tool feed, and tool rotation on responses such as material removal (MR), cathode tool wear (TW), and anode wear (AW). Among these, applied voltage was identified as the most influential factor, significantly affecting both MR (maximum of 2.5 mg) and TW (minimum of 0.5 mg), whereas tool rotation had the least impact. The RSM-based mathematical models demonstrated good agreement with experimental results, confirming their reliability for predicting multi-response outcomes. Scanning Electron Microscopy (SEM) was employed to examine the machined surfaces, revealing thermal damage patterns and surface asperities. Additionally, the introduction of CTAB surfactant in the electrolyte was found to reduce oxidation and thermal degradation, thereby improving surface quality. Overall, Singh et al. demonstrated that ECDM, when combined with RSM and a proper electrolyte formulation, is an effective approach for precision micromachining of brittle substrates such as borosilicate glass.

Kumar et al. **[89]** investigated the electrochemical discharge machining (ECDM) of hard, non-conductive zirconia (ZrO_2) using an in-house-developed setup. The study focused on optimizing key process parameters DC supply voltage, electrolyte concentration, and inter-electrode gap using a Taguchi L_{16} (4^5) orthogonal array design. Experimental findings revealed that electrolyte concentration and voltage were the most influential factors, contributing 51.52% and 47.56%, respectively, to the material removal rate (MRR), and 49.16% and 50.34%, respectively, to overcut. Optimal conditions for maximizing MRR and minimizing overcut were identified as V4E4G3 and V1E1G2, respectively. Field emission scanning electron microscopy (FESEM) revealed machining-induced microcracks and surface irregularities at higher parameter levels. At the same time, energy-dispersive spectroscopy (EDS) confirmed tool-material diffusion, specifically iron from the steel cathode to the work surface, though zirconia's composition remained largely unaffected. Mathematical models were also developed to predict MRR and overcut, showing less than 7% error in validation, indicating strong predictive capability. While the study confirmed the feasibility of machining zirconia via ECDM, it also highlighted the need for further optimization to minimize surface defects and improve the quality of the machined features.

Arab et al. **[90]** conducted experiments to investigate the impact of the tool electrode feed rate (TEFR) on velocity-feed electrochemical discharge drilling (ECDD). The study, utilizing cylindrical tungsten carbide tool electrodes of different sizes, explored TEFR values ranging from 1 to 9 µm s−1. The research highlighted the delicate balance needed for TEFR, where higher values risked tool collisions, potentially causing cracks, while lower values reduced the material etch rate. Stable and uniform EC discharges were observed for TEFR values below 5 µm s−1. Optimal results, including minimal hole size and heat-affected zone, were achieved within the TEFR range of 3–4 µm s−1. The study recommended a TEFR within this range to enhance ECDD performance.

Alvarado et al. **[91]** introduced a pulse classification technique for real-time monitoring and control of the Electrochemical Discharge Machining (ECDM) process using a Fuzzy Inference System (FIS). ECDM performance is significantly influenced by discharge behavior, which is difficult to monitor and control due to the process's dynamic nature. The proposed system utilizes raw voltage and current signals from the machining gap to classify discharge pulses into four types, each representing different discharge characteristics. The FIS was initially designed using simulated gap signals and later validated with raw experimental data. Although initial testing required adjustments to membership functions—due to discrepancies between simulated and actual responses, such as discharge delay effects—the final system achieved accurate classification without requiring signal preprocessing. Notably, the classifier performed robustly even in the presence of electrical noise, making it practical for real-time applications. This technique eliminates the need for complex filtering or large-scale computation, enabling efficient classification regardless of data size or sampling rate. The pulse classifier presents a foundational step toward intelligent monitoring and control of ECDM, potentially enhancing machining precision, repeatability, and process automation by linking discharge behavior to quality outcomes.

Singh et al. **[92]** investigated the impact of discharge regimes on material removal mechanisms in electrochemical discharge machining (ECDM), particularly addressing challenges in deep hole drilling. Focusing on the limitations of the hydrodynamic regime, such as bubble accumulation and insufficient electrolyte supply, the study explored implementing ECDM with a titrated electrolyte flow to achieve consistent machining conditions. The results demonstrated that this approach efficiently drilled micro-through-holes in a 1350-μm-thick workpiece within approximately 30 seconds. Comparative analysis with conventional ECDM revealed a sevenfold reduction in machining time and a 1.25 times improvement in accuracy by reducing the hole entrance diameter. The study emphasized the prolonged discharge regime and provided valuable insights into the underlying mechanism of material removal, positioning the titrated flow of electrolyte as an effective strategy for micro-hole drilling at a notable speed in the ECDM process.

Rajput et al. **[93]** developed a transient thermal model using Finite Element Modeling (FEM) to simulate the temperature distribution resulting from a single spark in the Electrochemical Discharge Machining (ECDM) process, specifically targeting soda-lime glass. The model aims to predict the material removal rate (MRR) by evaluating the post-processed temperature fields within the work material. Validation was performed through both comparison with previously reported FEM and experimental data and direct experimentation, confirming the model's reliability. The FEM analysis revealed that MRR increases with rising electrolyte concentration and applied voltage. Specifically, a 5% increase in MRR was observed at 60 wt.% electrolyte concentration, while a 6% decrease in MRR occurred at 60 V, compared to results obtained using a 3D Gaussian spark distribution model. Experimental data showed a 14% increase in MRR at high electrolyte concentrations, consistent with FEM predictions. Minor deviations were attributed to differences in assumptions, such as spark radius and the fraction of spark energy transferred to the workpiece (Ep). Overall, the study affirms the potential of FEM-based thermal modeling to predict material removal in ECDM accurately. The authors suggest that future improvements could include modeling the chemical etching effects to provide a more comprehensive simulation of the ECDM process.

Kang et al. **[94]** presented a finite element modeling (FEM) approach to predict material removal behavior in electrochemical discharge machining (ECDM), specifically in the discharge regime. The study focused on simulating both single-pulse discharges on a tapered electrode and continuous discharges on a cylindrical electrode to understand energy distribution and material removal mechanisms. The single-pulse discharge was modeled using a uniform heat source, and simulations revealed that approximately 30.5% of the discharge energy is effectively transferred to the workpiece. The simulated crater shapes closely matched experimental observations, validating the model’s accuracy. For continuous discharges, material removal was shown to initiate at the outer edge of the cylindrical tool and progress inward during machining. The effective discharge energy contributing to material removal was 10.1% over an applied voltage range of 37–43 V. The FEM predictions of drilling depths at varying voltages were in strong agreement with experimental results, affirming the model’s reliability. This dual-model approach offers valuable insights into crater formation and energy utilization, providing a strong basis for optimizing ECDM process parameters to achieve greater accuracy, efficiency, and control in micromachining applications.

Mishra et al. **[95]** conducted a comparative study on the tool wear behavior of four different electrode materials—brass, SS304, molybdenum, and tungsten—during the fabrication of long (>15 mm) and deep (>200 µm) microchannel arrays using the multi-pass Electrochemical Discharge Machining (ECDM) process. The objective was to evaluate the material's suitability for prolonged machining, with all process parameters held constant across trials. The findings revealed that brass exhibited the highest tool wear rate, rendering it unsuitable for extended ECDM operations beyond 15 minutes. Molybdenum and tungsten demonstrated moderate wear characteristics but experienced tip necking and breakage near the electrolyte-air interface, limiting their usability to approximately 35 minutes. In contrast, SS304 showed minimal wear, consistent tip geometry, and stable microchannel depths even after 65 minutes of machining. These results suggest that SS304 is the most robust and durable material for multi-pass ECDM, offering superior dimensional stability and tool longevity. Additionally, the study demonstrated successful fabrication of a dual serpentine flow field in glass using SS304 line-array electrodes, highlighting its potential for advanced microfluidic device manufacturing. The findings underscore the critical role of tool material selection in achieving precision and durability in prolonged ECDM-based microfabrication processes.

Singh et al. **[96]** explored an enhanced Electrochemical Discharge Machining (ECDM) approach for drilling micro-holes in Yttria-stabilized zirconia (YSZ), a hard and brittle ceramic. The study implemented an integrated method combining electrolyte flow with a pressurized feeding system to improve machining efficiency, accuracy, and tool life. The experimental findings revealed that material removal in YSZ primarily occurs through thermal spalling rather than the typical melting, evaporation, or chemical etching seen in other glass-based ceramics. The introduction of electrolyte flow significantly improved the machining performance by increasing the electrochemical discharge (ECD) frequency and enabling more stable, crack-free hole formation. Notably, a 42% increase in hole depth and a 33% reduction in hole diameter were achieved with the same machining duration as standard ECDM setups. Additionally, the electrolyte flow helped maintain consistent discharge characteristics and reduced tool wear, allowing sustained precision over longer machining periods. The process achieved a maximum penetration speed of 126 μm/min, successfully producing deep, clean micro-holes up to 630 μm in depth. This integrated technique represents a promising advancement in micromachining ceramics such as YSZ, where conventional methods face challenges due to their low machinability and thermal sensitivity.

Wang et al. **[97]** proposed a novel approach to electrochemical discharge machining (ECDM) that integrates a non-metallic paraffin backing layer with electrochemical reaming to enhance the precision of micro-hole machining. The backing layer ensures continuous electrolyte supply via reverse flushing once the electrode penetrates the workpiece, effectively mitigating electrolyte depletion. Simulation of flow dynamics within the paraffin layer confirmed sufficient fluid distribution, comparable to pre-penetration forward flushing. Experimentally, this method significantly reduced hole taper, improved orifice roundness, and produced smoother internal walls. Electrochemical reaming further refined the machined features, with optimal parameters identified as 1.5 g/L electrolyte concentration, 60 V machining voltage, and 12 s reaming duration. This hybrid strategy led to improved surface quality and dimensional accuracy of the holes, demonstrating its potential for high-precision microfabrication. The effectiveness of this method is evident in the reduced exit defects and enhanced uniformity of hole geometry. Wang et al.'s work highlights the importance of managing electrolyte flow dynamics and integrating post-processing strategies to address limitations of conventional ECDM, especially during deep-hole machining. This development opens new opportunities in micro-manufacturing of hard, brittle materials such as glass and ceramics, where precise geometry and minimal taper are critical.

Zhao et al. **[98]** conducted comprehensive ECDM experiments focusing on the fabrication of micro-holes, microgrooves, and complex three-dimensional (3D) microstructures in glass. The study emphasized how key parameters, namely power supply voltage, pulse frequency, electrode feed rate, and rotation speed, influence machining performance. It was found that increasing voltage enhanced spark energy, leading to improved machining efficiency and deeper micro-holes; however, it also resulted in larger entrance diameters and degraded edge quality. In contrast, lowering the pulse frequency improved discharge duration and machining depth, though at the cost of entrance quality. For microgroove machining, surface roughness was positively correlated with voltage and negatively correlated with both pulse frequency and electrode feed speed. Interestingly, electrode rotation speed had minimal impact on surface finish. The best surface finish achieved was R_a = 0.605 µm. Based on the findings, a voltage of 21 V, a frequency of 600 Hz, a rotation speed of 1000 rpm, and a feed rate of 7 µm/s were recommended for optimal performance. Additionally, their layer-by-layer machining strategy demonstrated ECDM's capability to fabricate intricate 3D microstructures on glass surfaces. This work showcases the potential of ECDM in precision micromachining applications, especially when proper parameter tuning and stepwise machining are applied to balance efficiency and accuracy.

Xu et al. **[99]** conducted a comprehensive study on the electrochemical discharge machining (ECDM) of micro-holes, microgrooves, and complex 3D microstructures in glass. The research explored the effects of key process parameters, including pulse voltage, frequency, electrode feed rate, and rotation speed, on machining efficiency and quality. It was observed that increasing the pulse voltage improved machining efficiency and hole depth, but also enlarged the entrance diameter and deteriorated entrance morphology. Conversely, higher pulse frequencies reduced machining efficiency but improved surface quality. For microgroove fabrication, surface roughness showed a direct relationship with voltage and an inverse relationship with frequency and feed rate. Electrode rotation speed had minimal influence on roughness. The optimal parameters identified were 21 V, 600 Hz, 1000 rpm, and 7 µm/s. Using these parameters and a layer-by-layer machining approach, the team successfully fabricated intricate 3D microstructures with high precision.

The study highlighted the importance of balanced parameter selection to achieve high efficiency and quality, demonstrating ECDM's capability for producing complex microstructures in brittle, non-conductive materials such as glass, with potential applications in MEMS and microfluidics.

Arab et al. **[100]** investigated the impact of the initial T-W (tool-workpiece) gap, varying machining time, and electrolyte concentrations on blind microhole formation in glass and tool wear in velocity-feed Electro-Chemical Discharge Drilling (ECDD). Microholes with superior quality and reduced overcut were successfully produced using lower concentrations of KOH electrolyte. A novel numerical model that introduced inverse heat flux reduction for different initial T-W gaps was compared to experimental results, which revealed an initial increase and subsequent decrease in microhole opening size with increasing T-W gap, with critical values identified as 20 µm for NaOH and 10 µm for KOH. Microhole depth was highest under zero-gap conditions, albeit with severe tool wear. The study recommended maintaining a specific initial T-W gap, suggesting values between 10-30 µm for NaOH and 5-20 µm for KOH. The experimental findings highlighted the inadequacy of the conventionally used gravity-feed mechanism from a tool-wear perspective.

Torabi et al. **[101]** investigated the impact of tool characteristics and electrolyte properties on microchannel fabrication through electrochemical discharge machining (ECDM), demonstrating the process's capability to achieve lithography-comparable precision. The study systematically analyzed how variations in tool geometry and electrolyte conditions influence material removal and surface quality. One key observation was that increasing the tool-workpiece distance from 20 µm to 150 µm led to a substantial 356% increase in surface roughness, attributed to weakened discharge localization and dispersed thermal effects. It was also found that the use of grooved tools intensified stray discharges, thereby enhancing material removal but compromising surface integrity. Furthermore, increasing the electrolyte temperature from 25°C to 65°C resulted in higher surface roughness due to intensified bubble activity and instability of the gas film, both of which are critical for spark discharge consistency. Tool miniaturization also proved significant; a 20% reduction in tool diameter led to a 33% reduction in surface roughness and a slight 3% reduction in microchannel width, indicating enhanced precision and reduced overcut. These findings emphasize the importance of optimizing both tool geometry and electrolyte properties to enhance the control, efficiency, and accuracy of microchannel fabrication in ECDM, positioning it as a promising technique for microfabrication of glass and other non-conductive materials.

Rajput et al. **[102]** developed a comprehensive three-dimensional thermal model using finite element modeling (FEM) to estimate the temperature distribution during electrochemical discharge drilling (ECDD) of silica glass, with a particular focus on predicting the material removal rate (MRR). The model incorporated transient thermal conditions and discharge energy distribution to simulate the thermal response of silica glass under various machining conditions. The simulation results were validated against experimental data and existing literature, demonstrating good agreement in the predicted MRR values. To address the common issue of rapid tool wear in ECDD, the study further introduced an adaptive tool-feed-based closed-loop machining strategy that dynamically adjusted the feed rate based on real-time tool-workpiece interaction. Additionally, the researchers applied response surface methodology (RSM) to establish empirical relationships between key input parameters, namely, tool feed rate, applied voltage, and electrolyte concentration, and critical output responses such as MRR, tool wear rate, and the number of tool-workpiece contacts. Finally, a multi-response optimization using a desirability-function approach was implemented to simultaneously maximize MRR while minimizing both tool wear rate and tool-workpiece contact. The study provides a robust framework for enhancing both the efficiency and tool longevity in precision ECDM of silica glass.

Mallick et al. **[103]** conducted systematic experiments on microchannel fabrication in silica glass using micro-electrochemical discharge machining (μ-ECDM), focusing on the influence of various process parameters on machining depth (MD) and surface roughness (R_a). The study explored a wide range of input conditions, including electrolyte composition (NaOH and KOH in different ratios), electrolyte concentration, applied voltage, pulse frequency, and duty ratio. Both direct and reverse polarities were tested to evaluate their effect on machining outcomes. Automated tool systems were employed to ensure precision and consistency during experimentation. The results indicated that a NaOH:KOH ratio of 3:1 under direct polarity yielded the best performance in machining depth, achieving a maximum MD of 1850 μm and improved surface quality. Conversely, when the polarity was reversed, a NaOH:KOH ratio of 1:3 resulted in a significantly lower Tool Electrode Wear Ratio (TEWR), indicating its suitability for prolonging tool life. The comparative analysis highlighted the trade-offs between achieving greater depth and minimizing tool wear, providing valuable insights for optimizing μ-ECDM parameters for enhanced microchannel fabrication on silica glass.

Harugade et al. **[104]** investigated the application of electrochemical discharge machining (ECDM) as a novel and precise method for removing delaminated fibers in fiber-reinforced polymer (FRP) composite materials. The study aimed to address the common issue of fiber protrusion around drilled holes, which often compromises structural integrity and dimensional accuracy in FRP components. Two machining strategies, top machining and inside machining, were employed to eliminate these delaminated fibers. Top machining targeted the surface fiber protrusions, while inside machining focused on removing fibers extending into the hole interior. The performance of ECDM in both approaches was evaluated based on the completeness of fiber removal and the extent of thermal damage induced in the material. Key metrics included the heat-affected zone (HAZ) and hole overcut (OC), both critical to maintaining dimensional precision and avoiding structural degradation. The results demonstrated that ECDM could effectively eliminate delaminated fibers with minimal thermal impact. Both methods showed significant potential for precision post-processing in composite drilling, offering a cleaner finish and preserving the mechanical integrity of the FRP. This study highlights ECDM as a promising non-traditional technique for enhancing the quality of holes in advanced composite materials.

Oza et al. **[105]** explored the fabrication of microslits on quartz substrates using a magnetohydrodynamic (MHD)-assisted traveling wire electrochemical discharge micromachining (TW-ECDM) process. In this innovative setup, the application of a magnetic field induced MHD convection within the electrolyte, which significantly enhanced the removal of gas bubbles from the machining zone. This improved bubble evacuation contributed to a more stable discharge environment, thereby enhancing machining performance. The study reported substantial process improvements, including an 85.28% increase in material removal rate (MRR), a 48.86% increase in cut length, and a 30.39% reduction in surface roughness compared to conventional ECDM techniques. To systematically evaluate the influence of various process parameters, the researchers adopted a crossover methodology incorporating the Taguchi design of experiments and analysis of variance (ANOVA). This allowed them to optimize the process conditions and confirm the statistical significance of the observed effects. The combination of TW-ECDM with MHD assistance introduced a novel hybrid micromachining strategy that demonstrated clear advantages in precision, efficiency, and surface quality over traditional

ECDM methods. The findings highlight the potential of MHD-assisted ECDM processes for high-accuracy micromachining of hard, brittle materials like quartz.

Rajput et al. **[106]** investigated the Electrochemical Discharge Machining (ECDM) process for micro-hole drilling in silica (quartz), focusing on optimizing multiple machining responses. To systematically analyze the influence of key process parameters, namely applied voltage, electrolyte concentration, and inter-electrode gap, the study employed Taguchi's L9 orthogonal array in conjunction with Grey Relational Analysis (GRA). This hybrid approach allowed for multi-objective optimization while minimizing experimental runs. The results highlighted electrolyte concentration as the most significant factor influencing overall machining performance, followed by applied voltage and inter-electrode gap. Among the tested parameter combinations, the optimal settings of 35 V applied voltage, 15 wt.% electrolyte concentration, and a 25 mm inter-electrode gap yielded the best performance in terms of machining depth, overcut, and material removal rate. The study validated these findings by successfully fabricating micro-holes in quartz, confirming ECDM's suitability for precision micromachining of hard, brittle materials. The integrated use of Taguchi and GRA methods further demonstrated an effective framework for parameter optimization in ECDM processes, supporting its application in advanced micromachining tasks.

Kumar et al. **[107]** analyzed the effects of machining parameters on various responses, using various graphs for evaluation. The study used a Taguchi method-based L16 (45) orthogonal array to optimize machining parameters. The experimental results indicated that the primary factors governing machining performance were the DC supply voltage and electrolyte concentration. Optimal material removal rate was observed at 65 V, 16 g/l electrolyte concentration, and a 60-mm inter-electrode gap. Examination of Field Emission Scanning Electron Microscopy (FESEM) images revealed microcracks on the machined hole surface under elevated parameter settings. Furthermore, Energy-Dispersive X-ray Spectroscopy (EDS) analysis detected iron (Fe), likely originating from the diffuse region of the steel cathode adhering to the machined surface.

Kannojia et al. **[108]** explored the fabrication of three-dimensional (3D) spiral inductors on fused silica substrates for high-frequency radio-frequency (RF) applications using a cost-effective Electrochemical Discharge Machining (ECDM) technique. The study focused on designing and fabricating inductors with tunable geometrical parameters to optimize their electrical performance. Through-holes were precisely etched in the fused silica substrate using ECDM and subsequently filled with copper to form vertical interconnections. Redistribution lines were then fabricated to complete the 3D inductor structure. The mechanical integrity of the fused silica substrates post-machining was evaluated using nanoindentation, confirming sufficient mechanical strength. Electrical characterization revealed favorable current-voltage (I-V) behavior, and the fabricated inductors achieved a maximum quality factor (Q) of 11.6 at 440 MHz, which closely aligned with the results predicted by electromagnetic simulations. The use of fused silica, known for its low dielectric loss, minimizes substrate losses, making these inductors highly suitable for integration into high-frequency RF circuits. This work demonstrates the feasibility of combining ECDM micromachining with conventional metallization techniques for realizing compact, low-loss passive components on glass substrates, offering a promising route for next-generation RF microsystems.

Ranganayakulu et al. **[109]** conducted experiments using an in-house Electrochemical Discharge Machining (ECDM) setup integrated with a MOSFET-assisted power module. Using an L9 orthogonal array, the study optimized three process variables (electrolyte concentration, applied voltage, and duty factor) at three levels each. A novel simultaneous multi-response optimization technique that combines the Graph Theory Algorithm (GTA) and the Desirability Function Approach (DFA) was introduced. Duty factor significantly influenced machining performance, with HE outperforming CE in MRR, overcut (OC), and taper angle (TA). SEM images confirmed surface differences. Confirmation tests validated the optimal values obtained by the proposed technique.

Rajput et al. **[110]** explored Closed-loop ECDM (CLECDM) using adaptive tool feed for material-contact retraction. This approach enhances micro-hole characteristics, yielding a significant 15.9% increase in material removal rate (MRR) and a 14.8% reduction in tool wear rate (TWR). The study investigates the impact of the number of tool contacts (NTC) on both MRR and TWR. Employing response surface methodology (RSM), the authors developed mathematical models, selecting applied voltage, electrolyte concentration, tool feed rate, and inter-electrode gap (IEG) as input parameters. Multi-response optimization, utilizing the desirability function, yielded optimal parameters: 50 V applied voltage, 25 wt.% concentration, 4 mm/min tool feed rate, and 42.35 mm IEG, achieving a desirability value of 0.7574. This approach by Rajput et al. effectively balances material removal enhancement, tool wear minimization, and tool contact optimization in CLECDM.

Zhao et al. **[111]** introduced a novel hybrid technique, laser-assisted Electrochemical Discharge Machining (ECDM), to enhance micro-grooving of glass substrates by combining the complementary advantages of lasers and ECDM. The study systematically compared the morphological characteristics of grooves produced by standalone ECDM, laser machining, and the proposed hybrid approach. Results showed that grooves created solely by ECDM often exhibited undesirable cylindrical protrusions due to localized thermal effects and uneven discharge energy distribution. However, when ECDM was followed by laser machining, these protrusions were effectively eliminated, yielding a smoother surface profile. Furthermore, the reverse approach, performing laser machining first to define the groove path and then applying ECDM, significantly improved edge quality and reduced tapering in the groove cross-section. The synergistic integration of laser precision and ECDM's superior surface finishing enabled better control over groove geometry, depth, and surface roughness. This hybrid strategy proved particularly advantageous for applications requiring high-precision features on brittle, non-conductive materials like glass. The study demonstrates that combining thermal and electrochemical mechanisms can overcome limitations of individual techniques, offering a powerful alternative for fabricating microfluidic channels and optical components in advanced microsystems.

Zhao et al. **[112]** delve into micro-hole and microgroove machining, focusing on the influence of power voltage and frequency on key parameters. Four factors affecting Electrochemical Discharge Machining (ECDM) were considered: the pulse power supply voltage and frequency, the tool electrode feed rate, and the rotation speed. Results indicated that micro-hole efficiency, entrance diameter, and limit depth increased with voltage but decreased with power frequency. Microgroove roughness showed a positive correlation with power voltage and a negative correlation with power frequency and electrode speed. Remarkably, the microgroove bottom surface roughness reached a minimum of 0.605 μm. The study demonstrated ECDM's potential in creating intricate 3D microstructures on glass surfaces using a layer-by-layer approach.

Charak et al. **[113]** investigated diverse approaches utilizing the same process, specifically focusing on electrode immersion depths and the impact of electrolytic stirring in Electrochemical Discharge Machining (ECDM). Experimental variables included applied voltage, electrolyte concentration, and electrode immersion depths, while outcomes comprised material removal, tool wear, and surface finish. The findings demonstrated effective material removal with equivalent electrode cross-sectional areas and optimal immersion depths. Examination of electrode immersion depth ratios, electrolyte concentration, and the effects of stirring on borosilicate glass highlighted improvements in process outcomes. The integration of stirring effects with appropriate electrode immersion depths significantly improved process performance, achieving surface finish values up to four times superior to standard ECDM. FESEM micrographs of fabricated microchannels revealed intriguing material-removal patterns, and EDS analysis shed light on the characteristics of the debris generated in this process.

Madhavi et al. **[114]** focused their research on the production of borosilicate glass nanoparticles using a μ-ECDM setup with a DC motor-actuated gear-reduction tool-feeding mechanism. Analysis of variance revealed that the most significant contribution was from voltage (V) at 73.77%, followed by concentration (C) at 14.76%, and duty factor (DF) at 6.05%. The optimal combination of parameters, specifically 40 V, 20 wt% concentration, and 40% duty factor, resulted in a minimal average diameter (AD) of 46.51 nm. Additionally, an empirical model was developed to predict responses for desired parametric combinations, with an average error of 5.63%. This work provides valuable insights into the controlled generation of borosilicate glass nanoparticles using μ-ECDM setups and the optimization of parameter conditions to achieve desired outcomes.

Paul et al. **[115]** documented a Finite Element Model (FEM) investigation of the Electrochemical Discharge Machining (ECDM) process within the discharge regime (less than 300 μm). Pulsed DC was applied in a 2D domain to characterize the Material Removal Rate (MRR) as a key process output response in borosilicate glass machining. Both model-based and experimental approaches were employed to determine the MRR values, yielding 0.373 mg/min and 0.414 mg/min, respectively. Remarkably, there was almost no difference in MRR between the experimental and model values, with a minimal 9.9% error. This close alignment between experimental and model results validated the model's accuracy, indicating a robust understanding of the ECDM process.

Torabi et al. **[116]** utilized electrochemical discharge machining (ECDM) to create microchannels on polydimethylsiloxane (PDMS), offering a cost-effective and efficient approach. The investigation focused on optimizing parameters such as electrolyte concentration, rotational speed, feed rate, and machining voltage for PDMS micromachining. Results showed that ECDM achieved microchannels with surface quality comparable to lithography, and higher machining voltage and electrolyte concentration increased material removal rates (MRR) while shifting the machining regime from contact to electrochemical. Varied rotational speeds reduced surface roughness. The study employed Response Surface Method with a Quadratic Equation model for predictive analysis, providing valuable insights into optimizing the ECDM process for PDMS micromachining.

Ma et al. **[117]** employed a non-pulsed direct current (DC) power supply and a 20 wt% NaCl solution for the Electrochemical Discharge Machining (ECDM) of Ti6Al4V. The experiments explored the effects of applied voltage, feed rate, and electrolyte pressure on machining performance, specifically, material removal rate (MRR), overcut width (WOC), and surface morphology. The results demonstrated that discharges significantly improved the MRR. To achieve a groove without a recast layer, the tool electrode wall thickness was reduced to reduce the discharge influence area and increase the MRR in Electrochemical Machining (ECM). A substantial improvement in MRR, by 38.8%, was observed when using a tool electrode with an inner diameter of 1.8 mm compared to 1.4 mm. The machined groove exhibited a surface roughness of merely 1.49 µm, with no recast layer or stray corrosion, indicating excellent surface quality and high machining efficiency.

Ranganayakulu et al. **[118]** investigated the implementation of periodic bi-directional tool rotation (PBTR) with a tungsten carbide helical drill, as employed in a study. Initially, COMSOL simulations with KOH electrolyte demonstrated superior electrolyte supply to the tool tip with PBTR compared to unidirectional tool rotation (UTR). Experiments, guided by an L16 array, revealed that PBTR significantly enhanced the material removal rate (MRR), depth of the machined hole (DOM), and circularity, while simultaneously reducing the heat-affected zone (HAZ), the radius of curvature (ROC), and tool penetration (TP). The study further employed the teaching-learning-based optimization (TLBO) algorithm for parametric optimization, successfully determining optimal values that were subsequently confirmed by experimental results.

1.4.4 Fabrication of Various Geometrical Shapes by ECD milling

Electrochemical Discharge Milling (ECD milling) offers versatile capabilities for fabricating various geometrical shapes with high precision and efficiency. Electrochemical Discharge Milling (ECD milling) is classified as a milling process because its tool kinematics, machining strategy, and material removal progression closely resemble those of conventional milling. The method employs a tool that moves along a defined CNC-controlled toolpath to progressively remove material and generate channel, groove, or cavity features, typically produced in mechanical milling. Although the underlying mechanism is thermo-electrochemical rather than mechanical cutting, the subtractive material removal occurs layer by layer, governed by feed rate, spindle speed, and tool geometry. Also, the material removal process is intermittent for conventional and ECD milling as shown in **Fig. 1. 5**.

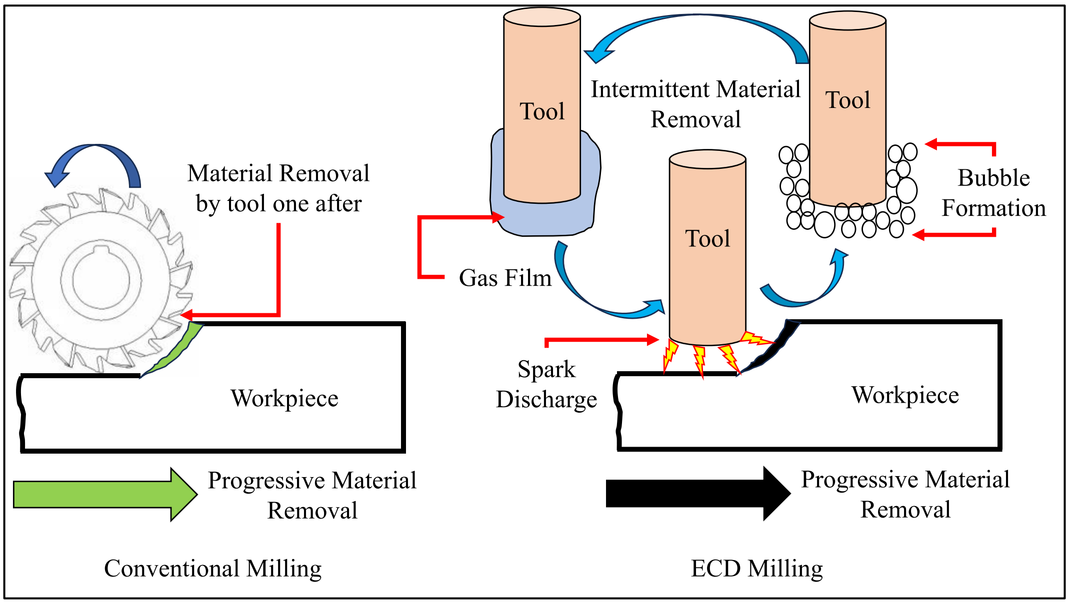

Fig. 1. 5 Schematic representation of conventional milling and ECD milling

Since the final geometry is shaped by the rotary tool during continuous feed motion, ECD milling meets the operational and geometric criteria for a milling operation, thereby justifying its classification as a milling process. This advanced machining process allows for the creation of complex geometries with intricate details. By employing suitable tool electrode designs and optimizing process parameters, ECD milling can effectively produce shapes such as pockets, slots, holes, contours, and even three-dimensional features. The key to fabricating different geometrical shapes lies in the precise control of spark discharge, electrolyte flow, and tool movement. For instance, to create straight slots or holes, controlled tool movements along specific paths combined with synchronized spark discharges enable precise material removal. Complex contours and three-dimensional shapes can be achieved by strategically adjusting process parameters to control material removal rates and electrode wear while maintaining dimensional accuracy. Additionally, using computer-aided design (CAD) software and advanced machining strategies, such as adaptive toolpath planning, further enhances the flexibility and accuracy of ECDM in fabricating various geometric shapes.

Cao et al. **[119]** generated various microstructures on 150 μm-thick soda-lime glass using a 30 μm-diameter tungsten carbide rod as the tool electrode in a potassium hydroxide (KOH) electrolyte. The machining was performed layer by layer, with a tool feed rate of 3 μm/sec per layer, achieving a maximum depth of 25 μm per pass. The study emphasized the importance of optimizing feed rate when using small-diameter electrodes, as high feed rates can cause tool breakage due to increased mechanical stress. In contrast, very low feed rates may lead to rough surfaces from prolonged thermal exposure. At an applied voltage of 25 V, Wang et al. achieved a remarkably smooth surface finish with a surface roughness (R_a) value of 0.099 μm. The work demonstrates the potential of Electrochemical Discharge Machining (ECDM) for precision micromachining of brittle, non-conductive materials such as soda-lime glass. The findings offer insights into the relationship among feed rate, tool diameter, and machining quality, suggesting that moderate feed rates are essential for balancing tool integrity and surface finish.

Nguyen et al. **[120]** addressed the paucity of information on milling conditions for quartz materials, distinct from those for glass, in electrochemical discharge machining (ECDM) processes, where the gas film and sparks are pivotal. Various machining parameters, such as electrolyte level, concentration, pulse voltage, and offset pulse voltage, were investigated to explore their impact on ECDM characteristics. Maintaining low electrolyte levels at 200 μm increased thermal energy due to reduced resistivity, thereby enhancing the discharge current. Moreover, electrolyte concentration directly influenced hydrogen film generation, a crucial factor in improving machining resolution. Configuration variations in offset pulse voltage, including pulse voltage, offset voltage, and pulse duration, were studied, demonstrating enhanced resolution and mitigation of tool erosion. The study also integrated dynamometer measurements to elucidate the relationship between tool feed rate and force, revealing that beyond a certain point, increased feed rate escalated force due to reduced discharge energy, underscoring its role in rough cutting 3D structures to minimize machining time.

A summary of the previous literature review is presented in **Table 1. 1**, covering their methodologies and key findings.

Table 1. 1 Summary of the previous research findings

First Author	Year	Methodology Used	Process / Material	Key Findings
Han et al. [70]	2017	FEM and experimental validation	Micro-groove machining	Micro-textured tools reduced taper and produced crack-free high-aspect-ratio grooves.
Hajian et al. [71]	2017	Experimental investigation	Magnetic-field-assisted ECDM	The magnetic field reduced the bending force and increased the optimum feed rate.
Goud et al. [72]	2017	Three-dimensional FEM with experiments	ECD drilling	Developed validated thermal model predicting material removal mechanism and MRR.
Gupta et al. [42]	2018	Experimental variation of electrolyte level	Glass micro-hole machining	Optimum electrolyte level (~1 mm) maximized MRR while minimizing HAZ and overcut.
Sabahi et al. [43]	2018	Experimental investigation using mixed electrolytes	ECDM	Equal NaOH–KOH mixture improved conductivity, surface finish and channel depth.
Liu et al. [44]	2018	Experimental analysis	Grinding-assisted ECDM	Grinding action removed clogging, stabilized machining and increased tool life.
Mehrabi et al. [73]	2018	Hollow-electrode with pressurized electrolyte	Deep-hole ECDM	Improved electrolyte supply increased machining depth by over 200% with better accuracy.
Arab et al. [31]	2019	Experimental using electrochemical finishing (ECF)-treated electrodes	ECDM of glass	Smoother tool electrodes reduced overcut and heat-affected zone while improving through-glass vias.
Madhavi et al. [45]	2019	Taguchi, S/N ratio and Grey Relational Analysis	μ-ECDM	Simultaneously optimized MRR, tool wear and channel width.
Kolhekar et al. [46]	2019	FEM multiphase simulation with experiments	Glass ECDM	Thinner and stable gas films reduced overcut and improved machining accuracy.

First Author	Year	Methodology Used	Process / Material	Key Findings
Zhang et al. [47]	2019	Experimental study on solution conductivity	ECDD	Optimum conductivity significantly reduced tool wear while maintaining hole quality.
Mishra et al. [48]	2020	Experiments with FEM validation	Soda-lime glass	NaOH produced deeper channels; larger tool-work gaps reduced tool wear.
Rathore et al. [49]	2020	Sonication-assisted experiments	ECDM	Sonication controlled gas-film thickness and improved spark intensity.
Singh et al. [32]	2021	High-speed imaging, discharge analysis, simulations and experiments	Ultrasonic-assisted ECDM	Ultrasonic vibration improved energy channelization, increased MRR, reduced HAZ and energy consumption.
Rashedul et al. [33]	2021	Comparative experimental study on six electrode materials	Precision ECDM	W70Cu30 electrode produced highest MRR, lowest wear and superior surface quality.
Torabi et al. [101]	2021	Experimental study	Micro-channel fabrication	Optimized tool geometry and electrolyte properties improved surface finish and dimensional accuracy.
Mallick et al. [103]	2021	Experimental investigation	ECDM	Improved process performance through optimized discharge conditions.
Ranganayakulu et al. [109]	2021	GTA, DFA and L9 Taguchi design	ECDM	Multi-response optimization identified duty factor as the dominant parameter.
Rajput et al. [110]	2021	Closed-loop ECDM with RSM	Adaptive ECDM	Adaptive tool feed increased MRR and reduced tool wear simultaneously.
Zhao et al. [111]	2021	Hybrid laser-assisted ECDM	Glass micro-grooving	Laser-assisted ECDM improved groove geometry, reduced taper and enhanced surface finish.

1.4.5 Various Tool Feeding Strategies

In Electrochemical Discharge Machining (ECDM), the heat source from the electrochemical discharges must be located close to the workpiece. However, as the tool is withdrawn and no longer touches the glass surface, the diameter of the machined area decreases compared to when there is no gap. For larger gaps, the machined area can become even smaller than the tool diameter. Therefore, the machining outcome will vary depending on the tool-feeding mechanism used. There are three primary tool feeding mechanisms, each involving a different method of tool movement. The simplest mechanism is gravity feed, in which a constant force ensures that the tool electrode remains in contact with the workpiece. Another method is constant-velocity feed, in which the tool-electrode moves at a feed rate lower than the average material removal rate, thereby maintaining a gap between the tool and the workpiece. The third approach involves controlling the tool feed using an XYZ stage driven by a servo motor and controlled via software.

1.4.5.1 Gravity-Feed

In a gravity-feed system, as shown in **Fig. 1. 6** the workpiece was advanced at a feed rate controlled by gravity. A weight was attached to the wire string, which was connected to the workpiece holder via a pulley system. The weight was responsible for maintaining contact between the tool electrode and the workpiece during machining **[4]**. However, this process also had a disadvantage due to mechanical contact between the tool electrode and the workpiece, and the gap between them was not controlled. This meant that machining progress could not be monitored in real time.

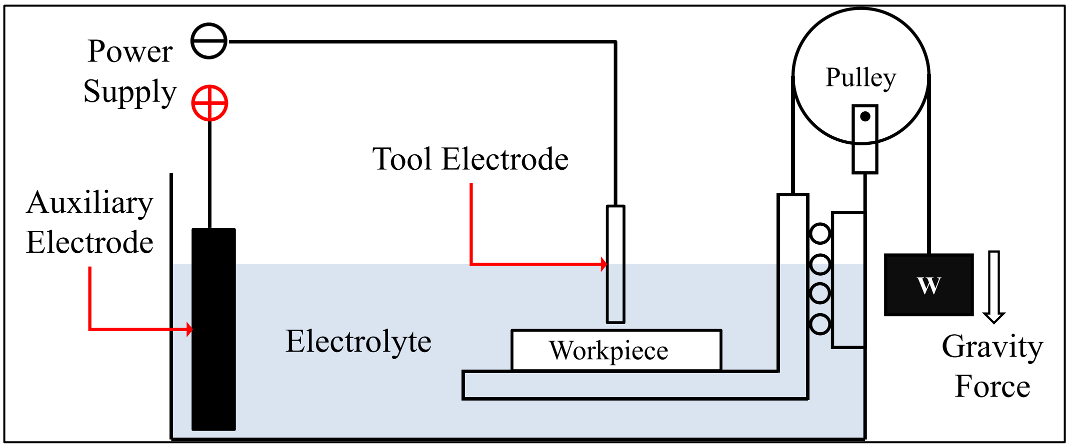

Fig. 1. 6 Schematic diagram of the gravity feed mechanism

Selecting the appropriate weight was crucial because if it was too high, it could bend the tool electrode under excessive contact forces, potentially damaging either the workpiece or the tool electrode. Conversely, very low weight could result in longer machining times and larger heat-affected zones around the hole.

1.4.5.2 Spring-Feed

In spring-feed systems, a steady force through a spring system was applied to the workpiece to keep it in close contact with the heat source, which was the tool electrode itself, heated by electrochemical discharges through a gas film. This ensured that the temperature in the machining area matched that of the tool electrode **[103]**. Although this technique was notably simple, as shown in **Fig. 1. 7** and yielded great results, its main drawback was that the mechanical contact between the tool and the workpiece limited effective flushing and could lead to hole deformation. The workpiece was guided vertically while a force was applied in the machining direction.

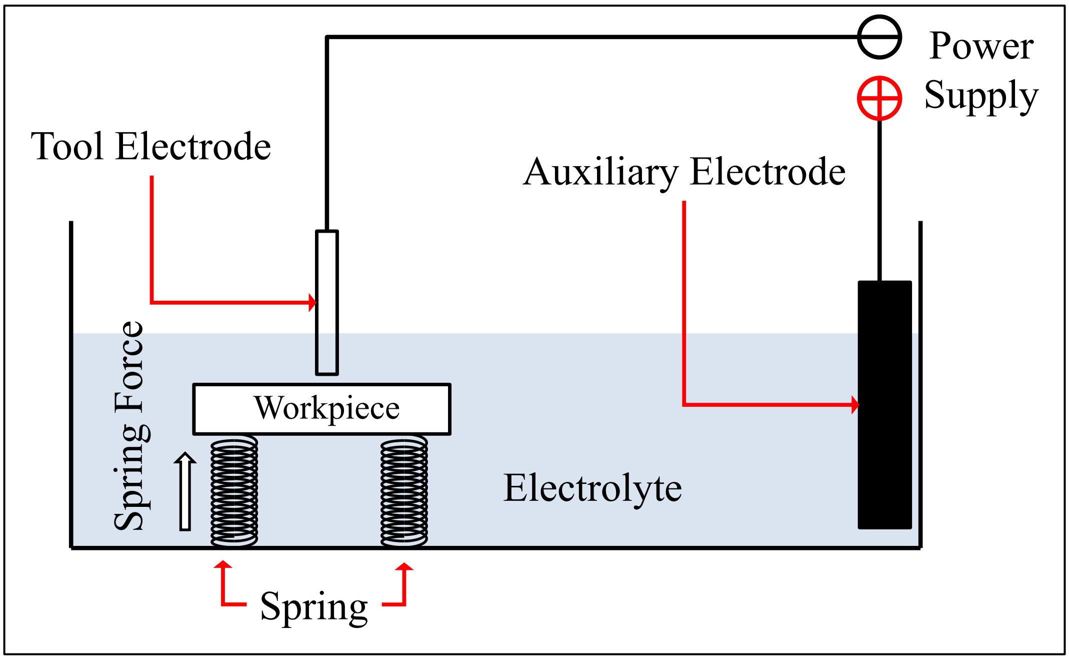

Fig. 1. 7 Schematic diagram of the spring feed mechanism

1.4.5.3 XYZ Stage Controlled Feed

This tool-feeding technique is still being used. In this method, the tool electrode movement is controlled using an XYZ stage via software, and the gap is controlled by issuing appropriate commands to the software **[120]**. An XYZ stage is involved in this method, and a setup of tool holding as well as a workpiece holding unit is attached as shown in **Fig. 1. 8**. The tool movement is controlled during milling, and a suitable machining gap is maintained throughout. This process reduces the likelihood of tool-workpiece contact, thereby diminishing the tool-bending problem during machining.

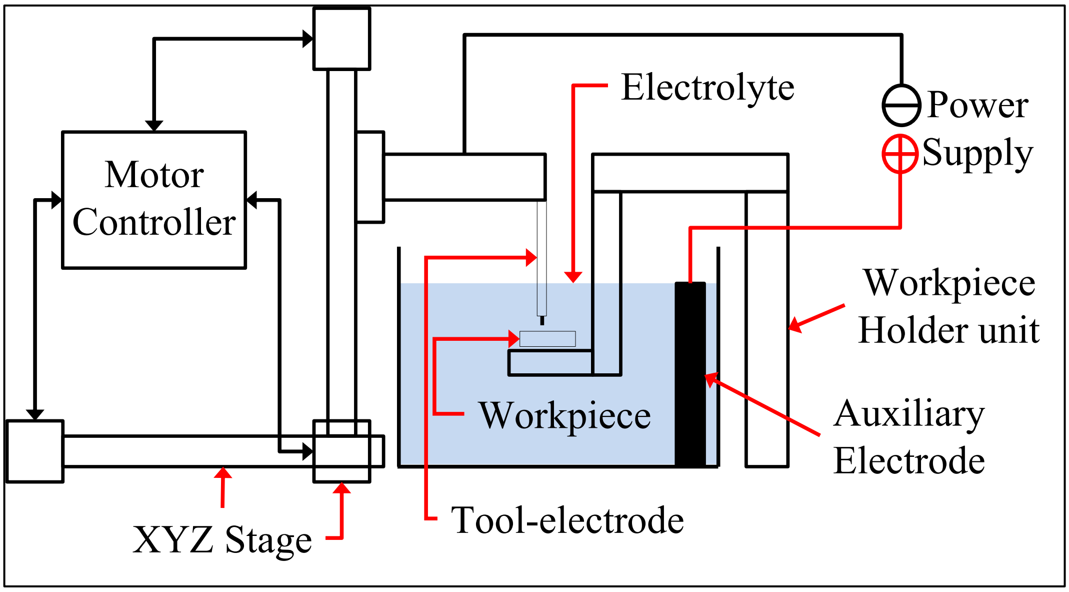

Fig. 1. 8 Schematic of XYZ-controlled feed mechanism

Although this process produced better machining results by controlling the optimal machining gap between the tool and workpiece, it cannot maintain a uniform machining gap during milling.

1.5 Research Gap Identification

Electrochemical Discharge Milling (ECD milling) has emerged as a promising technique for machining hard, brittle, and electrically non-conductive materials by combining the advantages of electrochemical and spark discharge processes. Despite its potential, the research landscape reveals several underexplored and partially addressed areas that necessitate further investigation. Extensive research has been conducted since the discovery of the Electrochemical Discharge Machining process. This technique has been widely used to make holes in electrically non-conductive materials. Few researchers have used this technique to create channels and various patterns on glass, ceramics, polymers, etc., but Electrochemical Discharge Milling has not been studied widely. Additionally, researchers have implemented various techniques and accessories within the ECDM setup to improve machining performance.

Most existing studies on Electrochemical Discharge Machining (ECDM) primarily focus on hole drilling and surface structuring on non-conductive materials such as glass, ceramics, and polymers. Although some progress has been made in extending the ECDM technique for milling operations, systematic research dedicated specifically to Electrochemical Discharge Milling (ECD milling) remains limited. In particular, the development of precise milling strategies, tool movement controls, and innovative tool feeding techniques for generating complex patterns and high-aspect-ratio features has not been extensively studied. Another critical challenge in ECDM is the inefficient evacuation of gas bubbles and the inadequate supply of fresh electrolyte in the machining zone, especially during deeper cuts. While researchers have attempted to overcome these limitations through methods such as tool vibration, rotation, magnetic field assistance, and altered tool geometries, there is a notable lack of work on tool feeding techniques, particularly those aimed at regulating gas bubble dynamics and ensuring continuous electrolyte refreshment. This remains a key bottleneck in achieving consistent spark discharges and uniform material removal.

Additionally, most research in ECDM has centered on glass as the primary workpiece material, with limited exploration of other advanced non-conductive materials such as engineering polymers. The performance of the ECDM process in terms of material removal rate, surface finish, and thermal damage mitigation across diverse materials also remains insufficiently characterized. Therefore, this research addresses these key gaps by:

- ❖ Developing a dedicated ECD milling setup capable of producing intricate features.
- ❖ Investigating tool feeding mechanisms to improve machining efficiency and electrolyte circulation.
- ❖ Extending the applicability of ECD milling to non-glass, non-conductive advanced materials.
- ❖ Exploring pattern fabrication and high-aspect-ratio structures through different milling strategies.

By targeting these underexplored areas, the study aims to enhance the understanding, control, and application of Electrochemical Discharge Milling in modern manufacturing.

1.6 Objectives of Present Research Work

Previous research has found that extensive experimental and theoretical studies have examined the effects of various factors, including electrolytes, tool vibration, and different types of tool electrodes. So far, the spark discharge mechanism, along with the stability of the gas film and the spark discharge, etc., is not clear to everyone. There have been a few studies on electrochemical discharge milling so far. So, keeping the drawbacks of the ECDM process in mind, the following objectives are set to be fulfilled during my Ph.D. (Engg.) research work:

(i) To develop an Electrochemical Discharge Milling set up.

(ii) To investigate the possibility of fabricating high aspect ratio features, such as channels, using Electrochemical Discharge Milling on glass.

(iii) To investigate the effects of different process parameters during Electrochemical Discharge Milling with vertically upward tool feeding technique.

(iv) To fabricate various patterns such as zigzag channels, rectangular-shaped cavity using Electrochemical Discharge Milling on glass.

(v) To investigate the effects of various process parameters on Electrochemical Discharge Milling of different types of polymers.

Chapter 2

DEVELOPMENT OF ELECTROCHEMICAL DISCHARGE MILLING SET UP

2.1 Introduction

The development of the Electrochemical Discharge Milling (ECD milling) setup was guided by an extensive review of prior research and by the fundamental concept of the electrochemical discharge process. Designing and developing an electrochemical discharge milling (ECD milling) setup represents a convergence of precision engineering, electrochemistry, and advanced manufacturing techniques. This innovative process combines the material removal capabilities of traditional milling with the enhanced precision and surface quality achievable through electrochemical machining. The integration of electrochemical discharge phenomena further enhances the machining capabilities by enabling high-precision machining of electrically non-conductive materials. Designing and developing an Electrochemical Discharge Milling (ECD milling) setup involves a comprehensive approach that integrates several intricate components to achieve precision machining of electrically conductive materials. At the core of the setup is the tool-holding unit, meticulously designed to grasp electrodes of varying sizes and geometries securely. This unit must withstand the harsh chemical environment of the electrolyte, requiring materials that are both durable and corrosion-resistant. Precision adjustment mechanisms enable precise positioning of the electrode relative to the workpiece, ensuring exact machining dimensions and geometry.

Complementing the tool holding unit and the workpiece holding unit, which play a crucial role in stabilizing and positioning the tool electrode and the workpiece, respectively, during machining. It incorporates robust clamping mechanisms that securely hold a wide range of workpiece shapes and sizes. This unit is designed for ease of loading and unloading to facilitate efficient workflow and minimize downtime between machining operations. The machining chamber, constructed from materials resistant to chemical corrosion, serves as the controlled environment where the machining process takes place. It houses the electrolyte solution essential for electrochemical reactions and provides seals to prevent leakage and maintain stability. Accessibility features are integrated to facilitate maintenance, electrode handling, and observation of the machining process.

Precision motion control systems form another critical component of the ECDM setup, enabling accurate positioning and movement of both electrodes and workpieces. These systems typically include multi-axis configurations (such as X, Y, Z axes) controlled by advanced software. Measuring instruments are indispensable for quality assurance and process optimization in ECDM setups. Surface profilers assess surface roughness and finish quality post-machining, while Coherence Correlation Interferometry (CCI) verifies surface topography of machined features.

Together, these integrated components form a sophisticated ECD milling setup capable of achieving high-precision machining results with exceptional surface finishes and dimensional accuracy.

2.2 Functional Elements of Electrochemical Discharge Milling Setup

Indigenously selected several elements are designed and integrated to form an ECD milling setup. Some readily available elements were purchased to reduce the time required to design the experimental setup. The main functional elements are as follows:

(i) X-Y-Z Translational Stage
(ii) Automated Programmed Tool (APT) Software
(iii) Tool and Workpiece Holding Device
(iv) Tool Electrode and Auxiliary Electrode
(v) Main Machining Chamber
(vi) Power Supply Unit
(vii) Measurements and Data Collection Equipment

All functional elements were integrated to form an indigenously developed ECD milling setup for experimentation. The details of each element are discussed below.

2.2.1 X-Y-Z Translation Stage

The primary and most adaptable component of the machining system is the mechanical unit, which consists of three linear stages that move along the three main Cartesian axes to position and maneuver the tool on the workpiece surface precisely. These stages, operating in X, Y, and Z directions, offer a minimum resolution of 0.1µm per incremental step driven by stepper motors. Each stage is positioned orthogonally and controlled by a central position controller. Specifically, the X-axis table facilitates tool movements towards and away from the workpiece, the Y-axis table enables lateral movements of the tool, and the

Z-axis table controls vertical movements. **Fig. 2. 1** shows the 3-D view and photograph of the XYZ stage with the attached tool-holding unit.

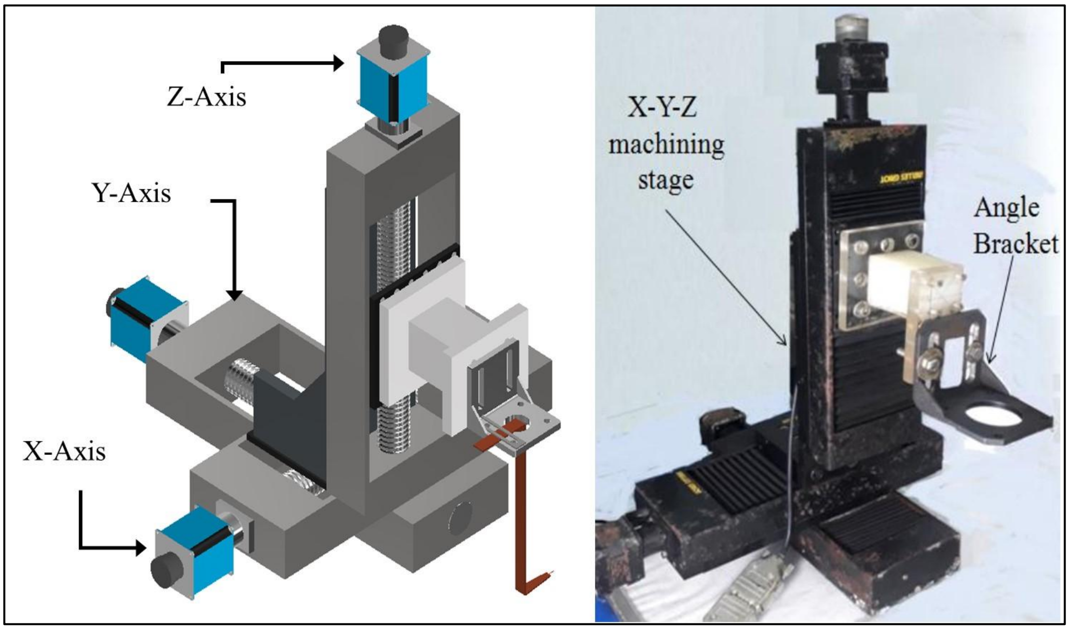

Fig. 2. 1 3-D view and photograph of the XYZ translational stage

To ensure smooth translational motion, recirculating ball carrier bearings are mounted on precisely aligned linear guide rails, paired with backlash-free precision lead screws. Each translation stage unit can travel up to 100mm, and is designed with robust construction. The X and Y stages can support loads of up to 20 kg each, while the Z-axis stage supports up to 5 kg. Movement across all stages is achieved through precise lead screw arrangements, ensuring continuous and accurate positioning.

2.2.2 Automated Programmed Tool (APT) Software

The APT software guides the programmed movement of stages by utilizing the X, Y, and Z axis columns displayed on the desktop computer interface, as shown in **Fig. 2. 2**. This software enables precise control over step-by-step translational motion, continuous motion, and vibratory feed motion of the tool electrode according to the programmed instructions. After completion of operations, all stages automatically return to their initial positions, establishing the starting point for subsequent tool movements.

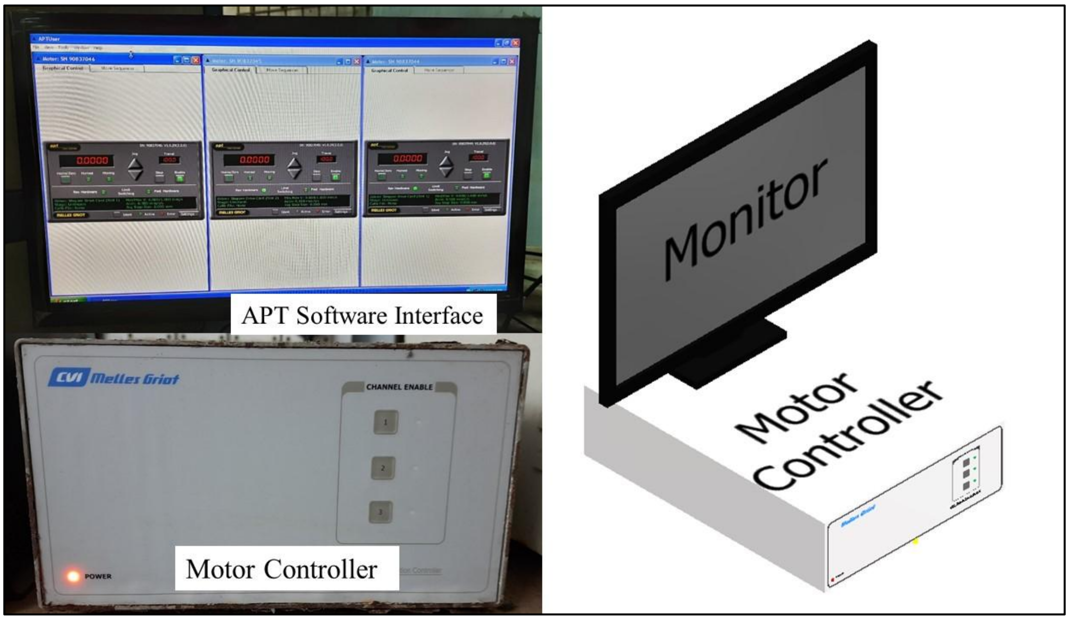

Fig. 2. 2 Photograph of the APT software interface and motor controller

This initial reference point in X, Y, and Z coordinates is crucial for offline sequential machining operations. The software interfaces via a graphical user interface to input stage positions and manage their movements within the system.

2.2.3 Tool and Workpiece Holding Device

The tool-holding unit is crafted from various solid, transparent plastic components, specifically polymethyl methacrylate (Perspex). Elements of the tool holding unit, with dimensions and assembled form, illustrate the detailed dimensions of these unit elements along with their assembled form. The dimensions of each component were determined based on the shape and size of the X-Y-Z translation stage, the dimensions of the machining chamber, and the total available height from the base of the chamber to the center of the tool holding block. The clamping plate, which is 10mm thick on the back side, is intricately cut to fit the stage precisely. Both the back plate and the front plate maintain a thickness of 10mm. A thin, 5mm-thick copper plate securely holds the tool to ensure efficient conduction of electric current during operations. Initially, the clamping plate is fastened to the Z axis of the stage using four screws. To maintain a specific distance between the table's Z axis and the machining chamber, a rigidly fitted central block measuring 40mm x 40mm x 55mm is positioned behind the assembly. A back plate is secured to the central block with four screws spaced equidistantly. A front plate is used to secure the angle bracket relative to the clamping plate, facilitating convenient loading and unloading of the tool-holding plate. The front plate is connected to the angle bracket using a screw arrangement, allowing efficient manual screwing and unscrewing to minimize the time required for tool electrode loading or removal.

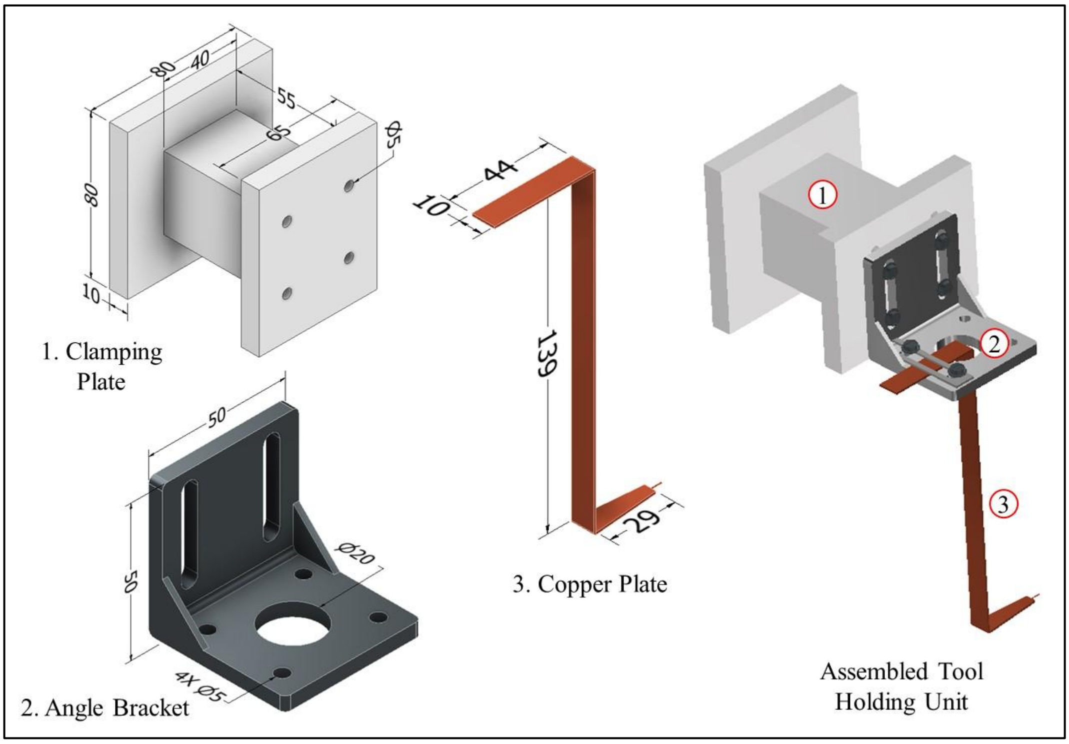

Fig. 2. 3 Elements of the tool holding unit with dimensions and assembled form

All components of the tool holding unit, except the tool holding plate and angle bracket, are made of acrylic to prevent electric current from reaching the X-Y-Z translation stage. The overall dimensions of the tool-holding unit are carefully managed to minimize space and weight, resulting in a compact, lightweight assembly. During the assembly, the negative terminal of the power supply connects to one end of the copper plate, while the tool is soldered at the other end. The dimensions of the 2 mm-thick copper tool holding plate are 140mm in length and 10mm in width.

The workpiece holding unit comprises a 10 mm-thick perspex sheet material cut to the required sizes. Key components include the main supporting stand, slotted plate, workpiece resting platform-I & II, and clamp, all drilled and assembled using stainless steel screws as **Fig. 2. 4** along with the assembled form of the workpiece holding unit. This arrangement allows for the accommodation of workpieces of various sizes, with portions submerged during machining made from lightweight, non-corrosive, transparent, and non-conductive perspex material to avoid vibration-induced errors. To minimize vibration-induced errors during machining, Z-shaped vertical stands made of robust 10 mm-thick mild steel were securely fitted to the machining table using nuts and bolts.

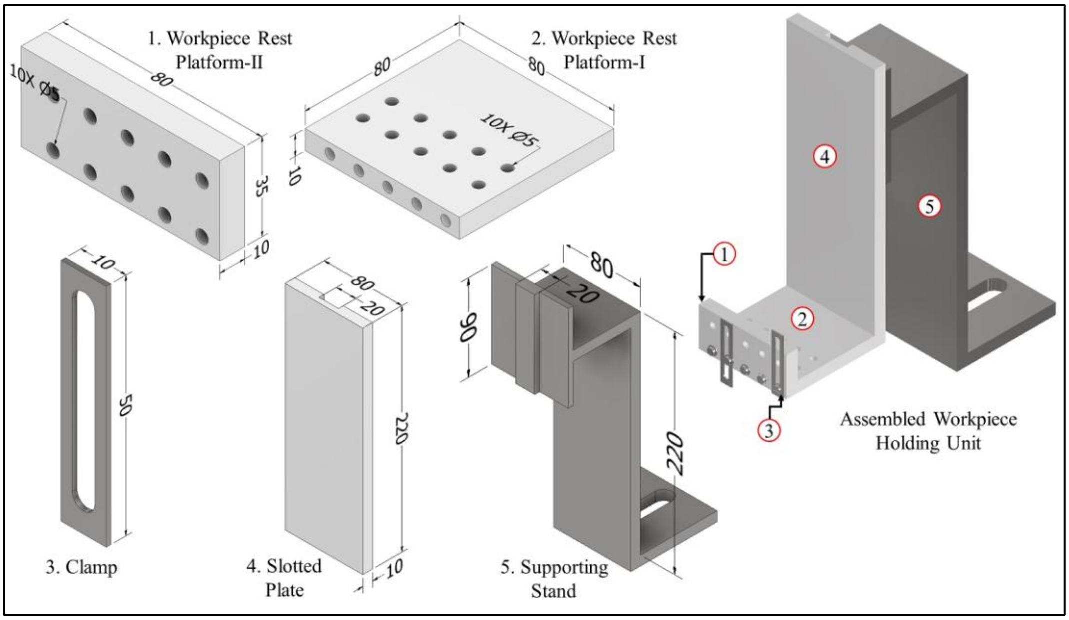

Fig. 2. 4 Elements of the workpiece holding unit with dimensions and assembled form

These stands were welded together to reinforce the structure and provide substantial support for the workpiece-holding unit. At the upper end of the supporting plate, another vertical steel plate was machined with a central vertical rib and slots on both sides, enhancing stability and vertical alignment of the slotted plate during its movement. The slotted plate features a groove on its backside for fitting into the upper plate of the supporting stand, with the slots in both the slotted plate and the supporting stand aligning after assembly. This configuration enables vertical adjustment of the plate relative to the Z-shaped stand, facilitating precise positioning of the workpiece with respect to the tool electrode.

During micro-ECM machining, the workpiece is connected to the positive terminal of the power supply unit. The vertical mild-steel stand is rigidly attached to the experimental table. The workpiece mounting unit's design also facilitates easy replacement of the electrolyte chamber without disturbing the tool or workpiece positions.

2.2.4 Tool Electrode and Auxiliary Electrode

The experimentation on electrochemical discharge milling (ECD milling) was carried out using a cylindrical copper tool with a flat end. The tool electrode was connected to the negative terminal of the power supply and attached to the tool-holding unit, as discussed earlier. The tool electrode diameter was 500 μm, as shown in **Fig. 2. 5(b)** and the length was 30 mm, as shown in **Fig. 2. 5(d)**. During the experiment, the tool electrode was cut into pieces, and after checking the diameter, it was soldered to the copper plate. The tool electrode was then insulated around the unwanted area of spark discharge. On the other hand, a graphite block of 100mm × 100mm was used as the auxiliary electrode, as shown in Fig. 2 .5 **(a)**. The auxiliary electrode was placed far from the tool electrode or sparking zone. The inter-electrode distance was 120mm between the tool electrode and the auxiliary electrode. The full image of the tool electrode is shown in **Fig. 2. 5(c)**.

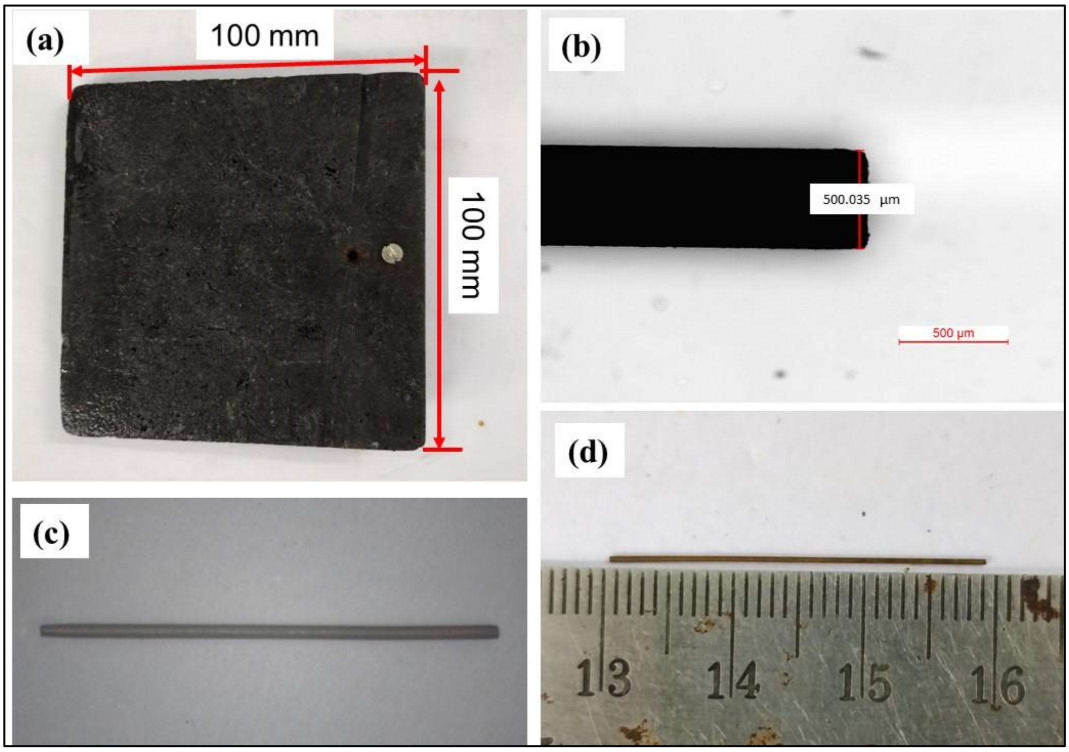

Fig. 2. 5 Photograph of the tool electrode and auxiliary electrode

The auxiliary electrode was connected to the positive terminal of the power supply and dipped into the electrolyte. The graphite block had high conductivity and helped start the electrolysis process quickly and smoothly throughout the experiments. Flexible power connections were used for both the tool electrode and auxiliary electrode so they could be plugged and unplugged easily.

2.2.5 Main Machining Chamber

This chamber serves as the primary location for electro-discharge milling processes. The figure depicts a 3-D view of the main machining chamber, which measures 200 mm in length, 160 mm in width, and 105 mm in height. Given its handling of corrosive electrolytes and the generation of high-intensity sparks, the material chosen for constructing the chamber must be non-corrosive, non-conductive, transparent, lightweight, and easily machinable to the desired specifications. Therefore, Perspex was selected to fabricate the main machining chamber as shown in **Fig. 2. 6**.

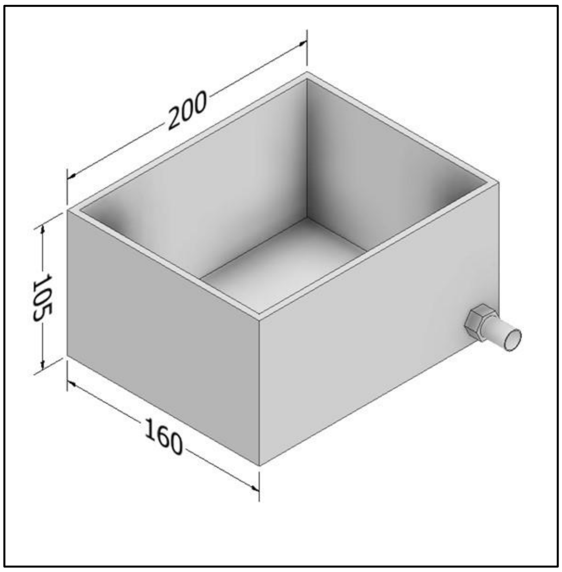

Fig. 2. 6 3-D model of the main machining chamber

Perspex sheets of 5 mm and 10mm thickness were available, and the chamber was constructed using 5 mm-thick sheets. Initially, these sheets were cut to the required dimensions and then securely fastened together using stainless steel screws. To ensure the chamber is leak-proof, all joints were sealed by applying chloroform. A steel valve with flexible piping is installed on the front face of the chamber to adjust the electrolyte level and facilitate drainage of used electrolyte from the machining zone. During fluid circulation mode in machining operations, this valve controls the electrolyte flow through the system.

2.2.6 Power Supply Unit

The newly developed ECD milling system setup is designed with a specialized power supply unit that is crucial for its operation, as shown in **Fig. 2. 7**. This power supply unit is connected to the main input power supply line, which is characterized by its 3-Phase configuration and a voltage rating of 440V AC. This configuration is necessary to meet the power demands of the ECD milling process. During ECD milling, the DC power supply plays a critical role by delivering a controlled voltage between the cathode tool (used for material removal) and an auxiliary electrode. This voltage application is essential for maintaining consistent polarity throughout the machining process, ensuring effective and precise material removal. A step-down transformer is employed to step down the high voltage from the mains supply (440V AC) to meet the specific requirements of the ECD milling process. This transformer reduces the incoming line voltage from 440V AC down to 220V AC, which is more suitable for further processing within the system.

Fig. 2. 7 Photograph of the power supply used in ECD milling

Following the transformer, a three-phase full-wave rectifier converts the AC voltage into DC. This rectification process is crucial because ECD milling typically requires pulsed DC power to achieve the desired machining effects effectively. The resulting DC power supply unit delivers voltages from 0 to 200 V and operates at 50 Hz. This setup ensures that the ECD milling process can be carried out with precision and reliability, meeting the specific operational requirements for machining a wide range of materials effectively.

2.3 Measurements and Data Collection Equipment

The optical photo of the machined channels was taken using an optical measuring microscope named Leica DM2500 M microscope, as shown in **Fig. 2. 8(a)** which is a versatile research-grade instrument designed for advanced scientific and clinical applications. It features a modular design with a variety of objective lenses (including 5x, 10x, 20x, 50x) for flexible magnification options. The microscope supports various contrast methods, such as phase-contrast, DIC, and dark-field microscopy, enhancing imaging versatility. The optical system provides high clarity and contrast, complemented by digital imaging capabilities for capturing high-resolution images.

The Coherence Correlation Interferometry (CCI) made by Taylor Hobson boasts exceptional capabilities for nano-scale surface analysis, as shown in **Fig. 2. 8(b)**. It is used for surface topography analysis, including surface roughness measurement of the machined surface by ECD milling. It offers an impressive vertical resolution of 1 nm, ensuring precise measurement and characterization of atomic-scale features. With a measurement range spanning from 0.36 mm to 1.8 mm in both X and Y directions, coupled with a lateral sampling resolution as fine as 0.35 µm, the CCI delivers detailed topographical imaging and accurate dimensional analysis. Operating at a maximum resolution of 1024 x 1024 pixels, it captures high-definition images and features a manual Z-stage resolution of 0.4 mm/revolution for precise positioning. The CCI's versatile stage accommodates components up to 300 mm in X and Y, and 100 mm in Z, with a weight capacity of up to 10 kg, ensuring compatibility with a wide range of samples for comprehensive material analysis and research applications.

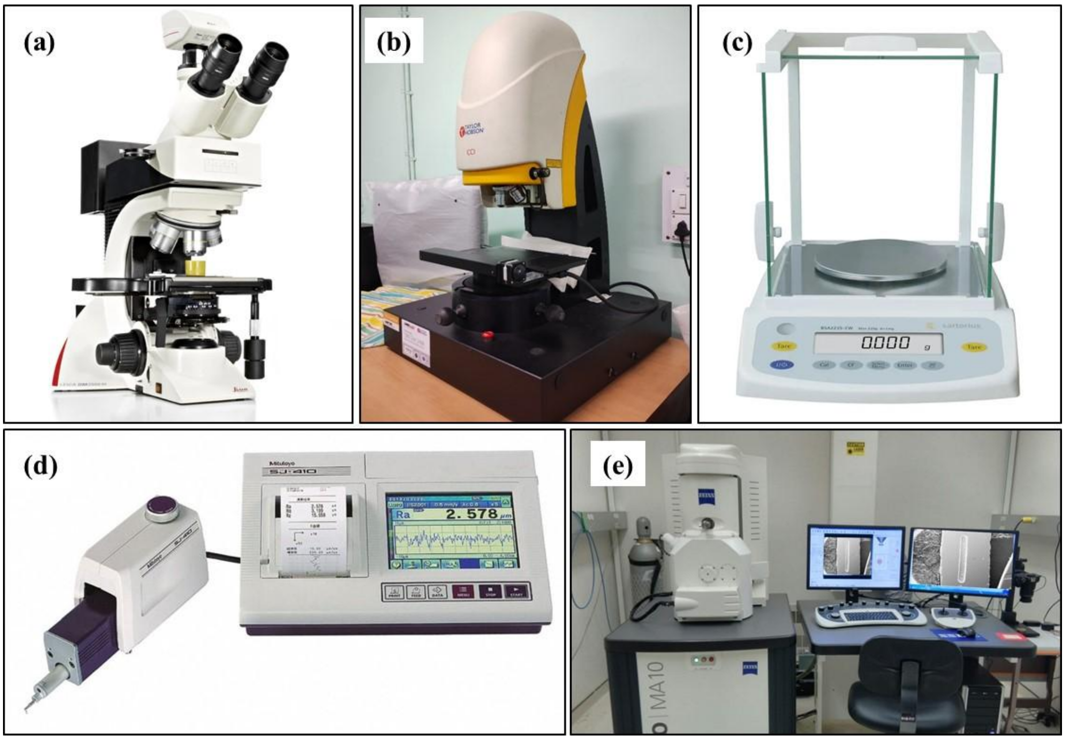

Fig. 2. 8 Photograph of Measuring instruments (a) Optical measuring microscope, (b) Coherence Correlation Interferometry, (c) Weighing machine, (d) Surface roughness tester, (e) Scanning Electron Microscopy

The Sartorius BSA model 224S-CW precision balance is shown in **Fig. 2. 8(c)** is used for measuring the weight of the machined sample before and after the ECD milling. It is an essential tool for accurate measurement in a variety of settings. With a capacity of 220g and a readability of 0.0001g, it ensures precise weighing and stabilizes in 2.5 seconds. It is enclosed in a draft-shielded chamber from the pan to the glass door, minimizing external influences and ensuring reliable results even in fluctuating environments. It enables straightforward operation and seamless data communication for efficient workflow integration.

The Mitutoyo SJ-410 surface roughness tester, as shown in **Fig. 2. 8(d)**. It is also used for measuring the surface roughness of the machined surface, which is a sophisticated instrument designed for precise measurement and analysis of surface roughness profiles. It offers a comprehensive range of measurement parameters, including R_a, R_z, R_y, and more, covering a measurement range of 360 µm (X) x 5.0 mm (Z) to accommodate various sample sizes. With a precise measuring force of 4 mN (0.4 gf) and adjustable cut-off lengths (0.08 mm to 2.5 mm), the SJ-410 ensures accurate and customizable evaluations of surface textures. It features a high-precision drive unit for smooth stylus traversing, a clear LCD for easy data readout, and connectivity options such as USB and RS-232C for data export and further analysis.

The scanning electron microscope, as shown in **Fig. 2. 8(e)**. It is used for collecting data related to the surface of the machined channels and also the element content on the surface of the machined channels. The JEOL JSM-7500F scanning electron microscope (SEM) is a highly capable instrument renowned for its exceptional imaging resolution and analytical versatility. Operating with a variable acceleration voltage typically ranging from 0.5 kV to 30 kV, it offers precise control over imaging conditions to suit various sample types and sizes. Equipped with advanced detector options including secondary electron (SE) and backscattered electron (BSE) detectors, the JSM-7500F delivers clear, high-resolution images and supports comprehensive analysis of sample surfaces. Its flexible sample stage accommodates a wide range of specimens, while intuitive software facilitates seamless operation, image acquisition, and data analysis.

2.4 Integrated Electrochemical Discharge Milling Setup

The ECD milling setup was designed and developed in-house by assembling various components. The detailed description of every piece of equipment and unit is discussed in the previous section. After assembling the equipment and units, the 3D image of the integrated ECD milling setup is shown in **Fig. 2. 9** and the actual setup is shown in **Fig. 2. 10**. All experiments were conducted in this setup by varying process parameters and machining techniques.

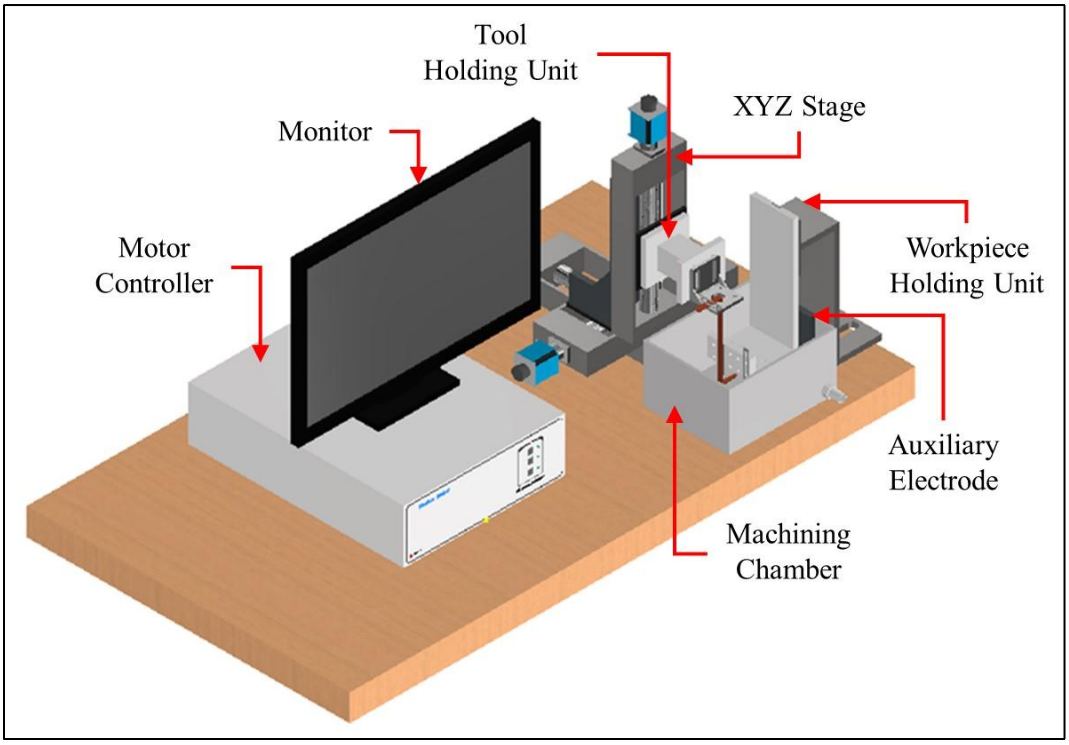

Fig. 2. 9 3D Image of the indigenously developed integrated ECD milling setup

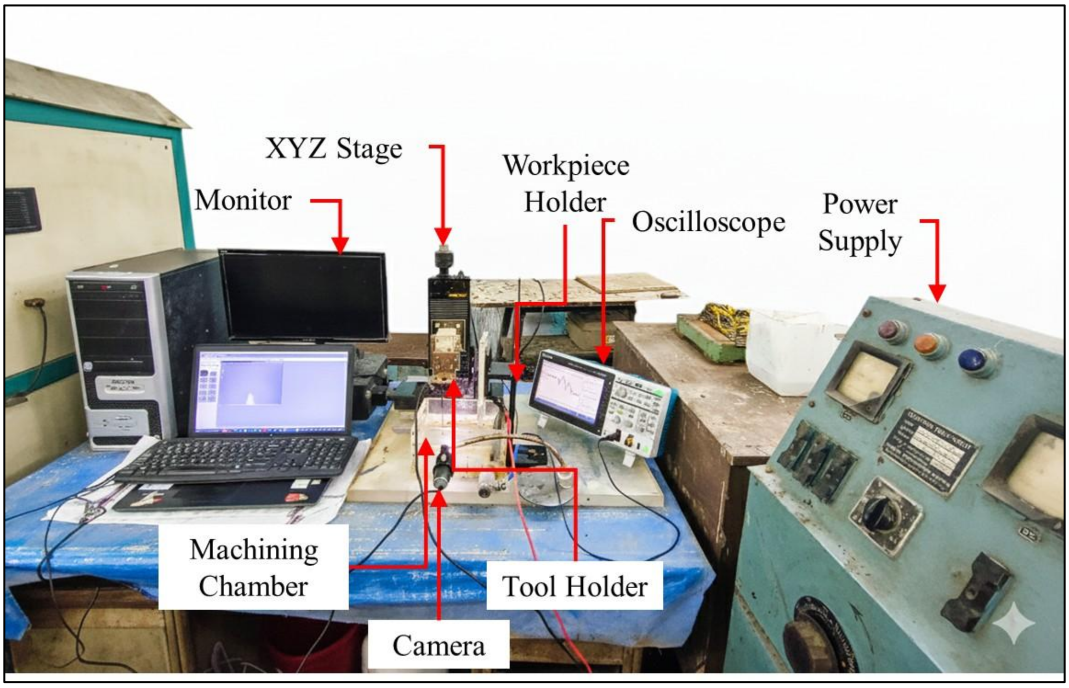

Fig. 2. 10 Actual image of the indigenously developed integrated ECD milling setup

Chapter 3

EXPERIMENTAL INVESTIGATION INTO THE PERFORMANCE OF ELECTROCHEMICAL DISCHARGE MILLING FOR DIFFERENT TOOL FEEDING TECHNIQUES

3.1 Introduction

In the realm of electrochemical discharge milling (ECD milling), understanding the dynamics of gas film shape generation is fundamental to improving machining processes. This chapter embarks on a detailed exploration of experimental methodologies and numerical analyses to elucidate the intricate mechanisms governing this phenomenon. The experimental plan is meticulously crafted to investigate key parameters that influence gas-film shapes, with a specific focus on their implications for tool-feeding techniques. This foundational research not only seeks to advance theoretical understanding but also aims to provide practical insights into enhancing machining precision and efficiency.

The chapter establishes a robust numerical analysis framework that serves as a predictive tool to improve gas-film shapes during ECD milling operations. This computational approach not only informs subsequent experimental investigations but also lays the groundwork for interpreting empirical findings. Later, practical experiments are conducted to validate and refine existing tool feeding techniques in ECD milling. Of particular interest is the comparative study of gas film shape generation, with a specific focus on upward tool feeding with a horizontal tool. This analysis aims to uncover subtle variations in machining dynamics and efficiency across different feeding orientations, thereby informing advancements in ECD milling technology. Simulation efforts are pivotal for a detailed examination of the temperature distribution within the machining environment. By simulating these thermal conditions, the study aims to elucidate the thermal effects influencing gas film formation and their consequential impact on machining outcomes. Through meticulous analysis and interpretation, correlations between experimental findings and theoretical predictions were elucidated, thereby enriching the understanding of gas-film shape generation in ECD milling. Furthermore, the chapter explores the intricate interplay of electrochemical spark-discharge phenomena across various tool-feeding techniques. Key investigations include assessing the effect of electrolyte concentration and feed rate on channel width, as well as conducting comparative analyses of channel dimensions and depth. These insights are crucial for improving ECD milling processes to achieve enhanced precision and reliability.

Finally, the chapter examines the effects of tool feeding on the electrode itself, addressing issues such as wear patterns and material deposition. These outcomes provide valuable feedback on machining efficiency and tool longevity, contributing to advancements in ECD milling technology. Through an integrated approach of experimental investigation, numerical analysis, and practical insights, this chapter significantly contributes to the understanding and application of gas film shape generation in electrochemical discharge milling.

3.2 Plan of Experiments

Three feeding techniques were used in this investigation. First, machining was done in the usual way, i.e., tool feeding at the top surface of the workpiece material in the downward direction (i.e., along the Z-axis) and tool movement in the X- and/or Y-axis directions, which is termed the existing tool feeding technique. The feeding of the tool electrode from the bottom surface of the workpiece in the upward direction (i.e., along the Z axis), along with tool movement in the X and/or Y axes, was the second technique, termed bottom tool feeding. In the third technique, the feeding of the tool electrode was given horizontally along the X or Y-axis, and the tool was moved vertically in an upward direction (i.e., along the Z-axis) as shown in **Fig. 3. 1** which is termed as vertically upward tool feeding with a horizontal tool electrode.

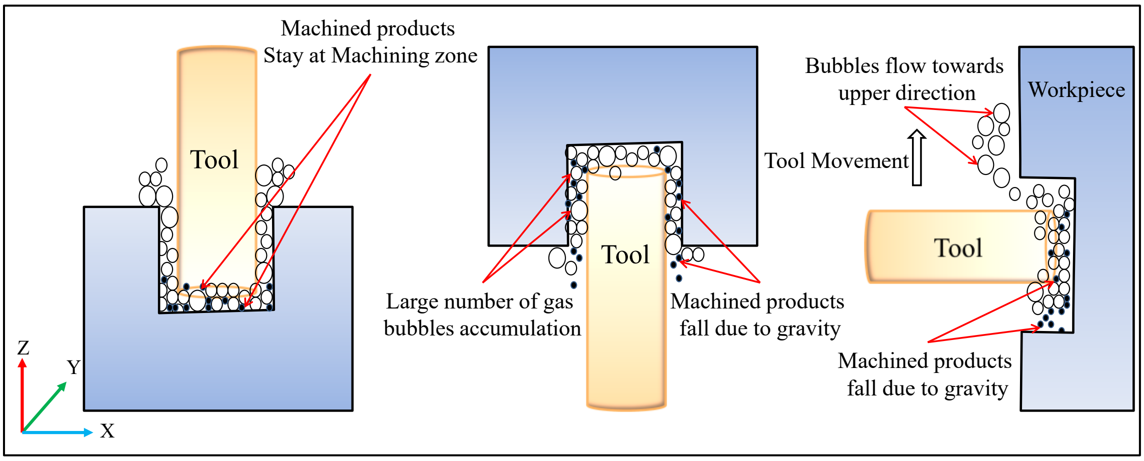

Fig. 3. 1 Schematic diagram of different tool-electrode feeding techniques

The second and third techniques were applied to keep the generated gas bubbles at the tool-electrode tip and at the upper level of the electrolyte solution. These three kinds of tool feeding techniques are referred to as the existing tool feeding technique, the upward tool feeding technique with a vertical tool, and the upward tool feeding technique with a horizontal tool. The positions of tool-electrode and workpiece during machining with three tool feeding techniques and tool path during machining with three kinds of tool feeding techniques are shown in **Fig. 3. 2**.

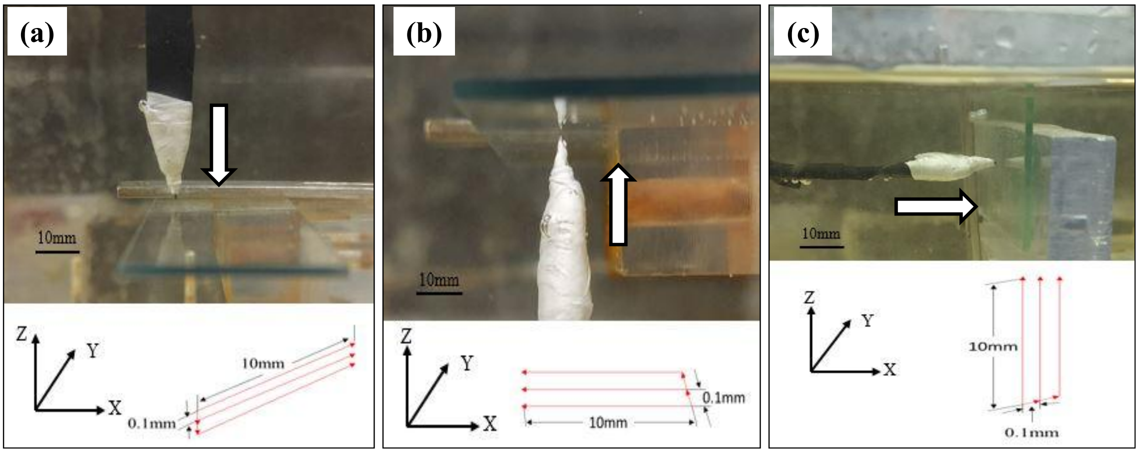

Fig. 3. 2 Positions of the tool-electrode and the workpiece for (a) existing tool feeding, (b) bottom tool feeding, (c) upward tool feeding with horizontal tool

Every channel was fabricated with five passes of tool-electrode, and during each pass of tool-electrode, 0.1 mm ‘depth of cut of 0.1 mm was given. This experimental study focused on creating channels on a 1mm-thick glass slide. The channel depth was observed to exceed 0.8 mm after five passes. Given the thickness of the glass slide, no further tool pass was given. The experiments were conducted by varying the electrolyte concentration and the tool feed rate. The applied voltage was kept constant at 40V throughout the experiments.

Initially, exhaustive experiments were conducted to determine the lowest applied voltage required to form a channel. In both first and third tool feeding techniques, discharge between the tool electrode and electrolyte was observed at 30 V. Still, the discharge was observed at 40 V in the case of the second tool feeding technique, and a prominent impression of tool movement was noticed on the workpiece surface. So, to compare three tool-feeding techniques, 40 V was chosen to make a channel in glass. To machine with the ECD process, the tool electrode was initially brought into contact with the glass workpiece, and then the machining depth was set twice, 100 µm each. From trial experiments, it was observed that the tool electrode reached a depth of approximately 100 µm after one pass. So, the machining depth of 100µm was set twice to facilitate the uninterrupted flow of fresh electrolyte and the easy removal of machining products from the machining zone. Several trial experiments were carried out to select the ranges of electrolyte concentration and tool-electrode feed rate. The discharge activity was identified at the lowest possible electrolyte concentration and the highest possible tool feed rate. It was observed that discharges occurred at 5wt% of aqueous NaOH electrolyte and 40 V. The maximum tool feed rate that could remove workpiece material continuously was 70 µm/sec. So, the range of electrolyte concentration from 5 wt% to 20 wt% and that of tool feed rate from 40 to 70 µm/sec were maintained during this experimentation. Before starting the machining, the tool electrode was always properly covered with insulating material to eliminate unwanted discharges from the side surface. If the tool electrode was exposed more to the electrolyte, discharges from its side damaged the workpiece surface. The details of the machining conditions are given in **Table 3. 1**.

Table 3. 1 Details of machining conditions

Items/Parameters	Materials/Value
Workpiece Material	Microscope Glass slide
Tool-electrode Material	Copper
Auxiliary Electrode Material	Graphite
Power Supply	Constant DC
Voltage	40V
Electrolyte	Aqueous NaOH
Electrolyte Concentration (wt %)	5, 10, 15, 20
Feed rate of tool (µm/sec)	40, 50, 60, 70
Inter-electrode gap (IEG)	120mm
Frequency	50 Hz
Duty factor	0.5

All the machined channels were put under the Olympus microscope (Model STM6) (LC 0.1 µm) to measure the channel width and depth. The machined channels were cut transversely to observe their cross-section and depth.

3.3 Numerical Analysis of Gas Film Shape Generation

The Electrochemical discharge phenomenon comprises many complex processes that occur during spark discharge. However, in this article, an in-depth analysis of the shape of the gas film and its effects on channel generation in electrically non-conductive material during ECD milling using a vertically upward tool-feeding technique with a horizontal tool was presented. In the existing tool-feeding technique, the tool electrode is positioned above the workpiece and then moved over its surface. This technique faces major problems, such as unwanted spark discharge at the periphery of the tool electrode and stagnation of the machined material in the machining zone, due to the buoyant force of the electrolyte. Alternatively, the vertically upward tool-feeding technique with a horizontal tool can overcome those limitations during ECD milling. This tool-electrode is placed horizontally, and it moves from bottom to top, releasing the machined products from the sparking zone and improving machining quality.

3.3.1 Gas Film Shape Generation for Existing Tool Feeding Technique

In the existing tool-feeding technique, each researcher employs various facilities, such as ultrasonic vibration, tool rotation, textured tools, and different shapes of tool electrodes, to improve the machining quality of ECDM. Researchers have identified various problems in ECDM, including the formation of a deeper machined channel, a smoother machined channel surface, and the MRR during machining. Some improvements in machining quality and channel depth were obtained by applying different strategies to the basic electrochemical discharge machining setup. The researchers have categorized the channel depth during ECD milling into two regimes: discharge and hydrodynamic. A depth less than 300 μm is called the discharge regime, and a depth greater than 300μm is called the hydrodynamic regime. The removal of material from the workpiece surface was easier in the discharge regime than in the hydrodynamic regime due to hurdles associated with the existing tool-feeding technique. The main problems with this technique were the absence of gas bubbles due to buoyancy in the machining zone and the difficulty of removing the machined product from the zone. The machined product accumulates at the bottom of the machined channel, preventing further entry of fresh electrolytes and halting the machining process. Due to electrochemical reactions and Joule heating in the electrolyte, hydrogen and vapor bubbles must form at the periphery of the tool electrode. The smaller bubbles are deflated to form bigger bubbles and ultimately a gas film due to surface tension and cohesive force. Bubbles always move against gravity due to the buoyant force. The primary forces acting on the gas bubbles and the gas film are buoyancy, surface tension between the gas and liquid, cohesion, and gravity. For the simplicity of the mathematical model, the drag force, cohesive force, or force due to spark discharge, and force due to tool movement were not considered in this article. The forces acting on the gas bubble and gas film are shown in **Fig. 3. 3**.

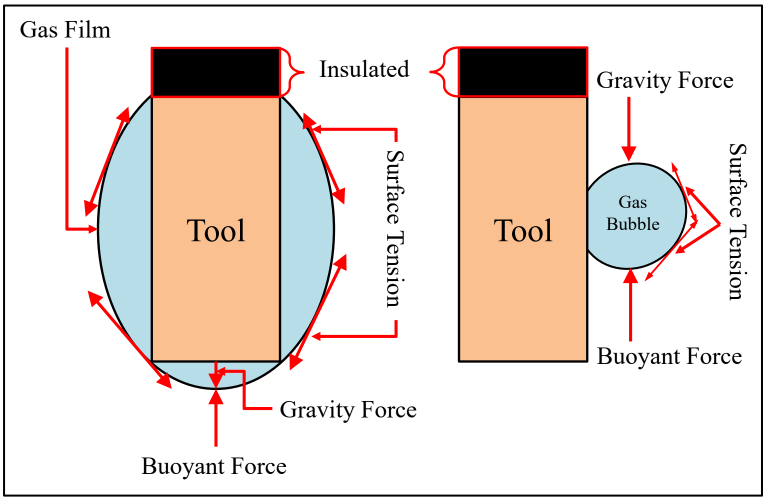

Fig. 3. 3 Schematic diagram of different forces acting on the gas bubble and gas film.

It was also assumed that the size of the generated bubbles that accumulate to form the gas film is equal, for simplicity in the calculation.

According to Archimedes' principle, the buoyant force depends on the volume of the object, which is the volume of the gas film in this case study. It also depends on the density of the liquid and gas. So, the buoyant force can be expressed as in equation (3.1) and shown in **Fig. 3. 3**:

$$F_B = \rho_g V_g \, g \qquad \dots (3.1)$$

Where, V_g is denoted as the volume of the gas film, ρ_g is the density of gas and g is the acceleration due to gravity.

To find out the expression of the gas film volume(V_g), the calculation of equivalent accumulated gas bubbles is required. The shape of a single gas bubble is spherical, and its volume is given by the standard equation (3.2).

$$V_b = \frac{4}{3}\pi r^3 \qquad \dots (3.2)$$

Where, V_b is the volume of a gas bubble and r is the radius of the gas bubble. If N The number of gas bubbles is merged to produce the gas film without overlapping, and the total volume of the gas film is given by the following equation (3.3).

$$V_g = \frac{4}{3}\pi r^3 \times N \qquad \dots (3.3)$$

It was observed that the generated gas film formed a layer around the tool electrode, specifically the cathode. The volume of the gas film was evenly distributed across the tool electrode's exposed area. When the gas film volume was uniformly distributed around the tool-electrode, its surface area became dependent on both the exposed area of the tool-electrode and the tool's diameter, as depicted in the **Fig. 3. 4**.

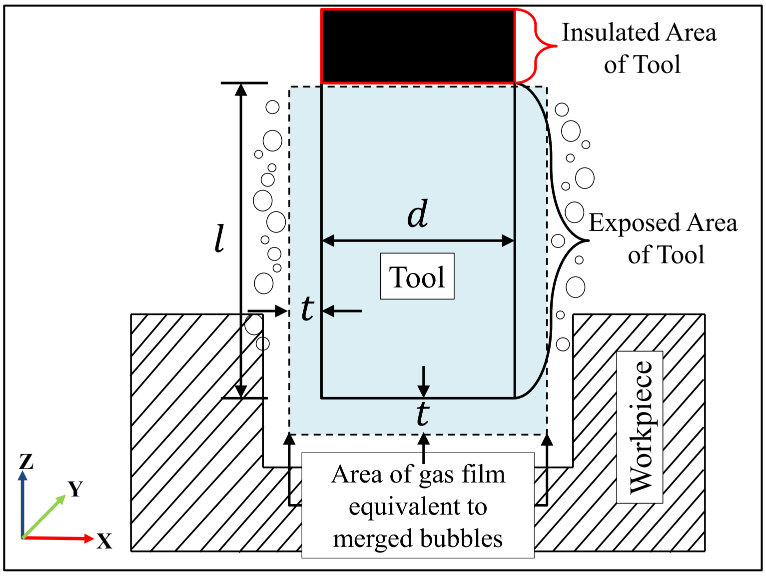

Fig. 3. 4 Schematic representation of the tool-electrode for the existing tool feeding technique with an equivalent area of gas film

The volume of the cylindrical gas film can be expressed differently in equation (3.4) due to the presence of the tool electrode, introducing an additional dimension.

$$V_c = \left\{\frac{\pi(d+2t)^2}{4} \times (l+t)\right\} - \frac{\pi}{4} d^2 l \qquad \dots (3.4)$$

Where V_c denotes the volume of cylindrical gas film, d is denoted as the diameter of the tool electrode, t is the thickness of the equivalent gas film and l is the length of the exposed tool-electrode. The gas film is assumed cylindrical to obtain the equivalent volume of the merged gas bubbles without surface tension, but in reality, the gas film is not cylindrical. According to fluid properties, the shape of a gas film or gas bubbles tends to minimize their surface area due to surface tension. The same phenomenon occurs with the generated gas film, which reduces its surface area as it converges toward the edge of the tool electrode, and no other sharp edge is present due to surface tension. Due to surface area convergence into a possible minimum value, the gas film will be reduced to a sphere with the same volume as a cylindrical gas film. The volume of a spherical gas film of radius R can be expressed as equation (3.5)

$$V_{sph} = \frac{4\pi}{3} R^3 - \frac{\pi}{4} d^2 l \qquad \dots (3.5)$$

Where, R is the radius of the spherical gas film and V_{sph} is the volume of spherical gas film. As the volume of gas film is the same for cylindrical and spherical shapes, from equations (4) and (5), the expression for the radius of the spherical-shaped gas film can be obtained as given in equation (3.6).

$$R^3 = \frac{3}{16}\{(d + 2t)^2(l + t)\} \quad \ldots (3.6)$$

Due to the presence of surface tension in the gas film, the film eventually took a curved shape, which is schematically represented in **Fig. 3. 5**.

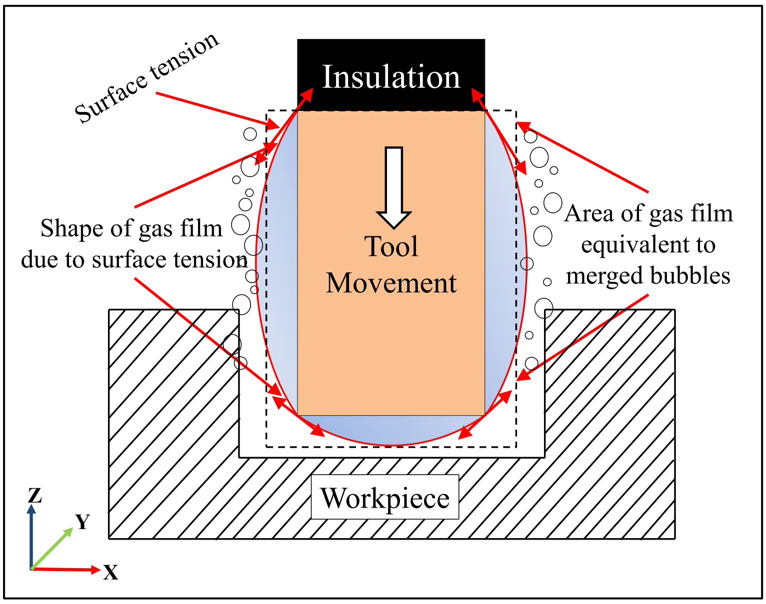

Fig. 3. 5 Schematic representation of the gas film shape due to surface tension for the existing tool feeding technique

From eq. (3.1) and (3.5), the final expression of the buoyant force can be expressed as (3.7)

$$F_B = \left[\left\{\frac{\pi}{4}\,(d + 2t)^2(l + t)\right\} - \frac{\pi}{4}d^2 l\right]\rho_g \times g \quad \ldots (3.7)$$

Furthermore, the buoyant force significantly impacted the shape of the gas film formed. This buoyant force acted on the generated gas film and influenced its shape. The gas film, which transformed due to surface tension, became more flattened at the tip of the tool-electrode when the buoyant force was introduced, as depicted in **Fig. 3. 6(a)**. Additionally, the buoyant force increased the thickness of the gas film around the tool electrode. Consequently, the shape of the gas film changes, resulting in a thinner film at the tool tip and a thicker film at the periphery of the tool electrode. The gas film that was generated during ECD milling was captured and compared with the numerically modeled gas film where many similarities are observed in terms of shape of the gas film during existing tool feeding technique as illustrated in **Fig. 3. 6(b)**.

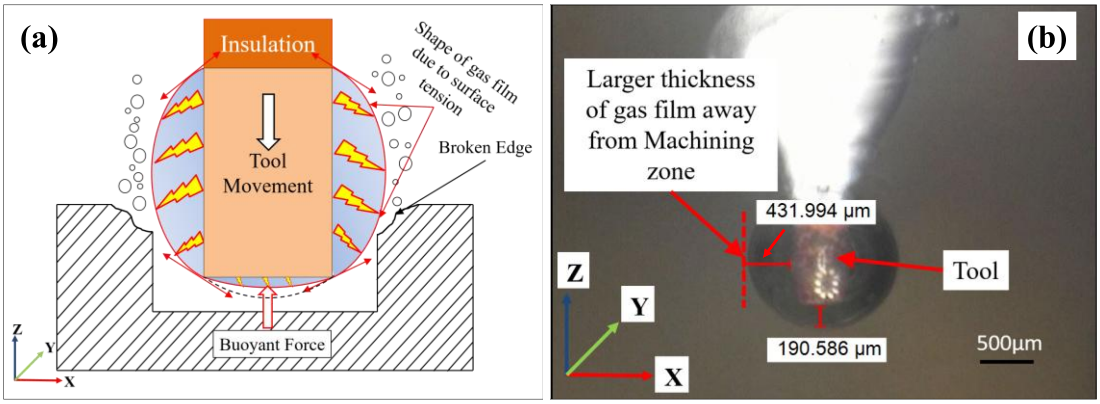

Fig. 3. 6 Shape of gas film due to surface tension and buoyant force for existing tool feeding technique (a) Schematic View and (b) Photographic view

The actual image also reveals that the thickness of the generated gas film around the tool electrode's periphery is larger than the thickness of the gas film at the tool tip. The thickness of the gas film around the periphery of the tool electrode was 431.994 µm, and at the tool tip, it was 190.586 µm. This kind of shape change in the gas film significantly affected the machined channel.

3.3.2 Gas Film Shape Generation for Bottom Tool Feeding Technique

In the bottom-tool feeding technique, the gas film shape differs from that of the existing tool-feeding technique. This difference in gas-film shape led to changes in machining performance across different tool-feeding techniques. The buoyant force, along with surface tension, plays an important role in determining the shapes of gas films. The schematic of the gas film shape during the bottom tool feeding technique is shown in **Fig. 3. 7(a)**. The shape of the gas film in bottom tool feeding technique protrude towards electrolyte surface and creates larger thickness of gas film at the tool electrode tip. This is also evidenced by the actual image of gas film during bottom tool feeding technique as shown in **Fig. 3. 7(b)**. The voltage required to break the protruded portion of the gas film is more than the gas film generated in existing tool feeding technique. The greater the energy of the spark discharge during the breakage of the protruded gas film, the greater its impact on machining performance under different tool feeding techniques. During bottom-tool feeding, the machined product is released from the machining zone by gravity as the tool feeds upward.

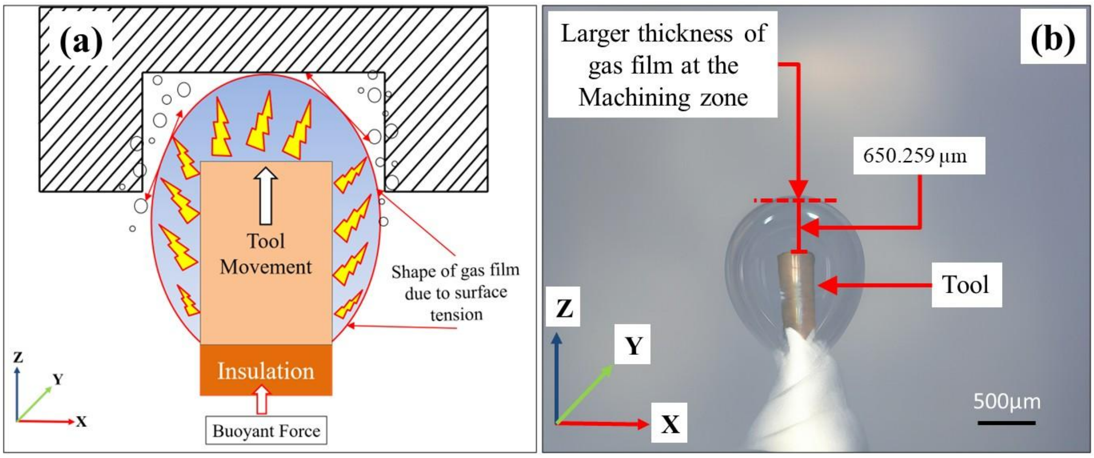

Fig. 3. 7 Shape of gas film due to surface tension and buoyant force for bottom tool feeding technique (a) Schematic View and (b) Photographic view

There are also some shortcomings in the bottom tool-feeding technique, including the thicker gas film. In this technique, the workpiece is placed over the tool tip, which prevents gas bubbles from escaping the machining zone and accumulating to form a larger, thicker gas film, thereby affecting machining quality during bottom tool feeding.

3.3.3 Gas Film Shape Generation for Upward Tool Feeding with Horizontal Tool

The gas film generation and spark discharge occur under different conditions in the newly developed novel tool-feeding technique, i.e., vertically upward tool feeding. The problems in the existing tool-feeding technique have been stated previously, and they can be overcome by using the novel tool-feeding technique. The tool electrode was kept horizontal and moved upward to achieve advantages for ECD milling. The dotted line that has been shown in **Fig. 3. 8(a)** is the gas film shape and thickness without buoyant force, according to equation (3.6), which is similar to the existing tool-feeding technique but in a different orientation. The shape of the gas film was further protruded towards the upward direction due to the buoyant force, as schematically depicted in **Fig. 3. 8(a)**. It is also noticeable from the actual image of the gas film, as shown in **Fig. 3. 8(b)** that the protruded portion is present towards the tool movement direction or towards the direction where machining is to be carried out. The advantage of this gas film shape was that the intense spark discharge, or the higher-energy spark discharge, occurred at the tool tip or the upper portion of the tool electrode.

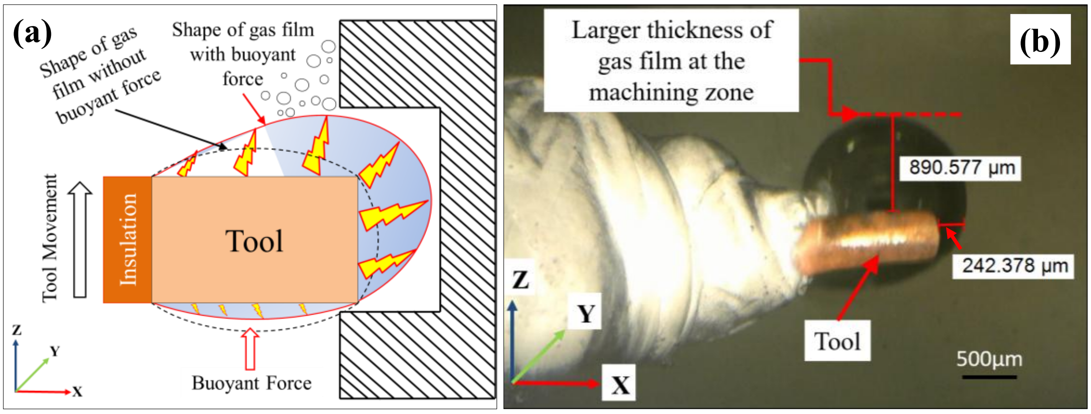

Fig. 3. 8 Shape of gas film due to surface tension and buoyant force for vertically upward tool feeding technique (a) Schematic view (b) Photographic view

Besides the advantageous shape of the gas film, the vertically upward tool feeding technique could help to remove machined materials from the machining zone due to gravity force, which allowed the replacement of new electrolytes into the machining zone which accelerated the machining process.

3.4 Simulation on the Temperature Distribution for Generated Gas Film Shapes

The nature and shape of the gas film during machining with both the existing and vertically upward tool-feeding techniques were analyzed in this study. Buoyancy plays a crucial role in determining the shape of the gas film across different tool-feeding techniques. A 2D computer simulation was performed using COMSOL Multiphysics 5.6 to numerically model the gas film and study the electrical field and temperature distribution along the gas film boundary for various tool feeding techniques. Several assumptions that were made for the simulation are as follows:

(i) The tool electrode material was homogeneous copper,

(ii) The gas film consisted of hydrogen gas,

(iii) The simulation considered the Equilibrium DC Discharge physics model, which accounts for the combined effects of electrostatics and heat transfer in fluids.

The simulation utilized a specific geometry for the existing tool feeding technique, represented by a finer physics-controlled mesh in **Fig. 3. 9(a)**, while **Fig. 3. 9(b)** and **Fig. 3. 9(c)** displays the corresponding geometry for the bottom tool and the vertically upward tool feeding technique, respectively.

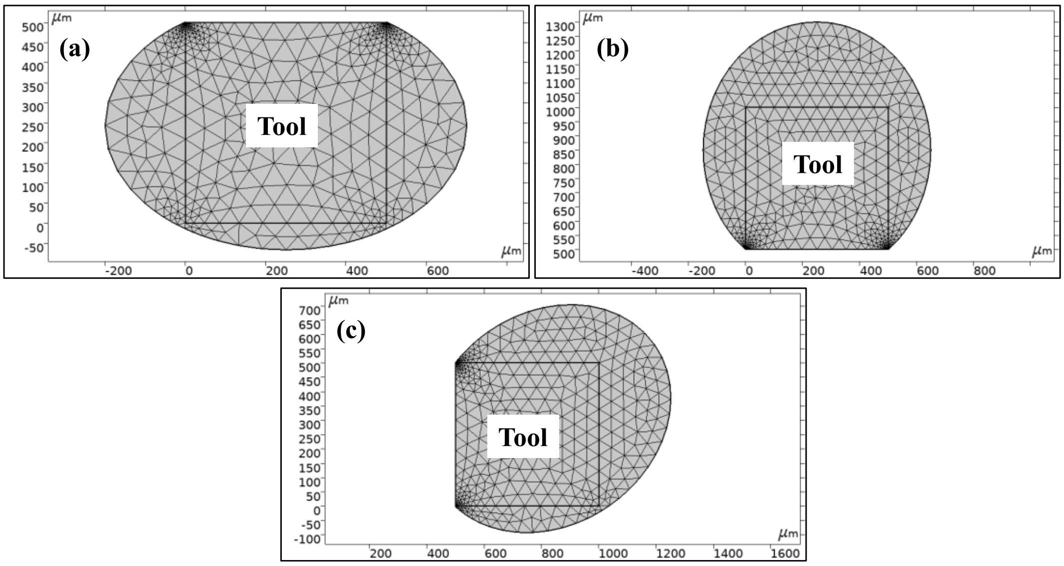

Fig. 3. 9 Geometry and mesh of (a) existing tool feeding, (b) bottom tool feeding, and (c) upward tool feeding with horizontal tool

After the simulation, the electric potential and temperature distributions were obtained, clarifying the effects of the gas film size and shape on heat and temperature variations over the gas film surface due to spark discharge. **Fig. 3. 10(a)** demonstrates the surface temperature for the existing tool-feeding technique at 0.001s and 30V of applied voltage, indicating a higher temperature around the periphery of the tool electrode than at the tool tip.

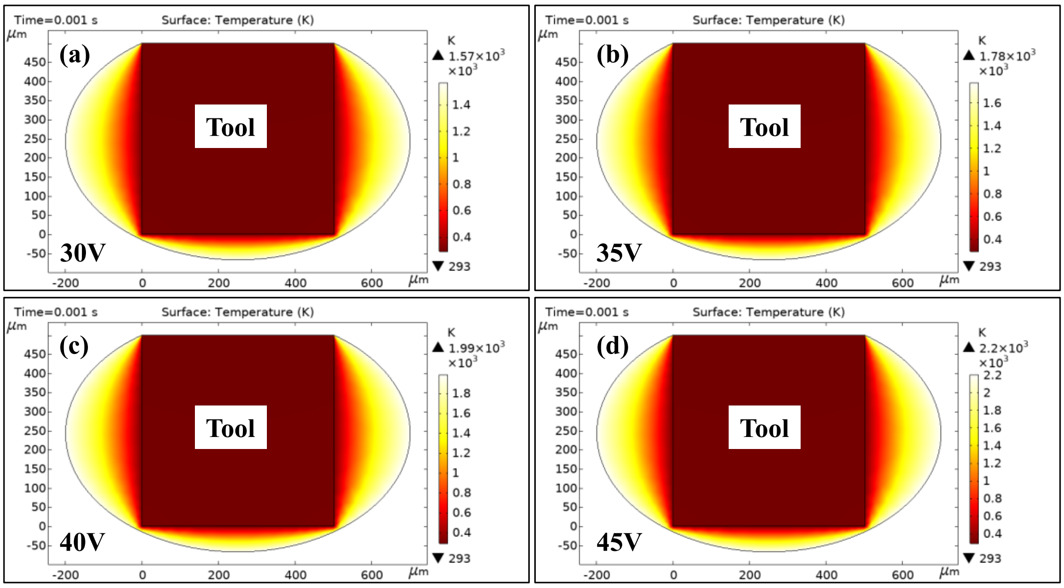

Fig. 3. 10 Simulated results of surface temperature distribution during the existing tool feeding technique at (a) 30 V, (b) 35V, (c) 40V, and (d) 45V

The maximum temperature was reached about 1.57×10^3K at 30V of applied voltage. The temperature of the spark discharge increased as the voltage was increased and reached up to 1.78×10^3K at 35 V as shown in **Fig. 3. 10(b)**. Further, the temperature was increased and reached up to 1.99×10^3K as shown in **Fig. 3. 10(c)** and 2.22×10^3K as shown in **Fig. 3. 10(d)** as the applied voltage was increased up to 40V and 45V respectively. This particular temperature distribution led to increased spark discharge intensity around the tool electrode periphery under the existing tool-feeding technique. Furthermore, the analysis revealed that, due to the shape of the gas film, higher temperatures are distributed along the gas film boundary, farthest from the tool electrode. **Fig. 3. 11(a)** to **Fig. 3. 11(d)** show a higher temperature line around the periphery of the tool electrode rather than the tool electrode tip or the machining zone for different applied voltages during the existing tool feeding technique.

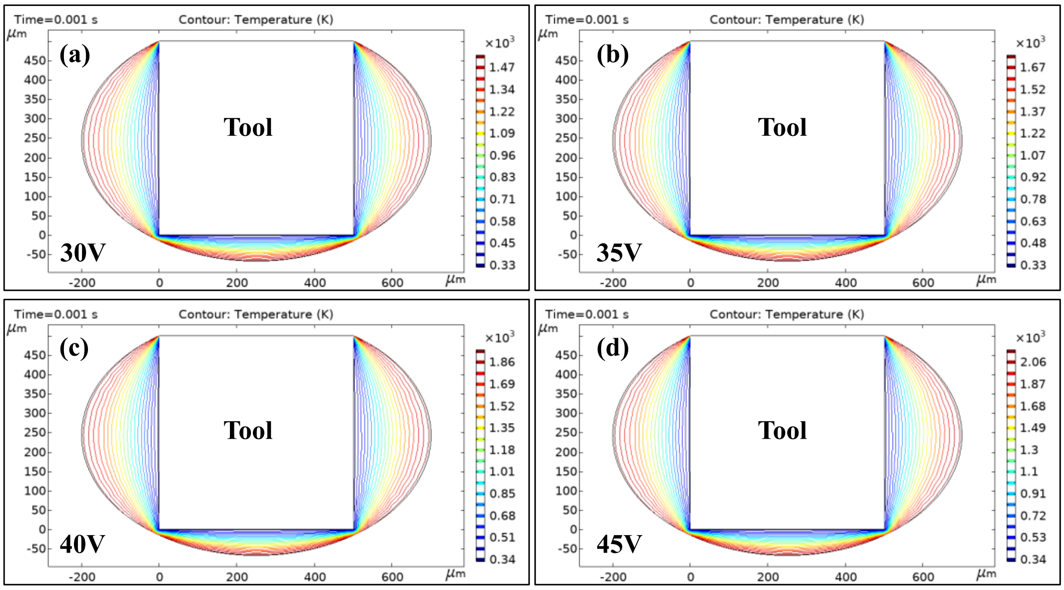

Fig. 3. 11 Simulated results of temperature contour diagram during existing tool feeding technique at (a) 30 V, (b) 35V, (c) 40V and (d) 45V

On the other hand, the bottom upward tool feeding technique resulted in a higher temperature distribution along the gas film border near the tool tip at 30V, as illustrated in **Fig. 3. 12(a),** leading to intense spark discharge at the machining zone and enhancement of material removal rate from the workpiece. The temperature rises up to 1.55×10^3K for 30V of applied voltage. The temperature increase was also noticeable as the applied voltage was raised from 30V to 45V. **Fig. 3. 12(b)** shows the simulated results at 35V where the temperature rises up to 1.76×10^3K. Similarly, at 40V and 45V applied voltage the temperature upsurges up to 1.97×10^3K and 2.18×10^3K as shown in **Fig. 3. 12(c)** and **Fig. 3. 12(d),** respectively.

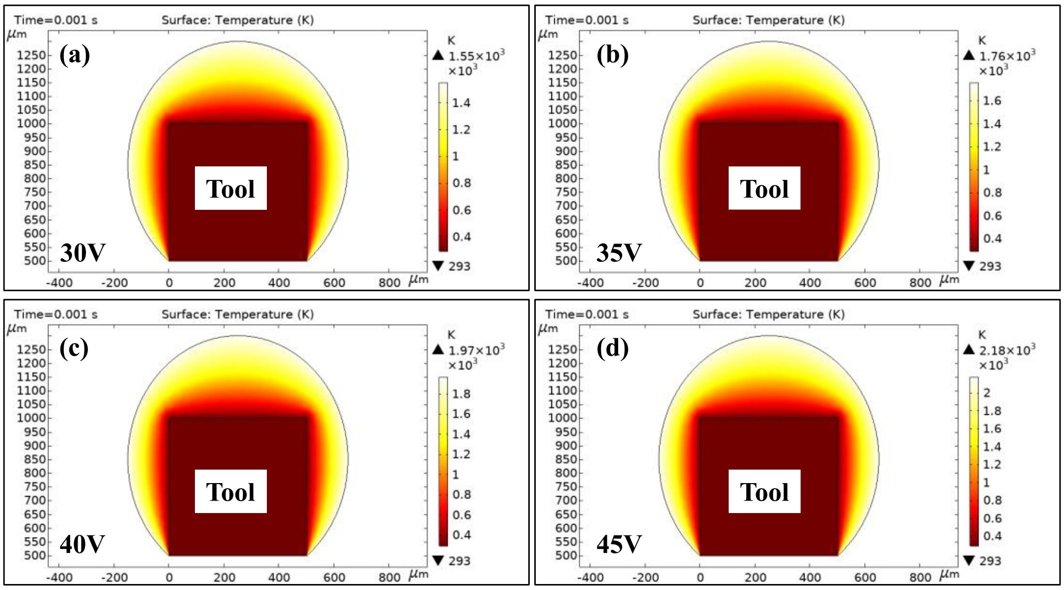

Fig. 3. 12 Simulated results of surface temperature distribution during bottom tool feeding technique at (a) 30 V, (b) 35V, (c) 40V, and (d) 45V

The temperature contour diagram also evidenced that the maximum temperature line is present at the tool electrode tip at 30V, as shown in **Fig. 3. 13(a)** and the thickness of the gas film is also higher at the tool electrode tip or in the machining zone. This result was similar for other applied voltages such as 35V, 40V, and 45V, as shown in **Fig. 3. 13(b), Fig. 3. 13(c),** and **Fig. 3. 13(d)** respectively. The bottom-tool feeding technique resulted in higher energy spark discharge, which helped remove material from the workpiece during ECD milling. There are some shortcomings in the bottom-tool feeding technique, including the accumulation of gas bubbles in the machining zone or their entrapment near the tool electrode. This entrapment led to the formation of larger gas bubbles or a gas film, resulting in abrupt or uncontrolled spark discharges. Besides these abrupt spark discharges, bottom-tool feeding can also generate side spark discharges and may reduce machining quality during ECD milling with this technique. Simulation results for the upward tool-feeding technique showed that the temperature around the gas film layer during ECD milling was higher in the machining area or at the tool tip.

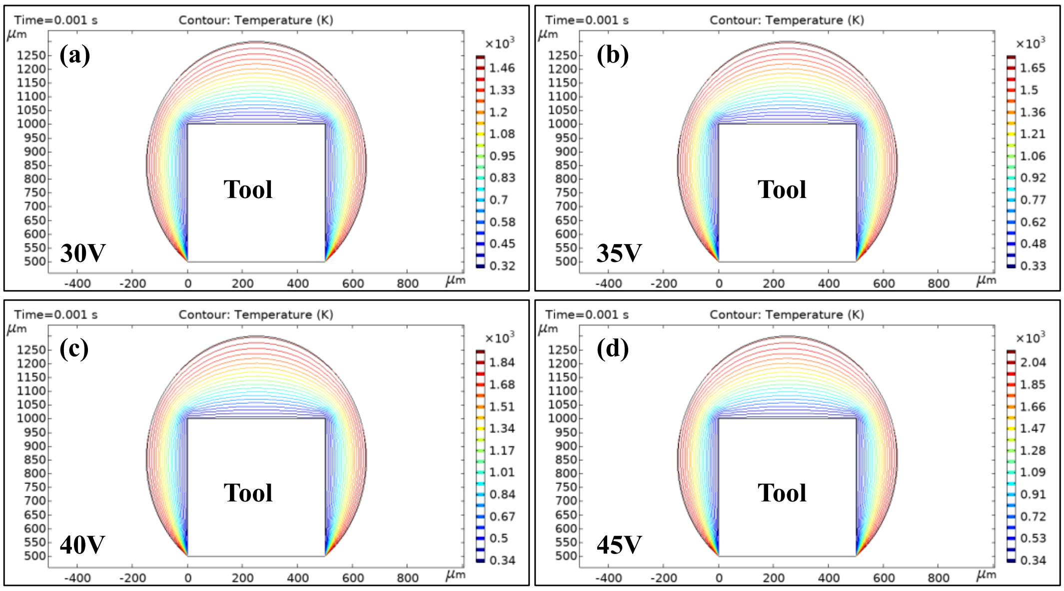

Fig. 3. 13 Simulated results of temperature contour diagram during bottom tool feeding technique at (a) 30 V, (b) 35V, (c) 40V, and (d) 45V

The temperature distribution around the gas film is the key factor in the removal of materials from the workpiece. **Fig. 3. 14(a)** shows the temperature distribution during upward tool feeding technique at 30V of applied voltage where the maximum temperature was reached about 1.56×10^3K. Unlike other tool feeding techniques, the temperature was increased in upward tool feeding technique also as the voltage was increased and reached up to 2.2×10^3K at 45V of applied voltage as shown in **Fig. 3. 14(d)**.

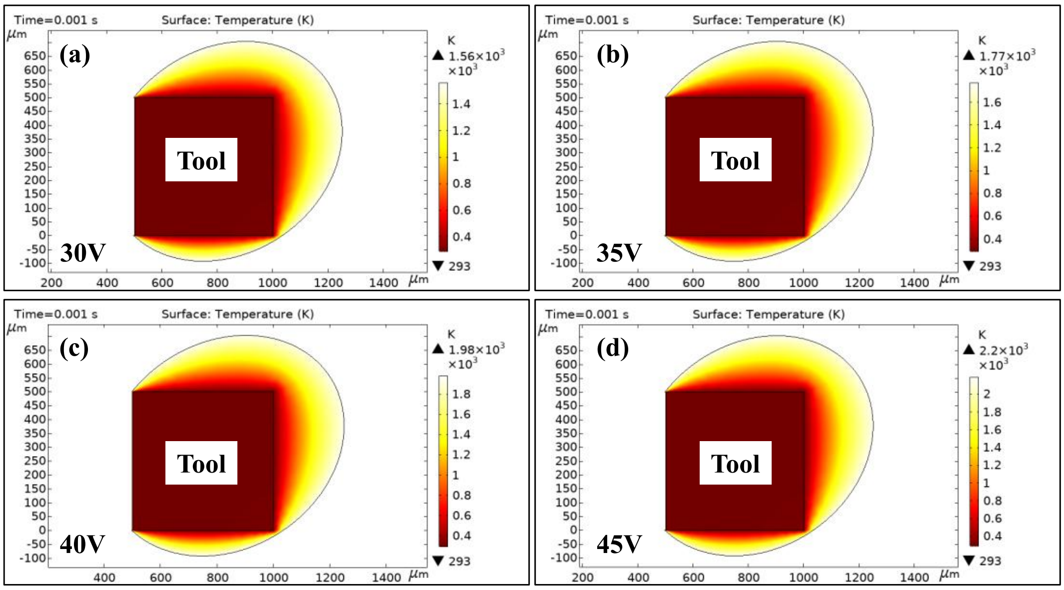

Fig. 3. 14 Simulated results of surface temperature distribution during upward tool feeding technique at (a) 30 V, (b) 35V, (c) 40V and (d) 45V

For every case during upward tool feeding technique as shown in **Fig. 3. 14(b)** and **Fig. 3. 14(c)** the maximum temperature was distributed towards the machining area or the tool tip which enhanced the machining performances. The temperature contour diagram of simulated results also revealed that the presence of maximum temperature line is near the machining zone during ECD milling with upward tool feeding technique as shown in **Fig. 3. 15(a)** at 30V. The lower temperature line is observed near the tool electrode surface around its periphery as shown in **Fig. 3. 15(b)** at 35V and it is similar for each applied voltage. This temperature distribution offers a significant advantage during ECD milling using the upward tool-feeding technique. Similar like 30V and 35V of applied voltage the maximum temperature distribution was observed around the tool electrode near tool tip for 40V and 45V of applied voltage as shown in **Fig. 3. 15(c)** and **Fig. 3. 15(d)** respectively.

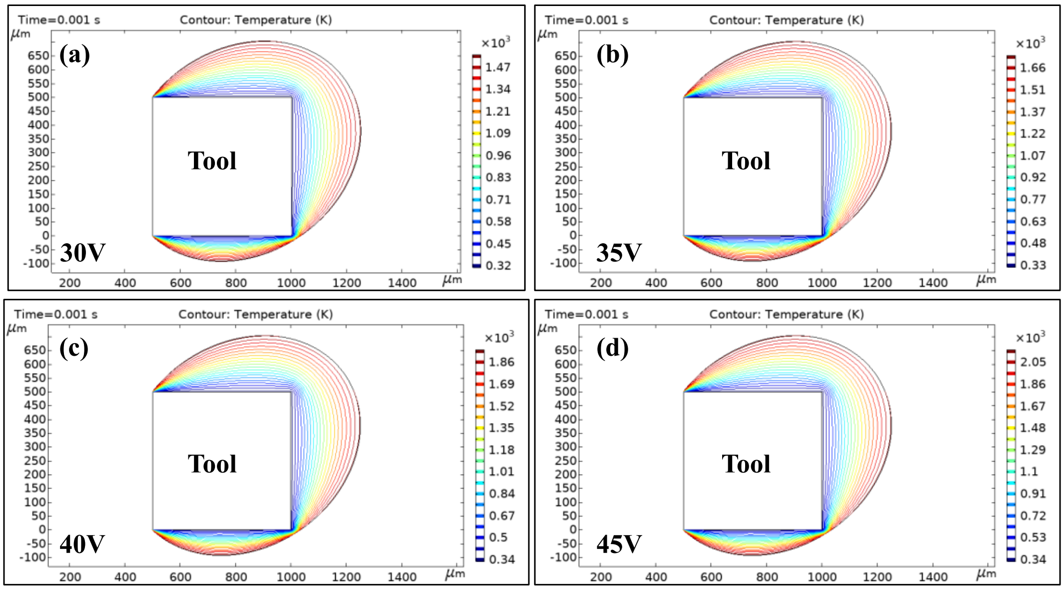

Fig. 3. 15 Simulated results of temperature contour diagram during upward tool feeding technique at (a) 30 V, (b) 35V, (c) 40V and (d) 45V

The simulation of three different tool feeding techniques confirmed the superiority of the upward tool feeding technique, which leverages the buoyancy and surface tension of the liquid to generate its unique shape. The buoyancy of the electrolyte can be leveraged to advantage in machining with the upward tool-feeding technique.

3.5 Results and Discussions

The spark discharges for different tool-feeding techniques, along with the effects of electrolyte concentration and tool feed rate on channel width and depth, have been analyzed during the ECD milling process. The impact of various tool feeding techniques on tool electrode wear was also investigated to identify a superior feeding method in ECD milling.

3.5.1 Electrochemical Spark Discharge for Different Tool Feeding Techniques

The most prominent factor of ECDM process is the generation of gas bubbles and gas film. During the experiment, when voltage is applied between the cathode (tool-electrode) and anode (auxiliary electrode), electrochemical reactions occur as both the cathode and anode are immersed in electrolyte at a certain distance apart. Due to the electrolysis process, hydrogen gas forms at the cathode and comes out. Also, vapor bubbles are formed due to joule heating or nucleate boiling of electrolyte. The number of bubbles increases with an increase in nucleation, which increases with an increase in applied voltage. Both the hydrogen gas and vapor bubbles are dispersed due to cohesion. These generated bubbles were accumulated around the tool-electrode and coalesced to produce the gas film when the voltage was increased. The gas film was broken down at a certain voltage, and electrons from the cathode jumped to the electrolyte, which is seen in the form of light. This phenomenon is referred to as discharge activity between the tool-electrode and the electrolyte. For other two techniques (bottom tool feeding and upward tool feeding), the gas film generation and discharge occurred in the same way as that took place for existing tool feeding due to electrochemical reactions and joule heating or nucleate boiling of electrolyte. The difference was the presence of gas bubbles in the machining zone. In the case of the existing tool feeding technique, the gas bubbles moved away from the tool-electrode tip due to buoyancy and a sufficient number of bubbles were not present at the machining zone. So, little spark discharges were concentrated at the tool tip rather than the scattered and uncontrollable discharge was observed at different regions of tool-electrode exposed to electrolyte during existing tool feeding of tool-electrode. But the machining with bottom tool feeding and upward tool feeding could be done at a deep region of electrolyte since there was high possibility of gas bubbles being assembled at the contact surface of workpiece and tool-electrode in the upward tool and bottom tool feeding techniques. Due to the buoyant force, bubbles reached at the tool-electrode tip end quickly to coalesce into an insulating gas film. More amount of gas bubbles was accumulated and formed thicker gas film during bottom tool feeding of the tool-electrode due to the presence of workpiece on the top of tool-electrode and this led to form dense, vigorous and uncontrolled discharges. In case of upward tool feeding, unwanted bubbles were free to escape out from the machining zone due to buoyancy of liquid that allowed the smaller bubbles to form thinner gas film and produce controllable discharge. So, more controlled spark discharges were found in the upward tool feeding technique than in the existing tool feeding and bottom tool feeding techniques. The spark discharges were captured during machining with three different technique and shown in the **Fig. 3. 16.**

Fig. 3. 16 Spark discharges for different feeding techniques at 15wt% NaOH and 30V (a) existing tool feeding (b) bottom tool feeding (c) upward tool feeding.

It was observed that during the bottom tool feeding, the spark discharge was noticed significantly at about 40V, as shown in **Fig. 3. 16(b).** The gas bubbles generation and spark discharge were observed in case of upward tool feeding, also as shown in **Fig. 3. 16(c).** More discharges were found at the upper portion of tool-electrode due to the presence of gas bubbles in that zone.

3.5.2 Effect of Electrolyte Concentration on Channel Width

The electrical conductivity of electrolyte solution is an important factor in ECDM process since the concentration can alter the electrical conductivity of electrolyte solution and influence the machining quality. If the electrolyte concentration is increased, the amount of sodium ion (Na^+) as well as hydroxyl ion (OH^-) is increased in the aqueous NaOH due to enhancement of chemical reactions and these promote the rise of electrical conductivity of electrolyte solution. The higher electrolyte concentration boosts the evolution of hydrogen gas bubbles at the tool-electrode and thereby diminishes the critical voltage to initiate the spark discharges. Though the channel width was increased in all three techniques with the increase of electrolyte concentration, overcut was found to reduce only during the upward tool feeding of tool-electrode. In all cases the channel width is found to be higher for 20wt% of NaOH solution. Comparatively larger channel width or overcut was obtained during machining with bottom tool feeding technique but the edge of machined channel was smoother than that obtained during existing tool feeding technique. A lot of peaks and valleys on the channel edge were noticed at lower concentrations of electrolyte, and this indicated the irregular removal of material at lower concentrations. The machining at lower concentration of electrolyte the width of channel was lower and less significant deviation was observed at 15wt% NaOH solution as per **Fig. 3. 17(a)**. A smaller deviation was observed at the 10 wt% concentration. Bottom tool feeding technique provided narrower channel width with bigger deviation at 5wt% concentration as shown in the **Fig. 3. 17(b).** The width of the channel was found lower than tool-electrode diameter at lower concentration due to absence of sufficient spark discharge.

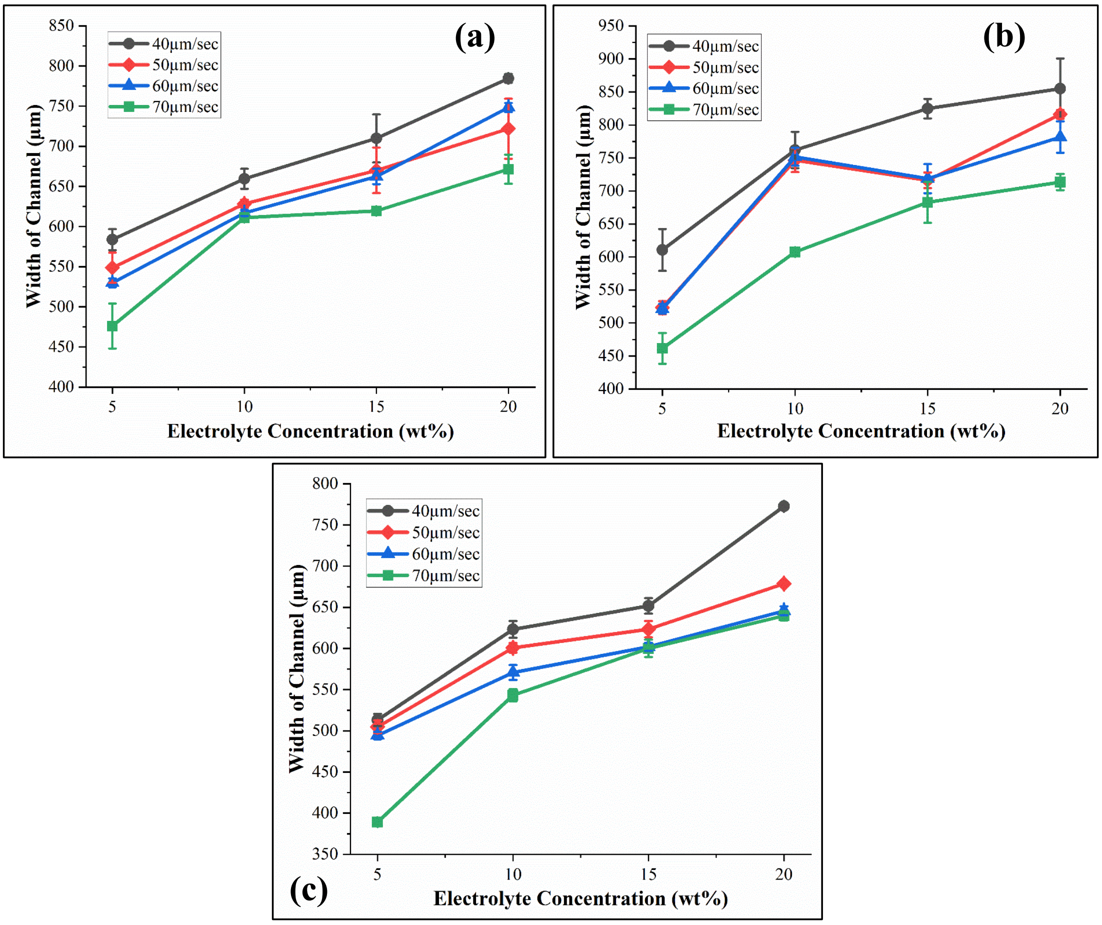

Fig. 3. 17 Effect of electrolyte concentration on channel width for different feeding technique, (a) Existing tool feeding, (b) Bottom tool feeding, (c) Upward tool feeding

A massive number of bubbles were stuck during bottom tool feeding as the generated gas bubbles could not escape from the surface due to the presence of workpiece above the tool-electrode. These accumulated gas bubbles created a thicker gas film. The accumulation of bubbles cannot be controlled at different location; as a result, it provides larger width deviation during channeling with bottom tool feeding technique. A smaller deviation was observed when upward tool feeding was introduced in the ECDM process. The upward tool feeding technique allowed the generated gas bubbles to move up to the top surface of electrolyte by avoiding a large accumulation of bubbles. **Fig. 3. 17(c)** shows that at 15wt% electrolyte concentration the deviations in channel width are smaller for upward tool feeding technique and the generated channel edge is found smoother than others. Optical images of machined channels are given in the **Fig. 3. 18** for three kinds of feeding technique.

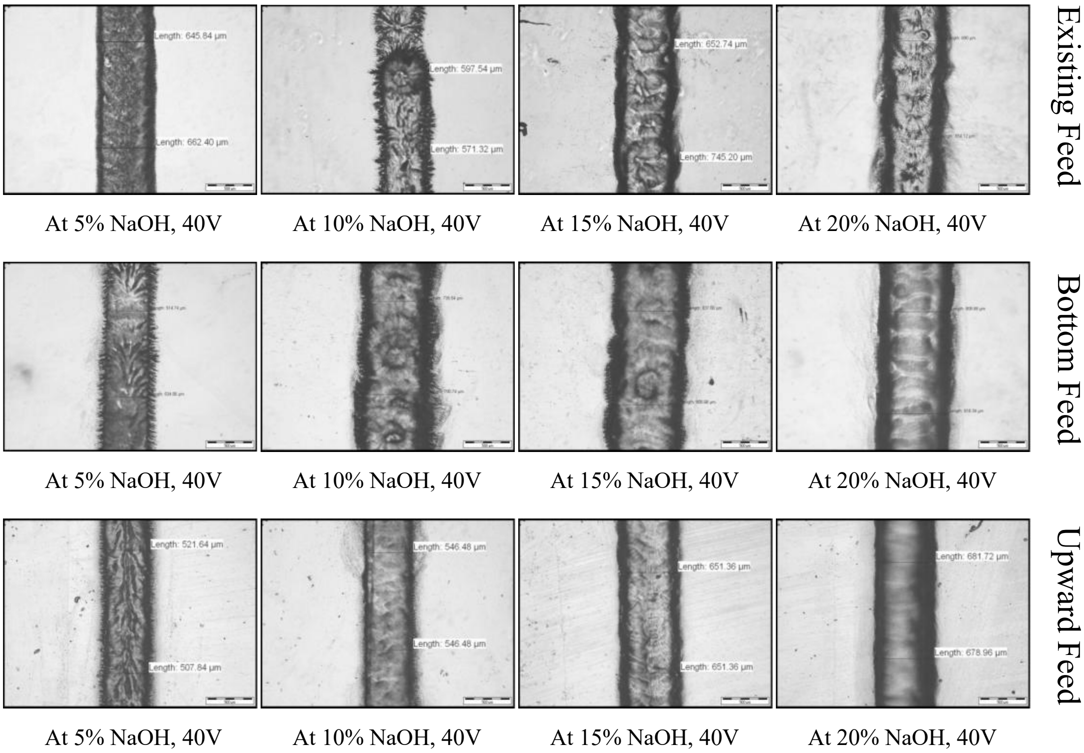

Fig. 3. 18 Optical images of channels during different tool feeding technique

3.5.3 Effect of Feed Rate of Tool on Channel Width

The feed rate of tool is responsible for the tool and workpiece contact time, which is a deciding factor for making a bigger or smaller channel width. The generated discharges strike the work surface very frequently at lower feed rate, which removes more amount of materials from the surface of glass workpiece. The frequency of spark discharge is reduced at higher feed rate of tool. **Fig. 3. 19(a)** and **Fig. 3. 19(b)** show the variation of channel width against feed rate during existing tool feeding and bottom tool feeding technique. At lower feed rate of tool, the width was bigger and it was smaller at higher feed rate of tool but the error bar was bigger in case of existing tool feeding and in bottom tool feeding. In both top and bottom tool feeding the channel width is increased with decrease in feed rate and decreased with an increase in feed rate of tool but at some points channel width increased at lower feed rate of tool. This type of irregularities was observed during top and bottom tool feedings and indicated uncontrollable discharge. **Fig. 3. 19(c)** shows the channel width against different feed rate for upward tool feeding technique and it was observed that at 10wt% and 15wt% concentration was linear which indicated smaller deviation during upward tool feeding.

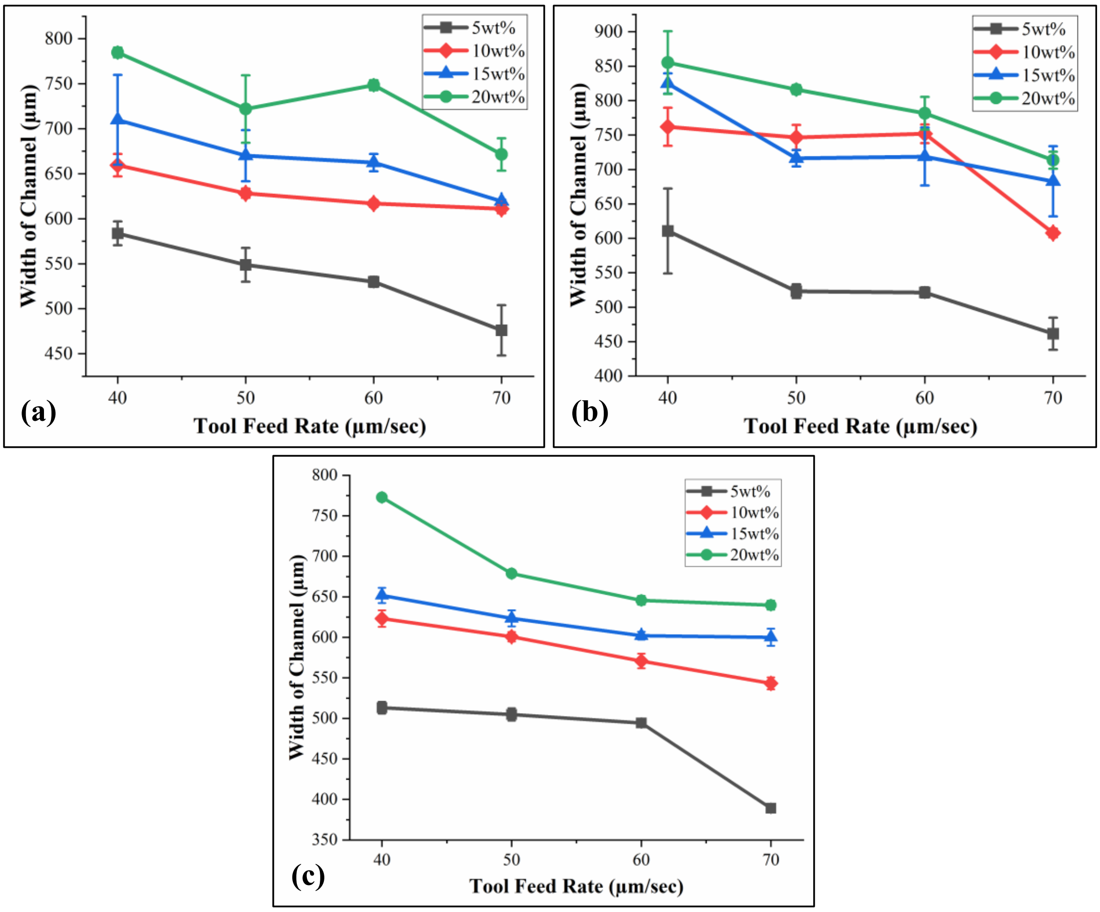

Fig. 3. 19 Effect of feed rate of tool on channel width for different electrolyte concentration, (a) Existing tool feeding, (b) Bottom tool feeding, (c) Upward tool feeding

The tool-electrode was moved quickly at higher tool feed rate without removing material from the workpiece which caused lower width of channel than tool-electrode diameter. If the tool-electrode moves slowly over the work surface then the amount of discharge at a particular region increases. These extra discharges remove more materials from the surface. It is needed to increase the tool movement or feed rate of tool to reduce the overcut. The materials were removed from the edge of the channel differently at different tool-feed rates which generated different edge profiles for different techniques.

3.5.4 Comparisons of Width and Depth among Three Tool Feeding Techniques

Different tool feeding techniques resulted in various width and depth of channel during ECD milling. Comparative analysis has been carried out among various tool-feeding techniques to identify the best or most appropriate technique for ECD milling.

3.5.4.1 Comparisons of Channel Width

The channel width was found to be smaller at higher feed rate of tool (70µm/sec) and was bigger at lower feed rate of tool (40µm/sec). It was observed that for machining with feed rate of 70µm/sec generated very small craters on the workpiece surface. For that speed the removal of materials was not found in some cases when machining was done from top surface. Material removal was taken place at the same conditions when machining was done from bottom surface as well as from side surface. It is more or less established by previous researchers that the generated gas bubbles come out from the tool-electrode tip due to buoyancy during machining with existing tool feeding. A lot of extra features are needed to add to the basic system to control these gas bubbles and gas film in existing tool feeding technique. Removal of machined product from the machining zone is also a challenging factor in existing tool feeding technique and to do that a proper flushing is required. The presence of gas bubbles at the tool-electrode tip makes the discharge easier at the deeper machining zone. In the bottom tool feeding technique the channel width was increased about 22% as compared to that of existing tool feeding technique. But the width was further reduced by 11% during upward tool feeding technique. **Fig. 3. 20** exhibits the channel width at different feed rates of tool for three techniques. In existing tool feeding technique materials removal irregularly took place from the job surface and it led to uneven channel edge as shown in the **Fig. 3. 20(a)**. Due to that, the channel width became different at different locations of tool-electrode during machining. Higher depth of channel was obtained in bottom tool feeding technique than that of existing tool feeding technique but the overcut was also found to be higher in that case, as shown in **Fig. 3. 20(b)**. The smoother edges of machined channel with lower channel width were obtained in case of side feeding as shown in **Fig. 3. 20(c).** The straightness of the channel edge was also improved in upward tool feeding technique. The gas bubbles always were adhered to the tool tip during bottom tool feeding and it provided larger amount of bubble's accumulation to form a thicker gas film that led to larger channel width. The main drawback of bottom tool feeding technique was the development of larger overcut, but the edge of the channel was found as smoother than existing tool feeding technique.

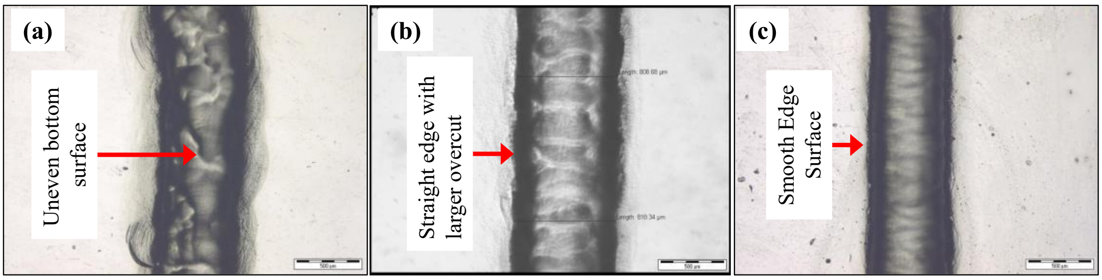

Fig. 3. 20 Optical images of machined channels (a) Existing tool feeding, (b) Bottom tool feeding, (c) Upward tool feeding

Despite of large channel width as shown in **Fig. 3. 21(a)**, the bottom tool feeding technique provided comparatively low undulated edge surface, which indicated the generation of uniform gas film and control discharge activity during machining with this technique. The drawback of bottom tool feeding technique was reduced further in upward tool feeding technique where the depth was obtained with considerable amount of overcut as shown in **Fig. 3. 21(c).**

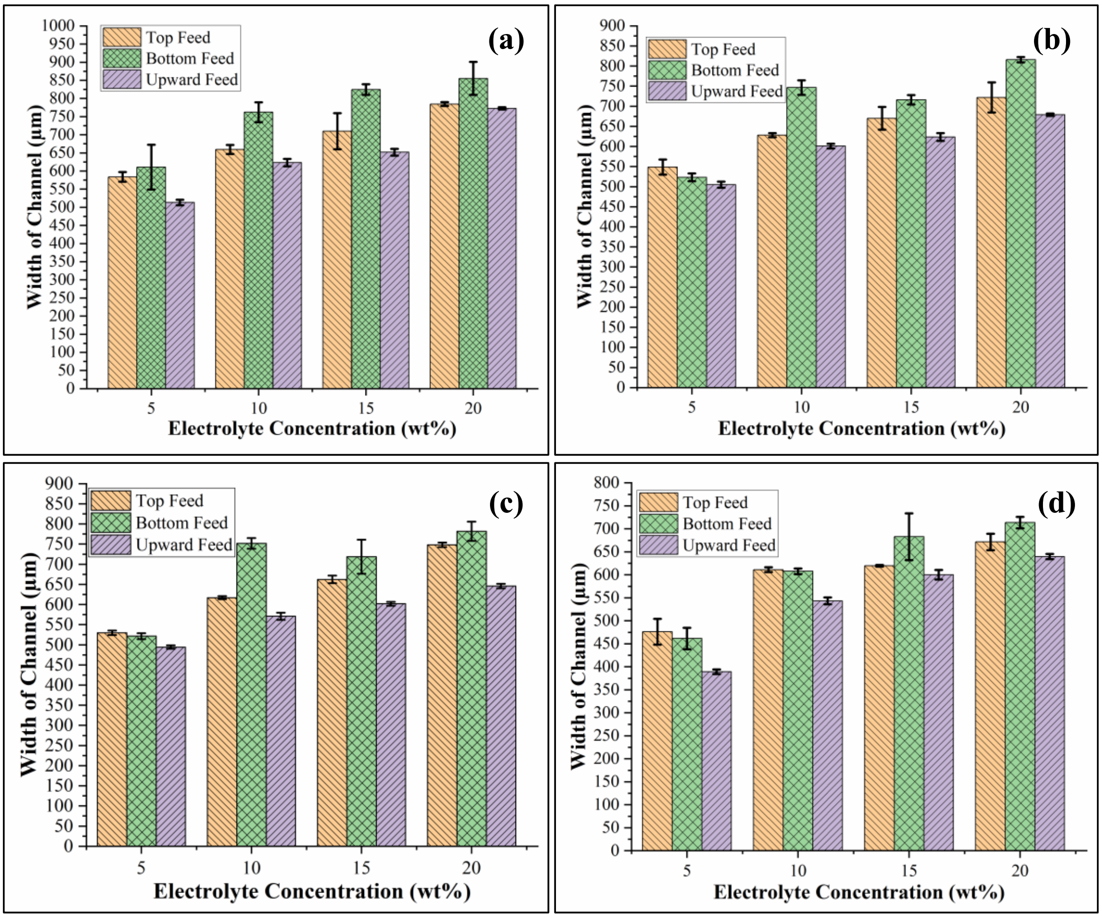

Fig. 3. 21 Width of channel for different tool feeding (a) 40 μm/sec tool feed rate, (b) 50 μm/sec tool feed rate, (c) 60 μm/sec tool feed rate, (d) 70 μm/sec tool feed rate

During upward tool feeding, the generated gas bubbles were free to come over the surface and chance of larger accumulation of bubbles was reduced. It was also noticed that the edge of the channel in upward tool feeding was smoother and straighter than bottom tool feeding. The variation of width of channel width was unpredictable for both top and bottom tool feedings if the feed rate of tool was increased except upward tool feeding technique. Further, smooth improvement in width of channels was noticed in case of upward tool feeding. Therefore, the upward tool feeding technique may be considered as the best feeding technique for ECD milling process. **Fig. 3. 21** shows that the lower channel width is found in upward tool feeding technique than top and bottom tool feeding techniques.

3.5.4.2 Comparison of Depth of Channel

In existing tool feeding technique, the minimum depth of the channel was found as 128.34µm at electrolyte concentration of 10wt% and feed rate of tool of 70µm/sec with an aspect ratio (height: width) of 1:3.7. The **Fig. 3. 22** shows the machining depth for three tool feeding technique.

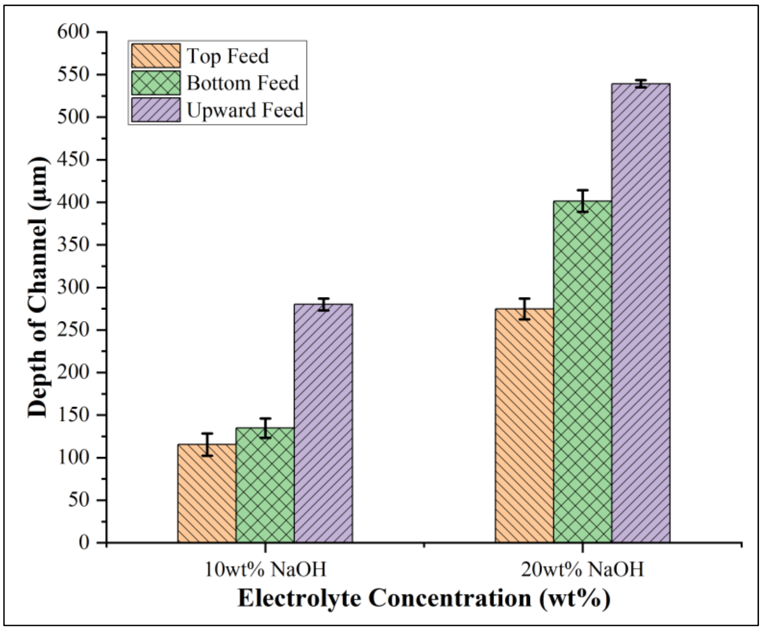

Fig. 3. 22 Channel depth for different kinds of feeding technique

The maximum depth of channel was obtained as 284.28 µm at 20wt% electrolyte concentration and 40µm/sec feed rate of tool with aspect ratio of 1:2.76. **Fig. 3. 23(a) & Fig. 3. 23(b)** show the depth of channel in existing tool feeding machining where the bottom surface of the machined channel was found to be uneven and curved. Though the depth of channel was increased in bottom tool feeding technique, the overcut of the channel was also increased compared to that of existing tool feeding technique. The availability of fresh electrolytes and generated gas bubbles at the tool-electrode tip promoted the continuous spark discharges even at a deeper tool penetration zone during bottom tool feeding. The machined products can fall from the machining surface easily due to gravity and it broadens the way of fresh electrolyte to enter. The depth of 147.66 µm was obtained at 10wt% electrolyte concentration and 70µm/sec TFR with aspect ratio of 1:3.13. The maximum channel depth of 414µm with aspect ratio of 1:2.07 was found during machining by bottom tool feeding technique but the surface of channel was of curvature in shape. **Fig. 3. 23(c)** & **Fig. 3. 23(d)** show the depth of channel obtained by bottom tool feeding technique. **Fig. 3. 23(e)** shows the optical images of machined channels with an aspect ratio of 1:1.4 obtained in upward tool feeding technique at different machining conditions.

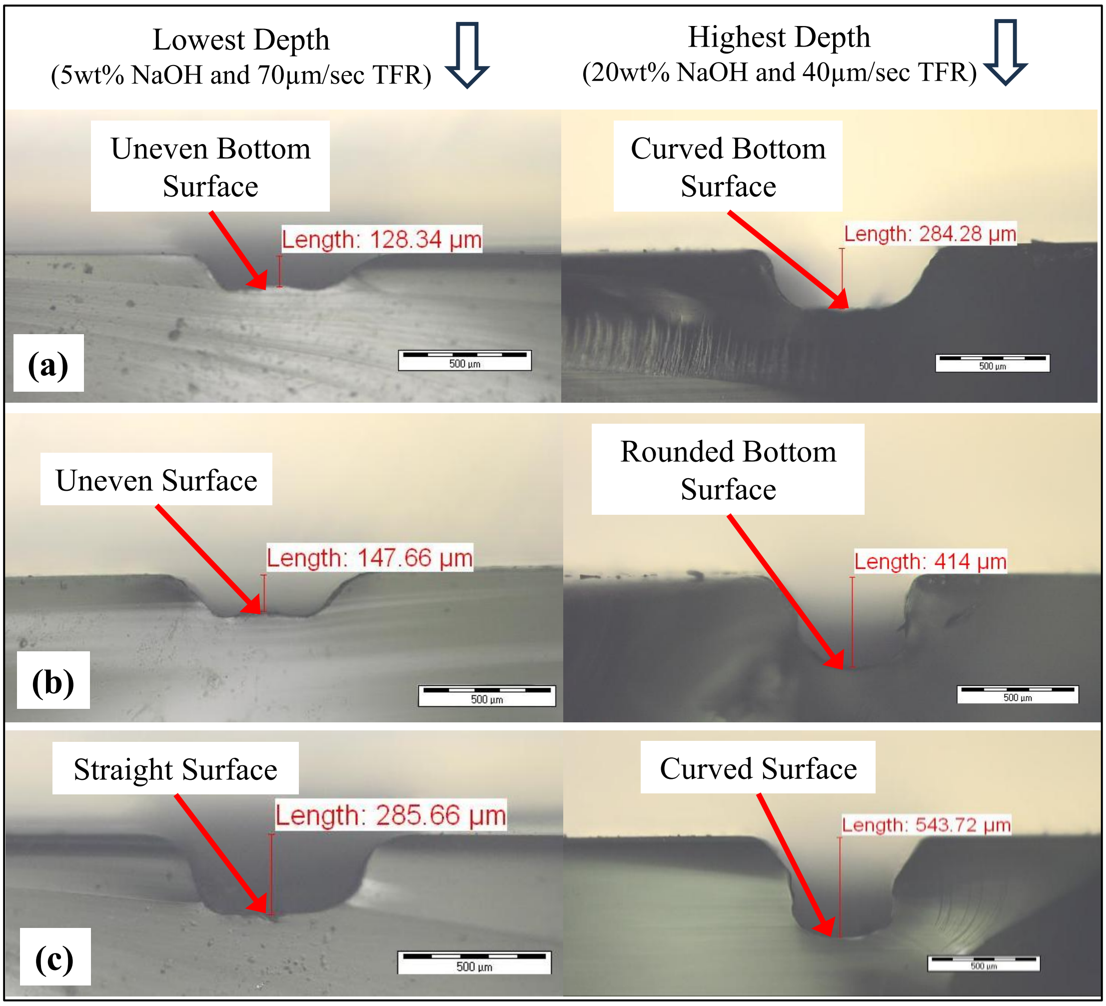

Fig. 3. 23 Optical images of cross-sections of channel for (a) existing tool feeding, (b) bottom tool feeding, (c) upward tool feeding

The machining depth of channel was found two times in upward tool feeding technique compared to existing tool feeding technique. **Fig. 3. 24** shows a channel with 800.40µm depth and 589.26μm width obtained by the upward tool feeding with copper tool at 15wt% NaOH solution and 60μm/sec tool-electrode feed rate after 5 passes of machining where every pass consists of 0.1mm depth feed.

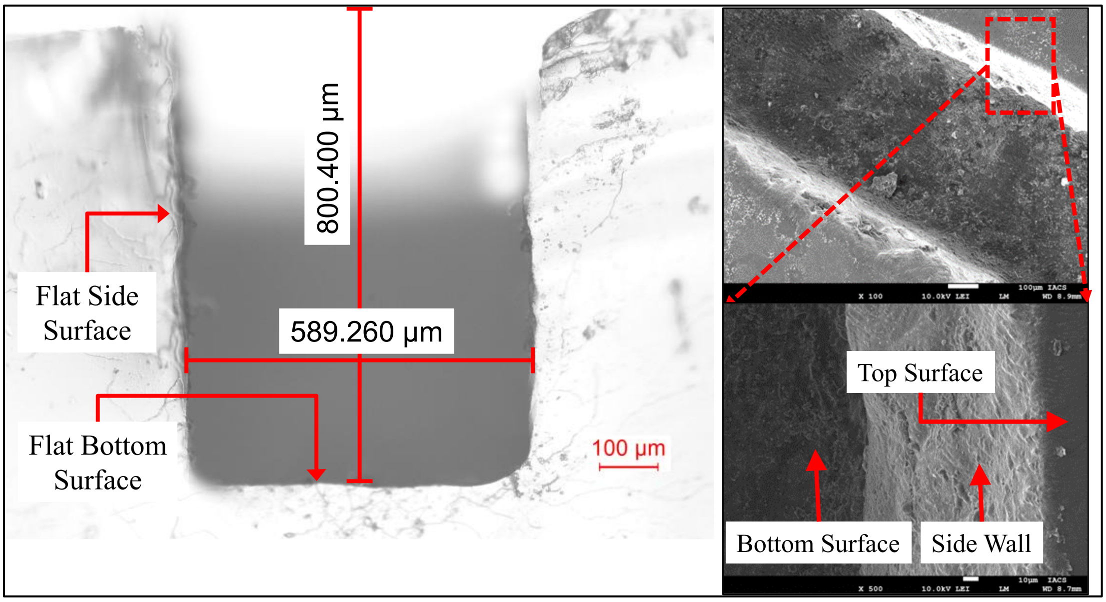

Fig. 3. 24 Optical and SEM image of channel at 5 passes using upward feeding technique

The depth of channel was increased and the channel width was reduced significantly in upward tool feeding technique. **Fig. 3. 25(a)** and **(b)** show the SEM images of machined channels with bottom tool feeding and upward tool feeding respectively. **Fig. 3. 25(b)** shows the SEM image of the channel obtained with upward tool feeding where the wall and bottom of the channel were crack-free and the edge of the channel was also found smooth.

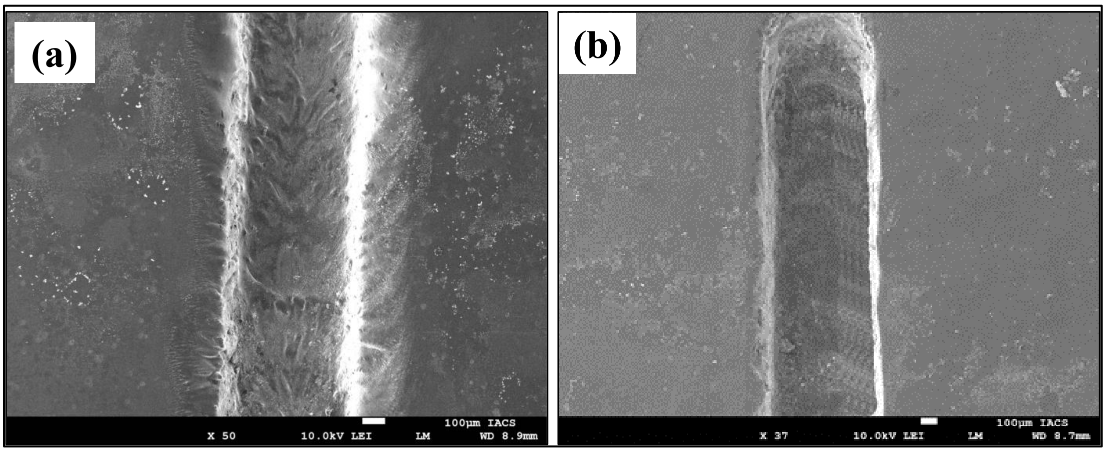

Fig. 3. 25 SEM images of channels at 15wt% NaOH/ 60 μm/sec, (a) Bottom tool feeding, (b) Upward tool feeding

A flat bottom surface of the machined channel was obtained in case of upward tool feeding technique where the tool-electrode was moved from bottom to upward direction vertically. This helped the generated gas bubbles reach the machining area, and consequently, spark discharges were observed to be evenly distributed around the tool-electrode, forming a flat surface.

3.5.5 Effect of Upward Tool Feeding on Tool-electrode

Copper tool with flat head as shown in **Fig. 3. 26(a)** was used in this experiment. It was found from the experiments with upward tool feeding that if the tool-electrode was exposed more than 500μm in electrolyte solution then irregular spark discharges were observed and it made the surface rougher and channel width larger. After making channel with upward tool feeding technique the tool-electrode was observed under SEM and the tool images were taken and depicted in the **Fig. 3. 26(b)**. This figure reveals that the surface of tool-electrode became rougher after machining than before machining.

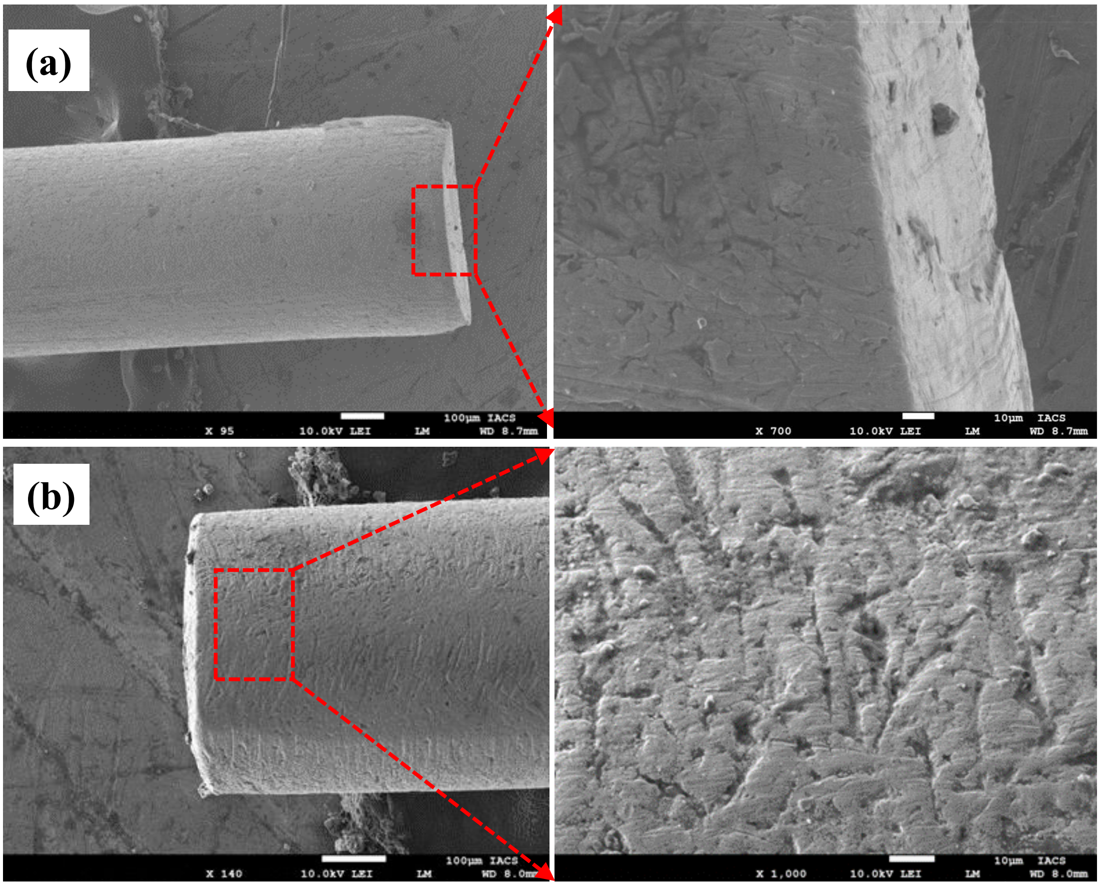

Fig. 3. 26 Images of tool-electrode (a) SEM image of Tool-electrode before machining, (b) Tool-electrode after machining at 15 wt% NaOH/ 60 μm/sec with upward tool feeding

A lot of pores and line of cracks were noticed on the tool-electrode surface after machining. It was also noticed that the front surface of the tool-electrode became curved shape after machining that helped to accelerate the electrolyte flow to the machining area. Further, **Fig. 3. 27(a)**, **Fig. 3. 27(b), Fig. 3. 27(c)** exhibit the optical images of tool-electrodes after machining with existing tool feeding, bottom tool feeding and upward tool feeding technique respectively.

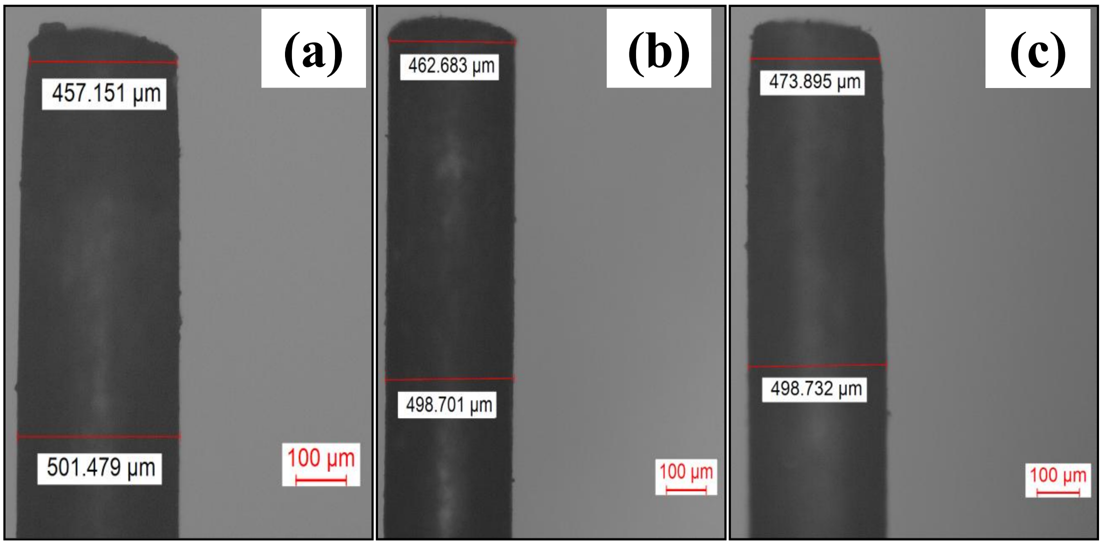

Fig. 3. 27 Tool after machining with (a) Existing tool feeding, (b) Bottom tool feeding, (c) Upward tool feeding

Tool-electrode diameters were reduced by 8.84% (501.479µm to 457.151µm), 7.22% (498.701µm to 462.683 µm) and 4.95% (498.732 µm to 473.895 µm) after machining with existing tool feeding, bottom tool feeding and upward tool feeding technique respectively. This indicates that tool-electrode wear is less during upward tool feeding technique as compared to other tool feeding technique.

3.6 Outcomes of the Study

In this study, three kinds of feeding technique have been used to make channels on glass workpiece surfaces. Among those, two novel techniques were introduced to obtain a higher depth of channel and ease of machining. Within the constraints of the investigation, the following conclusions are drawn:

(i) The simulation study revealed that the shape of the gas film significantly affects the temperature distribution during electrochemical discharge milling (ECD milling). In the existing tool feeding technique, higher temperatures were observed around the periphery of the tool electrode, leading to less efficient machining. In contrast, the vertically upward tool feeding technique concentrated higher temperatures at the tool tip, enhancing the intensity of spark discharge and improving material removal rates.

(ii) The vertically upward tool feeding technique demonstrated superior performance in terms of temperature distribution and machining quality. The simulation results showed that this technique maintained a higher temperature at the machining zone or tool tip across various voltages, ranging from 30V to 45V. This consistent high-temperature distribution at the tool tip is advantageous for more controlled and intense spark discharges, leading to better material removal and precision in machining.

(iii) Channel width is found to be lower than other feeding techniques and reduced by 11% during upward tool feeding than that of existing tool feeding at higher electrolyte concentration. The upward tool feeding technique resulted in the least tool-electrode wear among the three techniques. The diameter reduction of the tool-electrode was 4.95% (498.732µm to 473.895µm) for upward tool feeding, compared to 8.84% (501.479µm to 457.151µm) for existing tool feeding and 7.22% (498.701µm to 462.683µm) for bottom tool feeding.

(iv) The channel width was increased with the increase of electrolyte concentration. Also, the width of channel is reduced with an increase in feed rate of tool. In upward tool feeding technique tool wear is found to be less and tool-electrode diameter is reduced by 4.95% after machining. A smoother edge profile of channel is produced at 15wt% of NaOH solution and 60µm/sec of feed rate of tool. A maximum depth of 800.14µm and a width of 589.26µm are obtained at this parametric condition.

Chapter 4

INVESTIGATION INTO ELECTROCHEMICAL DISCHARGE MILLING ON SILICA GLASS USING UPWARD TOOL FEEDING TECHNIQUE

4.1 Introduction

Electrochemical Discharge Milling (ECD milling), also known as Spark Assisted Chemical Engraving (SACE), is a hybrid micromachining process that synergistically combines electrochemical dissolution and thermal (spark) erosion to machine hard and brittle materials such as silica glass materials that pose significant challenges for conventional machining methods. This chapter delves deeply into this advanced technique, with a particular focus on the novel upward tool feeding approach. By promoting a continuous supply of fresh electrolyte and more effectively regulating spark intensity, this method enhances machining stability, precision, and efficiency. Silica glass is one of the most important engineering materials for microfabrication because of its excellent optical transparency, high chemical resistance, biocompatibility, thermal stability, and electrical insulation. These properties make it an ideal substrate for applications such as MEMS, microfluidic devices, lab-on-chip systems, optical components, biomedical devices, and microreactors. However, its high hardness and brittle nature make conventional machining difficult due to crack formation, edge chipping, and poor dimensional accuracy. Electrochemical Discharge Milling (ECD milling), particularly with the proposed upward tool feeding technique, can successfully overcome these limitations by producing high-quality microchannels and intricate patterns with improved material removal rate, better surface finish, lower taper, and enhanced dimensional accuracy. This establishes ECD milling as a promising manufacturing process for precision machining of silica glass in advanced industrial and biomedical applications.

A key emphasis of this work is the systematic investigation of how critical process parameters applied voltage, electrolyte concentration, and Tool Feed Rate (TFR) affect milling performance. These variables influence not only the Material Removal Rate (MRR) but also the dimensional accuracy (channel width), surface quality (R_a), and channel taper angle, all of which are important for applications demanding high precision and consistent quality. The upward tool feeding method, in combination with parameter tuning, aims to minimize dimensional deviations, improve surface finish, and ensure more uniform channel geometry. In addition to conventional performance metrics, this study incorporates a quantitative energy analysis to correlate input and utilized energies with machining outcomes. The total electrical energy supplied during ECD milling is calculated as the product of instantaneous voltage and current over machining time. The actual energy consumed in material removal is estimated based on the mass and volume of the milled channels, factoring in channel taper geometry. The energy required for machining is decomposed into four stages:

(i) Heating the material from ambient to melting point,
(ii) Melting,
(iii) Heating from melting to vaporization point, and
(iv) Vaporization.

This energy framework enables calculation of the utilized energy (EU), which directly reflects the thermal and electrochemical contributions to localized material removal. The study also examines energy utilization efficiency i.e. the ratio of utilized to input energy and its influence on milling quality. It is observed that at lower energy levels, efficiency is high due to stable spark formation and minimal losses; however, as input energy increases, efficiency drops because of heat dissipation, gas film instability, and uncontrolled spark expansion. Such inefficiencies can result in greater sidewall erosion, increased taper, and reduced dimensional accuracy. By contrast, trends between used energy and performance metrics (e.g., channel width, taper angle) are more linear and predictable, indicating that controlling energy efficiency is a more reliable strategy for precision machining than simply increasing the input power. Experiments are conducted on silica glass using a 0.5 mm copper tool electrode (insulated except at the tip) and a graphite counter-electrode. Channels of 10 mm length are milled under varied applied voltages, electrolyte concentrations, and TFRs, with fixed baseline conditions determined from preliminary trials. Material removal is quantified via pre and post-machining weights, channel dimensions are measured using an optical measuring microscope, surface roughness is determined using a surface roughness tester, and surface topography is analyzed using coherence correlation interferometry. Taper angle is determined from entrance-to-bottom channel width variations.

The insights gained in this chapter extend beyond traditional process by linking energy-based modeling with experimental performance analysis. This integrated approach not only advances the understanding of ECD milling mechanisms but also guides the identification of an optimal energy window for maximizing precision, surface quality, and machining efficiency in industrial applications involving brittle, non-conductive materials.

4.2 Calculation of Energy Input and Output

Electrochemical Discharge Machining (ECDM), also called Spark Assisted Chemical Engraving (SACE), is a hybrid micromachining process that combines electrochemical and thermal (spark) energy to machine non-conductive materials such as glass and ceramics.

To analyze the energy input and output of ECDM numerically, it can be broken down into several phases and the energy transactions can be examined step by step.

- Electrolysis Energy Input:

The instantaneous electrical power input during electrolysis is as in equation (4.1):

$$P_{input} = V \times I \qquad \text{... (4.1)}$$

Here, Voltage V and Current I are the input values.

The total energy input for the time t is as shown in equation (4.2):

$$E_{input} = VIt \qquad \text{... (4.2)}$$

- Calculation of Volumetric Mass of Removed Materials

The energy used to melt and vaporize materials to get channels is calculated based on the material removed by the process. The mass is calculated from the channel volume, incorporating the taper angle and assuming a uniform taper throughout the channel depth. **Fig. 4. 1** shows a Schematic representation of the channel with dimensions used for the calculation of volume and mass.

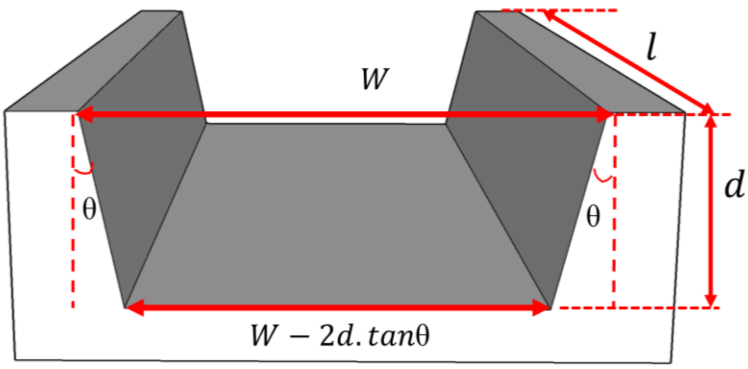

Fig. 4. 1 Schematic representation of the channel with dimensions

The mass of the material of the channel with taper angle θ is given in equation (4.3).

$$m = (w - d\tan\theta)dl\rho \qquad \text{... (4.3)}$$

Here, w and $(w - 2d\tan\theta)$ are the channel width of the top and bottom surfaces, respectively, and d is the depth of the channel, l is the length of the channel and ρ is the density of the material.

- Material Removal Thermal Energy (Continuous Thermal Input)

The thermal energy needed to melt and vaporize m mass of material is given in equation 10. The energy required to melt and vaporize materials from the workpiece is a combination of four steps.

(i) Energy required to raise the temperature from ambient to melting (E_1) is as shown in equation (4.4).

$$E_1 = mC_s(T_m - T_a) \qquad \text{... (4.4)}$$

(ii) Energy required to change the phase from solid to liquid (E_2) is as shown in equation (4.5).

$$E_2 = mL_f \qquad \text{... (4.5)}$$

(iii) Energy required to raise the temperature from melting to vaporizing (E_3) is as shown in equation (4.6).

$$E_3 = mC_l\Delta T_2 \qquad \text{... (4.6)}$$

(iv) Energy required to change the phase from liquid to vapour (E_4) is as shown in equation (4.7).

$$E_4 = mL_v \qquad \text{... (4.7)}$$

$$E_u = E_1 + E_2 + E_3 + E_4 \qquad \text{... (4.8)}$$

$$E_u = \left(C_s\Delta T_1 + L_f + C_l\Delta T_2 + L_v\right)m \qquad \text{... (4.9)}$$

Where, T_m is the melting temperature of the material, T_v is the vaporizing temperature of the material and T_a is the atmospheric temperature, $C_s$is the specific heat of solid material, and C_l is the specific heat of liquid material, L_f is the latent heat of liquefaction and L_v is latent heat of vaporization and $\Delta T_1 = T_m - T_a$, and $\Delta T_2 = T_v - T_m$ and m is the mass of material removed during machining.

Combining equations (4.3) and (4.9) the utilized energy can be obtained as equation (4.10).

$$E_u = \left(C_s \Delta T_1 + L_f + C_l \Delta T_2 + L_v\right)(w - d \tan\theta) dl\rho \qquad \dots (4.10)$$

Equation 10 has some constant part as well as some variable part, such as "$\left(C_s \Delta T_1 + L_f + C_l \Delta T_2 + L_v\right)$" and "$\rho$" are the constant parts for a particular material.

- Energy during Gas Film Breakdown (Spark Generation)

Assuming the breakdown occurs over a short time interval [t_1, $t_1+\Delta t$] with voltage $V_b(t)$ and current I_b (t), instantaneous electrical power is as shown in equation (4.11):

$$P_{breakdown} = V_b(t) \times I_b(t) \qquad \dots (4.11)$$

Total electrical energy during breakdown is as shown in equation (4.12):

$$E_{elec,2} = \int_{t_1}^{t_1+\Delta t} V_b(t) \times I_b(t) dt \qquad ... (4.12)$$

The spark energy discharged can be modeled (assuming capacitor C) as shown in equation (4.13):

$$E_{spark} = \frac{1}{2} C {V_{max}}^2 \qquad ... (4.13)$$

The voltage falls from V_{max} to 0 during the spark. In this study, the energy utilized for machining glass was calculated using Equation (4.10) and analyzed accordingly.

4.3 Plan of Experiments

In this study, the applied voltage, electrolyte concentration and TFR were varied during milling on silica glass by electrochemical discharge using upward tool feeding technique. This novel tool-feeding technique improved machining quality and spark intensity by regulating the flow of fresh electrolyte in the machining zone. One factor at a time was varied to observe the influences of process parameters on the milling performance of glass. The process parameters and their range were chosen based on pilot experiments. A copper tool with a diameter of 0.5 mm with a flat face end was used to make channel on glass slide where a counter electrode of graphite was used. The fixed machining conditions used during the experimentation have been given in **Table 4. 1**.

Table 4. 1 Constant Machining Parameters

Items	Material
Workpiece	Silica Glass
Tool Electrode	Copper
Auxiliary Electrode	Graphite Block
Electrolyte	NaOH
Power Supply	DC
Inter-Electrode gap	120mm

To prevent undesired spark discharges from the side surface, the tool was always adequately protected with insulation material before the machining process began. The workpiece surface may have been affected by discharges from the tool's side surface if more of the tool's surface was exposed to the electrolyte. The machining process parameters are given in **Table 4. 2**.

Table 4. 2 The machining process parameters settings

Parameters	Value
Applied Voltage (V)	30, 35, 40, 45
Electrolyte Concentration (wt%)	10, 15, 20, 25
Tool Feed Rate (TFR) (µm/sec)	40, 50, 60, 70

According to the plan, the experiments were conducted and three milling operations of 10mm length were performed on the glass so that total material removal can be observed. Each glass slide was weighed before as well as after the machining to evaluate the MRR. The width of each milled surface was observed and measured under an optical measuring microscope. The surface roughness in terms of R_a value of the bottom layer of the machined channel was studied using a surf test surface roughness measuring instrument to quantify the surface roughness. With the use of coherence correlation interferometry images, the surface topography and profile of the channel were observed.

Usually, the tapering means non-uniform material removal from the workpiece surface throughout the machining depth of the channel. It is the difference between width of the channel at the entrance and width of the channel at the bottom of the channel. The tapper angle is given as shown in equation (4.14):

$$\theta = \tan^{-1}\left\{\frac{\left(\frac{W_{Entry}-W_{Bottom}}{2}\right)}{D}\right\} \quad \text{... (4.14)}$$

Where, θ is the tapper angle, W_{Entry} is the width of channel at entry, W_{Bottom} is the width of the channel at exit and D is the depth of the channel.

Tapering during the fabrication of channels in glass using electrochemical discharge milling occurs for various reasons. The main cause is the nonuniform material removal from the workpiece along the channel depth. Now, this non-uniform material removal occurs due to uncontrolled spark discharge during ECD milling on glass. The formation of a gas film and its shape, along with process parameters such as applied voltage, electrolyte concentration, and tool feed rate, play a vital role in determining whether a spark discharge is controlled or uncontrolled. At a glance, it can be represented through a flow chart as given in **Fig. 4. 2**.

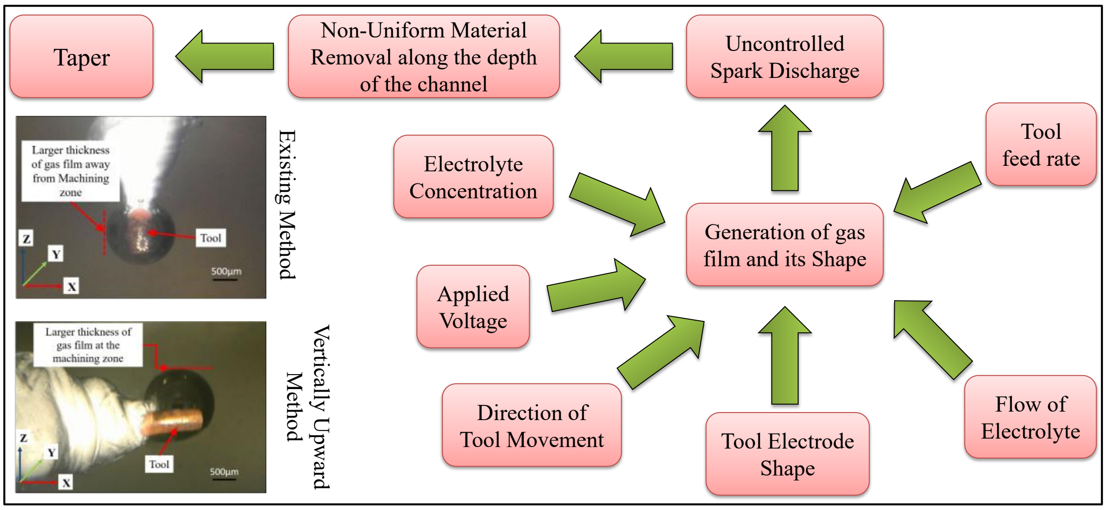

Fig. 4. 2 Flowchart diagram about the cause of taper during ECD milling

The causes of taper channel formation can be categorized into two parts: parametric combination and setup modification. Parametric combination is required to control the flow of current and current density in the tool electrode area of the machining zone, as well as the voltage difference between the tool electrode and the auxiliary electrode. The setup modification involves moving the tool electrode along the workpiece surface so that the generated gas film and spark discharge are in favorable conditions for smooth machining.

4.4 Results and Discussion

Thorough investigations were carried out, analyzing the influence of process parameters on material removal rate, channel width, surface roughness in terms of R_a and taper angle. After the analysis, the discussions are provided on the effect of process parameters on various machining outputs.

4.4.1 Influences of Process Parameters on Material Removal Rate

During the ECDM process, materials from the glass workpiece surface are removed due to thermal energy. However, the material removal mechanism is very complex in the case of electrochemical discharge milling. The availability of energy at the machining zone depends on the intensity of the spark discharge. High-intensity spark discharge is generated at higher voltage and electrolyte concentration, providing more energy at the machining zone, whereas low-intensity spark discharge provides less energy at the machining zone. The effectiveness of material removal is determined by the amount of energy from the spark discharge responsible for melting and vaporizing glass materials. Investigations have revealed that the applied voltage is the most crucial factor influencing Material Removal Rate (MRR). The rate of electrolysis increases with the rise in electric potential between the cathode and the auxiliary electrode, leading to the formation of massive amounts of hydrogen gas bubbles that cluster around the cathode. Spark discharge often occurred in the machining zone when there were enough gas bubbles present. The generated gas bubbles were merged to create an insulating gas layer surrounding the tool electrode, which cut off the current flow from the cathode to the electrolyte and this gas film breaks down with a high-intensity spark discharge at critical voltage. The high-energy spark discharge creates a larger crater on the glass material surface and removes more amount of material. The energy of the spark discharge is not fully used to remove materials from the workpiece because the spark discharge spreads around in all possible directions. In the case of the upward tool feeding technique, the discharge area at the machining zone is more than the existing tool feeding technique which removed a greater number of materials from the workpiece. **Fig. 4. 3(a)** shows the effect of supply voltage on MRR at 10 wt% electrolyte concentration where a great difference in MRR among different TFR was observed after 35 V. The MRR was higher for 40 μm/sec TFR for all electrolyte concentrations. From **Fig. 4. 3(b),** higher MRR can be observed at higher voltage at 15 wt% of electrolyte concentration and the MRR was lower for a higher tool-feed rate. The MRR was drastically improved during machining at higher electrolyte concentration due to the high rate of the electrolysis that escalated the generation of gas bubbles and gas films to produce high energy spark discharge more frequently as shown in **Fig. 4. 3(c)**. The tool feed rate (TFR) decides how fast the tool is moved from one position to another. Depending on this movement of the tool-electrode, the frequency of the spark discharge at the machining zone was increased or decreased. The tool electrode delivered more energy during spark discharge when it was moved slowly over the workpiece surface. The lower value of MRR was 0.517 µg/min at 10 wt% electrolyte concentration, 30 V and 70 µm/sec TFR and after that, the MRR kept on increasing as the voltage was increased and the TFR was decreased. The energy at the machining zone was higher at 25 wt% of electrolyte concentration and 45 V of applied voltage which led to achieving MRR of 6.097 µg/min which was the highest material removal rate among all other parametric conditions in this study as shown in **Fig. 4. 3(d)**.

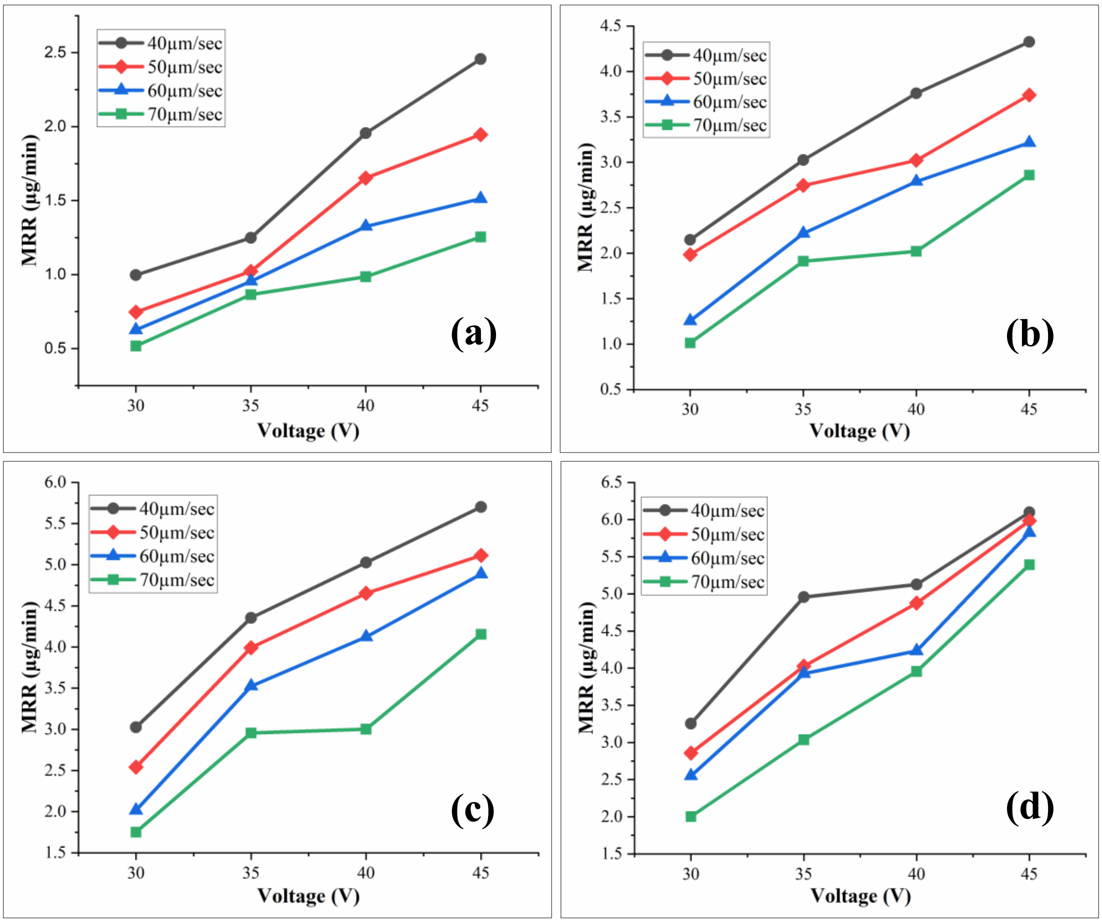

Fig. 4. 3 Influences of applied voltage on MRR at (a) 10 wt%, (b) 15 wt%, (c) 20 wt%, and (d) 25 wt% of electrolyte concentration for various TFR

The prerequisites for achieving a higher material removal rate were a higher electrolyte concentration and applied voltage; however, at the same time, the channel width also increased, and the channel surface was damaged.

4.4.2 Influences of Process Parameters on Surface Quality

The surface quality of machining depends on the surface roughness (R_a) of the machined channel. The surface roughness (R_a) of the channel was influenced by the voltage between electrodes, the concentration of the electrolyte and the TFR. **Fig. 4. 4(a)** shows that at 30 V the surface roughness is higher than all other applied voltages. Analysis after experiments revealed that both the lower and higher voltages were responsible for generating rough surfaces on the machined channel. R_a value was decreased as the supply voltage increased up to 40 V and beyond 40 V the roughness again increased. The surface roughness in terms of R_a value at 35 V was lower than that of 30 V but it was higher than 40 V. As shown in **Fig. 4. 4(a)**, the surface roughness (R_a) was higher at 10 wt% electrolyte concentration, 30 V, and 70 m/sec tool feed rate, whereas the surface roughness (R_a) was decreased at 15 wt% electrolyte concentration, 40 m/sec tool feed rate, and 40 V as presented in **Fig. 4. 4(b)**. Further increase of electrolyte concentration resulted in a reduction of the surface roughness of the channel but after 20 wt% of electrolyte concentration, the surface roughness again increased. The presence of hydroxyl ion in the solution ensured the high-temperature chemical etching which produced a smooth surface with lower surface roughness. The spark discharge became uncontrollable at 25 wt% of electrolyte concentration, which generated higher surface roughness. At 30 V, the energy level at machining zone was decreased and preventing it from removing materials from the glass surface. This low energy created uneven craters on the workpiece to generate higher surface roughness or more peaks valleys on the machined surface. It is also noticeable in **Fig. 4. 4(c)** and **Fig. 4. 4(d)** that at both 20 wt% and 25 wt% of electrolyte concentration, the surface roughness decreases as the voltage increases up to 40 V, after that the surface roughness again increases. MRR and surface quality have relationship. Higher machining energy increases the intensity and frequency of spark discharges, thereby removing more material per unit time and increasing MRR. However, the same high-energy discharges create larger craters and thermal effects, and more side sparking, leading to increased surface roughness. Therefore, the highest MRR does not necessarily produce a good surface finish.

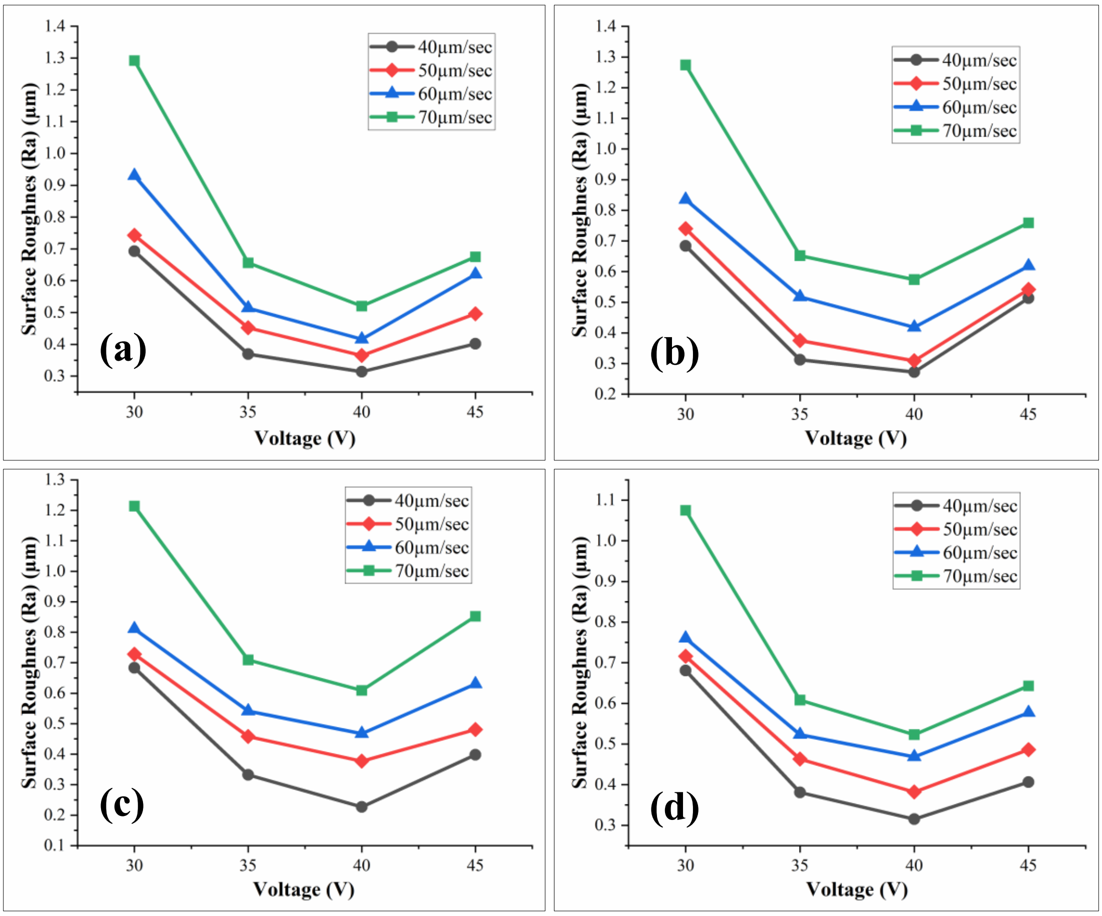

Fig. 4. 4 Influences of applied voltage on surface roughness (R_a) at (a) 10 wt%, (b) 15 wt%, (c) 20 wt%, and (d) 25 wt% of electrolyte concentration for various TFR

Higher electrolyte concentration led to a higher rate of the electrolysis process, which created more gas bubbles, resulting in a high-energy spark discharge. The higher voltage provided higher energy at the machining zone which generated a relatively lower rough surface than 30 V and the surface roughness eventually became lowest at 40 V. Further increase in voltage, created abrupt spark discharge that detoriated the surface to produce a higher rough surface. At 40 V, sufficient energy from spark discharge was available at the machining zone which removed materials uniformly than 30 V and produced a lower amount of peaks and valleys on the workpiece surface as shown in **Fig. 4. 5(d).** Irregular removal of materials creates a lump on the surface that increases the surface roughness as shown in **Fig. 4. 5(c).** The bottom layer of the machined channel developed a wavy structure when the TFR was 70 µm/sec as shown in **Fig. 4. 5(a)** whereas at a lower TFR, the surface of the channel turned into smoother which produced lower surface roughness as shown in **Fig. 4. 5(b).**

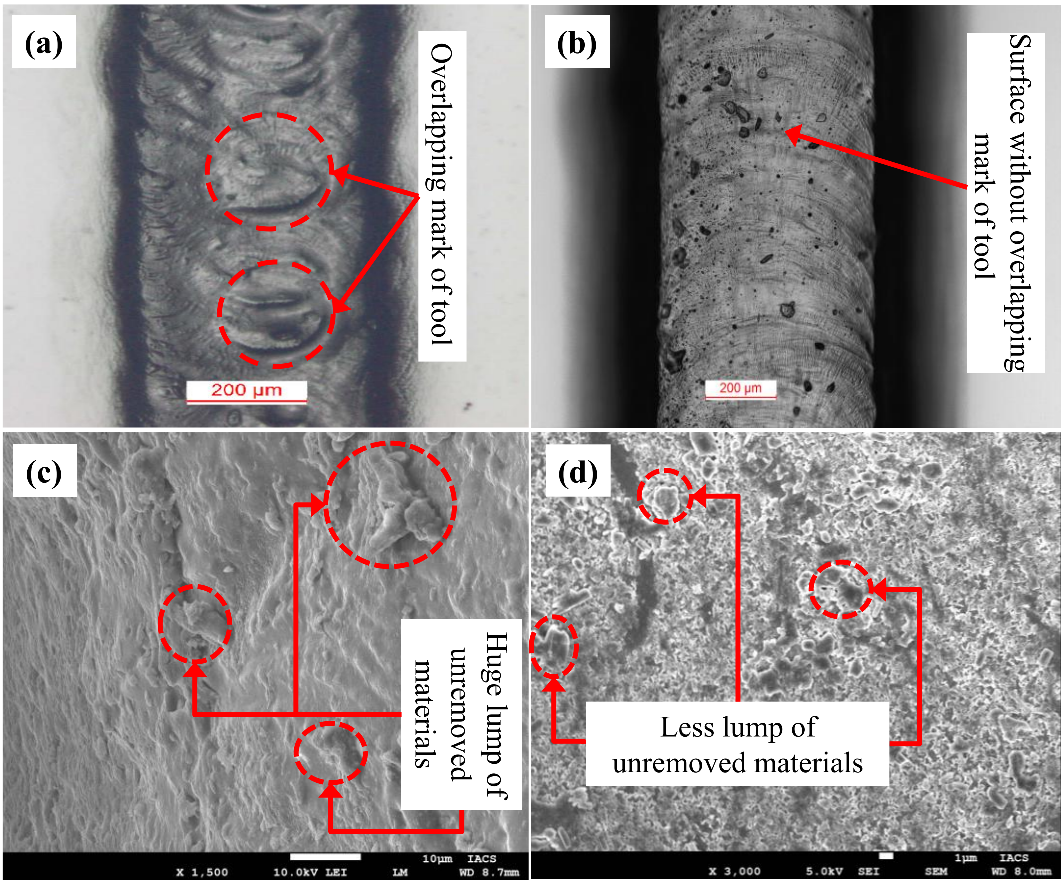

Fig. 4. 5 Optical and SEM images of machined channel (a) and (c) at 15 wt% of NaOH, 40 V and 70 µm/sec TFR and (b) and (d) 15 wt% of NaOH, 40 V and 50 µm/sec TFR

As it was previously mentioned that the rate of material removal was inversely related to the tool feed rate, but the rate of increase of surface roughness was directly proportional to the TFR. The R_a value of bottom surface increased with the increase of tool feed rate. According to the trial results, the surface roughness was found to be lower at a tool feed rate of 40 µm/s and increased as the tool-electrode speed was increased up to 70 µm/s. From **Fig. 4. 5(a)** to **Fig. 4. 5(d)** it is visible that in every electrolyte concentration, the roughness of the bottom layer that is the R_a value was higher for a higher TFR. It removes more materials evenly if the tool-electrode was moved at low speed across the workpiece surface. As a result of uneven material removal at a greater TFR, an overlapping mark was produced on the bottom layer of the machined channel, creating a wavy structure as shown in **Fig. 4. 6(a)**. The tool electrode created a path for itself as it advanced from one spot to another by melting the material of the workpiece. The quality of the machined surface would deteriorate if the movement of the tool-electrode was out of proportion to the quantity of material being removed.

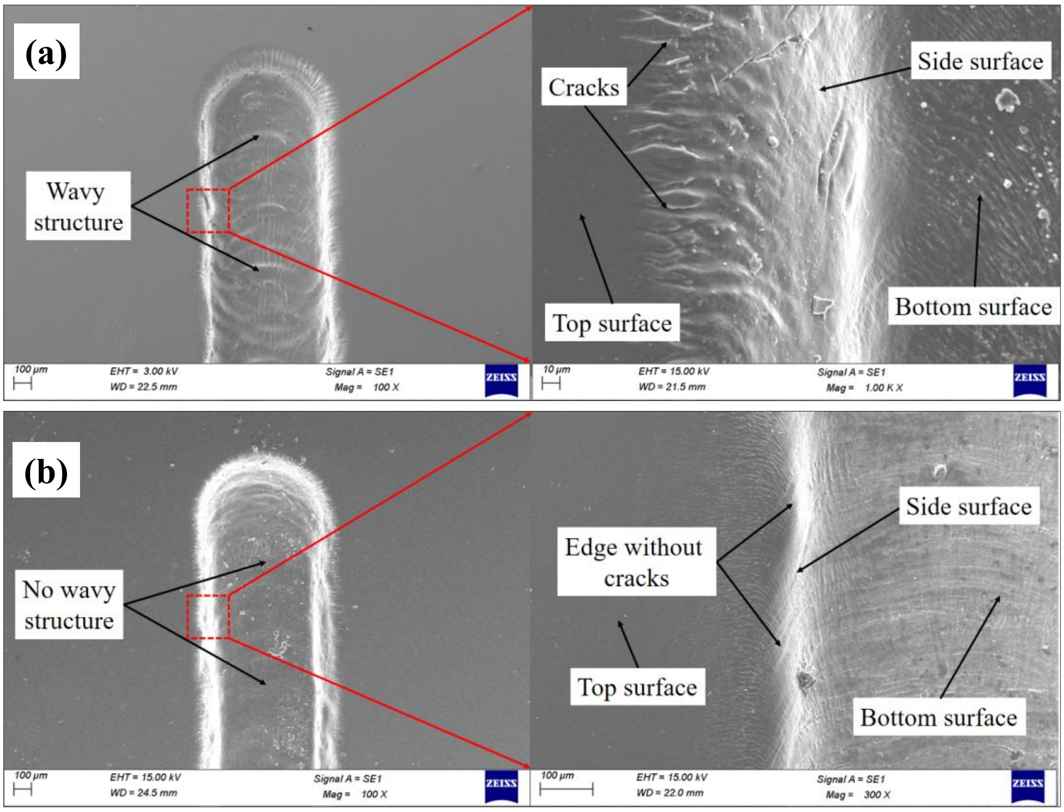

Fig. 4. 6 Scanning Electron Microscopy Image of the channel machined at (a) 20 wt% of NaOH solution, 45 V and 70 µm/sec TFR and (b) 20 wt% of NaOH solution, 40 V and 50 µm/sec TFR

When the TFR was higher, the tool-electrode was transferred from one location to another without removing materials from the workpiece. It is also noticeable in **Fig. 4. 6(a)** that at elevated tool feed rate, micro cracks were present along the edge of the channel as the speed of the tool electrode prevented to remove materials evenly from the edge of the channel. The wavy structure was diminished as the TFR decreased and also at higher voltage this wavy structure was not observed. A smoother edge was noticed at 40 V and also the wavy structure was not visible when the TFR was decreased to 50 µm/sec as shown in **Fig. 4. 6(b)**. Voltage and electrolyte concentration interact synergistically in ECD milling. Voltage increases the discharge energy, while electrolyte concentration increases the conductivity and promotes faster gas-film formation. When both increase together, spark generation becomes more frequent and energetic, resulting in higher MRR. However, beyond a level, the interaction produces side sparking and unstable gas-film breakdown, thereby increasing channel width, and surface roughness. A lower rate of electrolysis process occurred at a lower concentration of electrolyte and this resulted in less frequent spark discharge which produced an uneven edge and wavy bottom layer. Images from Coherence Correlation

Interferometry (CCI) reveal the surface topography of the machined bottom layer which is shown in **Fig. 4. 7**. The image shown in **Fig. 4. 7(a)** describes the channel at higher tool feed rate (TFR) that was unable to produce a smoother surface. A lower concentration of electrolyte caused uneven production of spark discharge from the tip of the tool that eventually created a lot of peaks and valleys at the bottom layer.

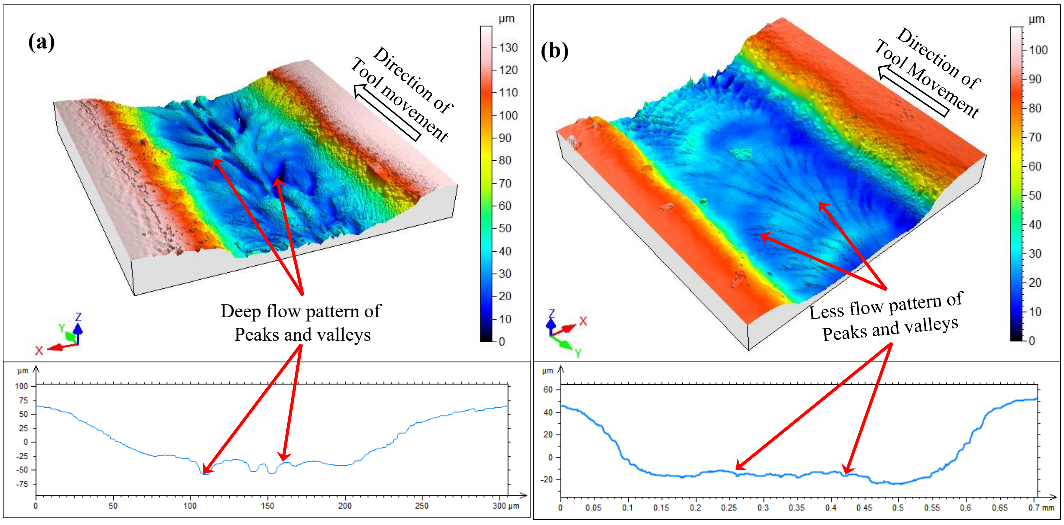

Fig. 4. 7 Surface topography and profile curve of machined channel at (a) 10 wt% of NaOH solution, 40 V and 50 μm/sec TFR and (b) 20 wt% of NaOH solution, 40 V and 50 μm/sec TFR

The flow of the peaks and valleys was always directed toward the movement of the tool during milling. This type of peaks valleys and their effect was diminished at elevated voltage and electrolyte concentration resulting in the production of smooth and lower rough surfaces that is shown in **Fig. 4. 7(b)**. The surface profile that is shown in **Fig. 4. 7(a)** contains an irregular pattern along the bottom layer and also it was flattened at the edge of the channel whereas the profile from **Fig. 4. 7(b)** denote a regular pattern and was less flattened at the edge. It is noticeable from both images of figure 8 that the flow of the valleys or the shape of the uneven surface made an interesting pattern toward the direction of the tool movement. Although the pattern was detectable at a lower concentration and it disappeared at higher voltage and concentration at same TFR of tool electrode.

4.4.3 Influences of Process Parameters on the Width of Channel

The width of the channel in ECDM depends on the intensity of the spark discharge and the nature of the spark discharge whether it is a controlled spark or an uncontrolled spark. It also depends on the TFR of electrode. In this study, the width of channel was analyzed against variation of the applied voltage, electrolyte concentration, and TFR. Voltage and concentration of electrolyte have major proportional effect on the intensity of the spark discharge as well as on the width of the channel whereas, the TFR alters the width of the channel inversely. An increase in supply voltage and electrolyte concentration increased the width of the channel. Higher voltage provided higher energy in the machining region and generated a large number of hydrogen gas bubbles. **Fig. 4. 8** shows the effects of supply voltage on the width of the channel at different TFR and electrolyte concentrations. The effects of supply voltage on MRR at 10 wt% electrolyte concentration are illustrated in **Fig. 4. 8(a)**, where it is evident that at lower voltages, the channel width was narrower than the tool electrode diameter. The lower rate of electrolysis was observed at lower concentration of electrolyte and lower voltage that produced less amount of gas bubbles. Due to insufficient gas bubbles being present at lower electrolyte concentrations and lower voltage, the gas film generated during the procedure was unable to completely cover the exposed tool-electrode surface. The generation of spark discharge and frequency of spark discharge reduced at 30 V and 10wt% of concentration that led to produce lower overcut during milling. But this width of the machined channel was increased if the voltage was increased from 30 V to 45 V. The channel width increases with applied voltage because higher voltage produces stronger, higher-energy spark discharges. The increased discharge energy causes greater thermal softening and chemical etching of the glass. At higher voltages, spark discharges also occur along the side surface of the tool electrode, leading to lateral material removal and overcut. Therefore, although higher voltage increases the material removal rate, it also produces wider channels. The tool feed rate (TFR) of the tool electrode was inversely proportional to the width of channel during ECD milling. If the tool electrode moves at slow speed over the workpiece surface, then it gets more time at a particular position to exert spark discharge energy that remove materials more than higher tool feed rate (TFR). In all cases as shown in **Fig. 4. 8(a)** to **Fig. 4. 8(d)** the width of channel was higher when the tool electrode moved at 40 μm/sec speed and the width decreased when the TFR was increased. The higher applied voltage produced unstable and vigorous spark discharge that led to the generation of different width of the channel at particular parameter. This kind of deviation has been given in terms of the Y-error bar in **Fig. 4. 8(a)** to **Fig. 4. 8(d)** and it has been observed that at 45 V as well as at a higher TFR the deviation of width was larger than other value of supply voltage and feed rate. The lower width of the channel was found as acceptable at 15 wt% of electrolyte concentration than that of 20 wt% and 25 wt% of electrolyte concentration as shown in **Fig. 4. 8(b)**.

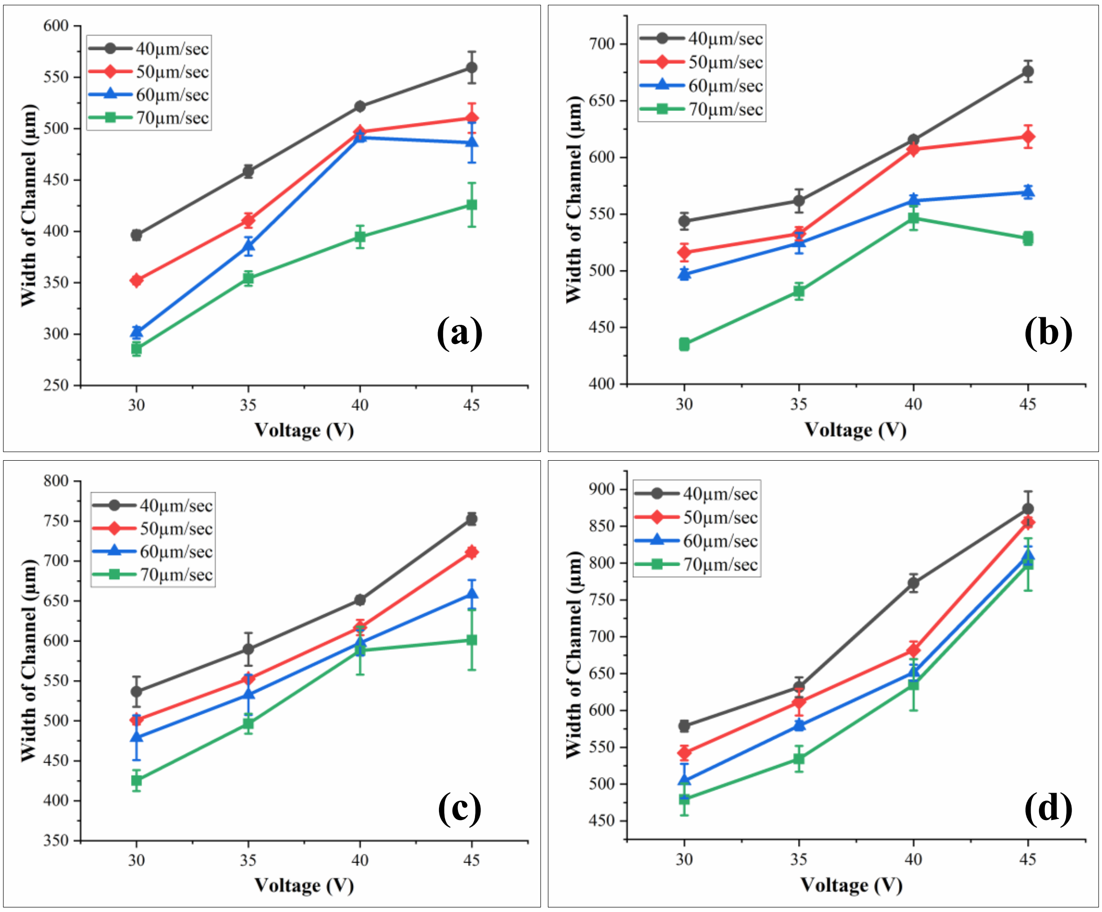

Fig. 4. 8 Effect of supply voltage on the width of channel at (a) 10 wt%, (b) 15 wt%, (c) 20 wt%, and (d) 25 wt% of Electrolyte concentration for different TFR

Fig. 4. 9(a) shows that the width of the channel was very lower at lower applied voltage due to insufficient spark discharge at the machining zone whereas the width was increased at a higher voltage. The width of channel at 30V was lesser than the tool electrode diameter which indicates that the spark discharge during milling at lower voltage was inadequate to create full replica of tool electrode on the workpiece. The width of channel increased as the voltage increased from 30 V to 35 V as shown in **Fig. 4. 9(b)** which shows that the width of channel was slightly higher than the tool electrode diameter due to adequate spark discharge energy at the tool tip. Although the width of channel at 35 V was higher than that of the channel at 30 V but the edge of the channel was fond uneven. **Fig. 4. 9(c)** shows the channel at 40 V that produced larger width of channel with smoother edge but if the voltage was increased even after 40 V, then the larger width of channel was noticed with evenly produced channel edge as descripted in **Fig. 4. 9(d)**.

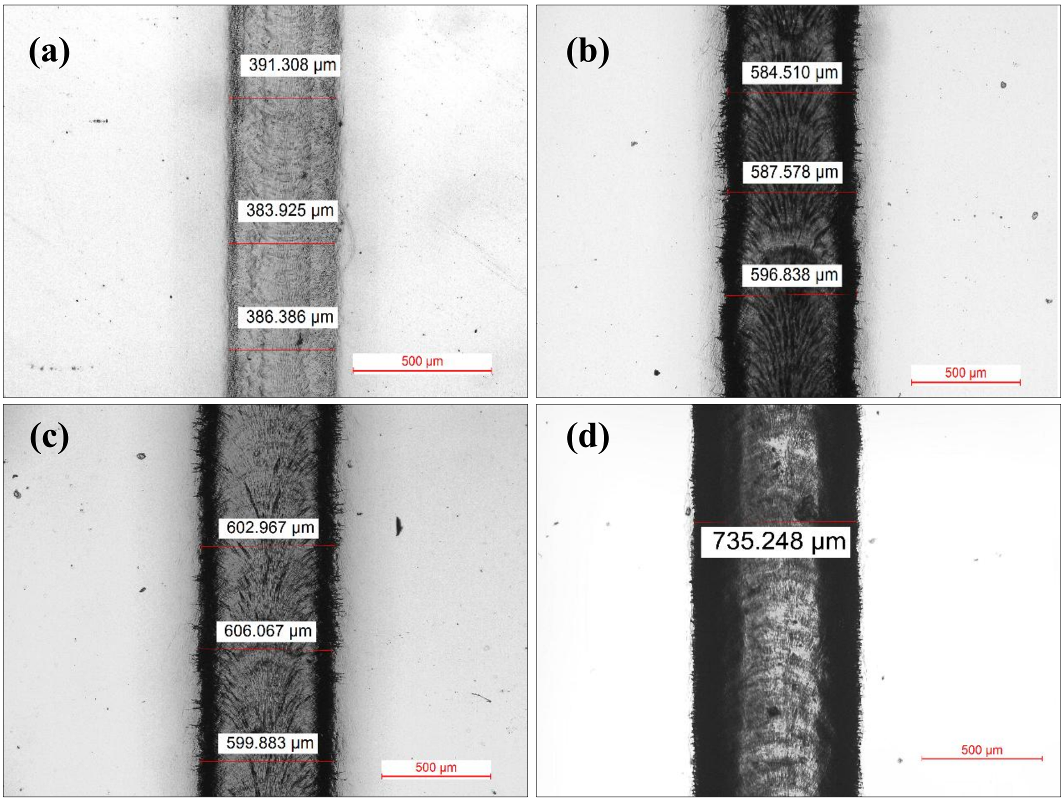

Fig. 4. 9 Optical image of the machined channel at (a) 30 V, 20 wt% and 50 µm/sec feed rate (b) 35 V, 20 wt% and 50 µm/sec feed rate (c) 40 V, 20 wt% and 50 µm/sec feed rate (d) 45 V, 20 wt% and 50 µm/sec feed rate

So, neither higher voltage nor lower voltage was appropriate for the milling on glass with ECD milling. The edge of the channel was diminished at both 40 V and 45 V but the channel at 45 V produced a larger width that was unacceptable.

4.4.4 Influences of Process Parameters on Channel Taper

One of the significant challenges in ECD milling is channel taper, which refers to the variation in the width of the machined channel from the top to the bottom of the workpiece. Several key parameters influenced channel taper, including voltage, electrolyte concentration, and tool feed rate. Voltage played a critical role in ECD milling by affecting discharges and electrochemical reactions. High voltage increased spark energy, resulting in more substantial material removal which cause larger taper angles as shown in **Fig. 4. 10**. Electrolyte concentration affected the conductivity and chemical activity in the machining zone. A high electrolyte concentration increased conductivity, leading to better current flow and more efficient material removal as shown in **Fig. 4. 10(d)**. However, it can also cause excessive gas bubble generation, creating unstable machining conditions that increase taper angle. On the other hand, a low electrolyte concentration decreases conductivity, resulting in less efficient material removal and potentially smaller tapers as shown in **Fig. 4. 10(a)**. Additionally, high voltage can enhance electrolyte decomposition, creating more gas bubbles that may disrupt machining stability and increase taper.

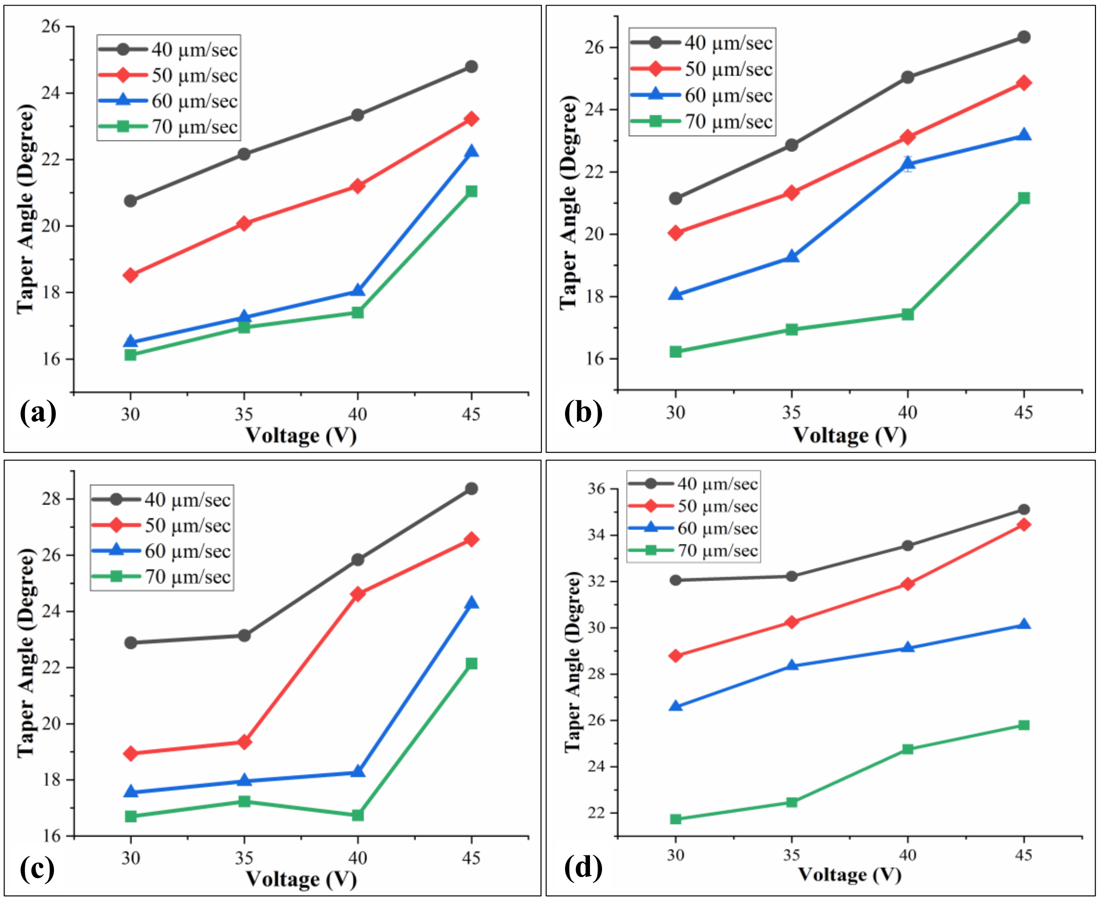

Fig. 4. 10 Effect of supply voltage on the taper angle at (a) 10 wt%, (b) 15 wt%, (c) 20 wt%, and (d) 25 wt% of Electrolyte concentration for different TFR

On the other hand, low voltage results in lower spark energy, reducing thermal damage and potentially producing smaller tapers. The tool feed rate, which determines the speed at which the tool moves through the material, also significantly impacts channel taper. **Fig. 4. 10(b)** and also in **Fig. 4. 10(c)** show that taper angle is higher if the tool feed rate is lower and taper angle is lower as the tool feed rate is increased. A high tool feed rate resulted in insufficient time for effective spark and electrochemical reactions, which reduced material removal and decreased taper angle. Conversely, a low tool feed rate allowed more time for spark discharges and electrochemical reactions that increased material removal but potentially caused larger tapers due to prolonged thermal effects. While this can enhance machining precision, it may be less efficient in terms of time. In Electrochemical Discharge Milling (ECD milling), upward tool feeding techniques significantly influenced the taper angle of machined channels due to the shape of the gas film and higher temperature distribution near the tool electrode tip. Upward tool feeding, where the tool moves in an upward direction during machining, improved material removal control, led to a more uniform channel width from top to bottom and reduced the taper angle. This technique also enhanced the flushing of electrolyte and debris from the machining zone, facilitated the removal of by-products like gas bubbles and eroded material that can otherwise accumulate and interfere with the process. In contrast, a combination of low voltage (i.e. 30V) and low tool feed rate (i.e. 40 µm/sec) produced minimal taper angle of 18.151 degree and depth of the channel was obtained about 60 µm as shown in **Fig. 4. 11(a)** but it was inefficient in material removal. Therefore, finding the right balance of these parameters is crucial for minimizing taper while maintaining efficient machining. **Fig. 4. 11(b)** shows the surface profile of channel performed at 35V of applied voltage and 25wt% of electrolyte concentration which resulted in generation of 20.484^0 taper angle. **Fig. 4. 11(c)** shows the surface profile of channel performed at 40V of applied voltage and 20wt% of electrolyte concentration which resulted in generation of 25.717^0 taper angle. The interaction effects of voltage, electrolyte concentration, and tool feed rate are interdependent. For example, a combination of high voltage (i.e. 45V) and high electrolyte concentration (i.e. 25wt%) exacerbated taper angle of 32.08 degree and depth of the channel was obtained about 200µm as shown in **Fig. 4. 11(d)** due to excessive energy and gas bubble formation, leading to unstable machining conditions. It is evidenced from the study that the taper angle of the machined channel was increased as the depth of the channel was increased due to the unavailability of fresh electrolyte at the machining zone. Upward tool feeding techniques in ECD milling can positively impact the taper angle by improving material removal control, enhancing electrolyte and debris flushing, reducing thermal effects, ensuring better spark distribution.

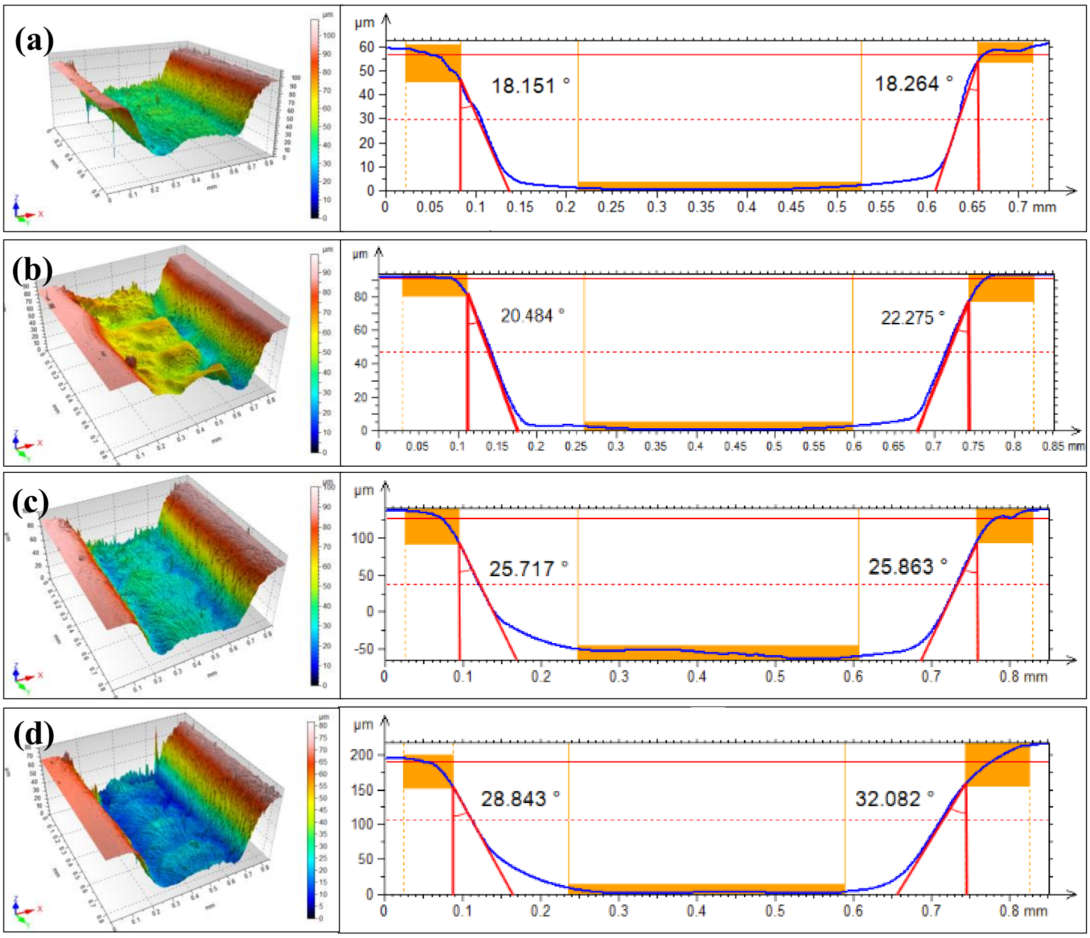

Fig. 4. 11 Channel fabricated at different conditions (a) 30V and 40 µm/sec TFR, (b) 35V and 25wt% electrolyte concentration, (c) 40V and 20wt% electrolyte concentration, (d) 45V and 25wt% electrolyte concentration

These benefits collectively contribute to achieving a more uniform channel width and reducing the taper angle, although careful consideration of machining parameters and potential challenges is necessary to obtain these benefits.

4.4.5 Effects of Energy Utilization on Milling Performance

A pattern that is initially linear but progressively gets closer to saturation is shown in **Fig. 4. 12**. This suggests that the majority of the incoming energy is efficiently used at lower energy levels. However, due to increased losses from heat dissipation, gas film instability, and spark inefficiencies, the percentage of energy used drops as energy levels rise. The majority of energy is expended at lower electrolyte concentrations. Although higher input voltage results in higher energy utilisation, the rate at which energy is used increases slowly in these situations.

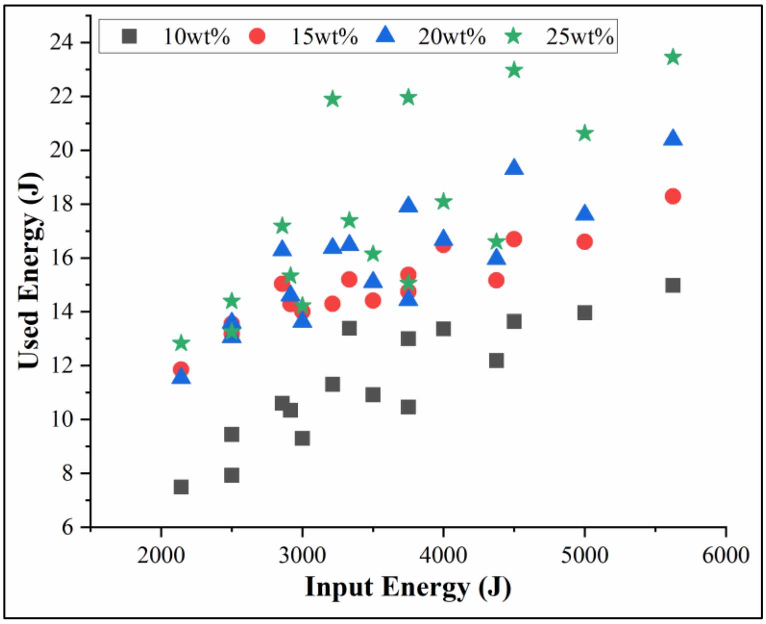

Fig. 4. 12 Energy utilization against input energy in ECD milling at different electrolyte concentrations

Beyond an ideal threshold, the energy input's diminishing returns are reflected in this nonlinear behaviour. Finding an appropriate energy window for effective machining is crucial, as the difference between input and consumed energy widens with increased input. A channel was created on glass using the input energy, and for every instance of energy utilised, the channel width varied. **Fig. 4. 13(a)** illustrates how the channel width gradually rises as the input energy increases. This is explained by improved spark production and more thermal energy entering the workpiece, which results in more thorough material removal and, as a result, wider channels.

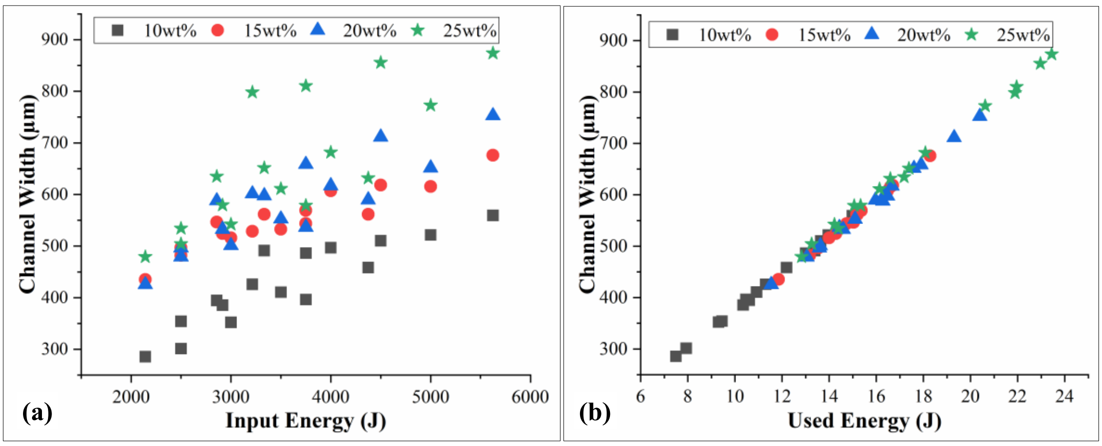

Fig. 4. 13 (a) Effects of input energy on channel width (b) Effects of used energy on channel width at different electrolyte concentrations

However, since high input energy tends to deteriorate the feature integrity due to uncontrolled energy dispersion, this also suggests an imbalance between dimensional precision and material removal rate. On the other hand, the relationship between channel width and consumed energy in **Fig. 4. 13(b)** is more straightforward and steadier. Used energy more closely matches real material removal since it represents the part of the input energy that actively contributes to the electrochemical discharge and localized heating. Used energy is a greater indicator of machining results than total input energy, as seen by the near-linear trend between used energy and channel width.

This finding provides credibility to the assumption that better control over channel dimensions can be achieved by concentrating on enhancing energy efficiency rather than just raising input energy. Further illustrating the drawbacks of excessive input energy is shown in **Fig. 4. 14(a)**. Greater sidewall divergence is indicated by an increase in taper angle with an increase in input energy. This is probably because of the uneven temperature distribution and the widening of the spark zone, which leads to more noticeable erosion along the sidewalls. Non-uniform channel profiles are the result of the discharge mechanism being unstable due to high energy input. Applications seeking vertical sidewalls and high precision are opposed to this result. On the other hand, **Fig. 4. 14(b)** illustrates a more controlled rise in taper angle as energy increases.

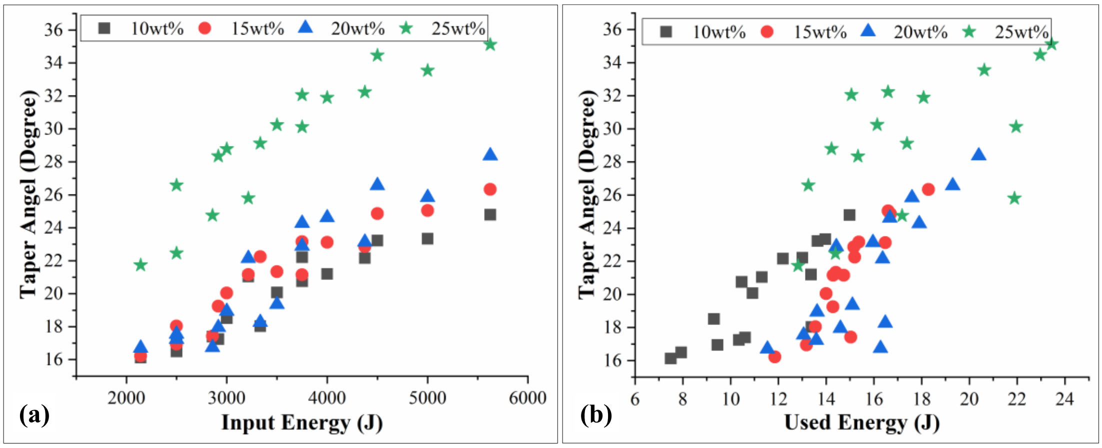

Fig. 4. 14 (a) Effects of input energy on taper angle (b) Effects of used energy on taper angle at different electrolyte concentrations

This implies that the influence on taper angle becomes more predictable and controllable when the energy that is effectively used is taken into account. The outcome suggests that taper creation is more closely related to the workpiece's localized energy absorption than to the system's gross input.

4.4.6 Generation of Various Patterns on Silica Glass

Electrochemical discharge milling (ECD milling) is a highly versatile method for generating various patterns on silica glass. This generation of patterns is usually done with proper control of process parameters and strategy of machining. In this study the patterns and various shapes were generated using upward tool feeding technique and with best parameters of ECD milling obtained from the study. **Fig. 4. 15** shows the various patterns and shapes fabricated on glass using ECD milling.

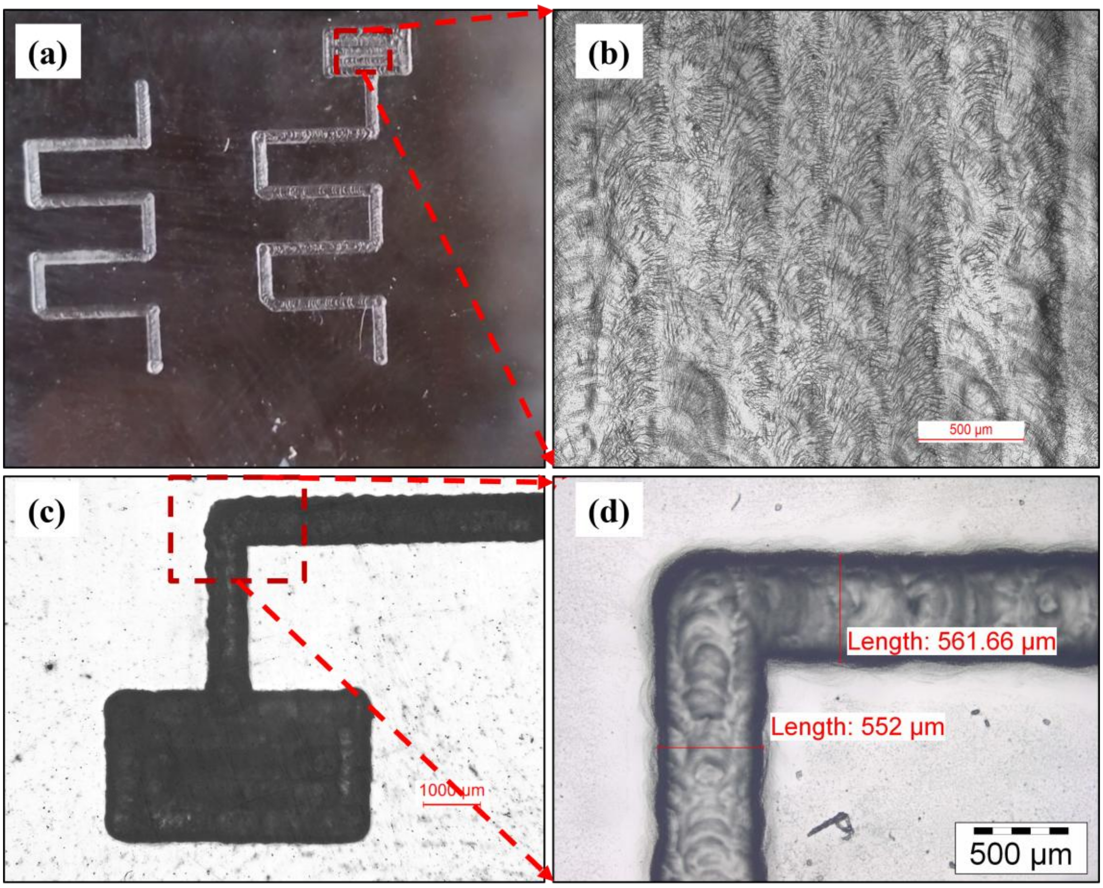

Fig. 4. 15 Zigzag patterns with rectangular shape cavity on glass (a) image of channel on workpiece, (b) smooth surface of the bottom, (c) optical image of cavity with channel, and (d) corner profile of the channel

Fig. 4. 15(a) shows the channels with rectangular-shaped cavities which are connected to the channel and can be used in microfluidics applications such as lab-on-chip devices. The bottom surface of the rectangular cavity at appropriate parameters is found to be smooth as shown in **Fig. 4. 15(b)**. The smoother bottom surface of the rectangular cavity is helpful for the flow of fluid. **Fig. 4. 15(c)** shows the optical image of channel with rectangular cavity where the corner of the channel is shown in the enlarged view in **Fig. 4. 15(d)**. It is

evidenced from the figures that the corners of the channel are perpendicular to each other which is possible in the upward tool feeding technique. Further, ECD milling was utilized to fabricate an E-shaped pattern on glass by adjusting tool movement and machining strategy as shown in **Fig. 4. 16(a)** along with an optical view of the E-shaped pattern as shown in **Fig. 4. 16(c)**. The ECD milling is also employed to generate other patterns of glass as shown in **Fig. 4. 16(b)**. All the patterns were fabricated to prove the feasibility of the upward tool feeding technique in ECD milling. Besides the patterns, the ECD milling also useful in making micro pillars on the glass by removing materials around the side of a particular area as shown in **Fig. 4. 16(d)**.

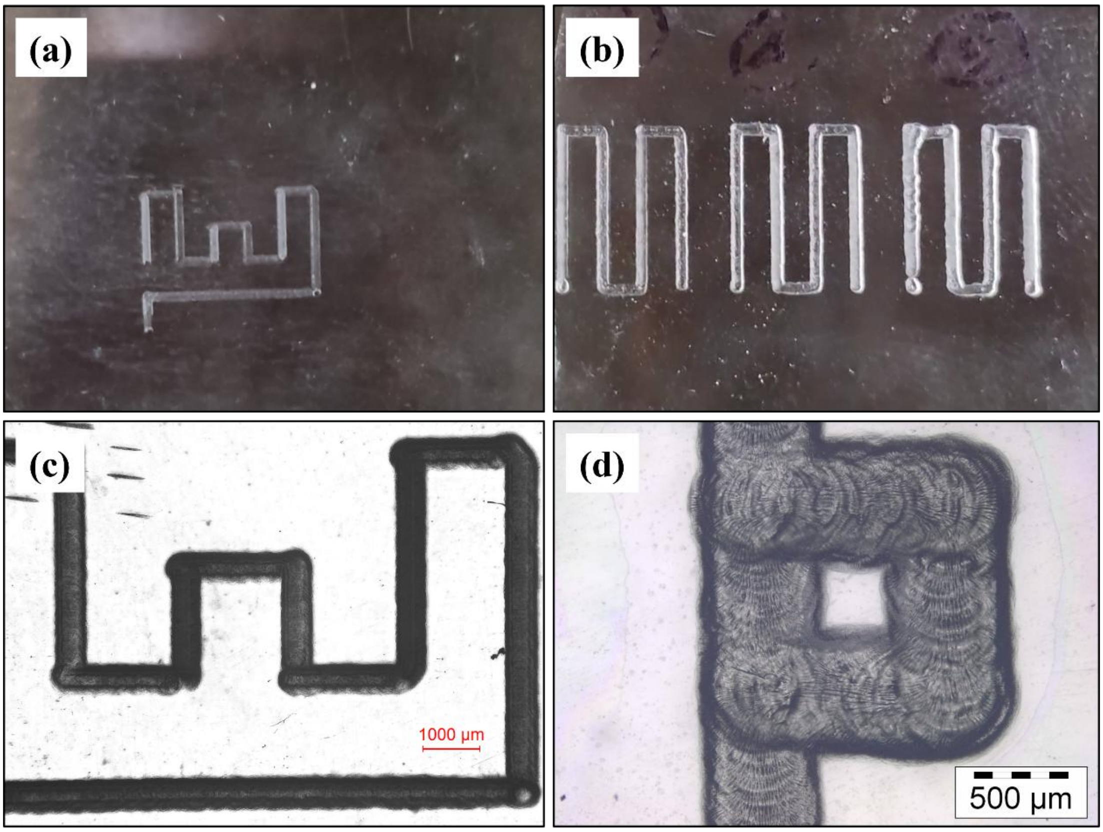

Fig. 4. 16 Various patterns on glass (a) E-shaped channel, (b) up and down pattern, (c) optical image of E-shaped channel, and (d) micro pillar formation

Besides the patterns shown in **Fig. 4. 16**, other fabrication of patterns was also attempted, as shown in **Fig. 4. 17**. Some patterns were fabricated with angular movement of the tool electrode and some multiple channels were generated that were connected to one source. These kinds of patterns and their integrated form can be used in various microfluidic devices, which were done using an upward tool feeding technique.

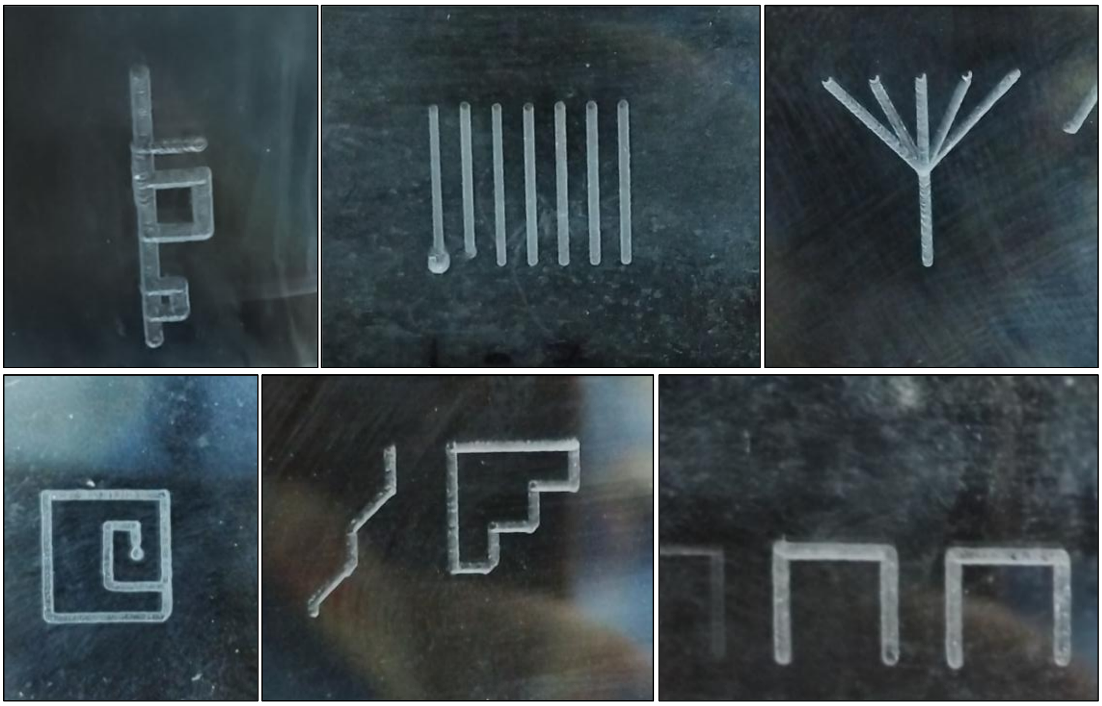

Fig. 4. 17 Other various patterns fabricated on glass using ECD milling

These generated patterns have numerous applications, including the production of microfluidic devices, optical components. For instance, precise microchannels and reservoirs can be created for lab-on-chip devices. Overall, ECD milling provides a highly controllable and precise approach to pattern generation on silica glass, making it a valuable technique for both industrial and biomedical applications.

The experimental results obtained in the present investigation show good agreement with previously reported studies on electrochemical discharge machining of silica glass. Similar to the observations of Rajput et al. **[102]**, applied voltage and electrolyte concentration were found to be the dominant parameters governing machining performance. In the present work, the material removal rate increased continuously with increasing voltage and electrolyte concentration, reaching a maximum value of 6.097 µg/min at 45 V and 25 wt% NaOH, confirming that higher discharge energy enhances thermal erosion and chemical etching. The relationship between applied voltage and channel geometry observed in the present work also agrees with the findings of Zhao et al. **[98]**, who reported that increasing discharge voltage improves machining efficiency but enlarges the entrance diameter and deteriorates dimensional accuracy. Similarly, the present investigation found that channel width increased with increasing voltage because of intensified side sparking and higher spark energy. The channel width reached 616.86 µm at 40 V and 20 wt% NaOH, indicating that excessive discharge energy causes greater lateral material removal. The influence of electrolyte concentration observed in this investigation further supports the conclusions of Mallick et al. **[103]**, who reported that electrolyte chemistry strongly influences machining depth and surface quality. The present study demonstrates that increasing electrolyte concentration increases conductivity and discharge intensity, thereby improving MRR. However, excessive concentration combined with high voltage generated unstable spark discharges, larger craters, and higher taper angles. The maximum taper angle of 32.082° was observed at 45 V and 25 wt% NaOH, whereas it decreased to 18.151° at 30 V, confirming that balanced discharge energy is essential for dimensional accuracy.

Although the above machining trends align well with previously published ECDM investigations, the present work makes a distinct contribution by applying the vertically upward tool-feeding technique. Earlier studies generally employed conventional gravity-feed or downward tool-feeding systems, whereas the proposed technique continuously removes gas bubbles from the machining zone through buoyancy and supplies fresh electrolyte to the discharge region. This resulted in more stable spark discharges, reduced side sparking, and improved machining quality. As demonstrated in Chapter 3, the upward tool feeding technique reduced tool wear to 4.95% and reduced channel width by approximately 11% compared with the conventional feeding method. These improvements provided the basis for the high-quality microchannels, intricate patterns, and rectangular cavities successfully fabricated in the present study.

4.5 Outcomes of the Study

The experimental study of electrochemical discharge milling focuses on the effects of applied voltage, electrolyte concentration and TFR on MRR using the novel upward tool feeding technique. Post-experimental analysis showed that the favorable conditions for higher MRR, lower width of the channel and lower R_a value were different for every case. The following conclusion can be drawn from the analysis done so far:

(i) In ECD milling, machining quality is governed more by used energy than total input energy. For instance, at an input energy of 2000 J, the used energy may be only 7-8 J due to heat dissipation and gas film instability, whereas at 5000 J input, the used energy rises only slightly to 16-20 J, despite a much larger input increase. While higher input energy increases spark generation and channel width (e.g., from 110 μm at 8 J used energy to 165 μm at 20 J), excessive input leads to taper growth (e.g., taper angle rising from 3.2° to 6.8°) and reduced dimensional precision.

(ii) A larger amount of material removal was observed at higher applied voltage and electrolyte concentration as well as at the lower TFR. At 25 wt% of aqueous NaOH solution and 45 V applied voltage the MRR was found to be 6.097 μg/min. The value of MRR decreases as the TFR increases.

(iii) High MRR was noticed at 45 V and 25 wt% of electrolyte concentration. Better surface finish was observed at 40 V, 20 wt% of NaOH solution and 40 μm/sec TFR in terms of R_a value of 0.222 μm surface roughness. The R_a value was increased at lower voltage and electrolyte concentration because of insufficient spark discharge which removed materials from the workpiece erratically and also at higher voltage and electrolyte concentration due to uncontrollable spark discharge that generates irregular crater on the workpiece surface.

(iv) With the increase of applied voltage, the width of channel increases due to side sparking and intense energy of spark discharge. Width of 616.86 μm and surface roughness, R_a of 0.377 μm were achieved at bottom layer at 40 V, 20 wt% of NaOH solution and 50 μm/sec of tool feed rate.

(v) High voltage increases spark energy, leading to greater material removal and larger taper angles due to heightened thermal effects and gas bubble formation. For instance, at 45V and 25 wt% electrolyte concentration, the taper angle reached 32.082 degrees, with a channel depth of about 200 μm. Conversely, lower voltage reduces thermal damage, resulting in smaller taper angles; at 30V and a tool feed rate of 40 μm/sec, the taper angle was 18.151 degrees, with a channel depth of about 60 μm.

(vi) Electrochemical Discharge Milling (ECD milling) effectively generates various patterns on glass, demonstrating its versatility and precision. By varying process parameters and employing an upward tool-feeding technique, intricate shapes such as zigzag patterns with rectangular cavities, E-shaped channels, and micropillars were successfully fabricated. Overall, ECD milling provides a controllable and precise approach for creating complex patterns on silica glass, suitable for industrial and biomedical uses.

The upward tool-feeding technique is also tested on other materials, such as polycarbonate and PMMA, in addition to glass. Chapter 6 of the study explored the possibility of milling on various polymers by altering process parameters.

Chapter 5

OPTIMIZATION OF ELECTROCHEMICAL DISCHARGE MILLING PROCESS WITH UPWARD TOOL FEEDING BASED ON RESPONSE SURFACE METHODOLOGY

5.1 Introduction

Electrochemical Discharge milling (ECD milling) is a hybrid machining process in which controlled spark discharges generated at the tool-electrolyte interface enable material removal from hard and brittle materials. The performance of this process is highly sensitive to variations in machining parameters, and small deviations in operating conditions can lead to substantial changes in channel geometry, surface finish, taper characteristics, and material removal rates. Because of this inherent complexity, a systematic and statistically robust experimental approach is necessary to understand the combined and individual influences of key process variables. Traditional trial-and-error methods or one-factor-at-a-time experimentation are not capable of capturing the nonlinear relationships, interactive effects, and curved response behaviour typically observed in ECD milling. Therefore, an advanced statistical design framework is essential for developing reliable predictive models and optimizing the machining process.

The optimization presented in this chapter is carried out using the upward tool-feeding technique because previous investigations (Chapters 3 and 4) have established its superiority over the conventional ECD milling approach. In the conventional top-feeding method, hydrogen gas bubbles generated during electrolysis accumulate around the machining zone, restricting the supply of fresh electrolyte and causing unstable spark discharges, increased side sparking, and higher tool wear. The upward tool-feeding technique uses the natural buoyancy of gas bubbles to facilitate their removal from the machining zone while continuously replenishing the electrolyte. This results in a more stable gas film, improved spark localization at the tool tip, reduced tool wear, narrower channel width, and enhanced surface quality. Since the upward tool-feeding technique provides a stable and reliable machining environment, it provides an appropriate basis for process optimization using Response Surface Methodology (RSM). Therefore, this chapter focuses on optimizing the applied voltage, electrolyte concentration, and tool feed rate under an upward tool-feeding configuration to achieve the best compromise among material removal rate, dimensional accuracy, surface roughness, and taper angle.

In this chapter, Response Surface Methodology (RSM) was employed to construct empirical models and evaluate the effects of electrolyte concentration, applied voltage, and tool feed rate on the machining responses. Among the available RSM designs, the Box-Behnken Design (BBD) was selected because it provides high modeling efficiency, requires fewer experimental runs, and avoids extreme corner points that could induce excessive sparking or thermal instability. The BBD approach allowed each of the three input factors to be studied at three coded levels, enabling the development of a full quadratic model capable of capturing linear, interaction, and squared effects. A total of 15 experimental trials, including 12 edge combinations and 3 centre-point replicates, were conducted to ensure accurate estimation of pure error and to facilitate lack-of-fit assessment. To evaluate machining performance comprehensively, four critical responses were measured for each experiment: width of channel, surface roughness (Ra), taper angle, and material removal rate (MRR). These responses collectively represent machining accuracy, surface integrity, dimensional uniformity, and productivity. The experimental data obtained from the BBD plan were analysed using Analysis of Variance (ANOVA) to determine parameter significance, model adequacy, and predictive capability. The RSM framework enabled the generation of response surfaces and optimization plots, supporting both single-response and multi-response optimization for identifying the most favourable machining conditions.

5.2 Plan of Experiments

To investigate the influence of electrolyte concentration, voltage, and tool feed rate on machining performance during Electrochemical Discharge milling (ECD milling), an organized, statistically robust experimental plan was developed using the Box-Behnken design (BBD) within the Response Surface Methodology (RSM) framework. Three machining parameters, such as electrolyte concentration, applied voltage, and tool feed rate, were selected based on preliminary trials and their importance in governing spark formation and material removal in ECD milling of Silica glass. Each factor was studied at three levels, allowing the development of a full quadratic response surface model capable of capturing both linear and nonlinear behaviour. The Box-Behnken design generated a total of 15 experimental runs, including 12 edge-point trials and 3 replicated centre-point trials. The centre points were incorporated to estimate pure error, assess model curvature, and enable lack-of-fit testing. The process variables and their levels are given in **Table 5. 1**

Table 5. 1 Process variables and their levels

Process Parameters	Unit	Symbol	Levels		
			-1	0	+1
Electrolyte Concentration	wt%	A	10	15	20
Voltage	V	B	35	40	45
Tool feed rate	µm/sec	C	40	50	60

Four critical machining responses were measured for each experimental run, such as the width of the machined channel, surface roughness (R_a), taper angle, and material removal rate (MRR). These responses collectively describe machining accuracy, surface quality, dimensional uniformity, and productivity, providing a comprehensive evaluation of the ECD milling process. The experimental data obtained from the BBD plan were fitted to second-order quadratic polynomial models, enabling estimation of linear, interaction, and squared effects. Analysis of Variance (ANOVA) was then performed to assess the statistical significance of each model and its individual terms. This experimental plan not only facilitated the construction of response surface plots but also enabled both single-response and multi-response optimization using desirability functions.

5.3 Results and Discussion

The outcomes of the study are derived from comprehensive statistical analyses using ANOVA, regression modelling, response surfaces, and optimization. These evaluations reveal the most influential machining parameters, their individual and interactive effects, and the optimal operating conditions that govern machining quality and efficiency in ECD milling.

5.3.1 Analysis of Width of Channel Using ANOVA and RSM

The ANOVA table for the width of the channel is shown in **Table 5. 2**, which shows that the developed quadratic RSM model is statistically significant, confirming that the factors included in the model can adequately explain the variation in channel width. The linear terms contribute most strongly to the model, with electrolyte concentration (Factor A) being the dominant parameter. Voltage (B) also has a significant effect, followed by tool feed rate

(C), which remains significant at the 5% level. The regression equation generated from RSM is given in equation (5.1).

Width of Channel (μm) = -2127 + 43.7A + 88.8B + 15.4C - 1.568 A^2- 0.874 B^2 - 0.025 C^2 + 0.592 AB - 0.117 AC - 0.347 BC ... (5.1)

The lack-of-fit is significant due to very low pure error, which is common in machining experiments with highly repeatable responses. The model exhibits a high coefficient of determination (R^2 = 96.23%). Overall, the ANOVA indicates that electrolyte concentration and voltage are the primary contributors to channel width, with a smaller but significant effect from feed rate. The response surface plots clearly show that the width of channel increases with increases in both electrolyte concentration (A) and voltage (B). In **Fig. 5. 1**, the surface exhibits a strong upward curvature toward the high-electrolyte concentration and high-voltage region, resulting in a broad, dome-shaped growth of channel width. This indicates that both concentration and voltage have a synergistic but non-linear influence on widening the width of channel.

Table 5. 2 Analysis of Variance for the width of the channel

Source	DF	Adj SS	Adj MS	F-Value	P-Value
Model	9	79395.1	8821.7	14.20	0.005
Linear	3	70172.0	23390.7	37.64	0.001
A	1	41878.6	41878.6	67.39	0.000
B	1	21785.3	21785.3	35.06	0.002
C	1	6508.1	6508.1	10.47	0.023
Square	3	7003.2	2334.4	3.76	0.004
A^2	1	5673.3	5673.3	9.13	0.029
B^2	1	1762.7	1762.7	2.84	0.003
C^2	1	24.0	24.0	0.04	0.032
2-Way Interaction	3	2219.9	740.0	1.19	0.002
A×B	1	875.5	875.5	1.41	0.009
A×C	1	137.5	137.5	0.22	0.048
B×C	1	1206.9	1206.9	1.94	0.002
Error	5	3107.0	621.4		
Lack-of-Fit	3	3107.0	1035.7	450.94	0.065
Pure Error	2	0.4	0.2		
Total	14	82502.1			
Model Summary		S	R^2	R^2(adj)	R^2(pred)
		24.9280	96.23%	89.46%	92.84%

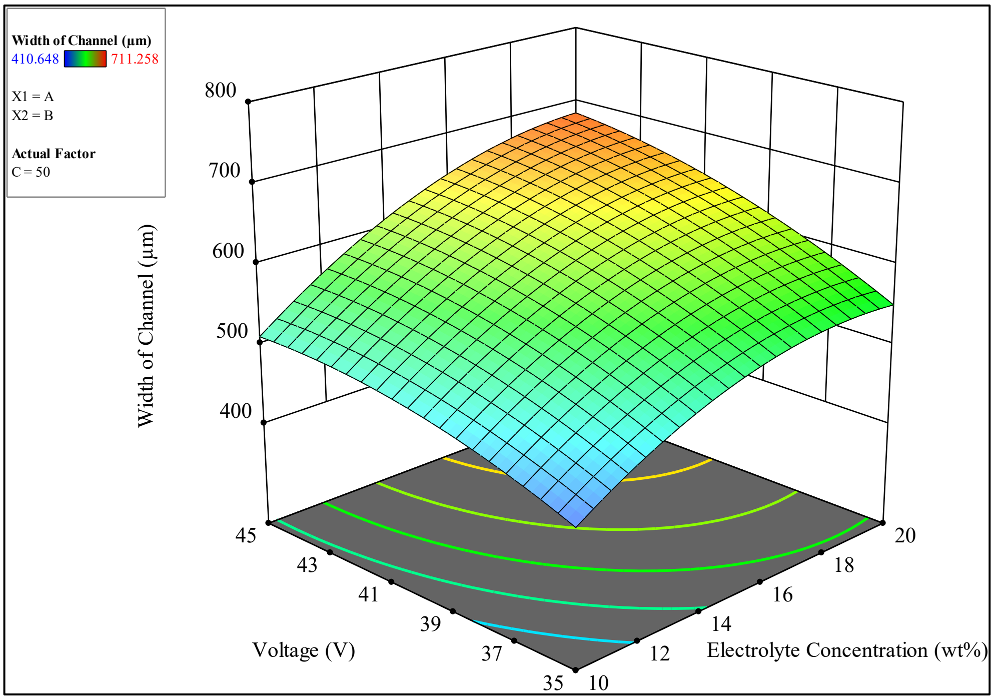

Fig. 5. 1 3D surface plot of width of channel as a function of voltage and electrolyte concentration.

Fig. 5. 2 shows that the surface trends upward with increasing electrolyte concentration, showing that concentration remains a dominant driver of channel enlargement.

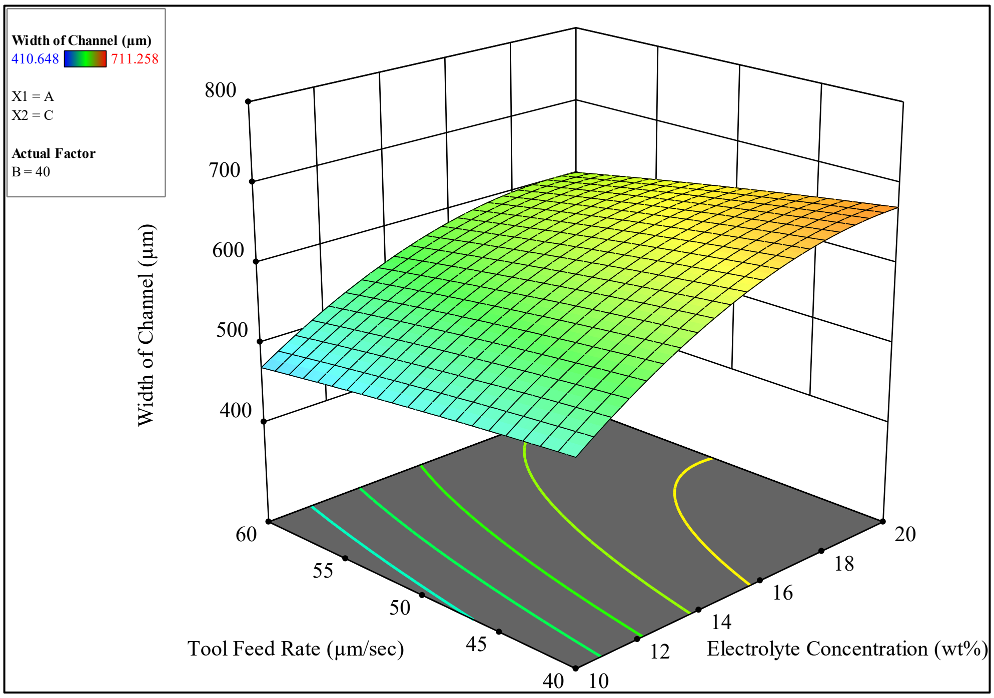

Fig. 5. 2 3D surface plot of width of channel as a function of tool feed rate and electrolyte concentration.

Feed rate (C), however, shows a milder effect: increasing C produces a gradual rise in WOC. The feed rate influences channel width but less aggressively than voltage. These plots highlight that electrolyte concentration and voltage are the primary variables controlling channel width, while feed rate plays only a moderate role.

5.3.2 Analysis of Surface Roughness Using ANOVA and RSM

The ANOVA table for the fitted quadratic model is given in **Table 5. 3** which shows that the overall model is statistically significant, indicating that the selected factors adequately explain the variation in the response. The model's R^2 (95.76%) indicates excellent fitting to the data. Overall, the ANOVA indicates that voltage and feed rate, particularly the quadratic effect of voltage, are the primary contributors to the response. The regression equation generated from RSM is given in equation (5.2).

$$\text{Surface Roughness } (\mu m) = 9.38 - 0.0445A - 0.4374B - 0.0148C + 0.000575A^2 + 0.005935B^2 + 0.000326C^2 - 0.000210AB + 0.000690AC - 0.000500BC \quad \text{... (5.2)}$$

Table 5. 3 Analysis of Variance for Surface Roughness (R_a)

Source	DF	Adj SS	Adj MS	F-Value	P-Value
Model	9	0.160748	0.017861	12.54	0.006
Linear	3	0.070411	0.023470	16.48	0.005
A	1	0.000253	0.000253	0.18	0.001
B	1	0.017020	0.017020	11.95	0.018
C	1	0.053138	0.053138	37.30	0.002
Square	3	0.082966	0.027655	19.41	0.003
A^2	1	0.000763	0.000763	0.54	0.037
B^2	1	0.081287	0.081287	57.07	0.001
C^2	1	0.003930	0.003930	2.76	0.038
2-Way Interaction	3	0.007371	0.002457	1.72	0.017
A×B	1	0.000110	0.000110	0.08	0.042
A×C	1	0.004761	0.004761	3.34	0.007
B×C	1	0.002500	0.002500	1.76	0.003
Error	5	0.007122	0.001424		
Lack-of-Fit	3	0.007122	0.002374	1017.46	0.071
Pure Error	2	0.000005	0.000002		
Total	14	0.167870			
Model Summary		S	R^2	R^2(adj)	R^2(pred)
		0.0377419	95.76%	88.12%	92.32%

The response surface for surface roughness as a function of electrolyte concentration (A) and voltage (B) at a fixed feed rate (C = 50 µm/s) shows a distinct bowl-shaped curvature, indicating a strong quadratic relationship, as shown in **Fig. 5. 3**. At low and high values of voltage, surface roughness increases, whereas moderate voltage levels produce the minimum surface roughness. This curvature is consistent with discharge behavior in ECD milling, i.e., very low voltage generates insufficient spark energy, causing uneven dissolution, while excessively high voltage leads to aggressive sparking, which increases roughness. Increasing electrolyte concentration gradually reduces surface roughness, reflecting enhanced ionic strength, more stable sparking, and better flushing, which collectively lead to smoother surfaces. In **Fig. 5. 4**, the surface shows a monotonic decrease in surface roughness as the feed rate increases, especially when combined with high electrolyte concentration. Higher feed rates reduce the duration of tool-workpiece thermal interaction, resulting in rougher micro-topography.

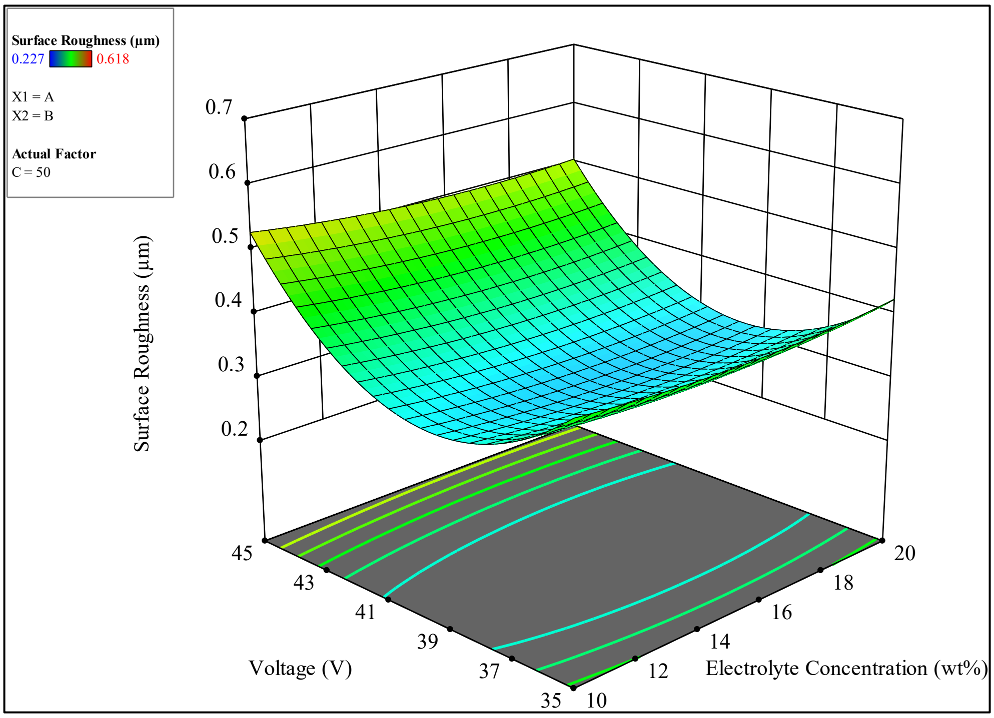

Fig. 5. 3 3D surface plot of surface roughness (R_a) as a function of voltage and electrolyte concentration.

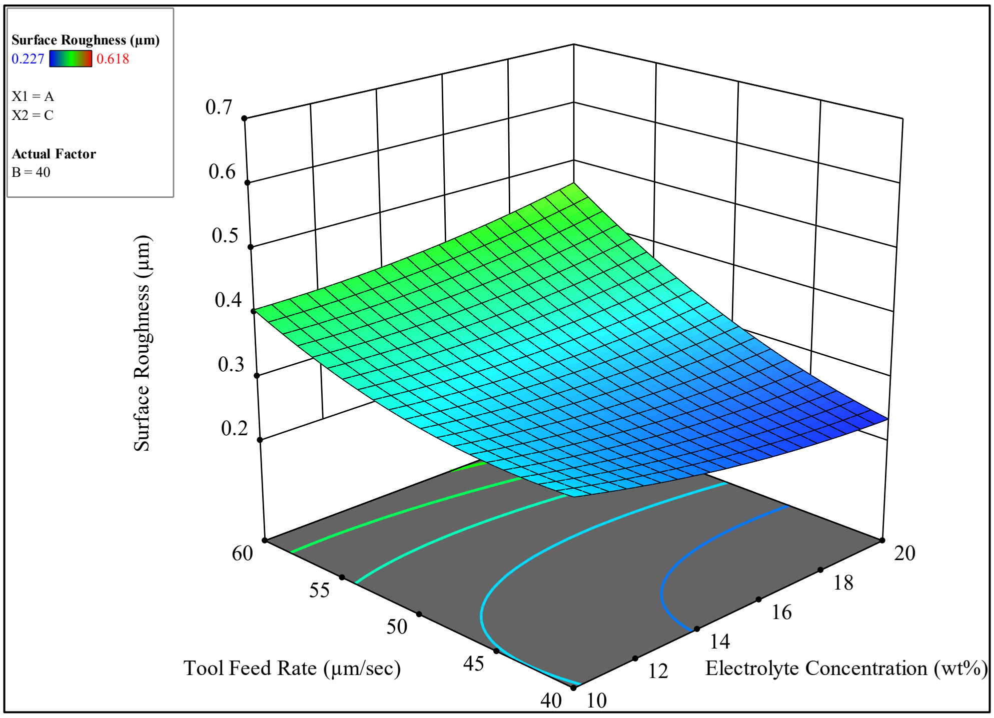

Fig. 5. 4 3D surface plot of surface roughness (R_a) as a function of tool feed rate and electrolyte concentration.

The two response surfaces demonstrate that surface roughness is minimized at high electrolyte concentration, moderate voltage, and low tool feed rate.

5.3.3 Analysis of Taper Angle Using ANOVA and RSM

The **Table 5. 4** shows the ANOVA results is statistically significant, indicating that the selected input factors collectively influence the response effectively. The linear component of the model is highly significant, demonstrating that most of the variability in the response is explained by the linear effects of the factors. Voltage (B) and feed rate (C) show very strong significance, making them the dominant contributors to the response. The model exhibits a high R^2 value (94.73%), showing an excellent fit to the observed data. The regression equation generated from RSM is given in equation (5.3).

$$\text{Taper Angle (Degree)} = 33.9 + 0.48A - 1.42B + 0.414C - 0.0469A^2 + 0.0143B^2 - 0.00577C^2 + 0.0407AB - 0.0114AC + 0.0022BC \quad \dots (5.3)$$

The **Fig. 5. 5** shows that the taper angle increases sharply with voltage, while electrolyte concentration has a milder but noticeable effect. The rising slope toward the high-voltage region indicates that stronger discharge energy at higher voltages causes excessive lateral erosion, widening the upper portion of the channel and therefore increasing taper.

Table 5. 4 Analysis of Variance for taper angle

Source	DF	Adj SS	Adj MS	F-Value	P-Value
Model	9	103.580	11.5089	9.98	0.010
Linear	3	91.271	30.4235	26.39	0.002
A	1	3.572	3.5716	3.10	0.039
B	1	39.367	39.3665	34.15	0.002
C	1	48.332	48.3325	41.93	0.001
Square	3	6.832	2.2773	1.98	0.006
A^2	1	5.078	5.0778	4.40	0.040
B^2	1	0.475	0.4751	0.41	0.009
C^2	1	1.230	1.2298	1.07	0.049
2-Way Interaction	3	5.477	1.8257	1.58	0.004
A×B	1	4.132	4.1317	3.58	0.037
A×C	1	1.297	1.2973	1.13	0.007
B×C	1	0.048	0.0482	0.04	0.016
Error	5	5.764	1.1528		
Lack-of-Fit	3	5.764	1.9213	7332.00	0.093
Pure Error	2	0.001	0.0003		
Total	14	109.343			
Model Summary		S	R^2	R^2(adj)	R^2(pred)
		1.07366	94.73%	85.24%	85.93%

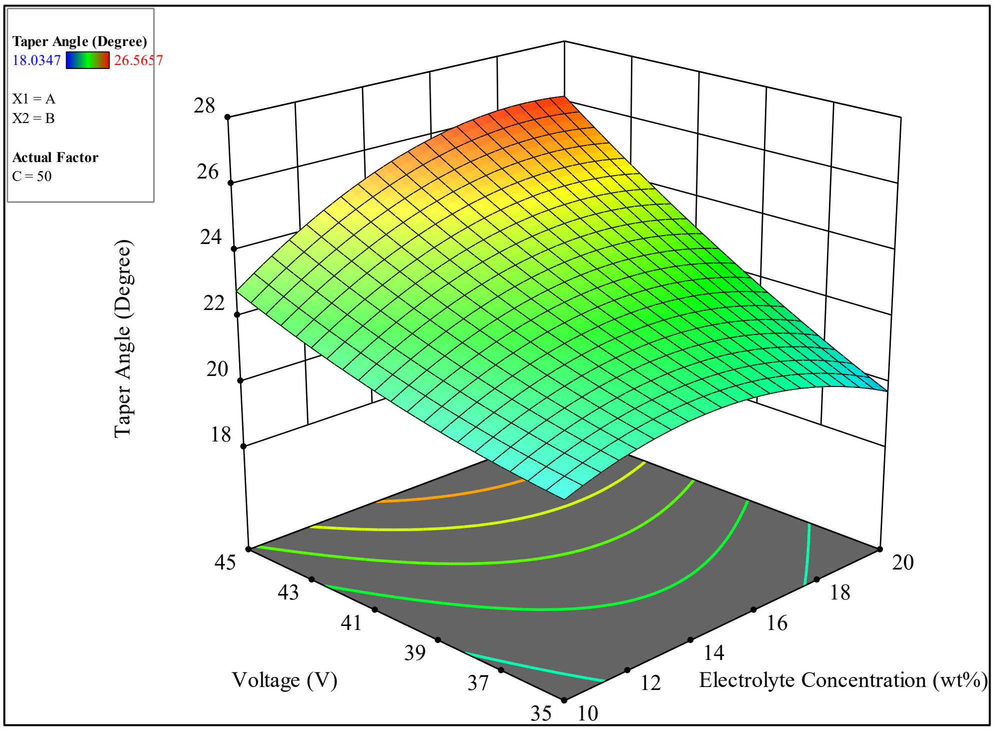

Fig. 5. 5 3D surface plot of taper angle as a function of voltage and electrolyte concentration.

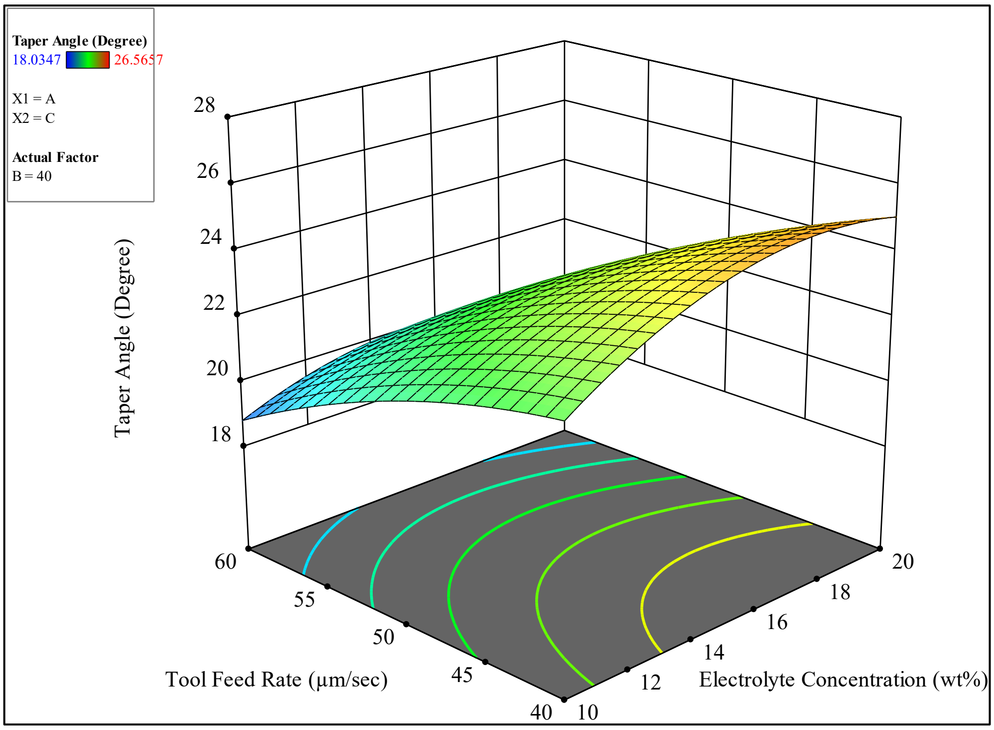

Fig. 5. 6 3D surface plot of taper angle as a function of tool feed rate and electrolyte concentration.

This behavior is typical in ECD milling, where elevated voltage enhances plasma channel expansion, leading to non-uniform side wall removal. Electrolyte concentration influences taper angle through its effect on discharge stability, i.e., at low concentrations, the spark is less stable, producing uneven side erosion, whereas at higher concentrations, ion availability increases, smoothing the thermal-chemical. In **Fig. 5. 6**, the surface shows a different trend, i.e., taper angle increases steadily with feed rate. As the feed rate increases, the tool spends less time at each point, causing incomplete material dissolution at the bottom while allowing more thermal spreading on the top surface, resulting in a larger taper. The voltage and feed rate are the primary drivers of taper angle, with voltage dominating taper angle behavior.

5.3.4 Analysis of Material Removal Rate Using ANOVA and RSM

The ANOVA table, which is given in **Table 5. 5** indicates that the fitted quadratic model is highly significant, demonstrating that the selected input factors explain nearly all of the variability in the response. Within the linear effects, electrolyte concentration is the most influential variable by a large margin, followed by voltage and tool feed rate, all of which are highly significant.

Table 5. 5 Analysis of Variance for Material Removal Rate

Source	DF	Adj SS	Adj MS	F-Value	P-Value
Model	9	21.8238	2.4249	380.50	0.000
Linear	3	21.7042	7.2347	1135.23	0.000
A	1	18.6152	18.6152	2920.99	0.000
B	1	1.8452	1.8452	289.54	0.000
C	1	1.2438	1.2438	195.16	0.000
Square	3	0.0618	0.0206	3.23	0.009
A^2	1	0.0042	0.0042	0.65	0.006
B^2	1	0.0015	0.0015	0.23	0.030
C^2	1	0.0525	0.0525	8.24	0.035
2-Way Interaction	3	0.0579	0.0193	3.03	0.002
A×B	1	0.0392	0.0392	6.16	0.006
A×C	1	0.0186	0.0186	2.92	0.018
B×C	1	0.0000	0.0000	0.00	0.043
Error	5	0.0319	0.0064		
Lack-of-Fit	3	0.0319	0.0106	45.52	0.072
Pure Error	2	0.0005	0.0002		
Total	14	21.8557			
Model Summary		S	R^2	R^2(adj)	R^2(pred)
		0.0798306	99.85%	99.59%	97.67%

The model performance metrics are outstanding, with R^2 = 99.85%, adjusted R^2 = 99.59%, and predicted R^2 = 97.67%, confirming excellent data fit and very strong predictive capability. The regression equation generated from RSM is given in equation (5.4).

$$MRR(\mu g/min) = -0.70 + 0.2551A + 0.101B - 0.1378C - 0.00134A^2 - 0.00080B^2 + 0.001192C^2 + 0.00396AB - 0.001365AC - 0.000011BC \quad ... (5.4)$$

The response surface in **Fig. 5. 7** shows a strong, steady, and almost linear increase in MRR with increases in electrolyte concentration and voltage. Higher electrolyte concentration improves ionic conductivity, promoting a higher frequency of spark discharge, while increasing voltage also enhances spark discharge strength. **Fig. 5. 8** shows that MRR increases with both electrolyte concentration and feed rate, although the effect of feed rate is more moderate compared to voltage. The MRR increase at a lower tool feed rate is noticeable but not as steep as with voltage or concentration.

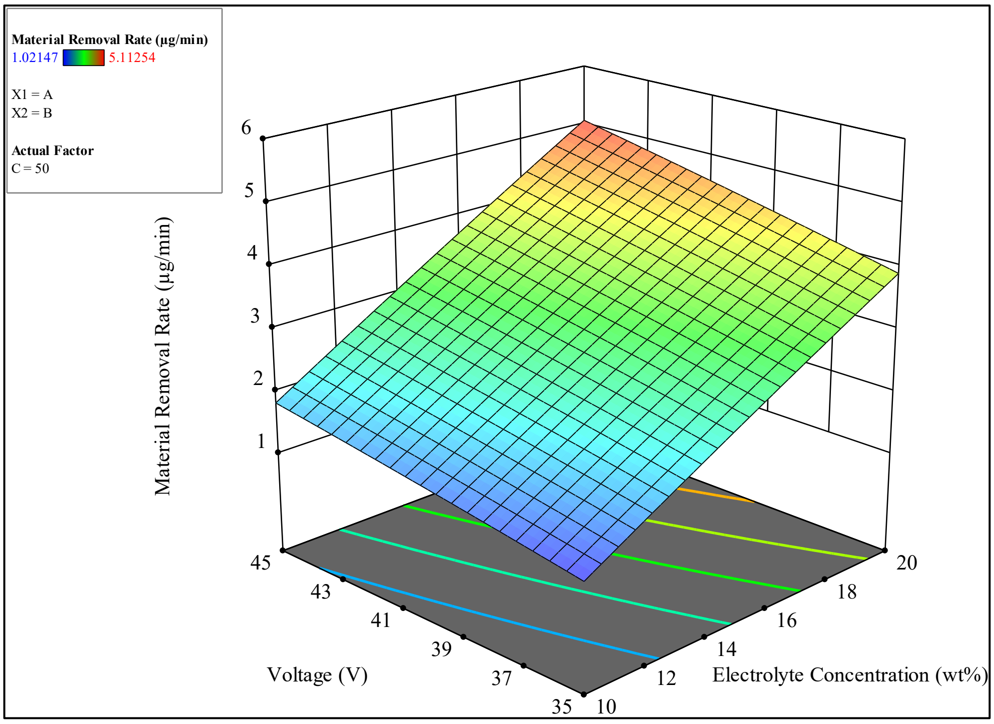

Fig. 5. 7 3D surface plot of material removal rate as a function of voltage and electrolyte concentration.

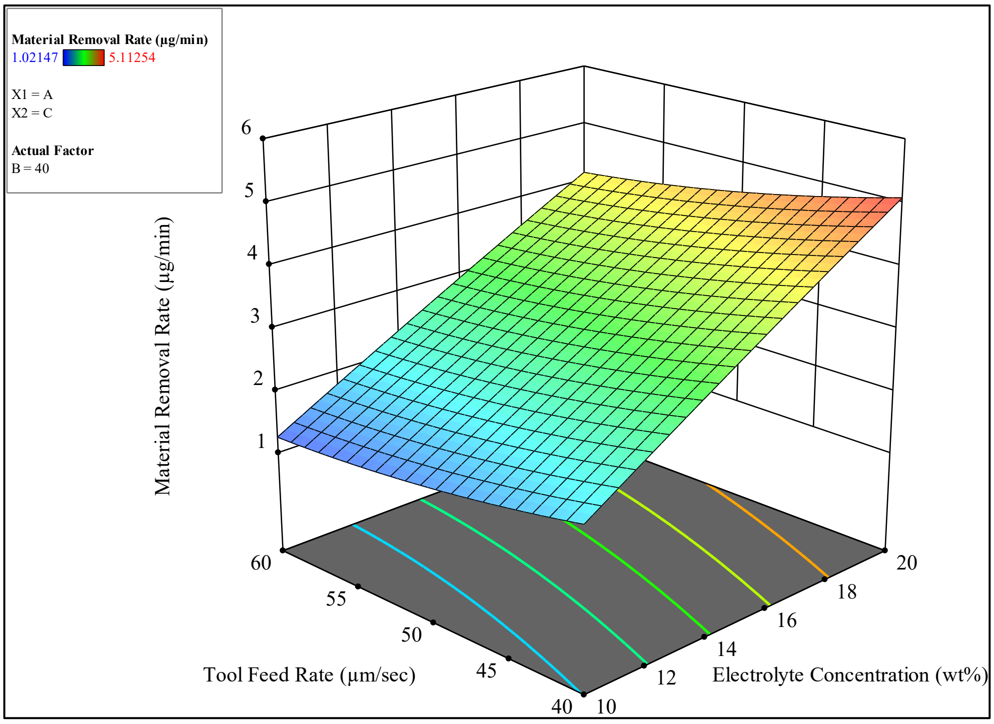

Fig. 5. 8 3D surface plot of material removal rate as a function of tool feed rate and electrolyte concentration.

Both plots demonstrate that electrolyte concentration is the most dominant factor, followed closely by voltage, in enhancing MRR. For maximizing MRR in ECD milling, operating at high concentration, high voltage, and low tool feed rate yields the most efficient material removal.

5.3.5 Single-Objective Optimization of ECD milling Responses

Optimization on width of channel, surface roughness, taper angle and material removal rate were performed separately using single-objective optimization as well as combined effects were also observed using multi-objective optimization.

5.3.5.1 Single-Objective Optimization on Width of Channel

The optimization plot for width of channel shows that a target value of 500 µm is achieved with a desirability of 1.0, indicating a perfect match between the predicted and desired output, as shown in **Fig. 5. 9(a)**. The plot reveals that the channel width increases with both electrolyte concentration (EC) and voltage, while the effect of tool feed rate (TFR) is mildly negative. The optimal solution is obtained at EC of 13.47 wt%, Voltage of 35 V, and TFR of 60 µm/s, where the predicted WOC equals the target value of 500 µm.

5.3.5.2 Single-Objective Optimization on Surface Roughness

For Surface Roughness, the optimization seeks the lowest possible value and achieves desirability of 0.9998, very close to perfect desirability. The plot shown in **Fig. 5. 9(b)** indicates that surface roughness in terms of R_a value decreases steadily as electrolyte concentration increases, showing that higher electrolyte concentration produces smoother surfaces. Voltage shows a strong quadratic effect, with surface roughness being minimized at a mid-range value of 38.94 V. Tool feed rate, on the other hand, increases surface roughness at higher levels, implying that slower feed rates allow better surface finishing. The optimum was therefore found at EC = 20 wt%, Voltage of 38.94 V, and TFR of 40 µm/s. This combination maximizes chemical dissolution while maintaining controlled spark energy and exposure time, leading to the lowest achievable roughness.

5.3.5.3 Single-Objective Optimization on Taper Angle

The goal for taper angle was to reduce side-wall divergence, and the optimizer again returns the maximum desirability value (d = 1.0). The taper angle decreases with increasing electrolyte concentration, reaching a minimum at an EC of 20 wt%, as shown in **Fig. 5. 9(c)**, indicating the importance of high conductivity in stabilizing spark locations. Voltage displays a strong linear effect, with taper increasing rapidly beyond 35 V due to stronger side discharges.

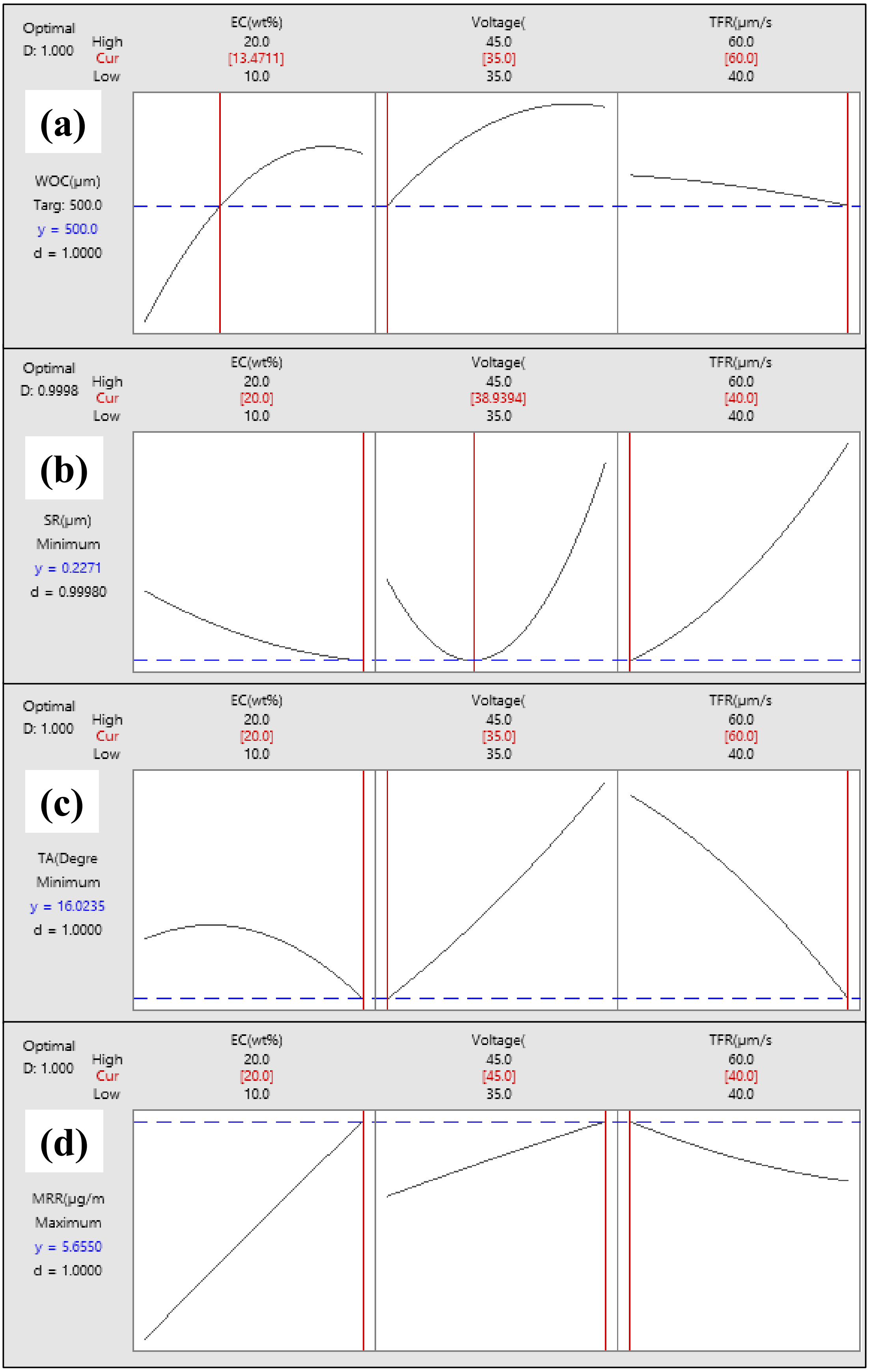

Fig. 5. 9 Single objective optimization plot for (a) width of channel, (b) surface roughness (R_a), (c) taper angle, and (d) material removal rate

The tool feed rate shows a negative slope; i.e. higher feed rates help reduce taper by minimizing thermal load and exposure time. The optimum is obtained at EC of 20 wt%, Voltage of 35 V, and TFR of 60 µm/s, yielding a minimum TA of 16.02°.

5.3.5.4 Single-Objective Optimization on Material Removal Rate

The MRR optimization reaches the highest desirability value (d = 1.0), showing an exact match to the maximum achievable removal rate. MRR increases sharply with electrolyte concentration and voltage, as both parameters intensify electrochemical reaction rates and spark discharge energy. TFR shows a peak in the middle range, indicating an optimal balance between exposure time and spark generation density. The optimized parameters are EC of 20 wt%, Voltage of 45 V, and TFR of 40 µm/s, resulting in the maximum predicted MRR of 5.655 µg/min.

5.3.6 Multi-Objective Optimization of ECD milling Responses

The multi-objective optimization plot in **Fig. 5. 10** shows how the combined desirability of all four responses, i.e., MRR, taper Angle, surface roughness, and width of channel is maximized simultaneously by adjusting the three machining parameters.

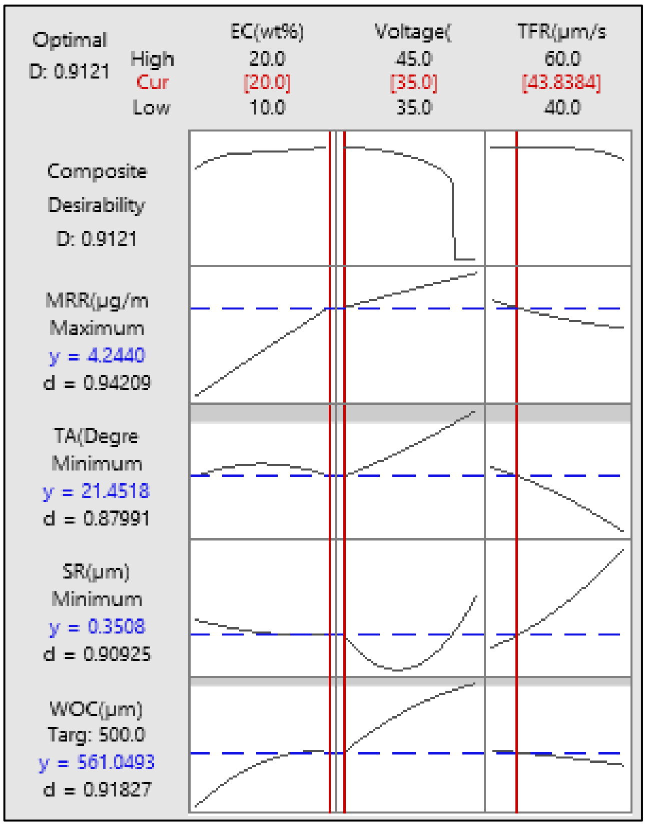

Fig. 5. 10 Multi-Objective optimization plot for width of channel, surface roughness (R_a), taper angle, and material removal rate

The composite desirability obtained is 0.9121, indicating an excellent compromise solution that balances conflicting machining requirements. At this optimum, the algorithm selects Electrolyte Concentration of 20 wt%, Voltage of 35 V, and Tool Feed Rate of 43.84 µm/s. These settings provide a balanced interaction between electrochemical dissolution and spark discharge mechanisms, enabling acceptable performance across all responses. For MRR, the desirability curve increases continuously with electrolyte concentration and voltage, but decreases with higher TFR. The selected point results in taper angle of 21.45°, achieving a high desirability of 0.8799 by keeping voltage lower and TFR moderate. For surface roughness, minimum roughness is favored; the curve shows a U-shaped behavior with respect to voltage and TFR. The selected region yields Ra 0.3508 µm, with high desirability of 0.9093 by choosing the optimal point close to the valley of the response curve. Finally, for width of channel, the target is 500 µm. The predicted output at this optimum is WOC of 561.05 µm, giving a desirability of 0.9183, reflecting a slight overshoot but still acceptable within the target range. The optimization identifies a parameter combination that provides the best possible balance between high MRR, low taper, low roughness, and near-target channel width, despite conflicting tendencies between these responses.

5.3.7 Validation Experiment Based on Optimized Parameters

The ECD milling performance was monitored over a range of applied voltage, electrolyte concentration, and tool feed rate. The fundamental concept of electrolysis makes it clear that the electrolytic process initiates upon the application of an external voltage between two electrodes, and it becomes more pronounced as the applied voltage is increased. The optimized parameters that were obtained during optimization are given in **Table 5. 6**.

Table 5. 6 Optimized process parameters and predicted responses

Parameters	Optimal Value	Predicted value of responses			
		Width of Channel	Surface Roughness	Taper Angle	Material Removal Rate
Electrolyte Concentration	20 wt%	561.049 µm	0.351µm	21.45^0	4.244 µg/min
Voltage	35 V				
Tool Feed Rate	43 µm/sec				

Experimental validation was conducted using the optimized process parameters as given in **Table 5. 6** and the obtained channel was produced with superior quality as given in **Table 5. 7**. The unevenness or broken edges were accelerated if the TFR was higher. The developed microcracks throughout the edge of the channels are observed through SEM micrograph as shown in **Fig. 5. 11(a)**, whereas the smooth edge of the machined channels that was developed during ECD milling is shown in **Fig. 5. 11(b)**. **Fig. 5. 11(a)** and **Fig. 5. 11(b)** show the SEM micrograph of edge of channel machined at TFR of 60µm/sec and TFR of 50µm/sec, respectively.

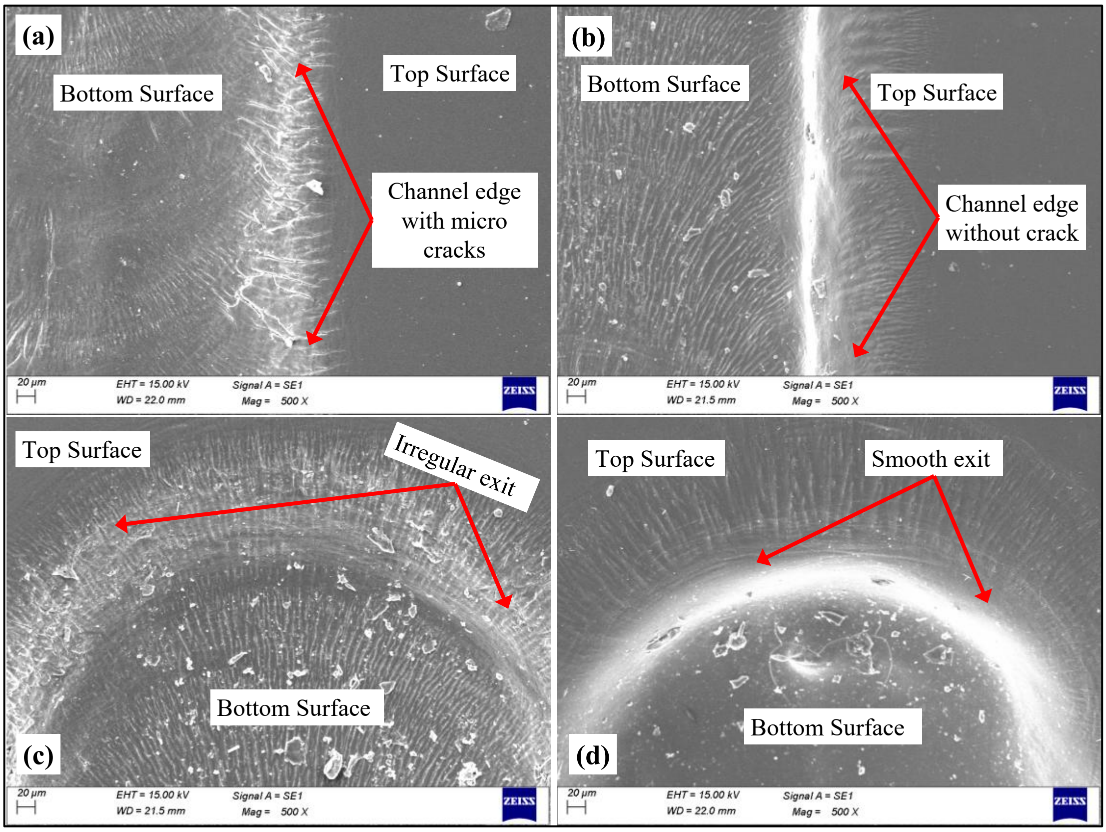

Fig. 5. 11 SEM images of machined channel edge and end point at (a) 35V, 15 wt% of NaOH and TFR of 60µm/sec (b) 35V, 20 wt% of NaOH and TFR of 43 µm/sec (c) 35V, 15 wt% of NaOH and TFR of 60µm/sec (d) 35V, 20 wt% of NaOH and TFR of 43µm/sec

The tool-electrode movements or the TFR influenced the quality of the channel edge by increasing the high-temperature chemical etching at lower TFR. Besides that, at a lower TFR, the spark discharge occurred frequently at a particular point of contact, which increased the chance of material removal for generating smooth and straight channel edges.

Table 5. 7 Experimental value of responses at optimized parameters

Parameters	Optimal Value	Experimental value of responses			
		Width of Channel	Surface Roughness	Taper Angle	Material Removal Rate
Electrolyte Concentration	20 wt%	581.604 µm	0.342 µm	20.48^0	4.335 µg/min
Voltage	35 V	3.66 % Error	2.56 % Error	4.50 % Error	2.14% Error
Tool Feed Rate	45 µm/sec				

Another aspect that was necessary for obtaining a better channel was the quality and shape of the end point of channel which was essential for making perfect shape of rectangle with parallel channels. **Fig. 5. 11(c)** represents the channel that was obtained at 15 wt% of electrolyte concentration and it consists of many irregular wrinkles on the edge of the channel. Lower concentration of electrolyte produced lower amount of ions, or more specifically, the hydroxyl ions in the electrolyte solutions which are responsible for high temperature chemical etching during the electrochemical discharge process. The increase of hydroxyl ions during ECD milling of glass accelerated the chemical etching of the channel edges that created smooth edges as well as smooth end points of the channel, as shown in **Fig. 5. 11(d)**.

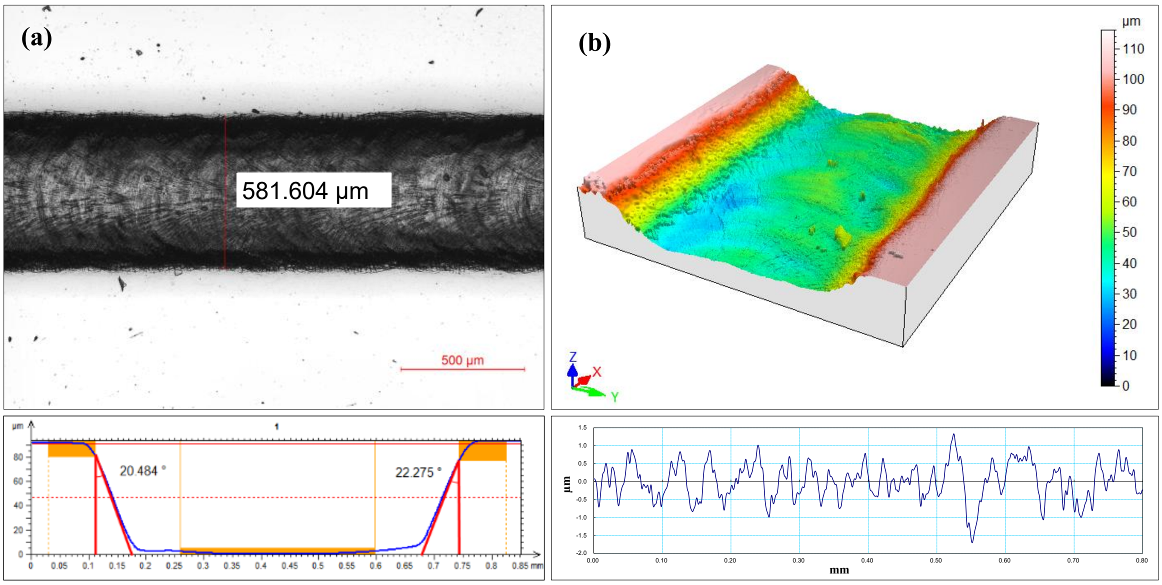

Fig. 5. 12 Optical and CCI image of single channel at 35V, 20 wt% of electrolyte concentration and TFR of 45µm/sec. (a) Optical image and (b) CCI image

After a certain amount of electrolyte concentration, the conductivity of the solution became much higher, creating high-intensity spark discharges that generated a rough surface, despite the presence of a greater amount of hydroxyl ions. It was found that at TFR of 45 μm/sec and 20 wt% of electrolyte concentration, and at 35 V, the produced channel was crack-free throughout its edges and endpoint. Finally, at an optimized parametric condition, a better-quality single channel with 581.604 μm width was generated, having uniform edges as shown in **Fig. 5. 12(a)**. The overall surface quality with crack-free edges and the bottom surface of the fabricated single channel is also shown in **Fig. 5. 12(b)** which reveals that the depth of the channel after a single pass is about 110 μm with no wavy or curvy pattern at the bottom surface. The taper angle is minimized under optimal conditions because the selected machining parameters produce stable, localized spark discharges. At 35 V, 20 wt% NaOH, and 44 μm/s tool feed rate, sufficient energy is available for efficient material removal at the tool tip, while excessive side sparking is suppressed. This reduces overcut at the channel entrance and maintains a more uniform channel width along the machining depth. Consequently, the difference between the top and bottom channel widths decreases, resulting in a lower taper angle and improved dimensional accuracy.

5.4 Outcomes of the Study

Based on the experimental plan developed using the Box-Behnken design and the detailed analysis of machining responses through ANOVA, regression modelling, response surfaces, and optimization studies, several key findings were obtained. These conclusions highlight the dominant process factors, response behaviours, and optimal operating conditions in ECD milling.

(i) The fitted second-order models for width of channel, surface roughness, taper angle, and MRR are statistically significant (ANOVA model p-values ≤ 0.05) and show very high goodness-of-fit ($R^2 = 96.23\%$ for WOC, 95.76% for SR, 94.73% for TA, and 99.85% for MRR). These results confirm that the Box-Behnken design and quadratic polynomials adequately capture the primary trends in the ECD milling data and are suitable for prediction within the selected range of process parameters.

(ii) ANOVA partitioning and coefficient magnitudes indicate that electrolyte concentration exerts the strongest influence on both width of channel and material removal rate, followed by voltage and then feed rate. In contrast, surface roughness and taper angle are primarily governed by voltage and tool feed rate.

(iii) Single-response optimizations produced ideal settings for each objective. Multi-objective desirability optimization returned a balanced setting (EC of 20 wt%, V of 35 V, TFR of 43.84 µm/s) with composite desirability of 0.9121, yielding MRR of 4.244 µg/min, Ra of 0.351 µm, TA of 21.45°, and WOC of 561.05 µm. This demonstrates the feasibility of obtaining high productivity while maintaining acceptable quality by compromising factor settings.

(iv) The optimized ECD milling parameters were found to produce high-quality microchannels with minimum taper, low surface roughness, and satisfactory material removal. The experimental results closely matched the RSM-predicted responses, with very low deviations of 3.66% for channel width, 2.56% for surface roughness, 4.50% for taper angle, and 2.14% for MRR, confirming the model's strong predictive capability. The SEM validation further supported the optimization outcome by showing smoother channel edges at optimized feed rates, while higher feed rates led to microcracks and edge damage.

Chapter 6

EXPERIMENTAL INVESTIGATION INTO ELECTROCHEMICAL DISCHARGE MILLING FOR GENERATION OF CAVITY ON GLASS

6.1 Introduction

Electrochemical discharge (ECD) milling is an advanced micromachining technique used for fabricating complex shapes on hard and brittle materials such as glass. This technique combines the principles of electrochemical machining and electrical discharge machining to achieve precision and intricate patterns, making it suitable for applications in microfluidics, lab-on-chip devices, and other fields requiring precise microstructures. The primary challenge in ECD milling is to control the surface roughness and minimize edge breakage during the machining process. This study aims to develop and improve the ECD milling process to produce high-quality rectangular cavities on glass with lower surface roughness and minimal edge breakage. This chapter focused on creating parallel channels on glass to form a rectangular shape with the goal of achieving lower surface roughness and minimizing edge breakage. The experiments aimed to identify suitable parametric settings for producing channels with smooth surfaces and minimal overcut. The materials and equipment used included sodalime glass as the workpiece, a copper tool-electrode, a graphite block as the auxiliary electrode, NaOH as the electrolyte, and a DC power supply. The parameters for generating single channels included a voltage range, electrolyte concentration, and tool feed rates. The best result from the single channel formation was used to fabricate a rectangular-shaped cavity through multiple parallel channels. Although the applied voltage and tool feed rate varied during the fabrication of rectangular cavities, the electrolyte concentration was kept constant. The process involved four consecutive parallel passes, utilizing different tool path movement strategies to achieve the best rectangular shape during ECD milling. The first strategy set the inter-channel distance equal to the width of a single channel. The second strategy spaced the parallel passes by the diameter of the tool-electrode, with movements along the Z-axis and repositioning along the Y-axis. The third strategy set the inter-channel distance to less than the tool-electrode diameter, considering the width overcut observed under optimal parametric conditions.

After creating the parallel channels, the total width of each rectangular cavity and the surface roughness were measured to evaluate the effectiveness of the different strategies. Surface characteristics were analysed using advanced techniques to investigate channel morphology, surface cracking, and other irregularities. Initial experiments produced single channels on the workpiece at various parametric settings using a vertically upward tool feeding technique. Channels were analysed based on width overcut, edge quality, and overall surface quality. This analysis guided the creation of parallel channels under optimal conditions to generate rectangular cavities on glass. The effects of process parameters such as voltage, electrolyte concentration, and tool feed rate on the width of single channels were monitored. It was observed that lower electrolyte concentrations and applied voltages produced narrower channels due to reduced spark discharge intensity. The influence of voltage on single-channel width revealed an increasing trend with higher voltage. Conversely, higher electrolyte concentrations facilitated chemical etching but led to rougher surfaces due to uncontrollable spark discharge. At lower voltages, channel overcut remained low, but edges became uneven or broke as the process progressed, especially at higher tool feed rates. Lower tool feed rates improved edge quality, as frequent spark discharges enhanced material removal. Higher electrolyte concentrations and lower tool feed rates resulted in smoother channel edges.

The study aimed to enhance the ECD milling performance for creating rectangular-shaped cavities on glass, with a focus on achieving lower surface roughness and precise dimensions. The various strategies and parametric settings explored provided insights into the optimal conditions for fabricating high-quality rectangular cavities, which can be applied in devices such as fluid reservoirs in lab-on-chip applications.

6.2 Plan of Experiments

In this study, parallel channels were made on the glass to obtain a rectangular shape, as shown in **Fig. 6. 1** with lower surface roughness and reduced edge breakage.

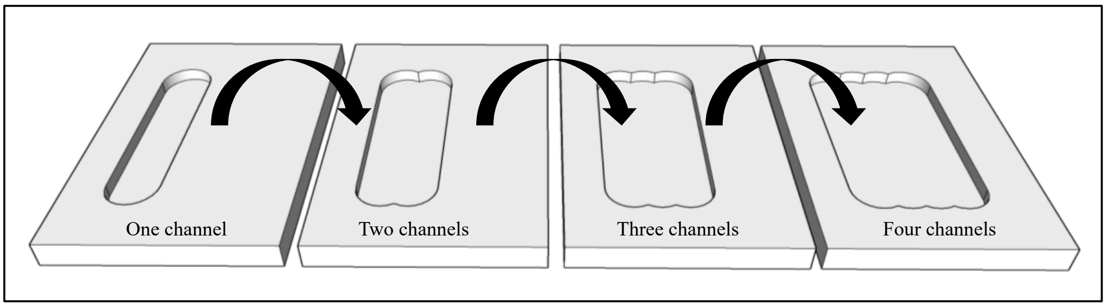

Fig. 6. 1 Schematic of making a rectangular cavity with parallel channels

Initial experiments were conducted to determine a range of suitable parametric settings that would achieve a channel with lower surface roughness and reduced overcut. After optimizing the process parameters, the best outcome was selected for the generation of a rectangular-shaped cavity on glass. The details of the parameters that were used to generate cavity are given in **Table 6. 1**.

Table 6. 1 Machining parameters for single channels

Parameters	Level/Sizes
Applied Voltage (V)	35
Tool-electrode diameter (µm)	500
Auxiliary electrode (sq. mm)	100mm X 100mm
Electrolyte Concentration (wt%)	20
Tool feed rate (TFR) (µm/sec)	45

The best result found during making a single channel on the workpiece was used for generating a rectangular-shaped cavity by utilizing multiple parallel channels. Although the applied voltage and TFR were varied during fabrication of the rectangular cavities, the electrolyte concentration was fixed at 20 wt% throughout the experimentation. Four consecutive parallel passes were given according to three different strategies of tool path movement to find out the better rectangular shape during ECD milling. Three strategies of tool path movement during ECD milling are stated here.

6.2.1 Inter-channel distance same as width of single channel

In the first strategy, the distance between two consecutive parallel passes was given as per the width of a single channel. After one pass of the tool electrode, the next consecutive pass was given at a similar distance to the channel width. The width of the channel was obtained from previously performed experiments aimed at achieving a better parametric condition for generating a single channel on the workpiece. After one pass of the tool-electrode, the distance was given as per the channel width, which was obtained at better parametric conditions, as shown in **Fig. 6. 2(a)**.

6.2.2 Inter-channel distance same as tool diameter

In the alternative method, the spacing between two parallel passes was set equal to the diameter of the tool electrode, and the impact on the surface quality of the rectangular shape was examined. The initial pass of the tool electrode was made in a bottom-up direction along the Z-axis, and then it was returned to its original position. After that, a parallel distance that was same as tool-electrode diameter was given along Y-axis and again tool was moved from bottom to upward direction as described in the **Fig. 6. 2(b)**. In this way, four consecutive parallel channels were generated to obtain the rectangular shape of the glass.

6.2.3 Inter-channel distance less than tool diameter

In the third and final strategy, the distance between two consecutive parallel passes was less than the tool-electrode diameter. The value of the width overcut that was found at better parametric conditions during generating a single channel was subtracted from the tool-electrode diameter and was used as the distance between two parallel channels, as shown in **Fig. 6. 2(c)**.

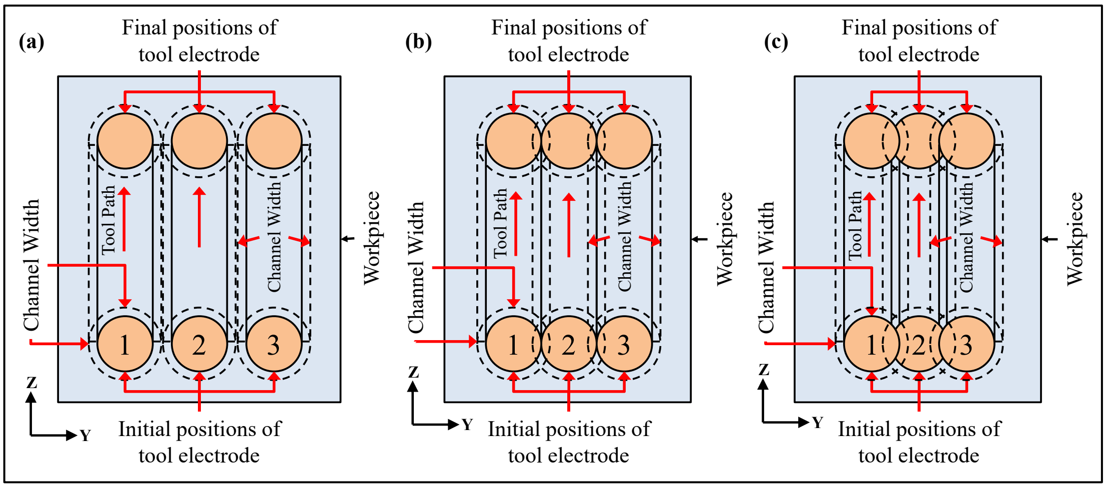

Fig. 6. 2 Schematic diagram of tool path movement and pass for (a) First strategy, (b) Second strategy, and (c) Third strategy

In the first two strategies, the tool-electrode diameter and single channel width were considered as the distance between two parallel passes. There will be some width overcut during the first two strategies, which were calculated and considered in the third strategy. After the generation of the parallel channels, the total width of every rectangular cavity and R_a were measured to investigate the effects of different strategies in fabricating rectangular-shaped cavities during ECD milling with vertically upward tool feeding technique. The surface characteristics of the rectangular-shaped cavity were observed under Coherence Correlation Interferometry (CCI) and analyzed. Scanning electron microscopy images were also taken to investigate channel morphology, surface cracking and various irregularities on the surface.

6.3 Results and Discussion

Single channel was generated on the workpiece at optimized process parametric settings by applying the vertically upward tool feeding technique. Those channels were analyzed in terms of width overcut, nature of channel edge, and overall surface quality. Based on the analysis, the parallel channels were made with the best parametric condition to generate rectangular-shaped cavities on glass.

6.3.1 Generation of Rectangular Cavity with First Strategy

The rectangular shape generation was tried on glass in three different strategies using ECD milling. The channel width that was obtained while generating a single channel on glass was used as the lateral distance between two passes. Significant changes on the milling surface were observed after milling with this approach. It was obvious that the total width of the rectangular area using first strategy was very large as compared to other two strategies, as the distance between two consecutive parallel passes was larger in this case. **Fig. 6. 3(a)** describes the influence of voltage on the total width of the generated rectangular-shaped cavity. It is noticeable from the **Fig. 6. 3(a)** that the width grows rapidly after 40V of applied voltage and it also increases at lower tool feed rate. The problem with this strategy is that the surface generated with this strategy was full of peaks and valleys. The surface roughness of bottom surface of rectangular cavity is also higher than other strategies. The surface roughness of the milling surface varies with applied voltage between tool and auxiliary electrode. The value of R_a decreases as the voltage increases up to 40V and it becomes lowest at 40V, but after that, R_a value of the surface was increased for all TFR, as shown in **Fig. 6. 3(b)**.

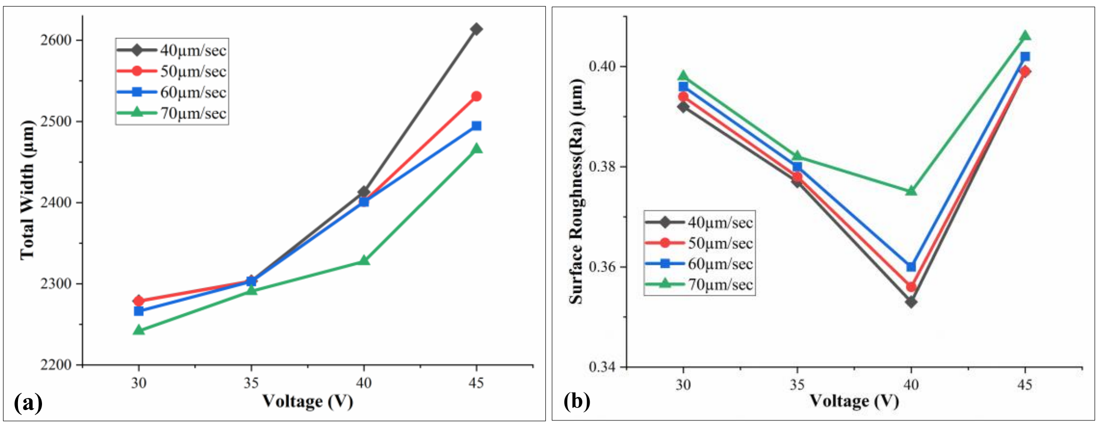

Fig. 6. 3 Variation of width and surface roughness (R_a) of rectangular-shaped cavity at different TFR for first strategy (a) Effect of voltage on total width and (b) Effect of voltage on surface roughness

The tool movement of two consecutive passes was separated by a distance equal to the single channel width. In this case, the border of two consecutive parallel channels was merged into each other which created heap of molten materials across the border line of the two adjacent parallel channels as shown in **Fig. 6. 4(a)** and this heap of materials abolished the uniformity of the bottom surface which increased the surface roughness (R_a). During the generation of single channels, the width of channels was found to be above 600µm at suitable parametric conditions. According to the first strategy, the distance between two consecutive tool path movements was similar to the width of a single channel. Due to that, the total width of rectangular cavity was found to be 2613.719µm including the overcut of initial and final tool movement. The surface roughness (R_a) across the parallel channels was observed as low as 0.406µm. The surface topography of the channel is shown in the **Fig. 6. 4(b)** where the profile of the surface was obtained after parallel ECD milling with the first strategy. The surface topography in **Fig. 6. 4(b)** shows the curvy nature of bottom surface of rectangular shape which was generated due to milling of parallel channels keeping the distance between two parallel channels as the width of single channel. **Fig. 6. 4(b)** also reveals that the variation in height across the surface reached about 80µm, as witnessed from the scale bar given in the figure. The edge portions of the bottom surface were much more irregular than the middle surface because of uneven material removal from the edge of the generated shape.

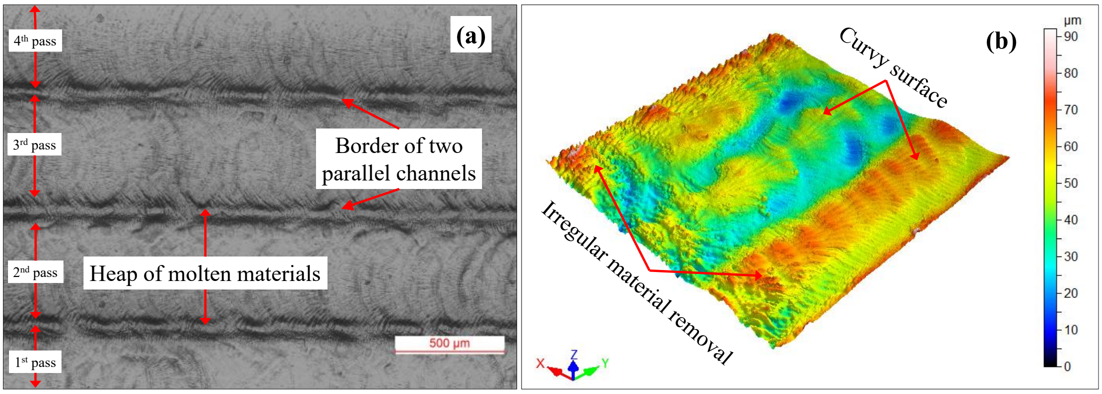

Fig. 6. 4 Images of bottom surface of rectangular shape (a) Optical image of parallel channels and (b) Surface topography of parallel channels

At lower voltage, the material removal happened unevenly from the surface due to lower energy that impact the workpiece surface. As the voltage was increased, the energy of spark discharge increased and consequently the materials were removed evenly from the surface.

R_a value again increased after 40V of applied voltage due to uncontrollable spark discharge at higher voltage.

6.3.2 Generation of Rectangular Cavity with Second Strategy

In the second strategy, the distance between two parallel channels was given as per the tool-electrode diameter. The copper tool-electrode of 500µm diameter was taken in this experiment and according to that, the distance between two parallel channels was taken as 500µm. The total width of the rectangular shapes was lower than the first approach as the inter-pass distance was reduced. The width was also varied for different applied voltages and different tool feed rate as shown in **Fig. 6. 5(a)**. The total width of rectangular shape increased as the voltage was increased because the overcut of the first and last channels was higher at higher voltage that decided the total width. As per the previous discussions about channel width of a single channel, the width of the channel was changed abruptly when the voltage was increased up to 45V. In this range of voltage, the electrolysis process became faster which influenced the formation of gas film and spark discharge frequently. Besides that, the energy of spark discharge at 45V was much higher compared to other lower voltages which led to uncontrollable high energy spark discharge that led to generation of cracked edges of rectangular shape cavities.

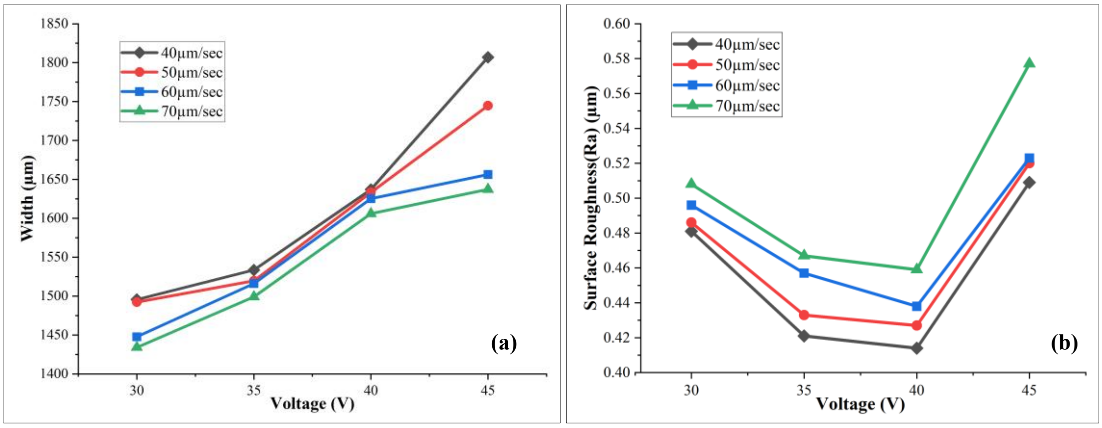

Fig. 6. 5 Variation of width and surface roughness of rectangular shaped cavity at different TFR for second strategy (a) Effect of voltage on total width and (b) Effect of voltage on surface roughness

It is also noticeable from **Fig. 6. 5(a)** that the width of the rectangular cavity tends to increase in the case of lower tool feed rate (TFR) i.e. 40µm/sec. The R_a value in this strategy also declined as the voltage increased up to 0.438µm with the application of 40V and 50µm/sec TFR and after 40V the surface roughness (R_a) increased rapidly as shown in **Fig.**

6. 5(b). The tool-electrode that moves on the workpiece provided more spark discharges at a particular point if the TFR was lower which caused the enhancement of total width of the channel. The heap of molten materials was accumulated along the border of two consecutive parallel channels in case of first strategy but during ECD milling with second strategy the inter-pass distance was given as 500µm which was the diameter of tool-electrode. The heap of molten materials was shifted towards the middle of adjacent channel as the distance between two consecutive parallel channels was reduced than the first strategy as shown in **Fig. 6. 6(a)**. The total width of the rectangular cavity was also reduced with the application of second strategy.

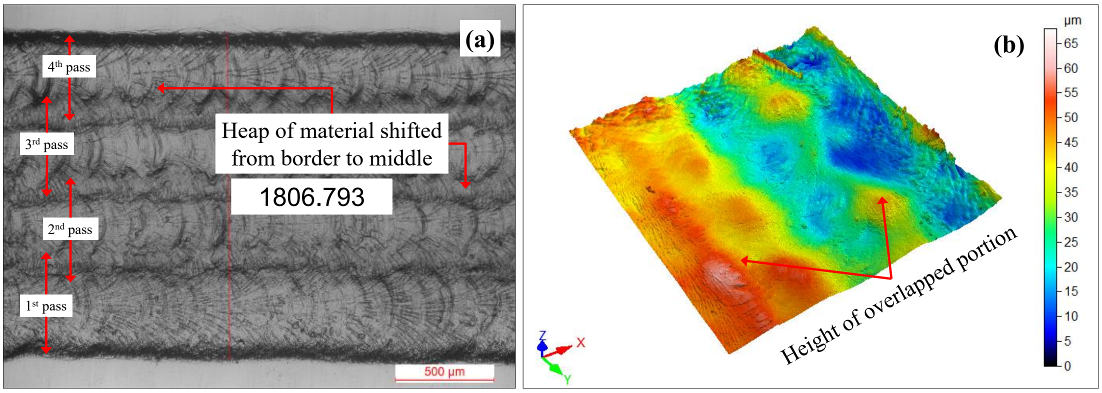

Fig. 6. 6 Image of rectangular shape and its surface topography machined by the second strategy (a) Optical image and (b) Surface topography

The variation in height within the bottom surface of rectangular shape cavity reaches up to 55µm as shown in **Fig. 6. 6(b)** which is lower than as it is obtained from the first strategy but till it generates surface roughness (R_a) of 0.438µm.

6.3.3 Generation of Rectangular Cavity with Third Strategy

The last strategy for generating a rectangular-shaped cavity on the soda lime glass was to reduce the distance between two adjacent parallel channels. In this case, the distance was considered depending upon the width overcut of single channel which was machined at 40V and TFR of 50µm/sec and tool-electrode diameter. According to the channel width and the tool-electrode diameter, the distance between two parallel channels was estimated by subtracting the width overcut from the tool-electrode diameter. Total width of rectangular shape cavity, which was machined with this strategy was reduced more than previous strategies due to lower inter-channel distance. As shown in **Fig. 6. 7(a),** the total width of the rectangular cavity increases gradually up to 40V of applied voltage but after that the width increases rapidly. The surface roughness (R_a) of the rectangular cavity decreases up to 40V and then it increases at 45V for every TFR as shown in **Fig. 6. 7(b).** It is also noticeable that the surface roughness at 40V and TFR of 40µm/sec is much lower. It indicates the occurrence of high-temperature chemical etching at that particular parameter setting. The chemical etching was responsible in making the surface smooth and crack-free as it removes material very slowly from the workpiece surface. This kind of high-temperature chemical etching is only possible if the tool-electrode moves over the workpiece surface very slowly. The TFR of 40µm/sec was the lowest tool feed rate compared to other TFR in this study. As a result, the high-temperature chemical etching occurred and the surface roughness in terms of R_a value was reduced significantly up to 0.247µm at 40µm/sec of TFR.

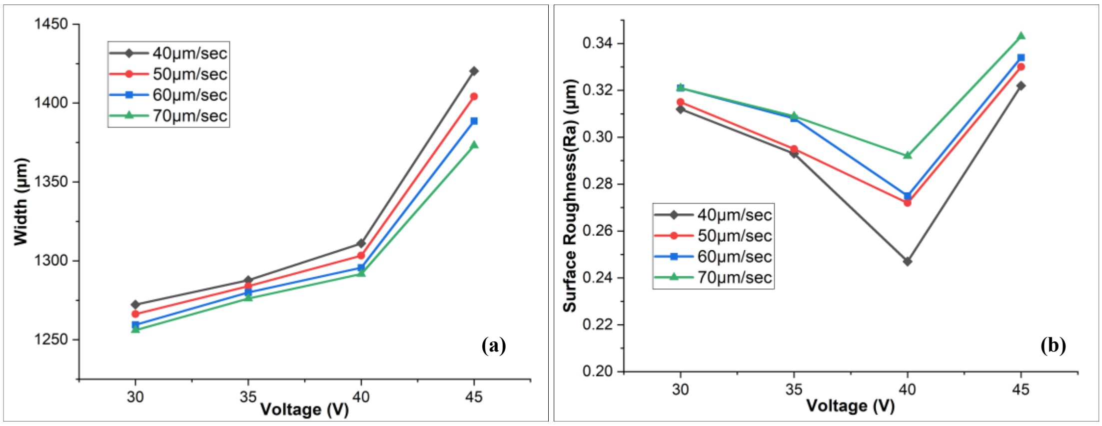

Fig. 6. 7 Variation of total width and surface roughness of rectangular shaped cavity at different TFR for third strategy (a) Effect of voltage on total width and (b) Effect of voltage on surface roughness

The total width of the rectangular shape cavity was larger at 40 µm/sec TFR as the tool-electrode took more time to stay at a particular spot and the frequency of spark discharge was increased at that spot resulting in widen the width of channel.

6.3.4 Generation of Rectangular Cavity with Suitable Strategy

The strategy with a lower inter-pass distance between two consecutive parallel channels was found to be suitable in fabricating rectangular-shaped cavities from the analysis of different strategies. This strategy not only provided a lower width but also it has generated uniform surface at the bottom of the rectangular cavity. Although several tool feed rates were considered for generating rectangular cavities, the safe option was the TFR of 50µm/sec which was considered throughout for fabricating of rectangular shape cavity and observed as better as shown in **Fig. 6. 8(a).** The heap of materials along the border of two adjacent parallel channels were shifted in case of second strategy which was further diminished in the third strategy of making rectangular shape cavity. In this strategy, the generated rectangular shape cavity was of smaller width of 1303.323µm and also resulted in lower surface roughness in term of R_a value. The surface topography as shown in **Fig. 6. 8(b)** reveals that the bottom surface of the rectangular cavity was smooth and it contained less amount of variation in height throughout the surface compared to other two strategies.

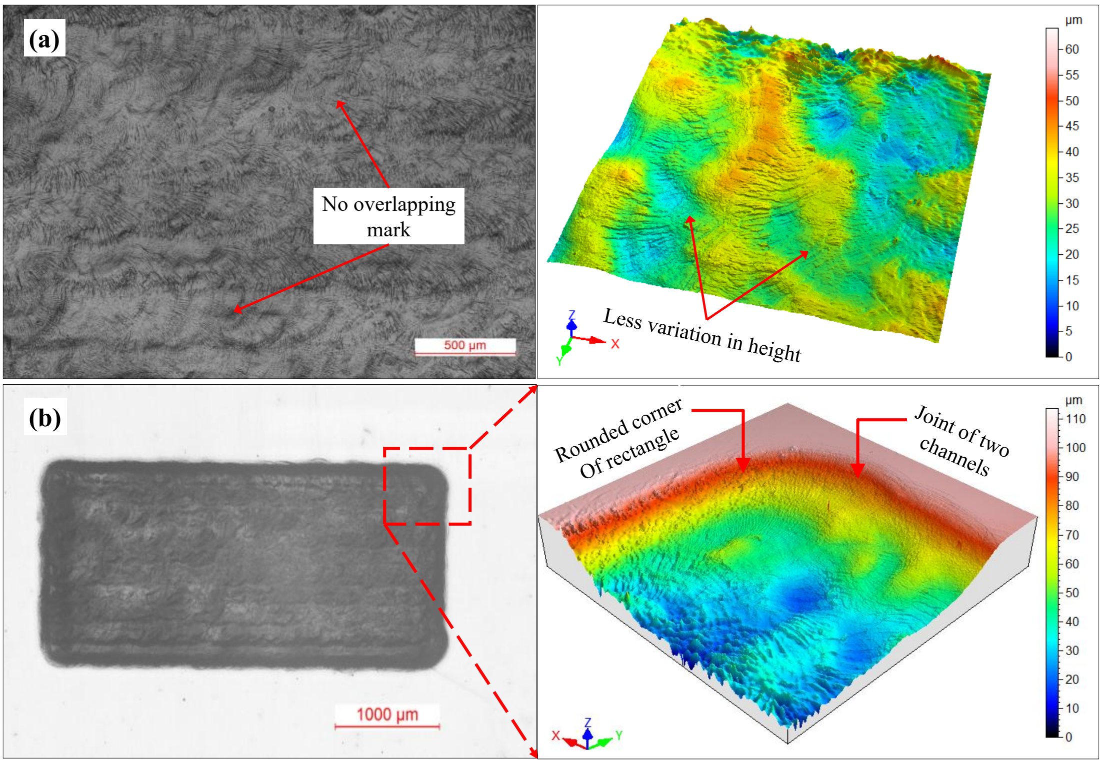

Fig. 6. 8 Images of rectangular shapes and their surface topography machined with third strategy (a) rectangular shapes machined with third strategy (b) surface topography of corner of rectangular cavity

The corner of the cavities was also impressive in terms of finishing and roundness which is described in **Fig. 6. 8(b)**. The border edge of two adjacent channels which was visible in case of previous two strategies but in this case, border was unidentified and made the rectangular cavities very precise.

6.4 Outcomes of the Study

The experimental study that was conducted and described in this chapter was about the gas film model development and fabrication of a rectangular cavity on glass by generating consecutive parallel channels with ECD milling using vertically upward tool feeding technique. During the generation of a rectangular-shaped cavity on glass, several strategies were tried to obtain the best possible method. From the study, the following conclusions can be drawn:

(i) With the application of vertically upward tool-feeding technique, the oval shape of gas film is used as an advantage and the thickness of gas film is enlarged at the machining area which resulted in intense spark discharge at the machining zone that helps in ECD milling on the workpiece surface.

(ii) Although the trend in increase of width of cut is linearly proportional to the applied voltage but the surface roughness reduces at 35V and then increases with the increase of applied voltage. The channel edge is smooth and uniform with width of 581.604 µm when the TFR is lower, i.e. 45 µm/sec, and voltage is 35V due to chemical etching at high temperature, but it did not occur at higher TFR.

(iii) Fabrication of a rectangular-shaped cavity is performed with three different strategies to reduce the surface irregularities. The first and second strategies that are described in this study produce a heap of molten materials either along the border of two adjacent channels or along the middle of the channels producing a higher width and surface roughness of rectangular cavity.

(iv) The good quality rectangular cavity with lower surface roughness (R_a) of 0.247 µm was fabricated by setting the inter-channel distance of less than tool-electrode diameter at 50 µm/sec of TFR, 40 V and 20 wt% of electrolyte concentration. Also, the width of rectangular cavity is reduced significantly to 1303.323 µm using third strategy as compared to the first and second strategies, which were 2613.719 µm and 1806.793 µm, respectively.

The rectangular-shaped cavity that has been fabricated utilizing ECD milling with lower surface roughness and lower width. The cavities can serve as channels for fluid flow, mixing chambers, or reaction chambers, depending on the specific requirements during the making of lab-on-chip devices. Besides rectangular shape cavities, other shapes like triangular, trapezoidal, can also be produced with ECD milling by adopting tool path movements with proper strategies.

Chapter 7

ANALYSIS OF THE PERFORMANCE OF ELECTROCHEMICAL DISCHARGE MILLING ON POLYMER MATERIALS

7.1 Introduction

In the realm of advanced manufacturing techniques, Electrochemical Discharge Milling (ECD milling) has emerged as a pivotal method for machining complex geometries in electrically non-conductive materials. However, machining of different polymers can also be done, such as thermoplastic and thermosetting polymers, polycarbonate, and PMMA (Polymethyl Methacrylate), respectively. This chapter presents an experimental investigation aimed at exploring the feasibility of ECD milling performances on these polymers. This chapter encompasses several critical aspects. Firstly, the relationship between applied voltage, tool feed rate, electrolyte concentration, and subsequent machining outcomes, specifically channel width and surface roughness, is thoroughly analyzed for both polycarbonate and PMMA. Additionally, simulated analyses of heat propagation through these polymers during the machining process provide insights into thermal effects on material removal and surface quality. The study also delves into the surface characteristics of machined channels, emphasizing differences observed when using NaOH and KOH electrolytes. Key findings from the experimentation highlight distinct behaviors of PMMA and polycarbonate under varying conditions. PMMA, known for its brittle properties, tends to exhibit larger channel widths and rougher surfaces when machined with KOH. In contrast, NaOH electrolyte results in smoother surface finishes and narrower channels. Polycarbonate, being a thermoplastic material, presents challenges during ECD milling, particularly with NaOH, where irregular material removal and rough surface finishes are noted. Conversely, KOH provides more consistent channel widths and smoother finishes despite some irregularities. The influence of electrolyte choice emerges as a critical factor in determining machining outcomes. KOH proves advantageous for PMMA, producing larger channels with improved surface finishes. For polycarbonate, the results vary significantly with electrolyte type, highlighting the intricate interplay between material properties and chemical processes during ECD milling. Moreover, detailed analysis of the Spark Affected Zone (SAZ) reveals insights into its formation and removal mechanisms, particularly notable in PMMA with NaOH and polycarbonate with KOH, where chemical etching effects are observed.

This chapter provides a comprehensive exploration into the electrochemical discharge milling of non-conductive polymers. The findings underscore the importance of parameter settings and electrolyte selection in achieving desired machining results for polycarbonate and PMMA.

7.2 Plan of Experiments

Experimentation on ECD milling was executed on both thermoplastic and thermosetting polymers to observe the characteristics and possibilities of milling with the adoption of upward tool feeding with a horizontal tool. Polymethyl methacrylate (PMMA) and Polycarbonate (PC) used during the milling are thermosetting polymers and thermoplastic polymers, respectively. Initially, the milling on both PMMA and Polycarbonate was done using aqueous sodium hydroxide (NaOH) solution as electrolyte. Aqueous potassium hydroxide (KOH) solution was used as an electrolyte to overcome the limitations of the NaOH electrolyte during the machining of Polycarbonate. Applied voltage, electrolyte concentration, and tool feed rate were altered during ECD milling on both polymers, where two electrolytes were used throughout the process. 'One factor at a time' (OFAT) was employed during the milling operation, where other parameters were kept constant. The type and size of workpiece and electrode used during ECD milling are given in **Table 7. 1**.

Table 7. 1 Details of the workpiece and the electrode material

Items	Specifications
Workpiece	PMMA, Polycarbonate (PC)
Tool Electrode Material	Copper
Tool Electrode Diameter	500µm
Auxiliary Electrode Material	Graphite
Auxiliary Electrode Dimension	100mm X 100mm

Voltage was altered from 30V to 45V with an increment of 5V, and electrolyte concentration was varied from 10wt% to 25wt% with an increment of 5wt%. A tool feed rate of 40 to 70 µm/sec was varied to carry out the experiments and observe the effects of various parameters during ECD milling on polymers. The parametric conditions are given in **Table 7. 2**.

Table 7. 2 Parametric conditions

Parameters	Type/Values
Voltage (V)	30, 35, 40, 45
Electrolyte	Aqueous NaOH, Aqueous KOH
Concentrations of Electrolytes (wt%)	10, 15, 20, 25
Tool feed rate (μm/sec)	40, 50, 60, 70

During the experimentation, when the applied voltage was varied from 30 V to 45 V then the electrolyte concentration was fixed at 20 wt%. Similarly, the voltage was fixed at 40 V when the electrolyte concentration was altered. As per the previous experimentation, 40 V of applied voltage and 20 wt% of electrolyte concentration provide better results than other parameters.

7.3 Simulation of Heat Propagation through Different Materials

Simulating heat propagation through materials in Electrochemical Discharge Milling (ECD milling) is crucial for collectively enhancing the precision and efficiency of the machining process. ECD milling involves the generation of localized heat due to electrochemical discharges between the tool electrode and the electrolyte. Understanding how this heat propagates through the material is essential for effectively managing thermal effects during machining. By predicting and controlling thermal gradients, thermal damage such as material degradation, surface roughness, and dimensional inaccuracies can be mitigated. Simulations on heat propagation through materials like glass, polycarbonate, and PMMA are carried out to understand the progress of heat during ECD milling on these materials and their effects on milling performances. **Fig. 7. 1** shows the surface temperature distribution during heat propagation through glass at different times. The initial condition is shown in **Fig. 7. 1(a),** where no heat flow is observed. As time flows, the heat propagation through glass starts, which is shown in **Fig. 7. 1(b)**. After 0.02s, the heat spread more through the materials as shown in **Fig. 7. 1(c)**. Similarly, **Fig. 7. 1(d), Fig. 7. 1(e), Fig. 7. 1(f)** show the further flow of heat at different time spans. The flow of heat through the materials is important during ECD milling, and it can affect the machining performance.

The temperature distribution in the material can clearly be seen from the temperature contour diagram.

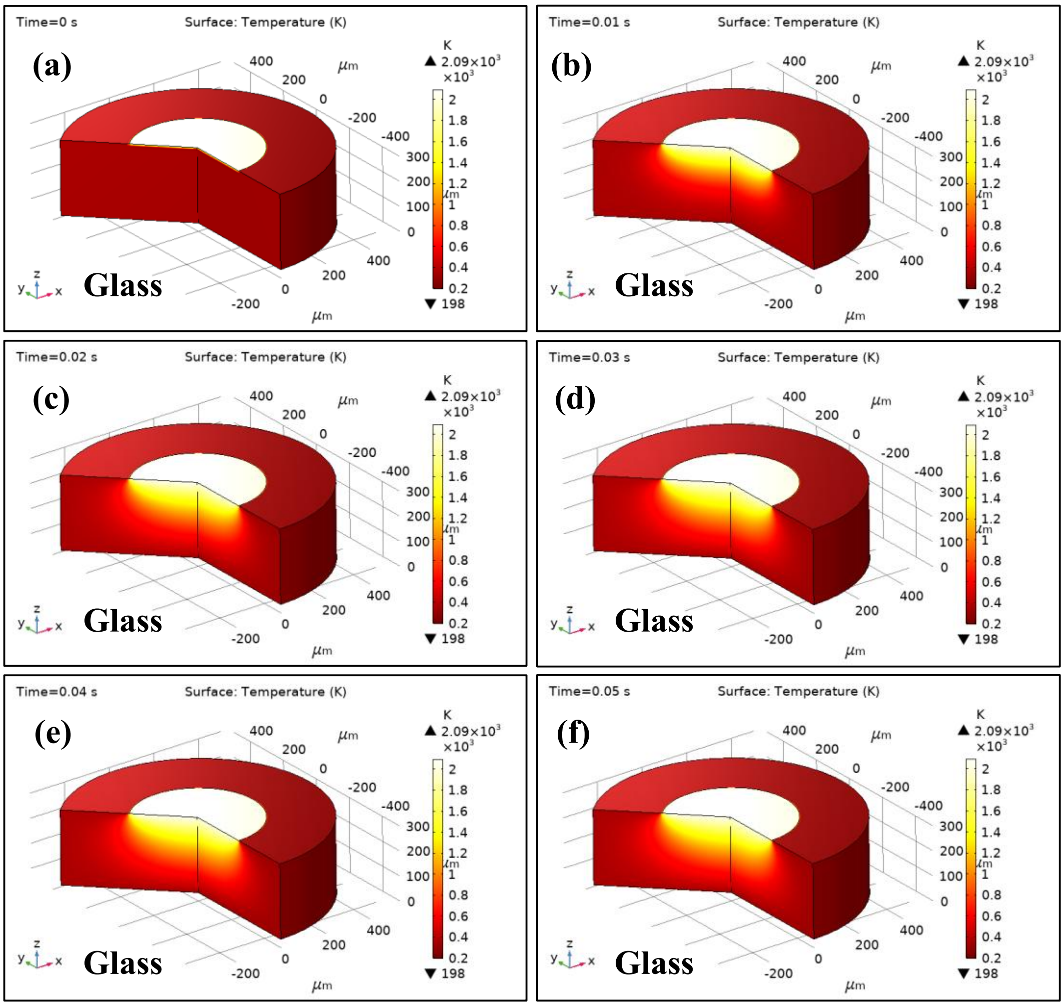

Fig. 7. 1 Simulation of heat propagation through glass at different times (a) 0s, (b) 0.01s, (c) 0.02s, (d) 0.03s, (e) 0.04s, and 0.05s

Fig. 7. 2(a) shows the initial condition of the heat flow, which changes with time, and can be seen as a spread about 250 µm depth at 0.01s for glass, as shown in **Fig. 7. 2(b)**. This spread of heat in terms of temperature distribution reaches about 350 µm at 0.02s, as shown in **Fig. 7. 2(c)**. Further, as the time progresses, the heat flow reaches about 400 µm, 450 µm, and 500 µm, which is shown in **Fig. 7. 2(d), Fig. 7. 2(e)** and **Fig. 7. 2(f)** respectively.

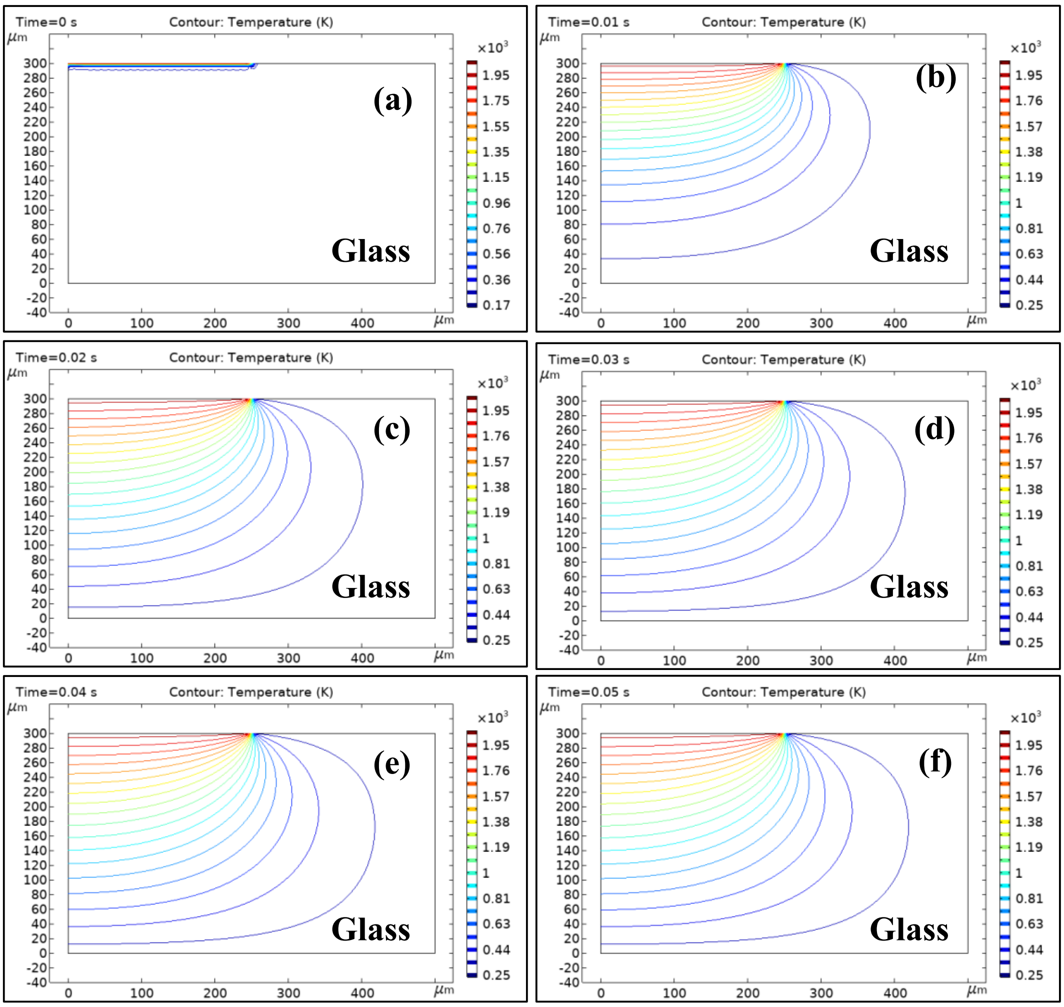

Fig. 7. 2 Temperature contour diagram for glass at different times (a) 0s, (b) 0.01s, (c) 0.02s, (d) 0.03s, (e) 0.04s, and 0.05s

Fig. 7. 3 illustrates the surface temperature distribution during heat propagation through polycarbonate at various time intervals. The initial condition, depicted in **Fig. 7. 3(a)**, shows no observable heat flow. As time progresses, heat begins to propagate through the polycarbonate material, as seen in **Fig. 7. 3(b)**. By 0.02 seconds, the heat has spread further through the material, as depicted in **Fig. 7. 3(c)**. Subsequently, **Fig. 7. 3(d), Fig. 7. 3(e),** and **Fig. 7. 3(f)** demonstrate the continued propagation of heat at subsequent time intervals. It is noticeable that the heat flow in polycarbonate material is slow compared to glass material, which ultimately affects the machining performance and differs in machining quality.

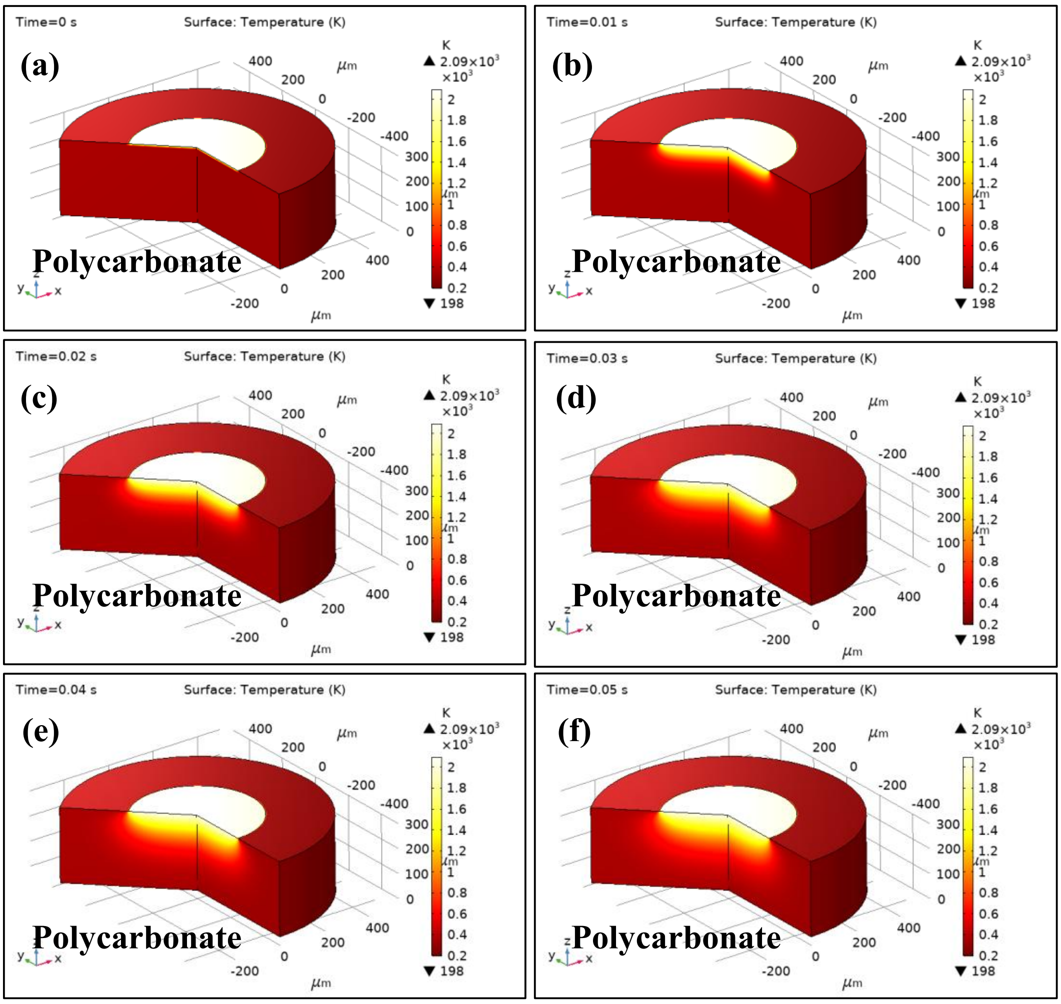

Fig. 7. 3 Simulation of heat propagation through polycarbonate at different times (a) 0s, (b) 0.01s, (c) 0.02s, (d) 0.03s, (e) 0.04s, and 0.05s

The maximum temperature of the spark discharge area reaches about 2.09×10^3K for polycarbonate material as per the simulation. The heat flow through polycarbonate is quite slow compared to glass material because of the distinct material properties. The process starts with an initial condition, as shown in **Fig. 7. 4(a)** where no heat flow is observed. After 0.01s, the temperature contour diagram shows that the heat flows about 100 µm, as shown in **Fig. 7. 4(b)** which is slower than the heat flow through glass. Further at 0.02s, the temperature contour diagram indicates the heat up to 150 µm, as shown in **Fig. 7. 4(c)**. It takes 0.05s to reach the distance above 200 µm in the case of polycarbonate, as shown in **Fig. 7. 4(f)**. Similarly, **Fig. 7. 4(d)** and **Fig. 7. 4(e)** shows the temperature contour diagram at 0.03s and 0.04s, respectively.

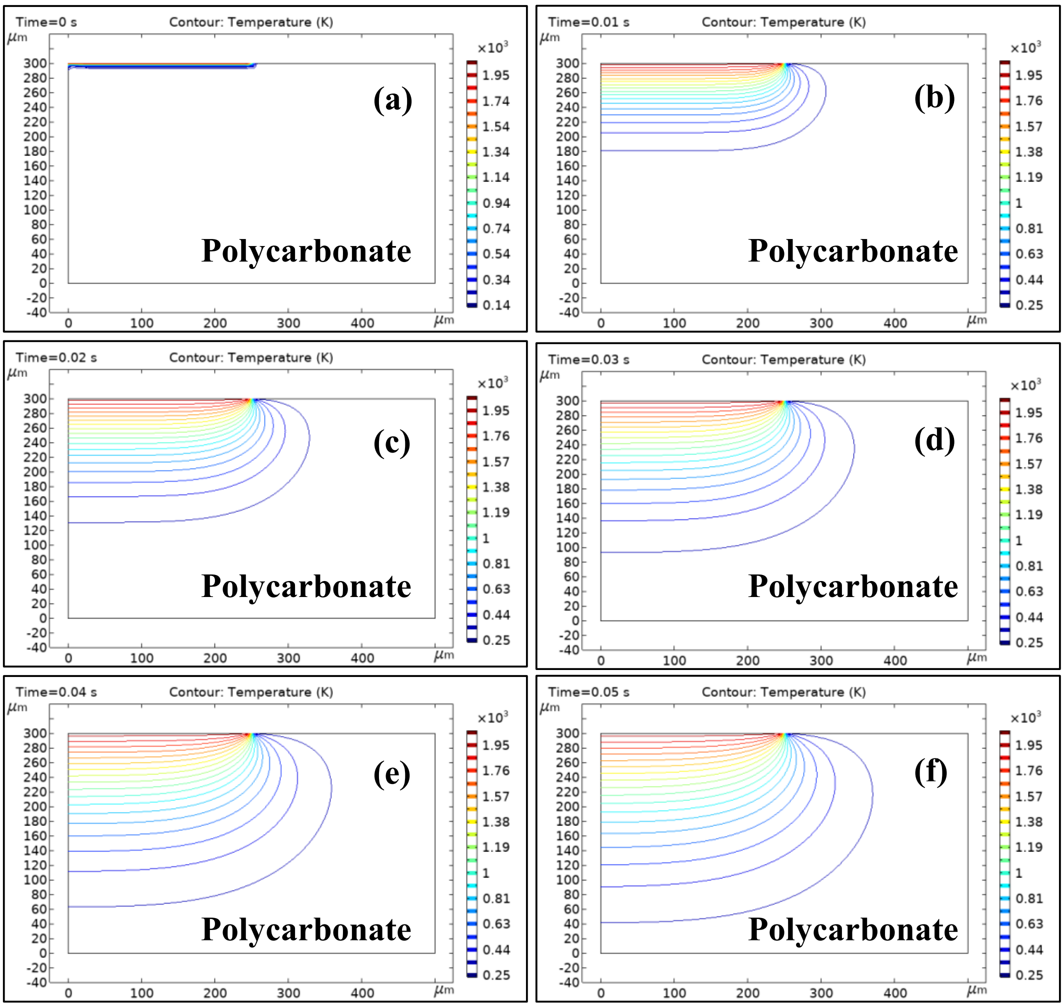

Fig. 7. 4 Temperature contour diagram for polycarbonate at different times (a) 0s, (b) 0.01s, (c) 0.02s, (d) 0.03s, (e) 0.04s, and 0.05s

Fig. 7. 5 provides a visual representation of the surface temperature distribution during the propagation of heat through PMMA at various time intervals. Initially, depicted in **Fig. 7. 5(a)**, no discernible heat flow is observed. As time progresses, heat begins to propagate through the PMMA material, becoming evident in **Fig. 7. 5(b)**. By the time 0.02 seconds elapse, the heat has expanded further within the material, as shown in **Fig. 7. 5(c)**. Subsequent figures, **Fig. 7. 5(d), Fig. 7. 5(e),** and **Fig. 7. 5(f),** illustrate the continuing propagation of heat at subsequent intervals. The slower heat conduction observed in PMMA compared to glass significantly influences machining performance and quality. This inequality in temperature distribution among three different materials made a great impact on the ECD milling process in terms of surface roughness, non-uniform channel edges due to irregular material removal.

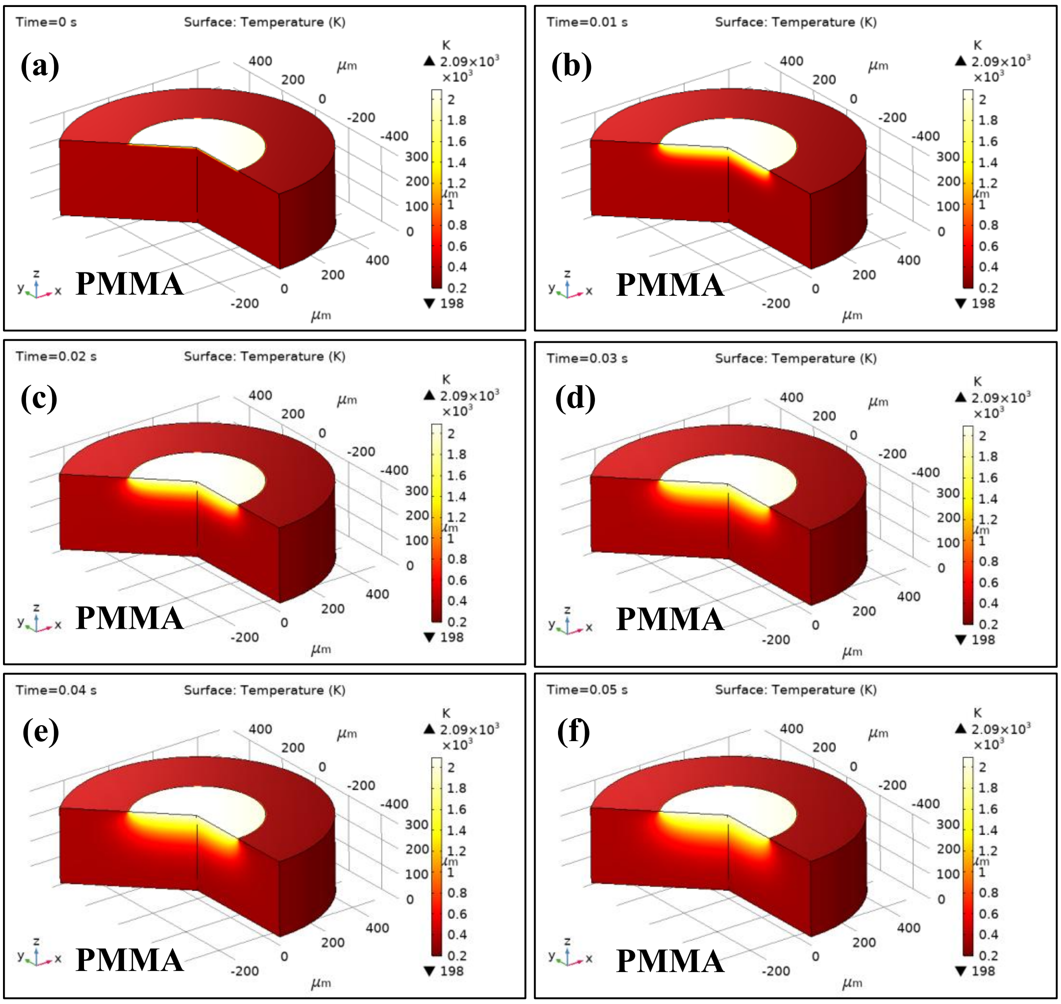

Fig. 7. 5 Simulation of heat propagation through PMMA at different times (a) 0s, (b) 0.01s, (c) 0.02s, (d) 0.03s, (e) 0.04s, and 0.05s

The simulation reveals that PMMA reaches a maximum temperature of approximately 2.09×10^3K in the spark discharge area. Due to its specific material properties, PMMA exhibits slower heat conduction compared to glass. Initially, at 0s as shown in **Fig. 7. 6(a)**, there is no observed heat flow. By 0.01s, heat has propagated approximately 100 µm, as shown in **Fig. 7. 6(b)**, which is slower than observed in glass. At 0.02s, as shown in **Fig. 7. 6(c)**, the heat has spread to about 150 µm. It takes until 0.05s to reach a distance greater than 200 µm, as shown in **Fig. 7. 6(f)** in PMMA. Additionally, **Fig. 7. 6(d)** and **Fig. 7. 6(e)** illustrate the temperature contour diagrams at 0.03s and 0.04s, respectively.

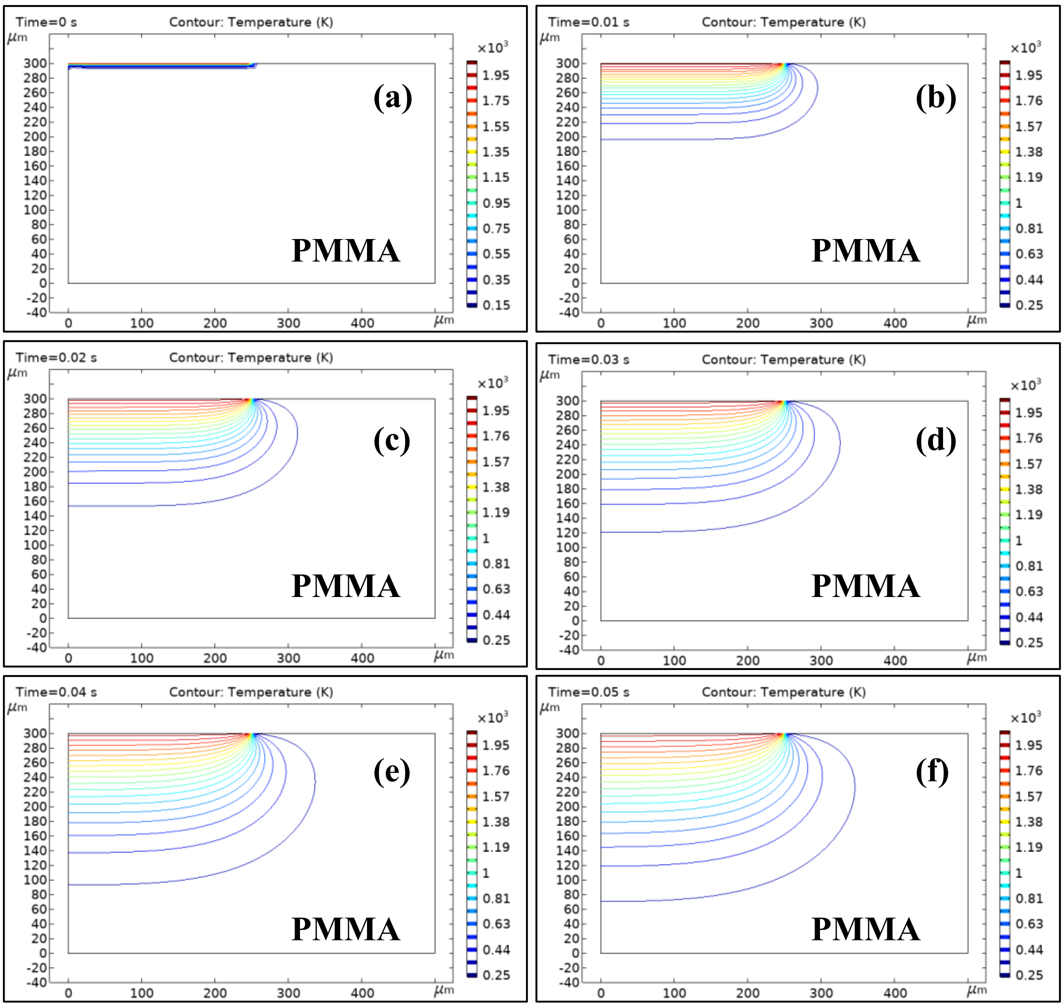

Fig. 7. 6 Temperature contour diagram for PMMA at different times (a) 0s, (b) 0.01s, (c) 0.02s, (d) 0.03s, (e) 0.04s, and 0.05s

After the simulation process, ECD milling of polycarbonate and PMMA was conducted with different electrolytes and tool feeding strategies than ECD milling of glass to ensure better machining performances.

7.4 Results and Discussion

The influence of process parameters on PMMA as well as on Polycarbonate with NaOH and KOH electrolyte has been analyzed. The surface roughness and spark affected zone (SAZ) and their variation with process parameters have been thoroughly analyzed. Due to numerous diverse characteristics, the results of ECD milling show an interesting phenomenon and convincing conclusions focused on several analyses and observations.

7.4.1 Influence of Process Parameters on PMMA with NaOH Electrolyte

The ECD milling on PMMA was conducted by varying applied voltage, electrolyte concentration, and tool feed rate. Initially, the milling operation was performed using aqueous sodium hydroxide (NaOH) as electrolyte. Sodium hydroxide disintegrates into sodium ion (Na^{+}) and hydroxyl ion (OH^{-}) when it dissolves in de-ionized water. The amount of ions in the electrolyte increases with the increase of electrolyte concentration and promotes the rise of electrical conductivity of the solution. The hydrogen gas bubbles along with water vapour are generated at the cathode, i.e. tool electrode, due to electrolysis, as the voltage between the two electrodes is increased. The rate of electrolysis increases at higher voltage compared to lower applied voltage. As a result, the width of the channel on PMMA is higher as the voltage increases from 30 V to 45 V for every tool feed rate, as shown in **Fig. 7. 7(a)**. The applied voltage is the driving force for altering the rate of the electrolysis process during ECD milling. Besides that, the electrolyte concentration also helps to increase the electrical conductivity of the solution, which further increases the rate of electrolysis. For this reason, the width of the channel in a higher electrolyte concentration is greater than the width of the channel generated at a lower electrolyte concentration. **Fig. 7. 7(b)** displays that the width of the channel under 10wt% of electrolyte concentration is much lower (i.e., 394.68 µm at 40V and 70 µm/sec tool feed rate) than the width of the channel fabricated under 25wt% of electrolyte concentration (i.e., 634.80 µm at 40V and 70 µm/sec tool feed rate).

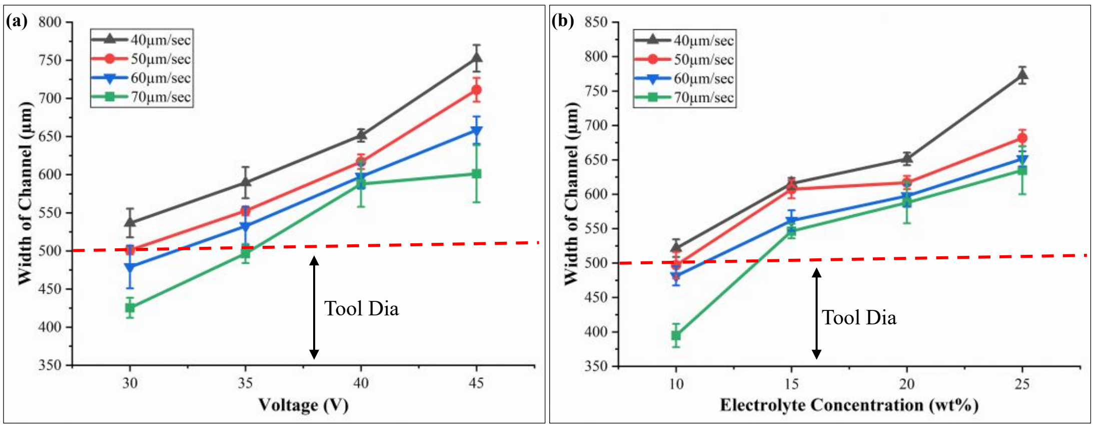

Fig. 7. 7 Impact of process parameters on channel width for PMMA in NaOH solution (a) Effect of Voltage at 20wt% of electrolyte concentration and (b) Effect of Electrolyte concentration at 40V of applied voltage

Although the tool electrode of 500 µm diameter was used for milling at lower voltage, such as 30 V, and at higher tool feed rate, such as 70 µm/sec, the full replica of the tool electrode was not generated. The spark discharge energy was lower at 30 volts at higher TFR lower energy of the spark discharge hitting the workpiece surface and causing a reduction in material removal. The width of the channel also became larger gradually when the electrolyte concentration increased from 10wt% to 20wt%, and after 20wt% of electrolyte concentration, the width increased rapidly at a lower tool feed rate. The increase in concentration influences the electrical conductivity of the solution, which leads to the generation of higher energy spark discharge with higher frequency and removes a large amount of materials from the workpiece surface. It is evidenced from the experiment that the rise of applied voltage influences the material removal rate, and the width of the channel increases, but this increase of applied voltage also generates uncontrollable spark discharge or unwanted spark discharge. Due to that, the surface of the milling area became irregular and rough, which generates a bad machining surface. Irregular removal of materials increased the surface roughness, which was measured in terms of R_a value. The surface roughness of the machined channel increases as the voltage decreases due to insufficient energy of the spark discharge at lower voltage, as shown in **Fig. 7. 8(a)**. The insufficient energy of the spark discharge leads to non-uniform material removal from the workpiece, creating higher surface roughness. As the voltage increases, the spark discharge energy also increases, which removes material uniformly from the workpiece and generates smooth surface by decreasing the Ra value as shown in **Fig. 7. 8(a)**. The R_a value of the bottom surface of the channel decreased up to 0.377 μm at 40 V, and after that, the R_a value again increased. The lower energy of the spark discharge at lower voltage caused the increase of the surface roughness, and as the applied voltage was increased, the surface roughness started to decrease up to 40V. After 40V, the spark discharge became uncontrollable, and it removed materials irregularly from the workpiece, which again generated higher surface roughness (i.e., 0.581 μm). The surface roughness of the channel is also significantly influenced by the electrolyte content. The high-temperature chemical etching process that produces a smooth surface and a lower R_a value is influenced by the hydroxyl ions present in the solution. Initially, at a lower electrolyte concentration, the electrical conductivity of the solution was lower, which produced lower energy of the spark discharge to create higher surface roughness of the channel as shown in **Fig. 7. 8(b)**. The higher electrolyte concentration increases the hydroxyl ions, which help to reduce the roughness of the channel. For this reason, the roughness of the channel at 10wt% of electrolyte solution is higher than the channel that is machined at 15wt% and 20wt% of electrolyte concentration. Upon reaching a 20wt% electrolyte concentration, the increased amount of hydroxyl ions improves the surface of the milling channel by escalating the high-temperature chemical etching. The electrical conductivity of the solution became too high to regulate the spark discharge after 20wt% of electrolyte concentration, which degraded the quality of the milling channel and resulted in R_a value of 0.586 µm.

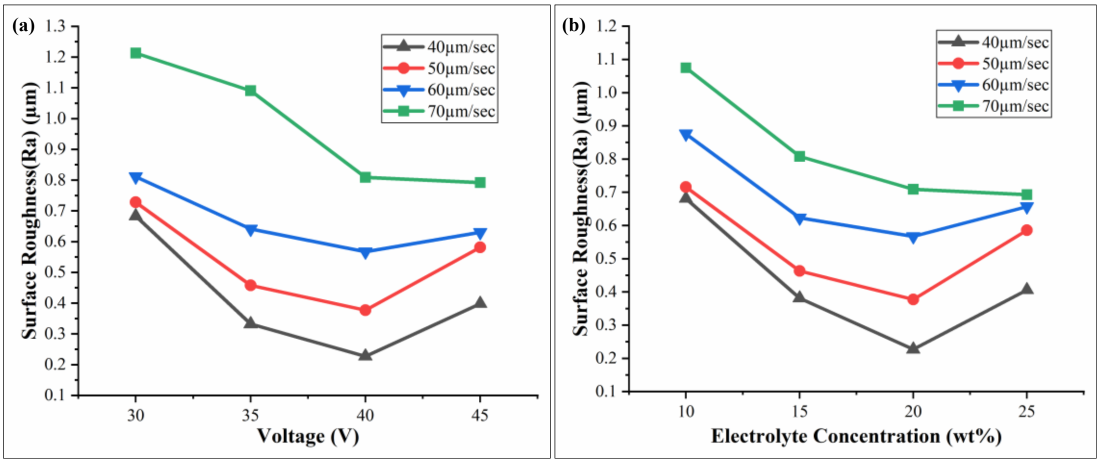

Fig. 7. 8 Impact of process parameters on surface roughness for PMMA in NaOH solution (a) Effect of Voltage at 20wt% electrolyte concentration, and (b) Effect of Electrolyte concentration at 40V of applied voltage

A lesser width of channel was obtained at 40V and 20wt% of NaOH electrolyte solution, as shown in **Fig. 7. 9(a)**. **Fig. 7. 9(b)** shows the 3D image of the channel, which reveals the uniform edges and smooth removal of materials to generate a better channel on PMMA.

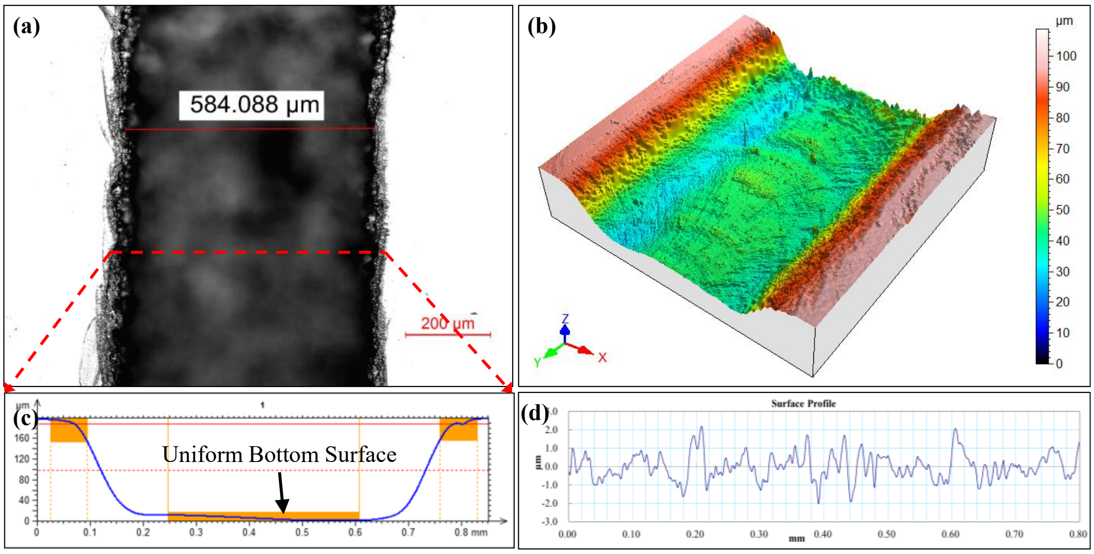

Fig. 7. 9 Milling channel on PMMA at 40V and 20wt% of NaOH electrolyte concentration with lesser width (a) optical image, (b) surface topography, (c) depth profile of channel, and (d) surface profile

In these parametric conditions, the surface of the bottom channel became smooth and uniform as shown in **Fig. 7. 9(c)**. **Fig. 7. 9(d)** shows the surface profile of the channel, which indicates the surface roughness of the channel. The maximum deviation was found to be very small when aqueous NaOH was used as an electrolyte. The R_a value was 0.377 µm at 40V of applied voltage and 20wt% of electrolyte concentration with a 50 µm/sec tool feed rate. Being a thermosetting polymer, the PMMA behaves like glass during milling, and the material is removed from the workpiece due to crack propagation and melting. Simultaneously, the high-temperature chemical etching in NaOH solution also promotes the uniform shape and channel edges throughout the milling on PMMA.

7.4.2 Influence of Process Parameters on PMMA with KOH Electrolyte

The energy of electrochemical discharge is more chemically active in aqueous KOH solution than in aqueous NaOH solution. Being a thermosetting polymer, PMMA acts like glass materials during electrochemical discharge milling. The spark discharges in KOH solution carry higher energy than NaOH solution, and it impacts the workpiece with high energy intensity, which leads to melting and vaporizing, and also to cracking of materials from the workpiece. The width of the channel generated through ECD milling using KOH as electrolyte was observed to be higher than that found in NaOH solution. **Fig. 7. 10** shows the impact of applied voltage on the channel width when ECD milling was done in aqueous KOH electrolyte at 50 µm/sec tool feed rate.

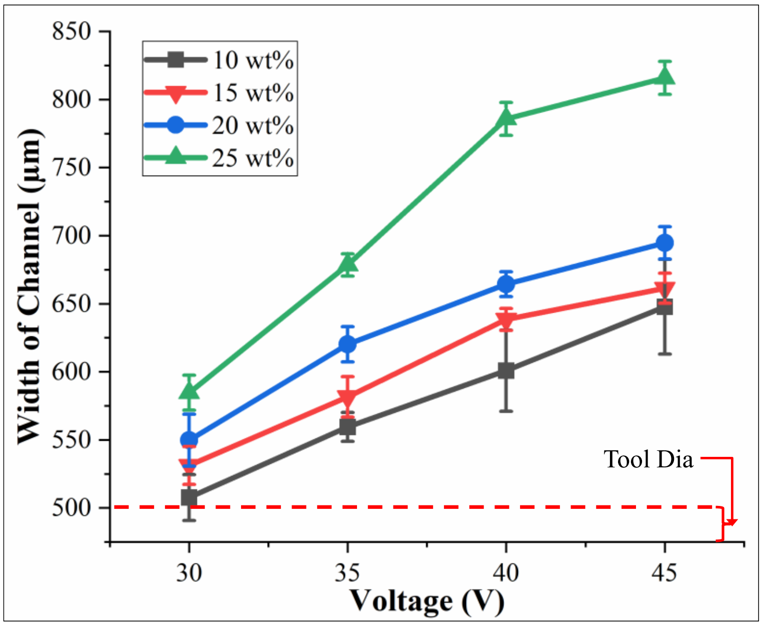

Fig. 7. 10 Impact of applied voltage on the width of the channel on PMMA for different KOH electrolyte concentrations at 50 µm/sec tool feed rate

The machined surface of the channel produced at other than 50 μm/sec tool feed rate was either rough or larger in width as per the previous study shown in **Fig. 7. 7** and **Fig. 7. 8**. The width of the channel is larger at 45V of applied voltage than at 30V of applied voltage. It is also noticeable from **Fig. 7. 10** that at lower electrolyte concentration, the channels are narrower than the width at higher electrolyte concentration. The size of potassium ions is bigger than the size of sodium ions as well, and the mobility of potassium ions is higher than sodium ions, which increases the electrical conductivity of potassium ions. Due to the higher electrical conductivity of the KOH solution, the potassium ions increased the electrolysis process and consequently the spark discharge that generates a greater impact on the workpiece and produces a larger width of channel. The lower width of channel with less amount of overcut was obtained at 30 V (i.e., 549.80 μm), but the channel quality, in terms of surface roughness, was poor. The surface roughness of the channel was decreased as the applied voltage was increased gradually, but after a certain voltage (i.e., 40V), the surface roughness was again increased. As shown in **Fig. 7. 11(a),** the R_a value is higher at 30V for every tool feed rate, but it gradually decreases up to 0.856 μm at 40V, and after that it again increases. It has been observed that the spark discharge generated at a lower 40V was unable to remove materials from the surface uniformly, and after 40V, the spark discharge became uncontrollable and vigorous. For this reason, the machined surface became rough at lower as well as higher voltage than 40 V. A Similar trend was observed with the varying electrolyte concentration. **Fig. 7. 11(b)** shows that the surface roughness was lower at 20wt% of electrolyte concentration than at other electrolyte concentrations for every tool feed rate.

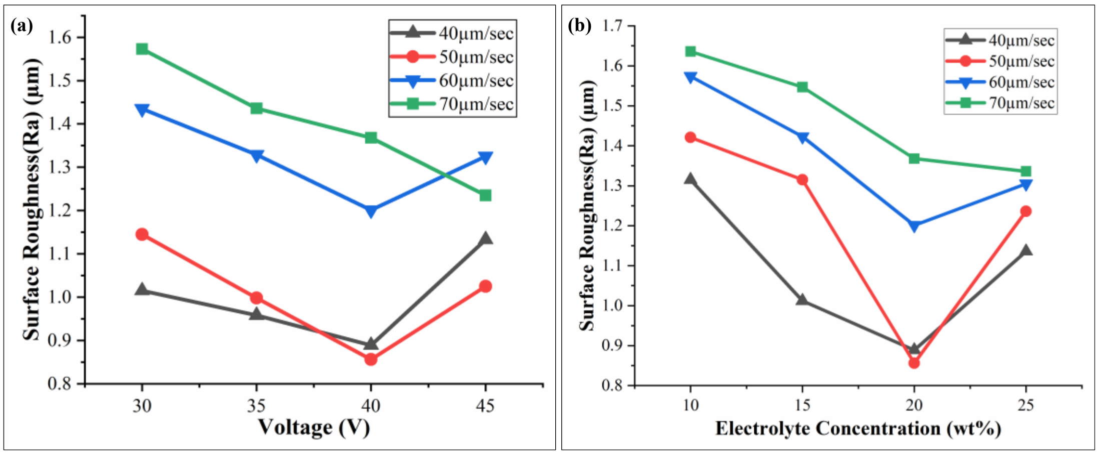

Fig. 7. 11 Impact of process parameters on surface roughness for PMMA in KOH solution (a) Effect of Voltage at 20wt% electrolyte concentration and (b) Effect of Electrolyte concentration at 40V of applied voltage

In ECD milling, a potassium hydroxide solution as electrolyte provides high-energy spark discharge, which removes large amounts of material from the workpiece. During the removal of materials from PMMA, larger-sized potassium ions generated larger craters on the surface of the material. Though the KOH solution provided high-temperature chemical etching during milling, it failed to smooth larger crater created by thermal energy of the spark discharge. At higher electrolyte concentration, large number of potassium ions enhanced the high-temperature chemical etching, which led to the reduction of surface roughness. After 20wt% wt% concentration, the solution conductivity was increased, which overpowered the chemical etching phenomenon and reduced the smoothness of the edge. The edges are irregular and non-uniform as shown in **Fig. 7. 12(a)** due to chaotic spark discharge in KOH solution. **Fig. 7. 12(b)** also reveals the irregular material removal during milling with KOH solution. This type of spark discharge generates a wavy bottom surface of the channel as shown in **Fig. 7. 12(c)** and **Fig. 7. 12(d)**. A non-uniform channel indicates less high-temperature chemical etching during milling with KOH solution as electrolyte.

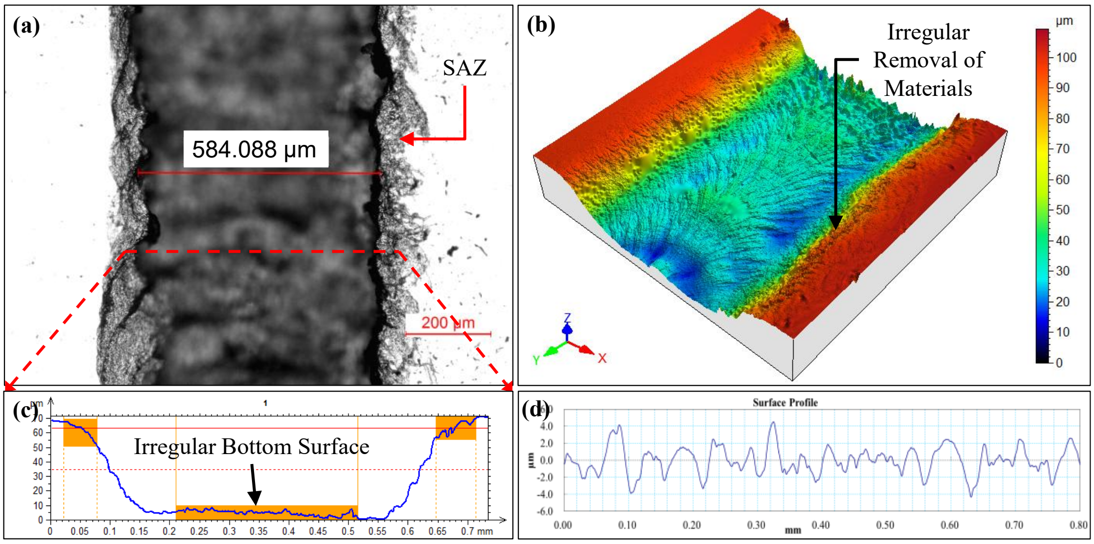

Fig. 7. 12 Milling channel on PMMA at 40V and 20wt% of KOH electrolyte concentration with higher width (a) optical image of channel, (b) Surface topography, (c) depth profile of channel, and (d) surface profile

Besides the irregular material removal and rough surface, the width of the channel that was fabricated using KOH electrolyte was higher than the width of the channel fabricated with NaOH solution.

7.4.3 Influence of Process Parameters on Polycarbonate with NaOH Electrolyte

Electrochemical Discharge Milling of polycarbonate was proved to be slightly more challenging than the milling of glass due to its unique properties as a thermoplastic polymer. Initial experiments were conducted using aqueous sodium hydroxide (NaOH) as the electrolyte, a common choice in ECDM for glass machining. However, when applied to polycarbonate, this electrolyte resulted in limited and irregular material removal from the workpiece surface. As a thermoplastic material, polycarbonate exhibited plasticity and was softened at elevated temperatures. Material removal during ECD milling on polycarbonate primarily occurred through processes involving melting, vaporization, and high-temperature chemical etching. These mechanisms played a crucial role in material removal at higher temperatures. In **Fig. 7. 13(a),** the impact of voltage on channel width is depicted at different tool feed rates. It was evident that higher tool feed rates led to narrower channels, whereas lower tool feed rates generated wider channels. This difference arose from varying tool-workpiece contact times; lower tool feed rates allowed for longer contact times, facilitating the generation of more spark discharges along the tool's path of movement. The applied voltage supplied the necessary energy to initiate and accelerate the electrochemical reaction, resulting in the production of hydrogen gas at the cathode and oxygen gas at the anode. The rate of electrolysis increased with higher applied voltage, leading to more frequent spark discharges and the generation of wider channels at higher voltages. Furthermore, as illustrated in **Fig. 7. 13(b),** the width of the channel increases with an elevated electrolyte concentration, reaching a maximum of 582.68 μm at 25 wt% electrolyte concentration.

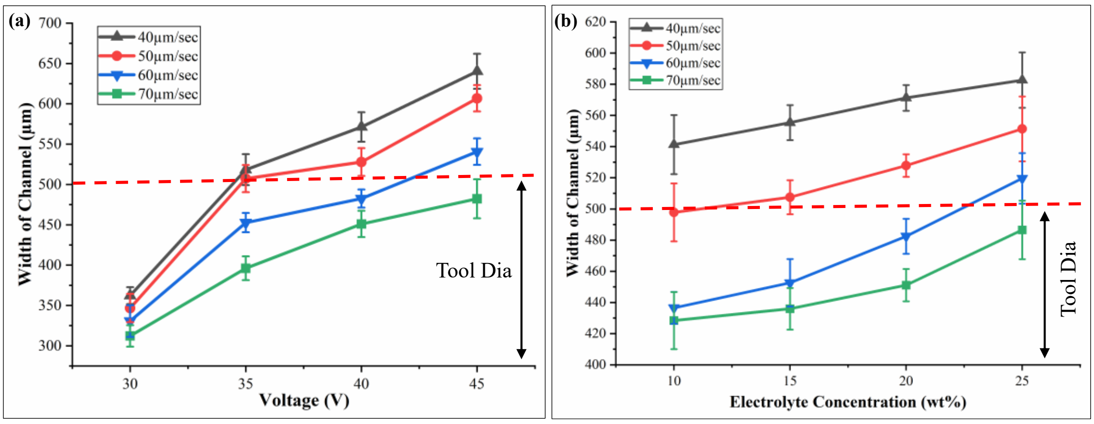

Fig. 7. 13 Impact of process parameters on channel width for Polycarbonate in NaOH solution (a) Effect of Voltage at 20wt% electrolyte concentration and (b) Effect of Electrolyte concentration at 40V of applied voltage

This increase in concentration enhanced the energy of the spark discharges, contributing to the formation of broader channels. The surface roughness of the bottom surface, measured in terms of R_a value, was measured for every channel generated on polycarbonate materials. It was noticed from the experimental results that the surface obtained by milling using aqueous NaOH as an electrolyte was rough and irregular. With lower voltage, removal of material from the workpiece surface happens irregularly and unevenly, creating a rough surface with R_a value of 0.785 µm at 30V. Although R_a value was reduced as the voltage was increased from 30V to 40V, and it was found to be lowest at 40V after that, the R_a value again increased, as shown in **Fig. 7. 14(a)**. It is also noticeable from **Fig. 7. 14(a)** that the R_a value is higher in the case of a higher tool feed rate compared to a lower tool feed rate. The intensity of spark discharge is greatly dependent on applied voltage, as it provides energy to the electrolysis process, and with the increase of voltage, the electrolysis process is also accelerated and leading to the generation of high-intensity spark discharge. The hydroxyl ion is increased in the solution at higher electrolyte concentration, which helps to etch the milling surface at high temperature and reduces the R_a value of the profile at higher concentration, as shown in **Fig. 7. 14(b)**. Due to the lower reactivity of sodium ions at higher temperatures, the surface of the milling channel was found to be rough, and non-uniform channel edges were produced.

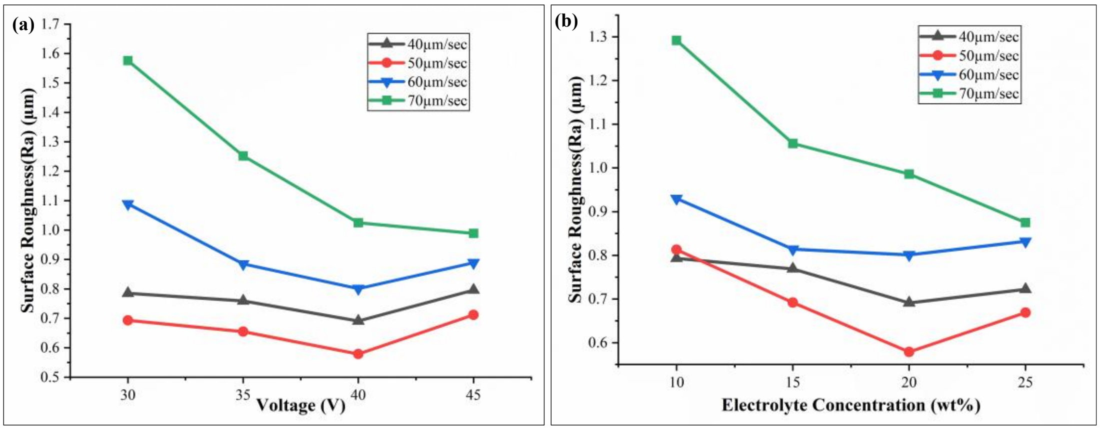

Fig. 7. 14 Impact of process parameters on surface roughness for Polycarbonate in NaOH solution (a) Effect of Voltage at 20wt% electrolyte concentration and (b) Effect of Electrolyte concentration at 40V of applied voltage

Channel width of 0.882µm R_a value of the bottom surface profile was obtained using aqueous NaOH solution as electrolyte. This is evidenced from the **Fig. 7. 15(a)** that the edges of the channel are irregular and non-uniform during milling with NaOH solution as electrolyte. Being a thermoplastic polymer, the polycarbonate behaves differently from PMMA during milling with NaOH electrolyte. The thermoplastic polymer melts at high temperature and flows along the edge of the channel to generate irregular channel edges as shown in **Fig. 7. 15(b)**. This also generates a wavy bottom surface due to insufficient material removal from the bottom surface of the machined channel, as shown in **Fig. 7. 15(c)**. The surface profile that was obtained during milling at 40V and 20wt% of electrolyte concentration is given in **Fig. 7. 15(d)**. The surface profile of the machined channel at other parametric conditions is very poor due to less and irregular material removal. The increase in electrolyte concentration influenced the electrical conductivity of the solution by increasing the ion content in the solution.

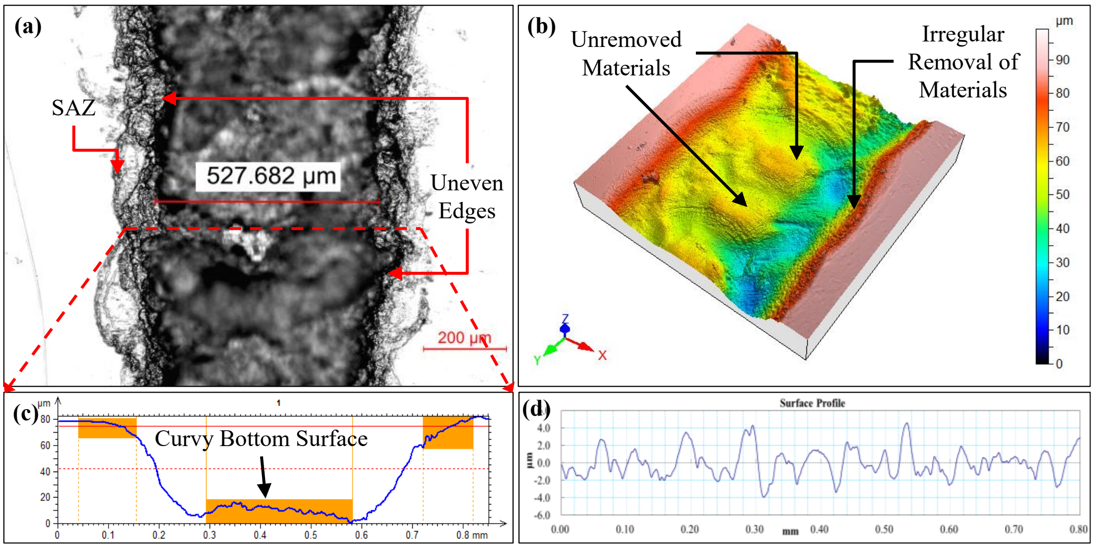

Fig. 7. 15 Milling channel on polycarbonate at 40V and 20wt% of NaOH electrolyte concentration with rough surface (a) optical image, (b) CCI image profile, (c) depth profile of channel, and (d) surface profile

Also, if the tool feed rate is increased, then the tool and workpiece interaction time is also reduced, which leads to insufficient spark discharge that removes materials irregularly.

7.4.4 Influence of Process Parameters on Polycarbonate with KOH Electrolyte

ECD milling was also conducted using aqueous potassium hydroxide (KOH) as an electrolyte to observe and compare the milling process on polycarbonate materials. The width of the channel was found to be higher and continued to increase as the applied voltage was increased while using KOH as the electrolyte. **Fig. 7. 16** shows the effect of voltage on the channel width generated using KOH electrolyte, and it can be noticed that the width of the channel increases with the voltage. Although the effect of voltage as seen in the case of NaOH solution is similar to the case of KOH solution but in the case of KOH electrolyte, the width of the channel was found to be larger than NaOH electrolyte. The width of the channel also increased with the increment of electrolyte concentration in the solution, as shown in **Fig. 7. 16**. Aqueous NaOH typically has higher electrical conductivity compared to aqueous KOH. This is because sodium ions (Na^+) have a lower molar mass and smaller ionic radius compared to potassium ions (K^+). As a result, sodium ions are more mobile in solution and can carry an electrical charge more effectively.

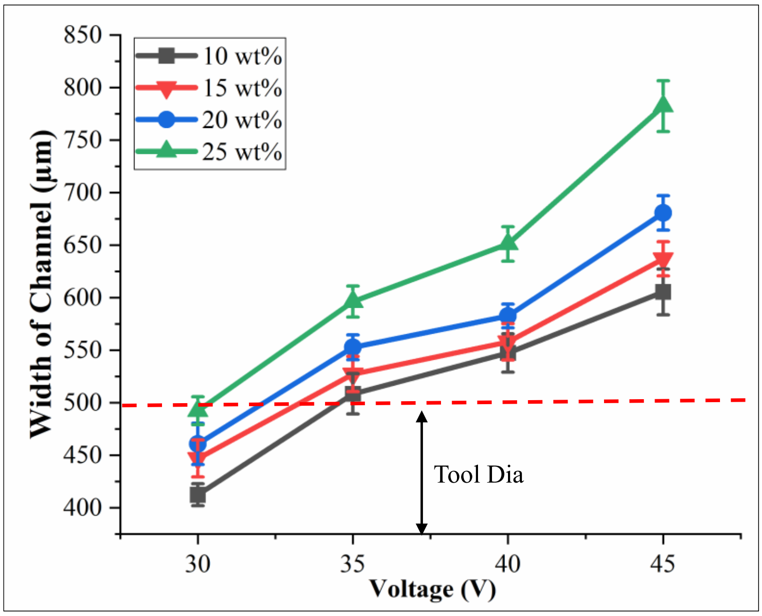

Fig. 7. 16 Impact of applied voltage on the width of the channel on Polycarbonate for various electrolyte concentrations at 50µm/sec TFR

Despite this, the temperature during electrochemical discharge in an aqueous KOH solution is higher than in an aqueous NaOH solution due to the greater resistance of the larger potassium ions. This phenomenon removes more material from the workpiece, producing a larger channel width in the case of KOH electrolyte. The lower tool feed rate resulted in generating a higher channel width. In contrast, the higher tool feed rate was responsible for producing a lower channel width as well as a rougher surface of the milling channel. Surface finish of the bottom surface of the milling channel with aqueous KOH electrolyte is better than that of aqueous NaOH electrolyte for polycarbonate, which was measured in terms of R_a value. As a thermoplastic material, polycarbonate exhibits a rough surface when treated with NaOH, primarily due to the lack of high-temperature chemical etching during processing. On the other hand, the channel generated using aqueous KOH produced a uniform channel edge and a smooth bottom surface during milling. High-temperature chemical etching of polycarbonate was more likely in an aqueous KOH solution than in an aqueous NaOH solution due to the size difference between the ions. The larger size of potassium ions increased the effect of chemical etching, which reduced the spark-affected zone by removing unwanted material from the edges of the channels. The R_a value of the milling channel is initially higher at lower voltage, and then it is reduced as the voltage is increased, but at more than 40V, the R_a value again increases, as shown in **Fig. 7. 17(a)**. A lower applied voltage results in lower spark energy, which removes materials from the surface erratically and creates a rough surface. As the voltage increases, the uniformity in material removal also increases, and surface roughness reduces up to 40V, but after that, the spark discharge becomes uncontrollable and removes materials non-uniformly again. The same phenomenon happens when the electrolyte concentration is varied from low to high. **Fig. 7. 17(b)** shows the effect of electrolyte concentration on the surface roughness of the milling channel.

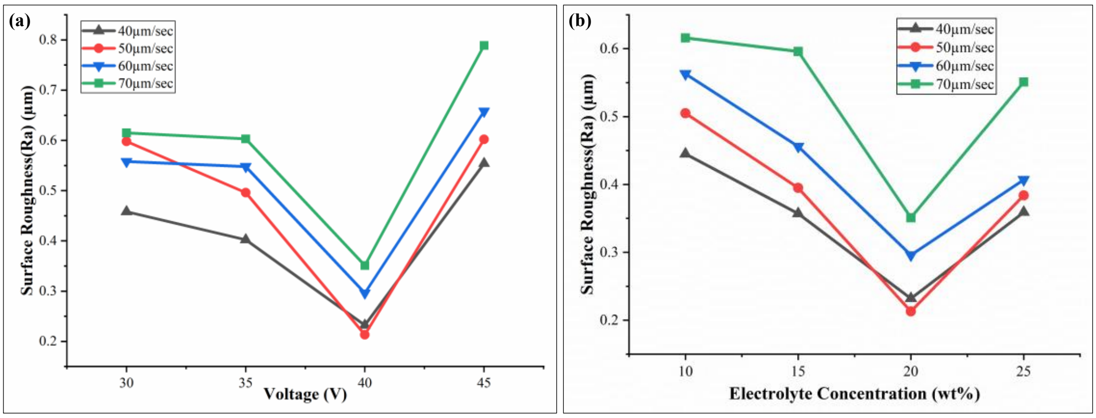

Fig. 7. 17 Impact of process parameters on surface roughness for Polycarbonate in KOH solution (a) Effect of Voltage at 20 wt% electrolyte concentration and (b) Effect of Electrolyte concentration at 40V of applied voltage

Along with the applied voltage, the surface roughness was greatly dependent on the electrolyte concentration, which was the main cause of high-temperature chemical etching. A higher electrolyte concentration increases the concentration of hydroxyl ions in the solution, and with more hydroxyl ions present, more etching is possible during machining. In this way, a channel with lower surface roughness was fabricated using a 20 wt% KOH electrolyte. **Fig. 7. 18(c)** shows the profile of the channel with an R_a value of 0.213 µm, which was fabricated at 40V and 50 µm/sec tool feed rate using 20 wt% aqueous KOH solution as electrolyte. It was observed from the experiments that the surface roughness of the channel increased further when the electrolyte concentration was raised above 20 wt%

due to the to the high electrical conductivity of the solution. As shown in **Fig. 7. 18(a),** the channel was obtained using a KOH electrolyte, revealing that the bottom surface as well as the edge of the channel is uniform. A lot of unevenness along the edge of the channel is removed due to high-temperature chemical etching and generates a uniform bottom surface, as shown in **Fig. 7. 18(b)**. The removal of unevenness of the bottom surface in KOH solution led to the generation of a smooth surface with a lower R_a value, as shown in **Fig. 7. 18(d)**.

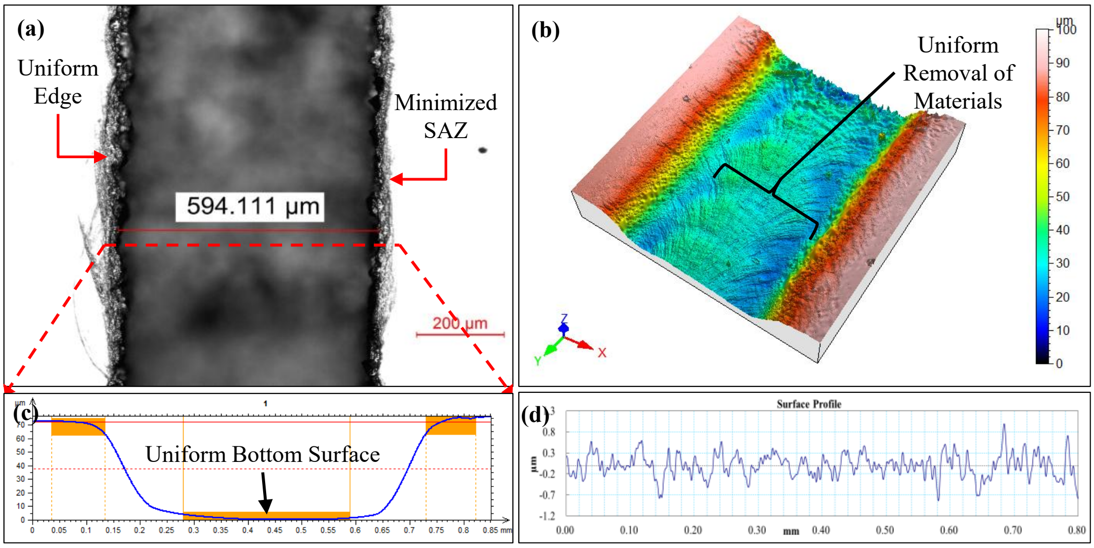

Fig. 7. 18 Milling channel on polycarbonate at 40V and 20 wt% of KOH electrolyte concentration with smooth surface (a) optical image, (b) CCI image profile, (c) depth profile of channel, and (d) surface profile

The re-deposited materials along the channel edge were removed by chemical etching during milling in KOH electrolyte. Finally, for polycarbonate with a 20 wt% KOH electrolyte, a 50 µm/sec tool feed rate, and 40 V, a smooth channel with a 0.213 µm Ra was achieved.

7.4.5 Influence of Process Parameters on Spark Affected Zone (SAZ)

The electrochemical discharge milling process generates heat energy during spark discharge. This heat energy is utilized to remove material from the workpiece to achieve a predetermined shape. Excess heat during spark discharge causes irregular material removal and rough surfaces along the edge of the machined channel in ECD milling. The area that is produced due to the effects of unwanted spark discharge is defined as the spark-affected zone (SAZ). The spark-affected zone results from unwanted, non-uniform spark discharge from the exposed surface of the tool electrode. The unwanted spark discharge generates spatter along the channel edge, reducing the quality of the milling channel. Several factors contribute to unwanted spark discharge and spatter along the channel edge. In this study, polycarbonate and PMMA behave differently in NaOH and KOH electrolyte solutions. It is noticeable from **Fig. 7. 19(a)** that the SAZ is bigger in the case of polycarbonate than PMMA when it was machined in NaOH solution, whereas it is smaller than PMMA when machined in KOH solution. The removal of material from the workpiece usually occurs via melting and vaporization, but in the case of thermoplastic polymers, the molten material is redeposited along the edge of the channel during ECD milling of polycarbonate in NaOH solution. As a result, the spark-affected zone increased when polycarbonate was machined with an NaOH electrolyte. The PMMA polymer behaves like a glass during machining, producing and propagating cracks in the presence of heat, and undergoing melting and vaporization as material is removed from the workpiece. Additionally, the applied voltage plays an important role in generating a spark-affected zone along the channel edge. The SAZ was observed at lower applied voltage as well as higher applied voltage for both the polymer, irrespective of the type of electrolyte, during ECD milling, as shown in **Fig. 7. 19(b)**. **Fig. 7. 19(b)** shows that the SAZ for PMMA machined with both NaOH and KOH electrolytes is lower than that of polycarbonate materials machined with NaOH electrolyte.

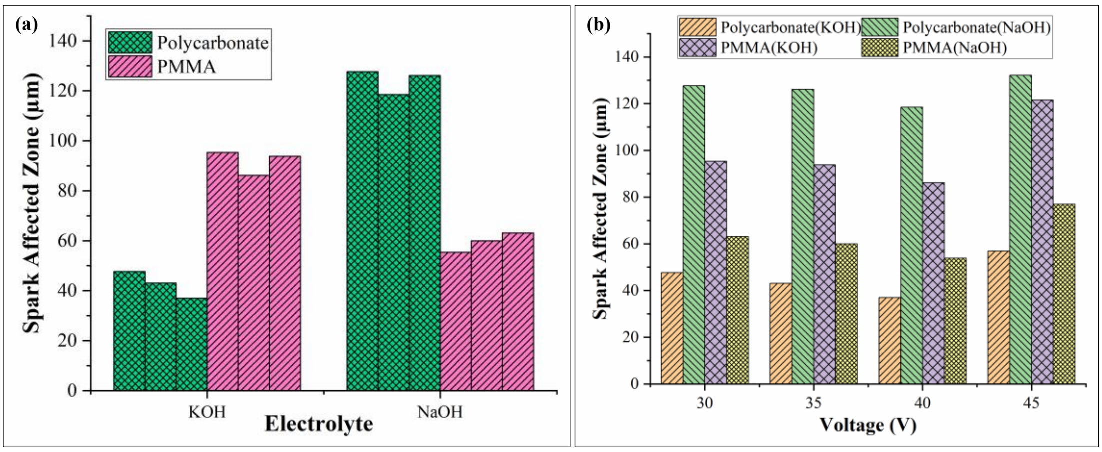

Fig. 7. 19 Variation of spark affected zone (a) for different electrolytes and (b) against applied voltage

The edges of the channel of PMMA, as shown in **Fig. 7. 20(a),** are full of unnecessary cracks with a lower channel width, which was machined at 40V and 20wt% of KOH electrolyte concentration, whereas the channel machined at 40V and 20wt% of NaOH electrolyte concentration produced a minimum spark-affected zone, as shown in **Fig. 7. 20(b)**. The voltage of less than 40V generates insufficient energy to erode materials along the edge of the PMMA channel uniformly. The edge of the PMMA channel was found to be full of cracks rather than re-deposited materials when machined at a lower voltage and KOH electrolyte solution. The impact of the spark discharge on the workpiece surface was vigorous, producing an irregular edge on the PMMA channel when machined at 40V with KOH solution. A smoother edge and a smaller spark-affected zone were observed when the channel was fabricated using NaOH as the electrolyte.

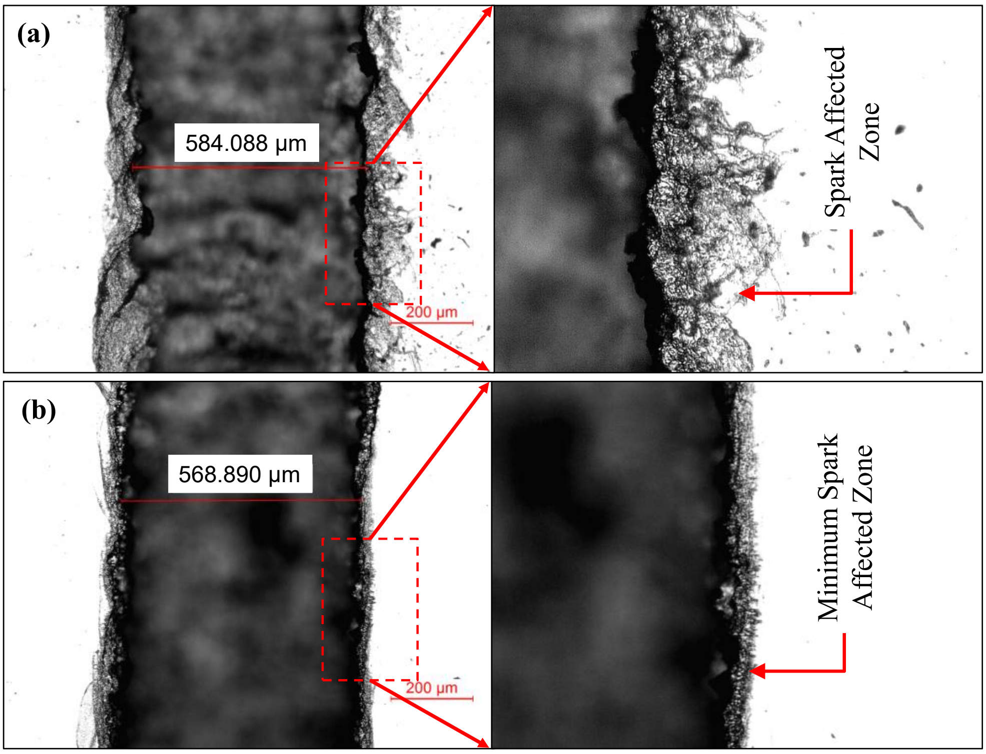

Fig. 7. 20 Image of channel fabricated on PMMA (a) at 40V and 20 wt% KOH electrolyte concentration and (b) at 40V and 20 wt% NaOH electrolyte concentration

Polycarbonate materials show a different nature under the machining conditions used for PMMA materials. In the NaOH solution, the polycarbonate channel generates a higher amount of spark-affected zone due to the absence of high-temperature chemical etching. The spark-affected zone was increased in the case of polycarbonate, not only because of high-temperature chemical etching but also due to the type of electrolyte used during machining. **Fig. 7. 21(a)** represents the machined channel produced by ECD milling at 40V and 20 wt% concentration using NaOH electrolyte solution, which shows a larger area of spark-affected zone along the edge of the channel. This SAZ is due not only to higher voltage or lower electrolyte concentration but also to the redeposited materials along the channel. During material removal, polycarbonate melts and disperses from the machining zone along the channel edge, creating a non-uniform surface of the machined channel. Experiments showed that when polycarbonate was machined with a KOH electrolyte solution, the generated channels exhibited a uniform edge and a smaller spark-affected zone. With the use of higher KOH electrolyte concentration and voltage, the deposition of the materials along the edge of the channel was reduced, as shown in **Fig. 7. 21(b)**.

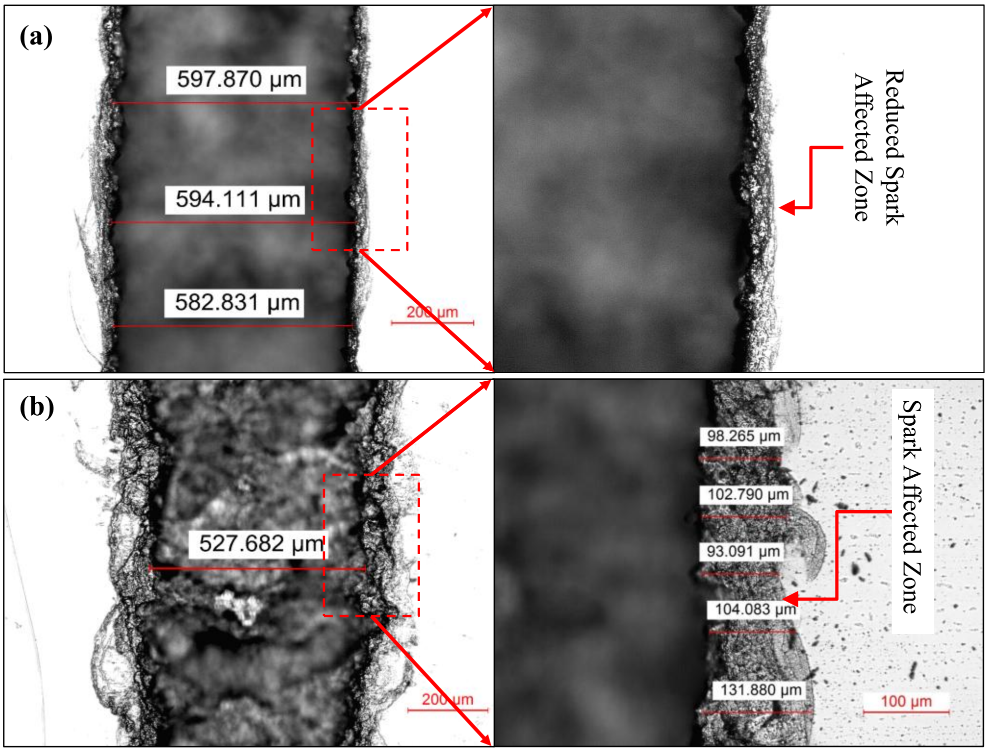

Fig. 7. 21 Optical image of spark-affected zone on Polycarbonate (a) at 40V and 20wt% of KOH electrolyte concentration and (b) at 40V and 20wt% of NaOH electrolyte concentration

The increase in $(OH)^-$ ions in the electrolyte solution enhances the chemical etching, which further accelerates when KOH is used as the electrolyte. The larger size of potassium ions relative to sodium ions influences the chemical etching process, and the greater impact of the spark discharge removes the deposited layer along the channel edge.

The experimental observations obtained in the present investigation agree well with those reported in previously published ECDM studies. Similar to Torabi et al. **[101]**, machining quality deteriorated with increasing discharge energy, resulting in wider channels and higher surface roughness. However, whereas Torabi et al. primarily related this behavior to tool geometry and electrolyte conditions in glass, the present study demonstrates that polymer type plays an equally important role. PMMA machined with NaOH produced a channel width of 584.088 μm and a surface roughness of 0.377 μm, whereas machining with KOH increased the channel width to 646.469 μm and the roughness to 0.856 μm under identical machining conditions. The observations are also consistent with Rajput et al. **[102]**, who showed that applied voltage, electrolyte concentration, and feed rate are the principal parameters governing ECDM performance. The present work confirms the same trend observed in polymer machining and further demonstrates that the optimal electrolyte depends on the material's thermophysical properties. Polycarbonate machined with NaOH exhibited irregular material removal with R_a = 0.579 μm, whereas KOH reduced the surface roughness to 0.213 μm while producing a wider channel of 594.111 μm because of enhanced chemical etching.

7.5 Outcomes of the Study

Electrochemical Discharge Milling was performed on Polycarbonate and PMMA to generate surface channels. As a thermoplastic material, polycarbonate exhibited some difficulties during milling with the ECD process. By altering process parameters such as voltage, electrolyte concentration, and tool feed rate, and using two distinct electrolytes, milling was performed, yielding the following experimental results.

(i) Simulation results revealed that materials like glass, polycarbonate, and PMMA show varying rates of heat propagation during ECD milling, affecting machining performance. Glass heats quickly, which can improve machining efficiency but may lead to thermal damage. Polycarbonate and PMMA heat up more slowly, affecting machining quality differently. Adjusting the ECD milling parameters to match each material's thermal properties is crucial for achieving better machining outcomes.

(ii) The PMMA material exhibited brittle material properties and generated a rough surface with a larger channel width in KOH solution. On the other hand, the fabricated channel in PMMA using NaOH electrolyte resulted in a smaller channel width and a smooth surface finish.

(iii) Larger channel width of 646.469 μm was obtained for PMMA at 40V, 50 μm/sec tool feed rate and 20wt% KOH with 0.856 μm R_a value whereas smaller channel width of 584.088 μm was obtained at 40V, 50 μm/sec tool feed rate and 20wt% NaOH with 0.377 μm R_a value which indicates the better results at KOH electrolyte during ECD milling of PMMA.

(iv) The milling on polycarbonate using the Electrochemical Discharge process exposed difficulties in removing materials from the surface using NaOH as an electrolyte, as it is a thermoplastic material. Experimental analysis revealed that thermoplastic materials melted and redeposited along the channel edge without vaporizing, thereby generating a rough, irregular surface during milling with the electrochemical discharge process.

(v) The width of the channel in case of Polycarbonate was found to be 527.682 µm with 0.579 µm R_a value at 40V, 50 µm/sec tool feed rate and 20wt% NaOH with irregular material removal and uneven channel edges, whereas 594.111 µm channel width with 0.213 µm R_a value was obtained using 20wt% KOH at the same parameters.

(vi) Polycarbonate material generated a larger spark-affected zone (SAZ) than PMMA during ECD milling with NaOH solution. In the case of PMMA, the spark-affected zone was removed using a NaOH solution, and the Polycarbonate material showed no spark-affected zone in a KOH solution due to high-temperature chemical etching.

ECD milling on polymers produced higher-quality channels using NaOH and KOH electrolyte solutions for PMMA and Polycarbonate, respectively. Due to their high transparency, both thermosetting and thermoplastic polymers are useful for making lab-on-chip devices generated by the ECD milling process. In addition to generating microchannels, several complex micropatterns can be fabricated not only on thermosetting polymers but also on thermoplastic polymers by proper selection of electrolytes and processing parameters.

Chapter 8

GENERAL CONCLUSIONS AND FUTURE SCOPE OF RESEARCH WORK

8.1 General Conclusions

The study provides a comprehensive understanding of Electrochemical Discharge Milling (ECD milling) by examining its mechanisms, including electrolysis, gas film formation, spark discharge, and material removal. Through this detailed analysis, the research clarifies how these phenomena work together to enable precise machining. A major contribution of the study is the evaluation of different tool-feeding techniques, comparing traditional and innovative methods to assess their effects on gas-film stability, spark behavior, and machining performance. These insights help identify strategies that improve material removal rates, channel geometry, and overall process efficiency. The study further demonstrates the versatility of ECD milling by applying it to materials such as silica glass and polymers. Upward tool feeding proved effective for glass, enhancing surface quality and enabling intricate pattern formation, while experiments on polymers showed how electrolyte choice and process parameters can reduce the Spark Affected Zone and improve machining outcomes. Additionally, the research offers guidance for fabricating complex shapes, such as rectangular cavities in glass, by adjusting inter-channel distances. These contributions not only address existing challenges but also open new possibilities for future research and technological development in the field of ECD milling. The insights gained from this study are expected to drive further advancements, making ECD milling a more effective and versatile tool in precision machining and manufacturing.

Based on experimental results and analyses, the following conclusions are drawn:

(i) The ECD milling setup was successfully developed by integrating several mechanical, electrical, and control components. The high-resolution X-Y-Z translation stage and APT software ensure accurate tool motion, while the specially fabricated tool- and workpiece-holding units provide stable alignment and insulation. The copper tool electrode, graphite auxiliary electrode, and Perspex machining chamber collectively create a safe and controlled environment for spark generation. A dedicated DC power supply delivers the required voltage for consistent discharge formation. Together, these functional elements form a compact, reliable ECD milling system.

(ii) The shape of the gas film plays a crucial role in the machining performance of ECD milling. In the upward tool-feeding technique, the gas film protrudes towards the machining direction due to buoyant force, thereby allowing intense and controlled spark discharges at the tool tip. This configuration leads to higher machining precision, reduced overcut, and minimal tool wear compared to existing horizontal and bottom-tool feeding techniques. The simulation study revealed that the shape of the gas film significantly affects the temperature distribution during electrochemical discharge milling (ECD milling). In the existing tool-feeding technique, higher temperatures were observed around the periphery of the tool electrode, resulting in less efficient machining. In contrast, the vertically upward tool-feeding technique concentrated higher temperatures at the tool tip, thereby enhancing the intensity of the spark discharge and improving material removal rates.

(iii) The vertically upward tool feeding technique demonstrated superior performance in terms of temperature distribution and machining quality. The simulation results showed that this technique maintained a higher temperature at the machining zone or tool tip across various voltages, ranging from 30V to 45V. This consistent high-temperature distribution at the tool tip is advantageous for more controlled and intense spark discharges, leading to improved material removal and machining precision. In upward tool feeding, the channel depth is greater than in existing tool feeding and bottom tool feeding techniques under the same machining conditions. Channel width is found to be lower than other feeding techniques and reduced by 11% during upward tool feeding than that of existing tool feeding at higher electrolyte concentration.

(iv) The upward tool feeding technique resulted in the least tool-electrode wear among the three techniques. The diameter reduction of the tool-electrode was 4.95% (498.732μm to 473.895μm) for upward tool feeding, compared to 8.84% (501.479μm to 457.151μm) for existing tool feeding and 7.22% (498.701μm to 462.683μm) for bottom tool feeding. The channel width increased with increasing electrolyte concentration. Also, the channel width decreases as the tool feed rate increases. In the upward tool feeding technique, tool wear is found to be less, and tool-electrode diameter is reduced by 4.95% after machining. A smoother edge profile of the channel is produced at 15 wt% NaOH solution and a tool feed rate of 60 µm/sec. A maximum depth of 800.14µm and a width of 589.26µm are obtained at this parametric condition.

(v) In ECD milling, machining quality depends more on the used energy than on total input energy. For example, with a 2000 J input, only about 7–8 J is effectively utilized due to heat loss and gas-film instability, whereas raising the input to 5000 J increases the effectively utilized energy only slightly to 16–20 J. Although higher input promotes greater spark generation and widens the channel (e.g., 110 µm at 8 J to 165 µm at 20 J), excessive input also causes taper growth (taper angle increasing from 3.2° to 6.8°), thereby reducing dimensional accuracy.

(vi) Multi-response RSM optimization (Box-Behnken) identified optimal ECD milling parameters: 20 wt% electrolyte, 35 V, and ~43–45 µm/s tool feed. Predicted responses were WOC of 561.05 µm, R_a of 0.351 µm, TA of 21.45°, and MRR of 4.244 µg/min. Experimental validation at 20 wt%, 35 V, and 45 µm/s produced WOC of 581.604 µm, Ra of 0.342 µm, TA of 20.48°, and MRR of 4.335 µg/min, with errors of 3.66%, 2.56%, 4.50%, and 2.14%, respectively. High electrolyte and moderate voltage improved MRR and surface finish, while feed rate controlled edge integrity.

(vii) The first strategy, i.e. inter-channel distance same as channel width for generating rectangular cavities using electrochemical discharge milling (ECD milling) on glass, led to a total cavity width larger than that obtained with other strategies, i.e. inter-channel distance same as tool diameter and less than tool diameter. The merging of borders between consecutive parallel channels formed heaps of molten material, thereby increasing surface roughness. The surface topography revealed a curved bottom surface with height variations of approximately 80µm, resulting in a lower surface roughness (R_a) of 0.406 µm.

(viii) The second strategy for generating rectangular cavities using ECD milling involved setting the distance between parallel channels equal to the diameter of the tool-electrode (500µm). This approach resulted in a narrower total cavity width compared to the first strategy due to the reduced inter-pass distance. Surface roughness (Ra) decreased with voltage up to 40V, reaching 0.438µm at 40V and 50µm/sec TFR, but increased rapidly beyond 40V. Unlike the first strategy, the reduced inter-pass distance in the second strategy caused heaps of molten material to shift toward the middle of adjacent channels, resulting in a narrower total cavity width and reduced height variation (up to 55µm).

(ix) The third strategy, i.e., inter-channel distance less than tool diameter, resulted in a narrower total cavity width compared to the previous strategies. This strategy also eliminated the accumulation of molten material heaps along the channel borders. Among the three strategies, the third strategy with the lowest inter-pass distance between parallel channels was identified as the most suitable for fabricating rectangular cavities. This method produced a smaller total width (1303.323µm) and lower surface roughness (R_a) compared to the other strategies, achieved at an applied voltage of 40V, an electrolyte concentration of 20 wt%, and a TFR of 50 µm/s.

(x) The simulation of heat propagation through different materials, e.g., glass, polycarbonate, and PMMA, reveals significant variations in heat distribution that directly affect machining performance in ECD milling. Glass exhibits the fastest heat propagation, leading to a deeper and more uniform temperature spread. Polycarbonate and PMMA show slower heat conduction. This discrepancy necessitates the use of different types of electrolytes for each material to achieve improved surface roughness and dimensional accuracy.

(xi) The ECD milling of PMMA with NaOH and KOH electrolytes shows that increasing voltage from 30V to 45V widens channels, and the better results are achieved at 40V and 20wt% NaOH electrolyte, producing the narrower channels with the smoother surfaces (R_a value of 0.377µm). In contrast, the KOH electrolyte generates higher-energy spark discharges, leading to larger channel widths. Higher KOH electrolyte concentrations enhance chemical etching but can also lead to irregular, non-uniform edges at concentrations exceeding 20 wt%. Overall, the NaOH electrolyte solution provides better control over surface quality and channel uniformity, whereas the KOH electrolyte yields larger, rougher channels.

(xii) In the case of polycarbonate using aqueous NaOH electrolyte, the material removal was less effective due to thermoplastic properties, leading to limited and irregular surface etching. In contrast, the KOH electrolyte, with its higher melting point due to larger potassium ions, facilitated greater material removal and yielded a smoother finish. Higher channel widths and better surface quality were achieved with the KOH electrolyte, especially at 40V and a 20 wt% electrolyte concentration, producing channels with an R_a value as low as 0.213µm.

(xiii) The influence of process parameters on the Spark Affected Zone (SAZ) in electrochemical discharge milling highlights significant variations based on the type of polymer and electrolyte used. For polycarbonate, the SAZ is more pronounced when machined with an NaOH electrolyte due to the redeposition of molten material along the channel edges, resulting in a larger SAZ than in PMMA. Conversely, the KOH electrolyte produced a smaller SAZ for Polycarbonate due to the larger potassium ions in KOH, which contributed to more effective chemical etching and smoother channel edges.

Overall, this comprehensive analysis offers valuable insights into the complex interplay of factors that influence ECD milling technology. By examining setup components, tool feeding techniques, material-specific considerations, and the effects of the electrolyte, the present research offers a deeper understanding of ECD milling processes for generating complex-shaped channels and cavities in different materials, especially glass and polymers. These findings are useful in advancing ECD milling technology and enhancing its applications across various manufacturing domains.

8.2 Future Scope of Research Work

Future research on Electrochemical Discharge Milling (ECD milling) can explore several promising avenues to enhance its effectiveness and broaden its applications.

(i) Incorporation of tool rotation with upward tool feeding Technique could potentially improve the uniformity of material removal and enhance surface finish by ensuring more consistent tool-workpiece gap and discharge distribution across the workpiece.

(ii) Generation of various geometrical cavities with patterns such as spiral, oscillatory, or complex geometrical paths may yield valuable insights into their effects on machining performance.

(iii) Addition of an advanced control system may provide precise control over discharge parameters, enabling adaptive adjustments based on real-time feedback. This would enhance the accuracy of ECD milling operations.

(iv) Various types of eco-friendly electrolytes can potentially reduce corrosion, enhance discharge stability, and improve the overall performance of ECD milling.

Bibliography

[1] Kurafuji, H., Suda, K., 1968. Electrical discharge drilling of glass. Annals of the CIRP 16, 415

[2] N.H. Cook, G.B. Foote, P. Jordan, B.N. Kalyani (1973). Experimental studies in electro-machining. Transactions of the ASME, Journal of Engineering for Industry, 945–950.

[3] H. Tsuchiya, T. Inoue, M. Miyazaiki (1985). Wire electro-chemical discharge machining of glasses and ceramics. Bulletin of the Japan Society of Precision Engineering. 19, 73.

[4] V.K. Jain, P.S. Rao, S.K. Choudhury, K.P. Rajurkar (1991). Experimental investigations into travelling wire electrochemical spark machining (TW-ECSM) of composites. Transactions of the ASME, Journal of Engineering for Industry. 113, 75.

[5] I. Basak, A. Ghosh (1997). Mechanism of material removal in electrochemical discharge machining a theoretical model and experimental verification", Journal of Materials Processing Technology. 71, 350-359.

[6] C.T. Yang, S.S. Ho, B.H. Yan (2001). Micro hole machining of borosilicate glass through electrochemical discharge machining (ECDM). Key Engineering Materials. 196, 149–166.

[7] V. Fascio, R. Wuthrich, H. Bleuler (2004). Spark assisted chemical engraving in the light of electrochemistry. Electrochimica Acta. 49, 3997

[8] R. Wuthrich, V. Fascio (2005). Machining of non-conductive materials using electrochemical discharge phenomenon: An overview. International Journal of Machine Tools and Manufacture. 45, 1095–1108.

[9] H. Vogt (1983). Comprehensive Treatise of Electrochemistry. 6, 445- 489.

[10] K. Allesu, A. Ghosh, M.K. Muju (1992). Preliminary qualitative approach of a proposed mechanism of material removal in electrical machining of glass. European Journal of Mechanical Engineering. 36, 202.

[11] A. Kulkarni, R. Sharan, G.K. Lal (2003). Measurement of temperature transients in the electrochemical discharge machining process. Temperature: Its measurement and Control in Science and Industry. 7, 1069.

[12] N. Gautam, V.K. Jain (1998). Experimental investigations into ECSD process using various tool kinematics. International Journal of Machine Tools and Manufacture. 38, 15.

[13] P. Maillard, B. Despont, H. Bleuler, R. Wuthrich (2007). Geometrical characterization of microholes drilled in glass by gravity-feed with spark-assisted chemical engraving (SACE). Journal of Micromechanics and Microengineering. 17, 1343–1349.

[14] V.K. Jain, S. Adhikary, (2008). On the mechanism of material removal in electrochemical spark machining of quartz under different polarity conditions. Journal of Materials Processing Technology. 200, 460–470.

[15] M.S. Han, B.K. Min, S.J. Lee (2008). Modeling gas film formation in electrochemical discharge machining processes using a side-insulated electrode. Journal of Micromechanics and Microengineering. 18, 045019.

[16] C.P. Cheng, K.L. Wu, C.C. Mai, Y.S. Hsu, B.H. Yan (2010). Magnetic field-assisted electrochemical discharge machining. Journal of Micromechanics and Microengineering. 20, 075019

[17] C.P. Cheng, K.L. Wu, C.C. Mai, C.C. Yang, Y.S. Hsu, B.H. Yan (2010). Study of gas film quality in electrochemical discharge machining. International Journal of Machine Tools & Manufacture. 50, 689–697.

[18] S. F. Huang, Y. Liu., J. Li, H. X. Hu, L. Y. Sun (2014). Electrochemical Discharge Machining Micro-Hole in Stainless Steel with Tool Electrode High-Speed Rotating. Materials and Manufacturing Processes. 29(5), 634-637.

[19] C. Gao, Z. Liu, A. Li. (2014). Study of Micro Drilling on Pyrex Glass Using Spark Assisted Chemical Engraving. Micro and Nanosystems. 6, 26-33.

[20] M.R. Razfar, A. Behroozfar, J. Ni. (2014). Study of the effects of tool longitudinal oscillation on the machining speed of electrochemical discharge drilling of glass. Precision Engineering. 38, 885-892.

[21] B. Jiang, S. Lan, K. Wilt, J. Ni. (2015). Modeling and experimental investigation of gas film in micro-electrochemical discharge machining process. International Journal of Machine Tools & Manufacture. 90, 8-15.

[22] H. Krotz, K. Wegener (2015). Spark assisted electrochemical machining: a novel possibility for micro drilling into electrical conductive materials using the electrochemical discharge phenomenon. The International Journal of Advanced Manufacturing Technology. 79, 1633-1643.

[23] S. Elhami, M. Razfar (2017). Analytical and experimental study on the integration of ultrasonically vibrated tool into the micro electro-chemical discharge drilling. Precision Engineering. 47, 424-433.

[24] S. Elhami, M. Razfar (2017). Study of the current signal and material removal during ultrasonic-assisted electrochemical discharge machining. The International Journal of Advanced Manufacturing Technology. 92, 1591-1599.

[25] N. Sabahi, M.R. Razfar., M. Hajian (2017). Experimental investigation of surfactant-mixed electrolyte into electrochemical discharge machining (ECDM) process. Journal of Materials Processing Technology. 250, 190-202.

[26] S. Elhami, M. Razfar (2018). Effect of ultrasonic vibration on the single discharge of electrochemical discharge machining. Materials and Manufacturing Processes. 33(4), 444-451.

[27] Y. Xu, J. Chen, B. Jiang, Y. Liu, J. Ni (2018). Experimental investigation of magnetohydrodynamic effect in electrochemical discharge machining. International Journal of Mechanical Sciences. 142-143, 86-96.

[28] T. Singh, A. Dvivedi (2018). On performance evaluation of textured tools during micro-channeling with ECDM. Journal of Manufacturing Processes. 32, 699-713.

[29] K.R. Kolhekar, M. Sundaram. (2018). Study of gas film characterization and its effect in electrochemical discharge machining. Precision Engineering. 53, 203-211.

[30] M.Y. Lin, T. H. Tsai, L.W. Hourng, W.K. Wang (2019). The effects of magnetic field and ethanol addition on the electrochemical discharge machining. The International Journal of Advanced Manufacturing Technology. 105, 2461-2467.

[31] J. Arab, H. K. Kannojia, P. Dixit (2019). Effect of tool electrode roughness on the geometric characteristics of through-holes formed by ECDM. Precision Engineering. 60, 437–447.

[32] T. Singh, A. Dvivedi, A. Shanu, P. Dixit (2021). Experimental investigations of energy channelization behavior in ultrasonic assisted electrochemical discharge machining. Journal of Materials Processing Technology. 293, 117084.

[33] I.M. Rashedul, Y. Zhang, K. Zhou, G. Wang, T. Xi, L. Ji (2021). Influence of Different Tool Electrode Materials on Electrochemical Discharge Machining Performances. micromachines, 12.

[34] J. W. Liu, T. M. Yue, Z. N. Guo (2010). An analysis of the discharge mechanism in electrochemical discharge machining of particulate reinforced metal matrix composites. International Journal of Machine Tools & Manufacture. 50, 86-96.

[35] C. Wei, K. Xu, J. Ni, A. J. Brzezinski, D. Hu (2011). A finite element based model for electrochemical discharge machining in discharge regime. The International Journal of Advanced Manufacturing Technology. 54, 987–995.

[36] H. Krotz, R. Roth, K. Wegener (2013). Experimental investigation and simulation of heat flux into metallic surfaces due to single discharges in micro-electrochemical arc machining (micro-ECAM). The International Journal of Advanced Manufacturing Technology. 68, 1267–1275.

[37] B. Jiang, S. Lan, J. Ni, Z. Zhang (2014). Experimental investigation of spark generation in electrochemical discharge machining of non-conducting materials. Journal of Materials Processing Technology. 214, 892-898.

[38] M. Hajian, M. R. Razfar, S. Movahed (2016). An experimental study on the effect of magnetic field orientations and electrolyte concentrations on ECDM milling performance of glass. Precision Engineering. 45, 322-331.

[39] S. Saranya, A. Nair, A. Ravi Sankar (2016). Experimental investigations on the electrical and 2D-machining characteristics of an electrochemical discharge machining (ECDM) process. Microsystem Technologies. 23, 1453-1461.

[40] N. Sabahi, M. Hajian, M. R. Razfar (2018). Experimental study on the heat-affected zone of glass substrate machined by electrochemical discharge machining (ECDM) process. The International Journal of Advanced Manufacturing Technology. 97, 1557-1564.

[41] T. Singh, A. Dvivedi (2018). On pressurized feeding approach for effective control on working gap in ECDM. Materials and Manufacturing Processes. 33(4), 462-473.

[42] P. K. Gupta (2018). Effect of Electrolyte Level during Electro Chemical Discharge Machining of Glass. Journal of The Electrochemical Society. 165(7), E279-E281.

[43] N. Sabahi, M. R. Razfar (2018). Investigating the effect of mixed alkaline electrolyte (NaOH + KOH) on the improvement of machining efficiency in 2D electrochemical discharge machining (ECDM). The International Journal of Advanced Manufacturing Technology. 95, 643-657.

[44] J. Liu, Z. Lin, T. Yue, Z. Guo, S. Jiang. (2018). An analysis of the tool electrode working mechanism of grinding-aided electrochemical discharge machining of MMCs. The International Journal of Advanced Manufacturing Technology. 99, 1369–1378.

[45] J. B. Madhavi, S. S. Hiremath (2019). Machining and Characterization of Channels and Textures on Quartz Glass Using μ-ECDM Process. Silicon. 11, 2919–2931.

[46] K. Kolhekar, M. Sundaram (2019). A multiphase simulation study of electrochemical discharge machining of glass. The International Journal of Advanced Manufacturing Technology. 105, 1597–1608.

[47] C. Zhang, Z. Xu., Y. Hang, J. Xing (2019). Effect of solution conductivity on tool electrode wear in electrochemical discharge drilling of nickel-based alloy. The International Journal of Advanced Manufacturing Technology. 103, 743–756.

[48] D. K. Mishra, K. Pawar, P. Dixit (2020). Effect of Tool Electrode-Workpiece Gap in the Microchannel Formation by Electrochemical Discharge Machining. ECS Journal of Solid State Science and Technology. 9, 034011.

[49] R.S. Rathore, A. Dvivedi (2020). Sonication of tool electrode for utilizing high discharge energy during ECDM. Materials and Manufacturing Processes. 35(4), 415-429.

[50] C.S. Jawalkar, A. K. Sharma, P. Kumar (2020). Innovations in electro chemical discharge machining process through electrolyte stirring and tool rotations. International Journal of Machining and Machinability of Materials. 22(6), 487-503.

[51] S. Elhami, M. R. Razfar (2020). Numerical and experimental study of discharge mechanism in the electrochemical discharge machining process. Journal of Manufacturing Processes. 50, 192-203.

[52] M. Singh, S. Singh, S. Kumar (2020). Environmental aspects of various electrolytes used in electrochemical discharge machining process. Journal of the Brazilian Society of Mechanical Sciences and Engineering. 42, 395.

[53] C.C. Ho, B. H. Huang, P. C. Chu (2021). A study based on electrochemical discharge assisted by hollow electrode and micro-nano bubble to process transparent non-conductive brittle materials. The International Journal of Advanced Manufacturing Technology. 115, 367–382.

[54] V. Rajput, M. Goud, N. M. Suri (2021). Multi-spark simulation of the electrochemical discharge machining (ECDM) process. Journal of Mechanical Science and Technology. 35(11), 5127-5135.

[55] V. Rajput, M. Goud, N. M. Suri (2021). Finite Element Modeling for Comparing the Machining Performance of Different Electrolytes in ECDM. Arabian Journal for Science and Engineering. 46, 2097–2119.

[56] M. S. Han, B. K. Min, S. J. Lee (2007). Improvement of surface integrity of electro-chemical discharge machining process using powder-mixed electrolyte. Journal of Materials Processing Technology. 191, 224-227.

[57] M. S. Han, B. K. Min, S. J. Lee (2009). Geometric improvement of electrochemical discharge micro-drilling using an ultrasonic-vibrated electrolyte. Journal of Micromechanics and Microengineering. 19, 065004.

[58] C. K. Yang, C. P. Cheng., C. C. Mai, A. C. Wang, J. C. Hung, B. H. Yan (2010). Effect of surface roughness of tool electrode materials in ECDM performance. International Journal of Machine Tools & Manufacture. 50, 1088–1096.

[59] C. K. Yang, K. L. Wu, J. C. Hung, S. M. Lee, J. C. Lin, B. H. Yan. (2011). Enhancement of ECDM efficiency and accuracy by spherical tool electrode. International Journal of Machine Tools & Manufacture. 51, 528-535.

[60] S. K. Jui, A. B. Kamaraj, M. Sundaram. (2013). High aspect ratio micromachining of glass by electrochemical discharge machining (ECDM). Journal of Manufacturing Processes. 15, 460-466.

[61] V. K. Jain, D. Priyadarshini (2014). Fabrication of Microchannels in Ceramics (Quartz) Using Electrochemical Spark Micromachining (ECSMM). Journal of Advanced Manufacturing Systems. 13(1), 5-16.

[62] A. B. Kamaraj, S. K. Jui, Z. Cai, M. Sundaram (2015). A mathematical model to predict overcut during electrochemical discharge machining. The International Journal of Advanced Manufacturing Technology. 81, 685-691.

[63] Y. Zhang, Z. Xu, D. Zhu, J. Xing (2015). Tube electrode high-speed electrochemical discharge drilling using low-conductivity salt solution. International Journal of Machine Tools & Manufacture. 92, 10-18.

[64] P. K. Gupta, A. Dvivedi, P. Kumar (2016). Effect of Pulse Duration on Quality Characteristics of Blind Hole Drilled in Glass by ECDM. Materials and Manufacturing Processes. 31(13), 1740-1748.

[65] A. Behroozfar, M. R. Razfar (2016). Experimental and Numerical Study of Material Removal in Electrochemical Discharge Machining (ECDM). Materials and Manufacturing Processes. 31(4), 495-503.

[66] A. Behroozfar, M. R. Razfar (2016). Experimental Study of the Tool Wear During the Electrochemical Discharge Machining. Materials and Manufacturing Processes. 31(5), 574-580.

[67] Y. Zhu, T. Liang, L. Gu, W. Zhao (2017). Precision machining of high aspect-ratio rotational part with wire electro discharge machining. Journal of Mechanical Science and Technology. 31(3), 1391-1399.

[68] M. Goud, A. K. Sharma (2017). On performance studies during micromachining of quartz glass using electrochemical discharge machining. Journal of Mechanical Science and Technology. 31(3), 1365-1372.

[69] N. Rattan, R. S. Mulik. (2017). Improvement in material removal rate (MRR) using magnetic field in TW-ECSM process. Materials and Manufacturing Processes. 32(1), 101-107.

[70] M. S. Han, K. W. Chae, B. K. Min (2017). Fabrication of high-aspect-ratio microgrooves using an electrochemical discharge micromilling process. Journal of Micromechanics and Microengineering, 27, 055004.

[71] M. Hajian, M. R. Razfar. A. H. Etefagh (2017). Experimental study of tool bending force and feed rate in ECDM milling. The International Journal of Advanced Manufacturing Technology. 91, 1677-1687.

[72] M. Goud, A. K. Sharma (2017). A three-dimensional finite element simulation approach to analyze material removal in electrochemical discharge machining. Proc IMechE Part C: J Mechanical Engineering Science. 231(13), 2417-2428.

[73] F. Mehrabia, M. Farahnakiana, S. Elhamib, M.R. Razfar (2018). Application of electrolyte injection to the electro-chemical discharge machining (ECDM) on the optical glass. Journal of Materials Processing Technology. 255, 665-672.

[74] Z. Y. Xu, Y. Zhang, F. Ding, F. Wang (2018). An electrochemical discharge drilling method of small deep hole. The International Journal of Advanced Manufacturing Technology. 95, 3037–3044.

[75] S. Saranya, A. Ravi Sankar. (2018). Fabrication of precise micro-holes on quartz substrates with improved aspect ratio using a constant velocity-feed drilling technique of an ECDM process. Journal of Micromechanics and Microengineering. 28, 125009.

[76] X. Kang, W. Tang (2018). Micro-drilling in ceramic-coated Ni-superalloy by electrochemical discharge machining. Journal of Materials Processing Technology. 255, 656-664.

[77] M. Hajian, M. R. Razfar, S. Movahed, A. H. Etefagh (2018). Experimental and numerical investigations of machining depth for glass material in electrochemical discharge milling. Precision Engineering. 51, 521–528.

[78] M. R. Dhanvijay, V. A. Kulkarni, A. Doke. (2019). Experimental Investigation and Analysis of Electrochemical Discharge Machining (ECDM) On Fiberglass

Reinforced Plastic (FRP). Journal of The Institution of Engineers (India): Series C. 100(5), 763–769.

[79] P. Antil, S. Sing, A. Manna (2019). Experimental Investigation During Electrochemical Discharge Machining (ECDM) of Hybrid Polymer Matrix Composites. Iranian Journal of Science and Technology, Transactions of Mechanical Engineering. 44, 813–824.

[80] M. Singh, S. Singh, S. Kuma (2019). Experimental Investigation for Generation of Micro-Holes on Silicon Wafer Using Electrochemical Discharge Machining Process. Silicon. 12, 1683-1689.

[81] R. K. Arya, A. Dvivedi (2019). Investigations on quantification and replenishment of vaporized electrolyte during deep micro-holes drilling using pressurized flow-ECDM process. Journal of Materials Processing Technology. 266, 217-229.

[82] B. Madhavi J, S. S. Hiremath (2019). Machining of micro-holes on borosilicate glass using micro-electro chemical discharge machining (μ-ECDM) and parametric optimisation. Advances in Materials and Processing Technologies. 5(3), 542-557.

[83] M. Sundaram, Y. J. Chen, K. Rajurkar (2019). Pulse electrochemical discharge machining of glass-fiber epoxy reinforced composite. CIRP Annals - Manufacturing Technology. 68, 169-172.

[84] J. C. Chena, Y. A. Lina, C. L. Kuob, C. C. Hoa, W. H. YAU (2019). An Improvement in the Quality of Holes Drilled in Quartz Glassby Electrochemical Discharge Machining. Smart Science. 7(3), 169-174.

[85] D. Singh, M. Goud (2019). A 3D Spark Model to Evaluate MRR in ECDM. Journal of Advanced Manufacturing Systems. 18(3), 435-446.

[86] P. Antil (2019). Modelling and Multi-Objective Optimization during ECDM of Silicon Carbide Reinforced Epoxy Composites. Silicon. 12, 275–288.

[87] D. K. Mishra, A. K. Verma, J. Arab, D. Marla, P. Dixit (2019). Numerical and experimental investigations into microchannel formation in glass substrate using electrochemical discharge machining. Journal of Micromechanics and Microengineering. 29, 075004.

[88] A. Charak, C. S. Jawalkar (2020). Experimental Studies in Micro Channelling on Borosilicate Glass Using RSM Optimization Technique. Silicon. 12, 1707–1721.

[89] M. Kumar, R. O. Vaishya, N. M. Suri, A. Manna (2020). An Experimental Investigation of Surface Characterization for Zirconia Ceramic Using

Electrochemical Discharge Machining Process. Arabian Journal for Science and Engineering. 46, 2269–2281.

[90] J. Arab, P. Dixit (2020). Influence of tool electrode feed rate in the electrochemical discharge drilling of a glass substrate. Materials and Manufacturing Processes. 35, 1749-1760.

[91] R. M. Alvarado, E. E. G. Gutiérrez, A. H. Rodríguez, R. J. P. Alejo (2020). Pulse Classification for an Electrochemical Discharge Machining Process Based on Fuzzy Logic Approach. International Journal of Precision Engineering and Manufacturing. 21, 1807–1820.

[92] T. Singh, A. Dvivedi (2020). On prolongation of discharge regime during ECDM by titrated flow of electrolyte. The International Journal of Advanced Manufacturing Technology. 107, 1819–1834.

[93] V. Rajput, M. Goud, N. M. Suri (2020). Finite Element Modelling for Analyzing Material Removal Rate in ECDM Process. Journal of Advanced Manufacturing Systems. 19(9), 815-835.

[94] X. Kang, W. Tang, W. Zhao, J. Qian, B. Lauwers (2021). Experimental and numerical investigations of material removal process in electrochemical discharge machining of glass in discharge regime. Precision Engineering. 72, 706-716.

[95] D. K. Mishra, P. Dixit (2021). Experimental investigation into tool wear behaviour of line-array tool electrode during the electrochemical discharge micromilling process. Journal of Manufacturing Processes. 72, 93-104.

[96] T. Singh, A. Dvivedi (2021). Fabrication of micro holes in Yttria-stabilized zirconia (Y-SZ) by hybrid process of electrochemical discharge machining (ECDM). Ceramics International. 47, 23677–22368.

[97] C. Wang, Y. Zhang., L. Ji, W. Yang, J. Wang. (2021). Improvement of machining accuracy in EDCM by enhanced electrochemical reaming based on a non-metallic backing layer. Chinese Journal of Aeronautics. 34(12), 251-264.

[98] D. Zhao, H. Zhu, Z. Zhang, K. Xu, J. Gao, X. Dai, L. Huang (2021). Influence of electrochemical discharge machining parameters on machining quality of microstructure. The International Journal of Advanced Manufacturing Technology. 119, 841–854.

[99] Y. Xu, B. Jiang (2021). Machining performance enhancement of deep micro drilling using electrochemical discharge machining under magnetohydrodynamic effect. The International Journal of Advanced Manufacturing Technology. 113, 883–892.

[100] J. Arab, D. K. Mishra, P. Dixit (2021). Measurement and analysis of the geometric characteristics of microholes and tool wear for varying tool-workpiece gaps in electrochemical discharge drilling. Measurement. 168, 108463.

[101] A. Torabi, M. R. Razfar (2021). The capability of ECDM in creating effective microchannel on the PDMS. Precision Engineering. 68, 10-19.

[102] V. Rajput, M. Goud, N. M. Suri (2021). Three-Dimensional Finite Element Modeling and Response Surface Based Multi-Response Optimization During Silica Drilling with Closed-Loop ECDM. Silicon. 13, 3583–3609.

[103] B. Mallick, B. R. Sarkar, B. Doloi, B. Bhattacharyya (2021). Improvement of Surface Quality and Machining Depth of μ-ECDM Performances Using Mixed Electrolyte at Different Polarity. Silicon. 14, 8223–8232.

[104] M. Harugade, S. Waigaonkar, N. Dhawale (2021). A novel approach for removal of delaminated fibers of a reinforced composites using electrochemical discharge machining. Proc IMechE Part B: J Engineering Manufacture. 235(12), 1949–1960.

[105] A. D. Oza, A. Kumar, V. Badheka, A. Arora, M. Kumar, C. I. Pruncu, T. Singh (2021). Improvement of the Machining Performance of the TW-ECDM Process Using Magnetohydrodynamics (MHD) on Quartz Material. Materials. 14, 2377.

[106] V. Rajput, S. S. Pundir, M. Goud, N. M. Suri (2021). Multi-Response Optimization of ECDM Parameters for Silica (Quartz) Using Grey Relational Analysis. Silicon. 13, 1619–1640.

[107] M. Kumar, R. O. Vaishya, N. M. Suri, A. Manna (2021). An Experimental Investigation of Surface Characterization for Zirconia Ceramic Using Electrochemical Discharge Machining Process. Arabian Journal for Science and Engineering. 46, 2269–2281.

[108] H. K. Kannojia, A. Sidhique, A. S. Shukla, J. Pednekar, S. Gupta, P. Dixit (2021). Design and fabrication of through-glass via (TGV) based 3D spiral inductors in fused silica substrate. Microsystem Technologies. 28, 955-964.

[109] J. Ranganayakulu, P. V. Srihari, K. V. Rao (2021). An Optimization Strategy to Improve Performance in Electrochemical Discharge Machining of Borosilicate Glass Using Graph Theory Algorithm and Desirability Index. Silicon. 14, 5241–5254.

[110] V. Rajput, M. Goud, N. M. Suri (2021). Performance analysis of closed-loop electrochemical discharge machining (CLECDM) during micro-drilling and

response surface methodology based multi-response parametric optimisation. Advances in Materials and Processing Technologies. 8(2), 1352-1382.

[111] D. Zhao, Z. Zhu, H. Zhu, Z. Cao, K. Xu (2021). An Investigation into Laser-Assisted Electrochemical Discharge Machining of Transparent Insulating Hard-Brittle Material. Micromachines. 12, 1-12.

[112] D. Zhao, H. Zhu, Z. Zhang, K. Xu, J. Gao, X. Dai, L. Huang (2022). Influence of electrochemical discharge machining parameters on machining quality of microstructure. The International Journal of Advanced Manufacturing Technology. 119, 841–854.

[113] A. Charak, C. S. Jawalkar (2022). Experimental Investigation and Analysis on Borosilicate Glass Using Electrochemical Discharge Machining Process. Silicon. 14, 1823-1829.

[114] J. B. Madhavi, S. S. Hiremath (2022). Generation and Characterization of Borosilicate Glass Nanoparticles using in-House Developed μ-ECDM Setup. Silicon. 14, 1713–1729.

[115] L. Paul, S. S. Hiremath (2022). Model Prediction and Experimental Study of Material Removal Rate in Micro ECDM Process on Borosilicate Glass. Silicon. 14, 1497-1510.

[116] A. Torabi, M. R. Razfar (2022). Investigating the effects of electrochemical discharge machining (ECDM) on the dimensional accuracy and surface integrity of the PDMS microchannel. SN Applied Science. 4, 274.

[117] Y. Ma, N. Qu, X. Yue, Y. Liu (2022). Electrochemical discharge machining grooves without recast layer in 20 wt% NaCl solution. The International Journal of Advanced Manufacturing Technology. 121, 5413–5425.

[118] J. Ranganayakulu, P. V. Srihari, K. V. Rao (2022). A strategy to improve performance in electrochemical discharge machining using periodic bi-directional tool rotation. The International Journal of Advanced Manufacturing Technology. 123, 1459–1476.

[119] X. D. Cao, B. H. Kim, C. N. Chu (2009). Micro-structuring of glass with features less than 100 μm by electrochemical discharge machining. Precision Engineering. 33, 459–465.

[120] K. H. Nguyen, P. A. Lee, B. H. Kim (2015). Experimental Investigation of ECDM for Fabricating Microstructures of Quartz. International Journal of Precision Engineering and Manufacturing. 16, 5-12.

Original Article

Institution of MECHANICAL ENGINEERS

Journal of ENGINEERING MANUFACTURE

Proc IMechE Part B:
J Engineering Manufacture
2023, Vol. 237(8) 1207–1219

DOI: 10.1177/09544054221123479
journals.sagepub.com/home/pib
SAGE

Investigation through novel tool-electrode feeding approach on electrochemical discharge machining of glass

Sudip Santra, Biplab Ranjan Sarkar, Biswanath Doloi and Bijoy Bhattacharyya

Abstract

The electrochemical discharge machining (ECDM) process is a promising advanced machining process to remove material from electrically non-conductive materials like glass, ceramics, etc. Till now fabricating a channel with a high aspect ratio on the glass surface is a challenging job as the generated gas bubbles are escaped from the machining area without developing gas film and consequent discharges. In this study, two novel approaches of tool feeding such as side feeding and bottom feeding along with usual top feeding approach have been introduced to keep the gas bubbles at the tool-electrode tip so that the development of gas film and spark discharge are taken place uniformly at the machining zone. Tool-electrode feeding at the bottom surface and at the side surface of workpiece have been employed and compared with the usual top feeding tool-electrode at the top surface of workpiece. The concentration of aqueous sodium hydroxide electrolyte and the feed rate of tool are varied for experimental investigations. The side feeding of tool-electrode has been found as the most suitable feeding approach for ECDM process. During side feeding approach, the overcut of the machined channel has been reduced by 11% as compared to that of top feeding. Also, depth of the channel has been increased significantly during machining by side feeding and bottom feeding. The tool wear has been reduced more in case of side tool-feeding approach than other two tool-feeding approaches.

Keywords

ECDM, side feeding, bottom feeding, machining depth, width, glass workpiece

Date received: 25 February 2022; accepted: 7 August 2022

Introduction

Advance machining processes have been using for machining of hard, brittle, and difficult-to-machine materials like glass, ceramics, metal matrix composites, etc. Further, the development of micro electro mechanical system (MEMS) pushes forward the micromachiningas well as non-traditional machining processes. Electrochemical discharge machining (ECDM), a non-traditional process, can machine electrically non-conductive materials and it is oneof thelow cost machining processes. In biomedical field, fabrication of lab-on-chip device needs channeling of glass materials, whichcanbe done by ECDM process. The development of a micro pattern with better surface finish is possible only for electrically conductive materials with the helpof electrochemical machining. [1] The limitationof EDM and ECM processes for machining of electrically non-conductive materials can be overcome by employing ECDM.[2] Another process to fabricate grooves on hard materials can also be done by creep feed profile grinding technique.[3,4] During grinding, the material removal process occurs due combined action of rubbing, ploughing, and cutting which causes residual stress on the workpiece.[5–7] In ECDM, two electrodes are immersed into an aqueous electrolyte and among them, one electrode is a cathode generally used as a tool, and another electrode is an anode used as an auxiliary electrode. Being an electrically non-

Production Engineering Department, Jadavpur University, Kolkata, West Bengal, India

Corresponding author:
Biplab Ranjan Sarkar, Production Engineering Department, Jadavpur University, 188, Raja S.C. Mallick Road, Jadavpur, Kolkata, West Bengal 700032, India.
Email: sarkarbiplab_s@rediffmail.com

Sādhanā (2024)49:128
https://doi.org/10.1007/s12046-024-02476-1

Electrochemical discharge milling on silica glass using vertically upward tool feeding technique

S SANTRA*, B R SARKAR, B DOLOI and B BHATTACHARYYA

Production Engineering Department, Jadavpur University, Kolkata, West Bengal 700032, India
e-mail: sudip16santra@gmail.com

MS received 11 July 2023; revised 23 November 2023; accepted 22 January 2024

Abstract. Machining of silica glass is a challenging task due to its physical properties like brittleness, electrically insulated, etc. Although with the use of electrochemical discharge, it is possible to make holes and channels in silica glass, but the generation of spark discharge and removal of materials is a complex phenomenon in the electrochemical discharge process. Several research works were carried out previously to control the spark discharge as well as machining accuracy using rotational tool, the addition of ultrasonic vibration, including a magnetic field, and the use of different electrolytes, etc. A novel tool feeding technique i.e. using a horizontal tool and vertically upward tool feeding technique was used during milling on glass. The effects of voltage, the tool feed rate (TFR) and the concentration of electrolyte on the material removal rate and machining quality were studied in this work. The machined channel was examined under an optical measuring microscope as well as scanning electron microscope. The machining surface was also observed using a coherence correlation interferometry image to analyze in-depth surface topography of machined channels. Material removal rate and Ra value of the bottom layer were measured. The material removal rate of 6.097 μg/min was noticed at 25 wt% of electrolyte concentration, 40 μm/s of TFR and 45 V of applied voltage. The bottom layer's surface roughness (Ra) was found as low as 0.222 μm (Ra) at parametric conditions of 40 V, 40 μm/s TFR, and 15 wt% electrolyte concentration by employing the developed novel tool feeding technique.

Keywords. Electrochemical discharge milling; vertically upward tool feeding; glass; MRR; surface roughness.

1. Introduction

The machining by Electrochemical discharge has achieved tremendous improvement in the machining of electrically non-conductive materials such as polymers, glass, ceramic, etc. Initially, this process was used to create holes in the workpiece, and nowadays, it can successfully produce channels even in exotic materials. The electrochemical discharge process was discovered by Kurafuji and Suda in 1968. Similarly, the electrolysis process which uses cathode and anode, milling with electrochemical discharge also involves the use of cathode and anode. Usually, the tool acts as a cathode and another separate electrode termed as auxiliary electrode acts as an anode in this machining process. The auxiliary electrode and the tool electrode are fully immersed in an aqueous alkaline solution. Electricity is allowed to pass through the anode, electrolyte, and cathode. Being an electrically non-conductive material the workpiece is not used as a part of the electrical circuit in ECD milling. The auxiliary electrode that is used in this process should be significantly larger than the tool in size. The electrochemical reaction processes can be categorized into two types i.e. reactions at the cathode, where hydrogen gas is evolved as a result of the evaporation of electrolytes, and reactions at the anode, where oxygen gas is evolved. Due to electrolysis process, the hydrogen bubbles are generated at the tool electrode when the current starts to flow between the anode and cathode through the electrolyte. Those generated bubbles gathered around the exposed area of the cathode and produce an insulated gas film that discontinues the electrical circuit [1]. With the increase of applied voltage, the gas film breakdowns and spark discharge is observed between the cathode and electrolyte. Several research works asserted that the heat produced in spark discharges is significantly higher than the temperature at which the glass melts and occasionally even reaches the vaporization temperature [2, 3]. This demonstrates that heat produced by spark discharges is the main factor in material removal. The removal of materials from the glass surface also occurred as a result of high-temperature chemical etching [4]. According to Wüthrich *et al* [5], examination of the current signal during ECDM might be used to track the electrolyte temperature as well as the availability of a gas film. For better machining quality and

*For correspondence
Published online: 04 April 2024

Journal of Advanced Manufacturing Systems
(2025) 1–26

DOI: 10.1142/S0219686725500143

Experimentation into Electrochemical Discharge Milling for the Generation of Cavity on Glass

Sudip Santra*, Biplab Ranjan Sarkar, Biswanath Doloi and Bijoy Bhattacharyya

Department of Production Engineering
Faculty of Engineering & Technology
Jadavpur University, Kolkata 700032, West Bengal, India
**sudip16santra@gmail.com*

Received 29 December 2023
Accepted 16 July 2024
Published 27 September 2024

The development of electrochemical discharge machining (ECDM) and the use of electrically nonconducting materials in microelectromechanical systems (MEMS), biomedical applications and making lab-on-a-chip devices are increasing tremendously. In this study, the performance of electrochemical discharge milling was improved by introducing the bottom-up movement of tool-electrode, i.e. vertically upward tool-feeding technique. The development of gas film model was compared with the actual gas film shapes to find out the problems associated with the existing tool-feeding technique and the advantages of vertically upward tool-feeding technique. Single channels were generated on the soda lime glass workpiece to analyze and obtain appropriate process parameters for good-quality channels. Applied voltage, electrolyte concentration and tool feed rate (TFR) were varied to get good-quality channel. It was achieved at the process parameters of an applied voltage of 40 V, an electrolyte concentration of 5 M and a TFR of 50 μm/s. With this parametric setting, four consecutive parallel channels were generated to get cavity on the soda lime glass. Rectangular-shaped cavities were fabricated by adopting three different strategies to minimize the problem of material deposition along the border of two adjacent parallel channels. These rectangular cavities were observed under a microscope to measure and obtain the surface topography which revealed the usability of third strategy of generating smooth and uniform cavity with lower surface roughness (R_a). A rectangular cavity of 0.247-μm surface roughness with smooth corners and edges was obtained at 40 V of applied voltage and 50 μm/s of TFR.

Keywords: Electrochemical discharge milling; vertically upward tool-feeding; rectangular cavity; soda lime glass.

1. Introduction

Electrochemical discharge machining (ECDM) is widely used for making holes and channels on electrically nonconductive materials as a hybrid machining to counter the shortcomings of electrochemical machining (ECM) as well as electrical

*Corresponding author.

JMEPEG
https://doi.org/10.1007/s11665-025-11241-2

1059-9495/$19.00

ORIGINAL RESEARCH ARTICLE

Fabrication of Microchannels on Polycarbonate Using Electrochemical Discharge Milling

S. Santra, B.R. Sarkar, B. Doloi, and B. Bhattacharyya

Submitted: 14 November 2024 / Revised: 9 January 2025 / Accepted: 31 January 2025

Electrochemical discharge milling (ECD milling) is a widely recognized process for machining electrically non-conductive materials, offering significant advantages over conventional methods. Unlike traditional milling, which relies on mechanical cutting or abrasion, ECD milling removes material through spark discharge and chemical etching. This results in minimal tool wear, reducing both heat generation and environmental impact. Conventional methods, on the other hand, experience higher tool wear and produce more heat and waste. ECD milling is especially effective for precision machining in industries like aerospace, where minimal wear and fine surface finishes are critical. In this study, a new tool-feeding technique was employed to improve the removal of machined products by self-circulating electrolytes in the machining area. Electrochemical discharge milling was performed on polycarbonate, a thermoplastic polymer, using aqueous KOH as the electrolyte. The process parameters were set to 40 V, a tool feed rate of 50 μm/sec, and an electrolyte concentration of 20 wt.%. The results showed a channel width of 594.111 μm and a surface roughness (Ra) value of 0.410 μm. The enhanced electrical conductivity and chemical etching effects of the KOH solution contributed to smaller spark-affected zones (SAZ), improving machining quality.

Keywords ECD milling, polycarbonate, SAZ, vertically upward tool feeding

1. Introduction

Electrochemical discharge machining has made significant advancements in processing electrically non-conductive materials such as ceramics, glass, and polymers. Initially developed for hole drilling, it has since proven effective in creating complex channels and processing advanced and exotic materials. In contrast to conventional electrolysis, this milling method involves the use of both cathodes and anodes. Typically, the tool functions as the cathode, while a separate electrode, known as the auxiliary electrode, serves as the anode. These components are fully submerged in an electrolyte solution. Electricity passes through the cathode, electrolyte, and anode. Remarkably, the workpiece, being an insulating material, is not integrated into the electrical circuit during the electrochemical discharge milling process. Electrochemical reactions in this process have been classified into two categories: cathode reactions, which result in hydrogen gas due to electrolyte vaporization, and anode reactions, which generate oxygen gas. Upon the initiation of current flow, electrolysis begins, leading to the formation of hydrogen bubbles at the tool electrode. These bubbles, accumulating near the exposed cathode, form a gas film that disrupts the electrical circuit (Ref 1). As voltage increases, breakdowns of the gas film occur, resulting in visible spark discharges. The thermal energy generated by these discharges leads to the extraction of material from the workpiece through processes such as melting and vaporization. Several studies have highlighted that the heat generated during spark discharges in electrochemical discharge machining (ECDM) can significantly exceed the melting point of glass, sometimes reaching temperatures high enough to cause vaporization (Ref 2, 3). This emphasizes that the primary mechanism of material removal is the heat produced by the sparks. Furthermore, material removal from glass is also influenced by chemical etching at elevated temperatures (Ref 4). Wüthrich et al. (Ref 5) demonstrated that monitoring the current in ECDM can provide insights into both electrolyte temperature and the presence of the gas film. To enhance machining accuracy and avoid excessive material removal, maintaining thin gas films is crucial. Various strategies, such as applying tool vibration, using different electrode materials, and introducing magnetic fields, have been explored to improve control over the gas film and discharge behavior. The integration of ultrasonic vibration into the ECDM process resulted in a twofold increase in material removal rate (MRR) compared to vibration-free conditions (Ref 6), with a 10-μm amplitude yielding the best results, while larger amplitudes tended to reduce the effectiveness of the vibration (Ref 7). The inclusion of a magnetic field in the system generated magnetohydrodynamic (MHD) convection, facilitating the movement of electrolytes across the machining area. This, in turn, elevated the spark frequency, leading to an augmented MRR (Ref 8, 9). In the context of ECDM channel fabrication, better results were

This article is an invited paper selected from presentations at the 9th International & 30th All India Manufacturing Technology, Design and Research Conference, held December 8–10, 2023, in Varanasi, India, and has been expanded from the original presentation.

S. Santra, B.R. Sarkar, B. Doloi, and **B. Bhattacharyya**, Production Engineering Department, Jadavpur University, Kolkata, West Bengal 700032, India. Contact e-mail: sudip16santra@gmail.com.

Published online: 29 April 2025

On electrochemical discharge milling of glass with horizontal tool and vertically upward feeding technique

Sudip Santra*, **Biplab Ranjan Sarkar, Biswanath Doloi, Bijoy Bhattacharyya**

Jadavpur University, Kolkata, India

Presented in International Conference on Precision, Micro, Meso and Nano Engineering (COPEN - 12: 2022)
December 8 - 10, 2022 IIT Kanpur, India

KEYWORDS

ECD Milling,
Vertically Upward Feeding,
MRR,
Overcut,
Glass.

ABSTRACT

Electrochemical Discharge Milling (ECD milling) process encounters some problems like the uneven edge of the machined channel, lower machining depth, uncontrollable spark discharge, etc. The primary cause of those issues is a lack of gas bubbles in the machining area, which are necessary for good spark discharges. Due to the buoyancy of the liquid, gas bubbles cannot remain at the tool-electrode tip and poor flushing arises from feeding the tool-electrode on the top surface of the workpiece. In this study, horizontal tool-electrode and vertically upward feeding technique has been introduced to solve the problems that arise during the existing feeding technique. The material removal rate (MRR) and overcut during ECD milling are observed and analysed by changing the applied voltage, concentration of electrolyte and feed rate of tool. MRR and overcut are found as 5.025µg/min and 116.86µm respectively at 40V, 20wt% concentration of electrolyte and 50µm/sec of feed rate.

1. Introduction

A promising machining technique for removing components from electrically non-conductive materials is electrochemical discharge milling that have varieties of uses in MEMS, bio medical device, lab-on-chip devices etc. Two types of electrochemical reactions are occurred at the cathode, where hydrogen bubbles are generated, and at the anode, where oxygen gas is generated. Together, the hydrogen gas bubbles and the vapour bubbles that congregate around the tool electrode create an insulated gas sheet over its exposed surface (Bhattacharyya et al., 1999). This layer of gas film ruptures at a certain voltage, causing a spark discharge between the cathode tool-tip and electrolyte. The heat developed due to the spark discharges removes materials from the workpiece by causing it to melt and vaporize when the workpiece is placed close to the sparking zone. According to several studies, spark discharged heat often exceeds the glass melting temperature and approaches the glass vaporization temperature (Basak & Ghosh, 1997; AbouZiki et al., 2012). Additional studies have revealed that high-temperature chemical etching also causes the loss of components from the glass surface (Jain & Adhikary, 2008). According to Wüthrich et al. (2006), the current signal can be used to monitor the electrolyte temperature and the existence or absence of a gas film during ECDM. MRR grew twice as rapidly with ultrasonic vibration applied as compared to without vibration (Elhami & Razfar, 2017). The quantity of material removed increased when ultrasonic vibration was applied with a 10 µm amplitude compared to when it wasn't used (Elhami & Razfar, 2018). However, a big amplitude reduced the vibration's impact. MHD convection was produced by introducing a magnetic field to the system, enabling electrolytes to travel through the machining region and increasing the frequency of sparks, which increased MRR (Ratan & Mulik, 2017; Xu & Jiang, 2021). The *(OH)*¯ ion concentration increased with the electrolyte's reduced surface tension, whic led to a thinner gas layer and enhanced surface quality during surface machining (AbouZiki et al., 2012; Yang et al., 2010). The larger tool-to-workpiece gap enables the discharge to impact the workpiece with greater kinetic energy, causing the machined surface to be rougher and encouraging cracking. Maintaining an optimal tool-workpiece distance was important to provide a proper machined profile (Torabi & Razfar, 2021;

*Corresponding author E-mail: sudip16santra@gmail.com

https://

Materials Today: Proceedings 62 (2022) 6438–6444

Contents lists available at ScienceDirect

Materials Today: Proceedings

journal homepage: www.elsevier.com/locate/matpr

Investigation on electrochemical discharge milling by side feeding technique

Sudip Santra *, Biplab Ranjan Sarkar, Biswanath Doloi

Production Engineering Department, Jadavpur University, Kolkata-700032, West Bengal, India

ARTICLE INFO

Article history:
Available online 21 April 2022

Keywords:
ECD milling
Side feeding
Surface roughness
Glass

ABSTRACT

Electrochemical discharge milling is an efficient process for generating channels and patterns on electrically non-conductive, hard-to-machine materials which are applied in the biomedical field for making lab-on-chip devices as well as in MEMS industries. The usual process of ECD milling is the feeding of tool-electrode from the top surface of the workpiece. It creates problems during machining as the generated gas bubbles escape from the machining area. To overcome this problem a new kind of feeding technique named side feeding is applied in this study. The gas bubbles always remain at the tooltip and due to buoyancy, it makes the milling process easier. This study is carried out with an in-house developed ECD milling set up and focuses on the influences of voltage and feed rate of tool electrodes on the channel width and surface roughness (Ra) during milling on glass with side feeding technique. Using this technique the channel width of 532.68 µm with surface roughness (Ra) of 0.222 µm was obtained.

1. Introduction

The developments of advanced machining processes have increased the possibilities to machine hard and brittle materials. The ECDM process is more competent to remove material from electrically non-conductive materials among various advanced machining processes. Making of the lab-on-chip device, surgical instruments, etc. has provided the scope of ECD milling in a broader way. Ho et al. [1] documented that EDM is an effective machining process to machine advanced materials but this process is bounded within electrically conductive materials and it also generates higher roughness on the machining surface. Bhattacharyya et al. [2] stated that the ECM process can improve the surface roughness of machining products but again this process can machine only electrically conductive materials. ECDM process is a hybrid machining process that combines the principle of EDM and ECM and it is able to overcome the limitation of EDM and ECM. The concept of electrochemical discharge was presented for the first time in 1968 by kurafuji and Suda [3]. Since the invention of this process, a lot of research were done to understand the mechanism and to stabilize the continuous removal of materials. Different names and abbreviations were given by several researchers such as electrochemical spark machining (ECSM) by Jain et al. [4], spark assisted chemical engraving (SACE) by Fascio et al. [5], electrochemical anode machining (ECAM) by Kubota [6], discharge machining of non-conductors (DMNC) by Cook et al. [7], spark assisted etching (SAE) by Daridon [8].

Bhattacharyya et al. [9] documented that at higher voltage MRR increased but the micro-cracks were observed although better dimensional accuracy was found at 80 V and 25% NaOH solution. Basak et al. [10,11] investigated the spark generation and material removal mechanism theoretically as well as experimentally. Further research on ECDM revealed some important factors about the mechanisms of discharge activity and removal of materials. Wüthrich et al. [12] claimed that by analysing the current signal, various activities could be monitored during this process. Gas film generation and its thickness were manipulated by applying various techniques like addition of vibration to the tool-electrode, use of magnetic field, use of different electrolytes etc. Arab et al. [13] produced thin gas film and lower HAZ by using tool-electrode with lower surface roughness. Singh et al. [14] used textured tool to generate high frequency low intensity discharge which removed materials from the workpiece surface uniformly. Besides electrochemical discharge drilling process, this discharge has also been used for milling. Hajian et al. [15] prepared a FEM model to find

* Corresponding author. Tel.: +91-33-24146153.
E-mail address: sudip16santra@gmail.com (S. Santra).

https://doi.org/10.1016/j.matpr.2022.04.111
2214-7853/

Experimental Investigation into Electrochemical Discharge Milling of Glass by Bottom Feeding the Tool Electrode

S. Santra, B. R. Sarkar, B. Doloi, and B. Bhattacharyya

Abstract Electrochemical discharge milling is very prospective and hybrid technology to produce a channel on brittle, hard engineering materials. In this investigation, the possibility of milling of glass material has been identified by feeding the tool electrode from bottom to upward direction using a copper tool of 0.5 mm diameter. The electrochemical discharge milling operation has been done by an in-house developed machining set-up. The present paper highlights phenomena of generation of gas film and electrochemical discharges by placing the tool electrode beneath the workpiece in an electrolyte-filled machining chamber. The effects of three different parameters like voltages, electrolyte types and dwell time on performance characteristics have been studied. Good quality machining surface is obtained at lower voltage and higher dwell time in NaOH electrolyte solution.

Keywords Electrochemical discharge milling · Bottom tool feed · Non-traditional machining

1 Introduction

In this advanced machining era, many processes are available for machining hard, brittle, and difficult-to-machine materials like glass, ceramics, metal matrix, etc. The development of micro electromechanical system (MEMS) increases the demand for micromachining and advanced machining processes. Depending on the material removal mechanism, the advanced machining processes can be divided into four types such as thermal, chemical, electrochemical, and mechanical. Electrochemical discharge milling can machine electrically non-conductive materials, and it is a low-cost machining process. In the biomedical field, fabrication of lab-on-a-chip devices needs milling of glass materials, which can be done by electrochemical discharge milling process.

S. Santra (✉) · B. R. Sarkar · B. Doloi · B. Bhattacharyya
Production Engineering Department, Jadavpur University, Kolkata 700032, India
e-mail: sudip16santra@gmail.com

M. S. Shanmugam et al. (eds.), *Advances in Modern Machining Processes*, Lecture Notes in Mechanical Engineering, https://doi.org/10.1007/978-981-19-7150-1_6

Advancement of Electrochemical Discharge Machining Process—A Review

S. Santra, B. R. Sarkar, B. Doloi, and B. Bhattacharyya

Abstract Electrochemical discharge machining (ECDM) process, which is referred to as electrochemical spark machining, was known to the world due to the invention by Kurafuji and Suda in 1968. Research papers of the last few years have been reviewed to comprehend the process mechanism and its development up to the milling operation on electrically non-conductive materials. The basic mechanism and development of the ECDM process in terms of gas film stabilization, enhancement of MRR, and improvement of surface quality and dimensional accuracy have been discussed in this paper. The application of electrochemical discharge for milling operation and its development has also been incorporated in this paper. Further, the effects of the use of various electrolytes, tool electrode materials, tool electrode shape and application of vibration, magnetic field as well as the addition of various extra features to the basic process and the future scope of research have been discussed.

Keywords Electrochemical discharge machining · MRR · Microchannel · Micro-milling

1 Introduction

Machining is an essential manufacturing process toward the development of technology and its applications in various fields. Conventional machining ruled the field of manufacturing since stone from stone weapons to the development of CNC and artificial intelligence. Due to the presence of new and advanced materials, the development of machining technologies is also improving. In the age of non-traditional machining, there are a lot of processes, which have been used for machining hard, brittle, and difficult to machine materials like glass, ceramics, metal matrix, etc. Further, the development of a micro-electro-mechanical system (MEMS) pushed forward the micro-machining as well as non-traditional machining processes. Among

S. Santra (✉) · B. R. Sarkar · B. Doloi · B. Bhattacharyya
Production Engineering Department, Jadavpur University, Kolkata 700032, India
e-mail: sudip16santra@gmail.com

U. S. Dixit et al. (eds.), *Advances in Forming, Machining and Automation*, Lecture Notes in Mechanical Engineering, https://doi.org/10.1007/978-981-19-3866-5_15